

Copyright
By
Guanyu Hu
2011

**The Dissertation Committee for Guanyu Hu certifies that this is the approved
version of the following dissertation:**

Behavior of Beam Shear Connections in Steel Buildings Subject to Fire

Committee:

Michael D. Engelhardt, Supervisor

Karl H. Frank

Todd A. Helwig

Loukas F. Kallivokas

Ofodike A. Ezekoye

Behavior of Beam Shear Connections in Steel Buildings Subject to Fire

by

Guanyu Hu, B.S.; M.S.

Dissertation

Presented to the Faculty of the Graduate School of

The University of Texas at Austin

in Partial Fulfillment

of the Requirements

for the Degree of

Doctor of Philosophy

The University of Texas at Austin

December 2010

Dedication

To my beloved family members

Acknowledgements

I would like to express my sincere gratitude and appreciation to my advisor Dr. Michael Engelhardt for his guidance, encouragement and patience to the completion of this research work. I feel I am extremely lucky to be a graduate student under the supervision of Dr. Engelhardt, as his constant support and review are invaluable to the progress of this work, and his wisdom, insight and advice will be a benefit to me in my lifetime.

Special thanks to my committee members: Dr. Karl Frank, Dr. Todd Helwig, Dr. Loukas Kallivokas and Dr. Ofodike Ezekoye for their helpful discussion and assistance. They have always been tremendous sources of information and ideas.

I acknowledge Eric Schell, Dennis Phillip, Andrew Valentine and Blake Stasney for their help in the experimental part of this work. I am also grateful to my fellow students Jinwoo Lee and Mohammed Morovat for their kindly help.

My return to graduate school would not have occurred without the funding provided by the National Science Foundation (NSF Award 0700682), and this support is greatly appreciated.

Finally, I would like to express my gratitude to my parents, for their strong and consistent love, moral support and encouragement through the entire process of my Ph.D. study at The University of Texas at Austin.

Guanyu Hu

August 2011

Behavior of Beam Shear Connections in Steel Buildings Subject to Fire

Publication No. _____

Guanyu Hu, Ph.D.

The University of Texas at Austin, 2011

Supervisor: Michael D. Engelhardt

This dissertation presents the results of experimental and computational investigations on the behavior of steel simple beam end framing connections subjected to fire. While significant progress has been made in understanding the overall structural response of steel buildings subject to fire, the behavior of connections under fire conditions is not well understood. Connections are critical elements for maintaining the integrity of a structure during a fire. Fire can cause large force and deformation demands on connections during both the heating and cooling stages, while reducing connection strength and stiffness. Of particular importance are simple beam end framing connections. These are the most common type of connection found in steel buildings and are used at beam-to-girder and girder-to-column connections in the gravity load resisting system of a building. This dissertation focuses on one particular type of beam end connection: the single plate connection, also known as a shear tab

connection. This connection is very commonly used in U.S. building construction practice.

In this study, material properties of ASTM A992 structural steel at elevated temperatures up to 900°C were investigated by steady state tension coupon tests. Experimental studies on the connection subassemblies at elevated temperatures were conducted to understand and characterize the connection strength and deformation capacities, and to validate predictions of connection capacity developed by computational and design models. In the computational studies, a three-dimensional finite element connection model was developed incorporating contact, geometric and material nonlinearity temperature dependent material properties. The accuracy and limitations of this model were evaluated by comparison with experimental data developed in this research as well as data available in the literature. The computational studies investigated the typical behavior of the connection during heating and cooling phases of fires as well as the connection force and deformation demands. The finite element model was further used to study and understand the effects of several key building design parameters and connection details.

Based on the test and analysis results, some important finding and conclusions are drawn, and future work for simple shear connection performance in fire are discussed.

Table of Contents

CHAPTER 1 INTRODUCTION AND BACKGROUND.....	1
1.1 Introduction.....	1
1.1.1 Steel Buildings in Fire	1
1.1.2 Steel Beam End Framing Connection Behavior in Fire.....	4
1.2 Research Need And Objective.....	8
1.2.1 Research Need	8
1.2.2 Objective of research	10
1.3 Outline of Dissertation.....	11
CHAPTER 2 LITERATURE REVIEW AND RECENT WORK.....	13
2.1 Overview.....	13
2.2 Elevated-Temperature Properties of Structural Steel	13
2.2.1 Testing Methods.....	14
2.2.2 Past Investigations on Structural Steel Properties at Elevated Temperatures.....	15
2.2.3 General Observations.....	22
2.2.4 Variation of Yield Strength, Tensile Strength and Modulus with Temperature	23
2.2.5 Analytical Expressions for Stress-strain Relationships at Elevated Temperatures.....	29
2.2.6 Creep Behavior of Structural Steel at High Temperatures	32
2.2.7 Summary	35
2.3 Elevated-Temperature Properties of Structural Bolts	36
2.3.1 Test Methods.....	36
2.3.2 Code Recommendations	36
2.3.3 Past Investigations	37
2.3.4 General Observations.....	44

2.4	Simple Bolted Connections at Elevated Temperatures.....	44
2.5	Elevated-Temperature Properties of Welds.....	45
2.6	Steel Beams in Fire Conditions.....	46
2.6.1	Beam Tests.....	46
2.6.2	Numerical Modeling.....	51
2.6.3	Analytical Investigations and Design Equations.....	51
2.6.4	General Observations.....	52
2.7	Shear Tab Connections.....	53
2.7.1	Shear Tab Connections at Ambient Temperature.....	53
2.7.2	Shear Tab Connections in Fire Conditions.....	57
2.8	Summary.....	63
CHAPTER 3 ELEVATED TEMPERATURE PROPERTIES OF ASTM A992 STEEL.....		65
3.1	Overview.....	65
3.2	Experiments.....	66
3.2.1	Equipment.....	66
3.2.2	Specimens.....	66
3.2.3	Loading Control and Measurement.....	68
3.2.4	Temperature Control and Measurement.....	68
3.2.5	Strain Measurement.....	70
3.2.6	Testing Procedure.....	72
3.3	Test Results.....	72
3.3.1	Stress–Strain Curves.....	75
3.3.2	Analysis of Experimental Data.....	79
3.3.3	Yield Strength.....	82
3.3.4	Tensile Strength.....	86
3.3.5	Elastic Modulus.....	88
3.3.6	Proportional Limit.....	89

3.3.7 Effect of Crosshead Displacement Rates	90
3.3.8 Static Yield Stress	91
3.4 Conclusions.....	93
CHAPTER 4 DEVELOPMENT OF FINITE ELEMENT MODELS.....	95
4.1 Overview.....	95
4.2 Overall Approach for Thermal-Structural Analysis	95
4.3 Thermal Analysis Of Steel Beams in Fire	96
4.3.1 Heat Transfer Mechanisms	96
4.3.2 Analysis	99
4.3.3 Element Selection	100
4.3.4 Thermal Properties of Steel	100
4.3.5 Thermal Expansion of Steel.....	102
4.3.6 Thermal Properties of Insulation Materials	103
4.3.7 Heat Transfer FE Model Evaluation.....	104
4.3.8 Observations	112
4.4 Structural Analysis Of Steel Beams in Fire	112
4.4.1 Element Selection	113
4.4.2 Material Properties.....	113
4.4.3 Geometric Nonlinearity	115
4.4.4 Boundary and Load Conditions	115
4.4.5 Model Evaluation.....	116
4.4.6 Observations	122
4.5 FE Modeling of Simple Shear Connections at Ambient Temperature	122
4.5.1 Brief Description.....	122
4.5.2 FE Model Convergence Study	124
4.5.3 Evaluation of FE Model for A Simple Bolted Connection.....	127
4.5.4 Evaluation of the FE model for A Beam and Connection	130
4.5.5 Observations	134

4.6	FE Modeling of Simple Shear Connections at Elevated Temperatures.....	134
4.7	FE Modeling of Shear Tab Beam End Framing Connection in Fire	141
4.8	Other Types of Connections	143
4.9	Summary.....	146
CHAPTER 5 SHEAR TAB CONNECTION TESTS AT ELEVATED TEMPERATURES.....		147
5.1	Overview.....	147
5.2	High Temperature Test System	148
	5.2.1 Loading System	148
	5.2.2 Heating System.....	148
	5.2.3 Cooling System.....	149
5.3	Instrumentation	151
	5.3.1 Temperature Measurement	151
	5.3.2 Load and Displacement Measurement.....	152
5.4	Test Specimens	152
5.5	Testing Procedure	155
	5.5.1 Connections under Axial Tension.....	155
	5.5.2 Connections under Inclined Tension	157
5.6	Test Results.....	161
	5.6.1 Connections under Axial Tension at Elevated Temperatures.....	161
	5.6.2 Connections under Axial Tension after Heating and Cooling.....	169
	5.6.3 Connections under Inclined Tension at Elevated Temperatures.....	173
5.7	Comparison of Experimental Data with Finite Element Connection Models	181
5.8	Simplified Predictions of Connection Strength	187
	5.8.1 Bearing Failure.....	187
	5.8.2 Bolt Shear Failure	188
	5.8.3 Block Shear Failure.....	190

5.9	Summary	192
CHAPTER 6 ANALYSIS AND PARAMETRIC STUDIES OF SHEAR TAB CONNECTION PERFORMANCE IN FIRE.....		194
6.1	Overview	194
6.2	Model and Analysis	195
6.2.1	Model Description	195
6.2.2	Behavior of Shear Tab Connections	200
6.2.3	Behavior of Bolts	202
6.3	Parametric Study	204
6.3.1	Load Ratio.....	204
6.3.2	Beam Length.....	207
6.3.3	Stiffness of the Adjacent Structure	209
6.3.4	Initial Cooling Temperature.....	211
6.3.5	Non-Uniform Temperature Distribution.....	212
6.4	Effect of Connection Details.....	215
6.4.1	Short Slotted Bolt Holes	215
6.4.2	Pretension in Bolts	218
6.4.3	Shear Tab Location.....	219
6.4.4	Shear Tab Thickness	220
6.4.5	Shear Tab Width	221
6.4.6	Bolt Grade.....	225
6.5	Summary and Observations	225
CHAPTER 7 CONCLUSIONS AND FUTURE WORK.....		229
7.1	Brief Summary of Work Completed.....	229
7.2	Conclusions.....	230
7.3	Future Work.....	235

REFERENCES.....	238
VITA.....	250

List of Tables

Table 2.1 Yield strength and modulus of elasticity reduction factors (Eurocode 3 2006)	29
Table 2.2 Bolts strength reduction factors (Eurocode 3 2006)	37
Table 2.3 Welds strength reduction factors (Eurocode 3 2006)	46
Table 3.1 Summary of test results	73
Table 3.2 Tested tensile strength reduction factor	88
Table 4.1 Thermal conductivity of structural steel (Eurocode 3 2006)	101
Table 4.2 Density and thermal conductivity of different insulation materials (ECCS 1995)	104
Table 5.1 Measured material properties at ambient temperature	154
Table 5.2 Test results for connections with 3/4 inch A325 bolts under axial tension	165
Table 5.3 Test results for connections with 1 inch A325 bolts under axial tension	167
Table 5.4 Test results for connections with 3/4 inch A325 bolts under axial tension after heating and cooling	171
Table 5.5 Residual tensile strength of 3/4 inch A325 bolts after heating and cooling	171
Table 5.6 Test results for connections with 3/4 inch A325 bolts under inclined tension	175
Table 5.7 Test results for connections with 1 inch A325 bolts under inclined tension	179
Table 5.8 Comparison of results for connections with 3/4 inch A325 bolts	190
Table 5.9 Comparison of results for connections with 1 inch A325 bolts	191

List of Figures

Figure 1.1 Floor system response in Cardington fire test (Cardinton test report 2003) ...	3
Figure 1.2 Connection failure at tree column of WTC5 (FEMA 2002)	5
Figure 1.3 Connection tear out failure in WTC5 (FEMA 2002)	5
Figure 1.4 Simple shear beam end framing connection damage in heating (left) and cooling (right) (Cardington test report 1998).....	6
Figure 1.5 Simple shear beam end connection damage in fire (Cardington test report 2003)	7
Figure 1.6 Typical shear tab beam end connections	8
Figure 1.7 Echelon Building fire in Austin Texas (www.myfoxhouston.com , February 18 2010)	9
Figure 1.8 Connection damage in Echelon Building due to fire.....	10
Figure 2.1 Stress-strain curves for an ASTM A36 steel (Harmathy and Stanzak 1970) 16	
Figure 2.2 Strain-temperature curves of Grade 43A steel (Kirby and Preston 1988).....	17
Figure 2.3 Chen and Young's testing device (Chen and Young 2005).....	18
Figure 2.4 Stress-strain curves of stainless steel type EN 1.4301 at elevated temperatures (Chen and Young 2005)	19
Figure 2.5 Typical high temperature stress-strain curves for specimen from near the fire and impact zone of WTC 1 (NIST 2005).....	20
Figure 2.6 Outinen's high temperature tensile testing device (Qutinen 2006).....	21
Figure 2.7 Stress-strain curves of Grade 50 steel at elevated temperatures under loading rate of 0.1 in/min (Yu 2006)	22
Figure 2.8 Ultimate and yield strengths of an ASTM A36 steel (Harmathy and Stanzak 1970)	24
Figure 2.9 Elevated-temperature strength properties of a typical BS 4360: Grade 50B structural steel derived from steady-state tests (Kirby and Preston 1988).....	25

Figure 2.10 Yield strength ratio at elevated temperatures of different structural steels (Yu 2006)	26
Figure 2.11 Ultimate strength ratios at elevated temperatures of different structural steels (Yu 2006)	26
Figure 2.12 Young's modulus ratio at elevated temperatures of different structural steels (Yu 2006)	27
Figure 2.13 A typical creep strain versus time curve.....	33
Figure 2.14 Creep curves for the three steels at 600°C (Kelly and Sha 1999)	35
Figure 2.15 Tensile capacity (left) and double shear capacity (right) of Grade 8.8 bolts at elevated temperatures (Kirby 1995).....	38
Figure 2.16 Hardness change with different heating temperatures (Kirby 1995).....	39
Figure 2.17 Yu's bolt shear test setup (Yu 2006).....	40
Figure 2.18 Normalized shear capacity of A325 and A490 bolts at different temperatures (Yu 2006)	41
Figure 2.19 Residual shear capacity of A325 bolts (Yu 2006).....	41
Figure 2.20 Residual shear capacity of A490 bolts (Yu 2006).....	42
Figure 2.21 Strength reduction factors of different structural bolts at elevated temperatures	43
Figure 2.22 Residual strength reduction factors of different structural bolts after heating	43
Figure 2.23 Block shear connection failure at 800°C (Yu 2006)	45
Figure 2.24 Liu's test setup (Liu et al 2002).....	48
Figure 2.25 Li's test setup and arrangement of instruments (Li and Guo 2007)	50
Figure 2.26 Setup of Metzger's shear tab connection test (Metzger 2006)	56
Figure 2.27 Wald and Ticha's fin plate connection test (Sarraj 2007)	59
Figure 2.28 Lap joint component model (Sarraj 2007).....	60
Figure 2.29 Setup used in Yu's connection test (Yu et al 2008)	62
 Figure 3.1 Testing equipment	 67

Figure 3.2 High temperature testing coupon specimen	67
Figure 3.3 Coupon specimen in the furnace during a test (furnace is normally closed during test).	68
Figure 3.4 Strain and temperature measurement	69
Figure 3.5 Strain measurement with resetting extensometer	71
Figure 3.6 Coupons from elevated temperature tests - elongation	74
Figure 3.7 Coupons from elevated temperature tests - fracture section	74
Figure 3.8 Complete stress-strain curves at elevated temperatures – 0.01 inch/min	76
Figure 3.9 Complete stress-strain curves at elevated temperatures – 0.1 inch/min	76
Figure 3.10 Stress-strain curves up to 10% strain – 0.01 inch/min	77
Figure 3.11 Stress-strain curves up to 10% strain – 0.1 inch/min	77
Figure 3.12 Final elongations of tested coupons	78
Figure 3.13 Strain at the ultimate tensile strength	78
Figure 3.14 Stress-strain curve comparison between test data and Eurocode 3 - 400°C – 0.1 inch/min	80
Figure 3.15 Stress-strain curve comparison between test data and Eurocode 3 - 500°C – 0.1 inch/min	80
Figure 3.16 Stress-strain curve comparison between test data and Eurocode 3 - 600°C – 0.1 inch/min	81
Figure 3.17 Stress-strain curve comparison between test data and Eurocode 3 - 700°C	81
Figure 3.18 Stress-strain curve comparison between test data and Eurocode 3 - 800°C	82
Figure 3.19 0.2-percent offset yield strength reduction factor.....	84
Figure 3.20 0.5-percent yield strength reduction factor.....	85
Figure 3.21 2-percent yield strength reduction factor.....	85
Figure 3.22 Stress-strain curves compared at temperatures 20°C and 400°C	86
Figure 3.23 Tensile strength reduction factor $f_{u,T}/f_{y,20}$	87
Figure 3.24 Tensile strength reduction factor $f_{u,T}/f_{u,20}$	88
Figure 3.25 Elastic modulus reduction factor	89
Figure 3.26 Proportional limit reduction factor	90

Figure 3.27 Stress-strain curves compared at two different crosshead rates	91
Figure 3.28 Static yield phenomenon at elevated temperatures for ASTM A992 steel .	92
Figure 3.29 Stress relaxation test for ASTM A992 steel at 700°C	93
Figure 4.1 Three heat transfer mechanisms involved in structure-fire problems	99
Figure 4.2 Heat transfer FE model of steel beam and insulation.....	100
Figure 4.3 Thermal conductivity of carbon steel as a function of the temperature (Eurocode 3 2006).....	101
Figure 4.4 Specific heat of carbon steel as a function of the temperature (Eurocode 3 2006)	102
Figure 4.5 Thermal elongation of carbon steel as a function of the temperature (Eurocode 3 2006).....	103
Figure 4.6 Temperature (°C) distribution on the cross-section of Li's beam during heating obtained by FE model	106
Figure 4.7 Temperature-time comparison between FEA and Li's test (TF 1).....	107
Figure 4.8 Temperature-time comparison between FEA and Li's test (BF 1)	107
Figure 4.9 Temperature-time comparison between FEA and Li's test (TF 2).....	108
Figure 4.10 Temperature-time comparison between FEA and Li's test (BF 2)	108
Figure 4.11 Modeled temperature (°C) on Liu's beam during heating (a) & cooling (b)	110
Figure 4.12 Temperature-time comparison between FEA and Liu's test (TF).....	110
Figure 4.13 Temperature-time comparison between FEA and Liu's test (BF)	111
Figure 4.14 Temperature-time comparison between FEA and Liu's test (web).....	111
Figure 4.15 Steel properties used in FE model of Li and Guo's test.....	114
Figure 4.16 Deflection-time comparison between FEA and Li's test (test 1)	117
Figure 4.17 Deflection-time comparison between FEA and Li's test (test 2)	118
Figure 4.18 Axial force-time comparison between FEA and Li's test (test 1).....	118
Figure 4.19 Axial force-time comparison between FEA and Li's test (test 2).....	119
Figure 4.20 Beam deflection shape of fire test and FEA	119

Figure 4.21 Bottom flange temperature - mid span deflection response (FEA vs. Liu's test).....	121
Figure 4.22 Beam axial force - temperature response (FEA vs. Liu's test).....	121
Figure 4.23 Layout of bolted connection model.....	124
Figure 4.24 Mesh of FE model for convergence study.....	125
Figure 4.25 Convergence study on stress	126
Figure 4.26 Convergence study on displacement	126
Figure 4.27 Geometry and dimensions of steel lap joint used in Richard's test.....	128
Figure 4.28 Stress-strain curve of ASTM A36 steel.....	128
Figure 4.29 Stress-strain relationship of A325 Bolt used in FE model	129
Figure 4.30 Deformations and stress contours of FE model of steel lap joint.....	129
Figure 4.31 Load-deflection comparison between FEA and Richard's test.....	130
Figure 4.32 Dimensions of Metzger's shear tabs and test beams (Not in scale)	131
Figure 4.33 FE mesh of shear tabs and beam ends of Metzger's test.....	132
Figure 4.34 Deformations and stress contours of connection FE model of Metzger's test	133
Figure 4.35 Load-rotation comparison between FEA and Metzger's test.....	133
Figure 4.36 Single bolt connection setup and dimensions of Yu' test (Not in scale)...	135
Figure 4.37 Twin-bolt connection setup and dimensions of Yu's test (Not in scale)...	135
Figure 4.38 FE material model of plate steel at elevated temperatures used in Yu's test	136
Figure 4.39 FE material model of A325 bolt at elevated temperatures used in Yu's test	136
Figure 4.40 FE mesh of single and twin-bolt connection test.....	137
Figure 4.41 Deformations and stress contours of single bolt and twin-bolt connections	137
Figure 4.42 Single bolt load-deformation comparison between FEA and test (300°C)	139
Figure 4.43 Single bolt load-deformation comparison between FEA and test (600°C)	139
Figure 4.44 Twin-bolt load-deformation comparison between FEA and test (300°C).	140

Figure 4.45 Twin-bolt load-deformation comparison between FEA and test (400°C).	140
Figure 4.46 Twin-bolt load-deformation comparison between FEA and test (600°C).	141
Figure 4.47 FE model of Wald's test specimen	142
Figure 4.48 Deflection-time comparison between FEA and Wald's test.....	143
Figure 4.49 FE model of double angle and top-seat angle connection.....	144
Figure 4.50 Deformations of top and bottom seat angle connection of Daryan's test and FE model.....	145
Figure 4.51 Temperature-rotation comparison between FEA and Daryan's test (test 11)	145
Figure 5.1 Testing facilities	150
Figure 5.2 Temperatures collected on the different locations of specimen for a 400°C connection test	151
Figure 5.3 Axial tension test specimen dimensions.....	153
Figure 5.4 Inclined tension test specimen dimensions.....	153
Figure 5.5 Stress-strain curves of steel used in beam and shear tab.....	154
Figure 5.6 Layout of test setup for connections subject to tension (left) and specimens subject to inclined tension (right)	158
Figure 5.7 Test setup without furnace, for connections subject to tension (left) and specimens subject to inclined tension (right).....	159
Figure 5.8 Furnace used for heating and cooling.....	160
Figure 5.9 Testing device for bolt tensile strength	161
Figure 5.10 Connection failures after axial tension tests at 20°C (left) and 600°C (right) – W12×40	163
Figure 5.11 Connection failures after axial tension tests at 20°C (left) and 400°C (right) – W12×26 – 3/4 inch A325 bolts.....	163
Figure 5.12 Connection failures after axial tension tests at 500°C (left) and 550°C (right) – W12×26 – 3/4 inch A325 bolts.....	164

Figure 5.13 Connection failure after axial tension test at 700°C – W12×26 – 3/4 inch A325 bolts.....	164
Figure 5.14 Load displacement response of connections with W12x26 beams and 3/4 inch A325 bolts under axial tension.....	165
Figure 5.15 Connection failures after axial tension tests at 20° (top left), 500°C (top right) and 700°C (bottom) – W12×26 – 1 inch A325 bolts	167
Figure 5.16 Load-displacement response of connections with 1 inch A325 bolts under axial tension	168
Figure 5.17 Comparison between connections with different bolt sizes	168
Figure 5.18 Specimen after exposure to 900°C	170
Figure 5.19 Failure shape of specimen exposed to 1000°C and subsequently cooled and tested	170
Figure 5.20 Bolts fracture in tensile test after exposure to high temperatures (900°C-left two; 1000°C-right two) and cooling.....	171
Figure 5.21 Residual Strength Reduction Factor for A325 Bolts after Heating and Cooling.....	172
Figure 5.22 Load-displacement response of connections tested in axial tension after heating and cooling.....	172
Figure 5.23 Connection failures after inclined tension tests at 20°C(left) and 400°C (right) – 3/4 inch A325 bolts.....	174
Figure 5.24 Connection failures after inclined tension tests at 500°C (left) and 700°C (right) – 3/4 inch A325 bolts.....	175
Figure 5.25 Load-rotation response of connections with 3/4 inch A325 bolts under inclined tension	176
Figure 5.26 Load-displacement response of connections with 3/4 inch A325 bolts under inclined tension	176
Figure 5.27 Load-Rotation rotation response of connection with 3/4 inch A325 bolts under inclined tension - 500°C	177

Figure 5.28 Connection failures after inclined tension tests at 400°C (left) and 500°C (right) – 1 inch A325 bolts.....	178
Figure 5.29 Connection failure after inclined tension test at 700°C – 1 inch A325 bolts	179
Figure 5.30 Load-rotation response of connections with 1 inch A325 bolts under inclined tension	180
Figure 5.31 Load-displacement response of connections with 1 inch A325 bolts under inclined tension	180
Figure 5.32 Finite element model of connections under axial tension	182
Figure 5.33 Finite element model of connections under inclined tension	182
Figure 5.34 Comparison of test result and finite element analysis - 20°C – W12×40 ..	183
Figure 5.35 Comparison of test result and finite element analysis - 600°C – W12×40	183
Figure 5.36 Comparison of tension test and finite element analysis - 400°C – W12×26	184
Figure 5.37 Comparison of tension test and finite element analysis - 500°C – W12×26	184
Figure 5.38 Comparison of tension test and finite element analysis - 700°C – W12×26	185
Figure 5.39 Comparison of inclined tension test and finite element analysis - 20°C...	185
Figure 5.40 Comparison of inclined tension test and finite element analysis - 40°C...	186
Figure 5.41 Comparison of inclined tension test and finite element analysis - 500°C.	186
Figure 5.42 Comparison of inclined tension test and finite element analysis - 700°C.	187
Figure 5.43 Calculated connection strength under axial tension – 3/4 inch A325 bolts	191
Figure 5.44 Calculated connection strength under inclined tension – 3/4 inch A325 bolts	192
Figure 6.1 Layout of steel beam and shear tab connections for FEA (not to scale)	196
Figure 6.2 Stress-strain relationship of A992 beam material used in FE model	197

Figure 6.3 Stress-strain relationship of A36 plate material used in FE model	197
Figure 6.4 Deformed shape and stress contour of the shear tab connection.....	198
Figure 6.5 Beam Axial force – temperature response comparison between model with beam element and model with solid elements	199
Figure 6.6 Beam deflection – temperature response comparison between model with beam element and model with solid elements	199
Figure 6.7 Connection axial force - temperature response in fire.....	201
Figure 6.8 Connection rotation - temperature response in fire	201
Figure 6.9 Bolt shear forces during heating.....	203
Figure 6.10 Bolt shear forces during cooling.....	204
Figure 6.11 Connection axial force - temperature response for different load ratios ...	206
Figure 6.12 Connection rotation - temperature response for different load ratios.....	206
Figure 6.13 Connection axial force - temperature response for different beam lengths	208
Figure 6.14 Connection rotation - temperature response for different beam lengths ...	208
Figure 6.15 Beam connects to different boundaries	210
Figure 6.16 Connection axial forces - temperature response for different stiffness levels of adjacent structure	210
Figure 6.17 Connection rotation - temperature response for different stiffness levels of adjacent structure	211
Figure 6.18 Connection axial force - temperature response for different initial cooling temperatures	212
Figure 6.19 Gas temperature of Cardington fire test (Wald et al 2006)	213
Figure 6.20 Connection axial force for uniform and non-uniform temperature distribution	214
Figure 6.21 Connection rotation for uniform and non-uniform temperature distribution	214
Figure 6.22 FE mesh of standard holes and short-slotted holes	216
Figure 6.23 Connection force for standard holes and short-slotted holes.....	217

Figure 6.24 Top bolt shear for standard holes and short-slotted holes	217
Figure 6.25 Load-displacement behavior of Yu's twin-bolt connection at ambient temperature by FEA (bolt with and without pretension)	219
Figure 6.26 Top bolt shear for different shear tab locations.....	220
Figure 6.27 Top bolt shear for thick and thin plates.....	221
Figure 6.28 Initial gap length of shear tab connection assembly.....	222
Figure 6.29 Connection rotation - temperature response for different plate width	224
Figure 6.30 Top bolt shear-temperature response for different plate width	224

CHAPTER 1

Introduction and Background

1.1 INTRODUCTION

There is an increasing interest in the US in transforming building fire safety design from a prescriptive to a performance-based environment. This interest is driven by the need to provide more cost effective fire protection, to provide greater flexibility in fire safety design for complex and unusual buildings, and to provide tools to mitigate fire related hazards that follow other extreme events, including earthquakes and terrorist attacks (Cox 2001, Kodur et al 2007, FEMA 2002, NIST 2005). Studies on the collapse of the World Trade Center Towers (NIST 2005) and World Trade Center Building 7 (NIST 2008) on September 11, 2001 concluded that the technical basis for current U.S. practices in structural fire safety design is inadequate, and poses a safety concern. Other studies also point to the need to reduce the high cost of building fire protection in the US. With respect to the impact of fire on the cost of building construction, it has been estimated that 12-percent of the total cost of private, nonresidential structures in the US is for fire protection (IASIE 2005). The cost of providing fire protection in buildings, including the cost associated with structural fire protection, is large and is increasing. Hall (2008) notes that new building construction costs for fire protection have increased by 55% since 1980, after adjusting for inflation. A number of recent studies have identified the need for research on improved methods for fire safety design of building structures (NRC 2003, CERF 2004, Kodur et al 2007, NIST 2004, NIST 2005, NIST 2008).

1.1.1 Steel Buildings in Fire

Steel buildings are a class of structure that pose significant challenges with respect to fire safety. Steel buildings are generally viewed as being particularly

vulnerable to fire, due to the high thermal conductivity and low specific heat of steel (steel heats very quickly in a fire) combined with the loss of stiffness and strength of steel at elevated temperatures (Buchanan 2002). Consequently, structural steel members are normally protected by spray applied fire resistive coatings, or by other insulating barriers, such as gypsum-board. However, the cost of fire protecting steel is significant, and has been estimated to account for 30-percent of the total cost of a steel frame (Robinson and Latham 1986). Despite the large cost associated with fire protecting steel, little or no engineering calculations are typically conducted in designing the fire protection. Instead, highly simplified prescriptive code-based rules are followed to establish fire protection requirements for steel structures. The basis for these rules in the US is the standard fire resistance test used for building frame elements specified in ASTM E119 (ASTM 2000). This approach has changed little in the last 100 years, and has been widely recognized as an inadequate basis for structural fire safety design (Usmani et al 2001, Wang 2002).

A significant amount of experimental and analytical research on the performance of steel structures in fire has been conducted over the last fifteen years. Most of these research activities have been carried out in Europe. Useful summaries of recent research are provided by Plank (2000) and Wang (2002, 2005). One of the most significant experimental programs investigating fire behavior of steel buildings was the Cardington program, in which a full-scale eight story steel framed structure was studied under fire exposure at the Cardington, UK research facility of the Building Research Establishment (Cardington test report 1998). The steel building tested at Cardington was constructed with composite floors, and a number of steel beams in the composite floors were not fire protected and would not have satisfied US prescriptive fire protection requirements. Despite the absence of fire protection, the floor system and the entire structure was capable of sustaining severe fire exposure without collapse. The Cardington tests demonstrated the potential for significant cost saving in fire protection while still maintaining the safety of the steel structure under fire exposure.

One of the important outcomes of the Cardington research was the conclusion that the key behavioral factor that affects the ability of a floor system to survive a fire is the development of tensile catenary and membrane action resulting from the large vertical displacements which normally occur in a fire (Figure 1.1). This highly beneficial system behavior of a full composite floor system is not recognized in current US standards and typical practice, where fire protection requirements for structural steel beams are based on a standard fire test of isolated floor assemblies. Cardington and other related research have clearly shown that the fire behavior of a structural system is completely different from that seen in the standard fire test of a single structural element or assembly (Usmani et al 2001). However, catenary action in beams, while providing important reserve capacity, also subjects the beam end framing connections to very large axial forces and very large rotation demands; and these force and deformation demands are not well understood.



Figure 1.1 Floor system response in Cardington fire test (Cardington test report 2003)

1.1.2 Steel Beam End Framing Connection Behavior in Fire

Beam end framing connections are critical elements that transfer the floor load to supporting members (column or girder). In fire, large axial forces can often be generated in steel beams. Due to displacement restraint from adjacent portions of the structure, these forces are initially compressive, while later on with temperature increasing, these forces become tensile as catenary action starts to develop (Li and Guo 2008). Both the compression and tension developed during a fire are not normally considered in the beam end framing connection design process and thus can possibly lead to connection failure and potential beam collapse in a fire event. Failure of a beam-to-column connection was identified as a major contributing factor to the collapse of World Trade Center Building 7. Connection failure in this building resulted in a loss of bracing for a column, which in turn led to buckling of the column and collapse of the building (NIST 2008).

Beam end framing connection failure under tension due to the development of beam catenary action can be examined by considering the case of World Trade Center Building No. 5 (FEMA 2002). Figure 1.2 is a photo of a collapsed area within WTC 5 following fires on September 11, 2001. The connection failures at the ends of the column tree stubs are visible. A portion of a failed beam end connection recovered from the building is shown in Figure 1.3. These photos clearly illustrate the dominating influence of tensile forces on the failure; forces that are not normally accounted for in beam connection design.



Figure 1.2 Connection failure at tree column of WTC5 (FEMA 2002)



Figure 1.3 Connection tear out failure in WTC5 (FEMA 2002)

The large axial compressive forces developed early in the fire can lead to bolt shear failure and buckling of shear plates. The axial tension developed later in the fire can lead to bolt shear failure, to fracture of the welds connecting the shear plate to the column or girder, to bearing tear-out failure in the beam web or shear plate, and to block shear failure in the beam web or shear plate. During the cool down phase of the fire, the thermal contraction of the beams can lead to even larger axial tensile forces. An example of this was seen in the Cardington tests, where bolt shear failure occurred at a beam end connection during the decay phase of a test fire (Wang 2002). Figure 1.4 shows a photo of this connection failure. There appears to be very few previous studies which have examined beam connection forces during fire cool-down.



Figure 1.4 Simple shear beam end framing connection damage in heating (left) and cooling (right) (Cardington test report 1998)



Figure 1.5 Simple shear beam end connection damage in fire (Cardington test report 2003)

Furthermore, in the case of a beam subjected to fire, the rotational ductility demands at the connection as the beam develops catenary action will likely be significant and may lead to connection damage as well (Figure 1.5). Little analytical or experimental data are available to quantify these ductility demands.

To allow the beam to mobilize the reserve strength associated with catenary action, it is important to understand the force and deformation demands generated at the beam end framing connections during the heating and cooling phases of a fire, and to account for these demands in design.

1.2 RESEARCH NEED AND OBJECTIVE

1.2.1 Research Need

In US building construction practice for structural steel buildings, one of the most common types of simple beam end framing connections used is the shear tab connection, also referred to as a single plate or fin plate connection. Shown in Figure 1.6, the connection consists of a shear tab that is bolted to the beam web and then welded to the supporting element, which can be a column or a girder. Normally idealized as pinned connections and designed only for shear forces transferred by the supported beam, shear tab connections can be vulnerable to failure under large axial loads and rotation demands resulting from a fire. Therefore, a good understanding of the performance of this connection in fire is essential.

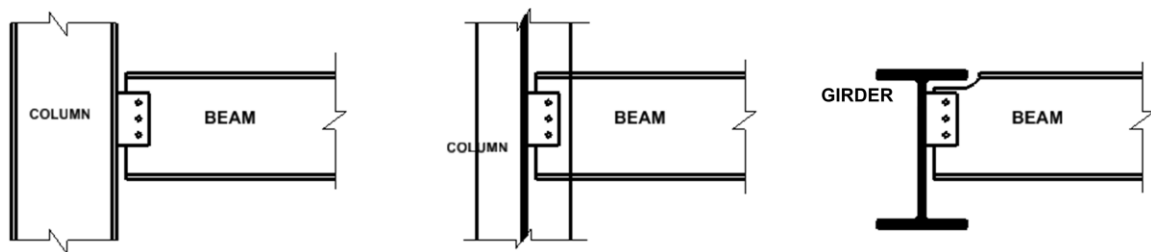


Figure 1.6 Typical shear tab beam end connections

On the other hand, although, this type of connection failure has been observed in some major fire events and the Cardington fire test, there is no clear evidence showing that shear tab beam end framing connections designed by current US specifications is not capable of performing well under severe fire exposure. An example of this can be illustrated by a fire event in the Echelon building in Austin Texas in February of 2010 (Pilot deliberately crashed into Texas building, CNN, February 18 2010). A large fire occurred in this steel framed office building following impact of a small aircraft (Figure 1.7). Severe damage caused by the large fire was observed in this structure, including

large deformations of the beams, open web steel joists and the concrete floor system. However, most of the steel shear tab beam end framing connections successfully survived this large fire despite the apparent development of significant catenary and membrane action in the floor system. Minor damage was observed at only one connection (Figure 1.8)



Figure 1.7 Echelon Building fire in Austin Texas (www.myfoxboston.com, February 18 2010)



Figure 1.8 Connection damage in Echelon Building due to fire

Nevertheless, the lack of understanding and the lack of data on the performance of shear tab beam end framing connections represent a critical gap in the knowledge base of steel building behavior under fire conditions, and represent an important research need to further enable performance-based structural-fire safety design.

1.2.2 Objective of Research

The objective of the research described in this dissertation is to develop an improved understanding of the performance of shear tab beam end framing connections in fire through experimental and finite element studies. More specifically, the objectives of the research are to better understand force and deformation demands on these connections, as well as to characterize the strength and deformation capacity of the connections at elevated temperatures.

1.3 OUTLINE OF DISSERTATION

In order to address the objectives listed above, a literature review was conducted, followed by a combined experimental and numerical study.

Chapter 2 of this dissertation discusses previous research that is pertinent to this dissertation. A literature review of steel simple shear connection behavior in fire is summarized. Also included is a review of recent research on steel properties at elevated temperatures.

Chapter 3 discusses tests conducted on samples of ASTM A992 structural steel at elevated temperatures. These tests were conducted because A992 steel is commonly used for rolled steel shapes in the U.S. and no data on the elevated temperature properties of this steel was found in the literature. This chapter discusses the test setup, test procedures and test results. Test results are compared to available models for elevated temperature stress-strain response of structural steel.

Chapter 4 describes the development of a finite element model of steel beams with shear tab connections. Three-dimensional nonlinear thermal and structural finite element simulations were performed to compare model predictions with existing test data in the literature. Included is a description of the development of detailed three-dimensional bolted connection models that were used in subsequent phases of this research.

Chapter 5 describes the experimental program on shear tab connections tested at elevated temperatures. The high temperature test setup and data acquisition system are introduced. Then test results for different temperatures and different connection variables are discussed. In addition, results from finite element analysis and simplified capacity calculations are compared to the test data.

Chapter 6 presents the results of a parametric finite element study of connection performance in both the heating and cooling phases of a fire. Connection force and deformation demands as well as individual bolt forces were systematically studied.

Effects of a fairly large number of parameters and connection details on connection performance were investigated.

Chapter 7 summarizes findings of the research program. Key observations and discussions from the literature review, experimental program, and numerical program are compiled. Finally, suggestions for further research are provided.

CHAPTER 2

Literature Review and Recent Work

2.1 OVERVIEW

Understanding the performance of steel simple shear connections in fire is an involved topic and requires a good understanding of several areas, including fundamental knowledge of general steel connection behavior and design, properties of structural steel, bolts and welds at elevated temperatures, and steel structure performance under thermal loading. Previous research conducted by other investigators on these topics is reviewed in this chapter.

The literature review for this research is divided into seven sections. The first section introduces investigations on the mechanical properties of structural steel at elevated temperatures. The second, third, and fourth sections review previous studies on the behavior of structural bolts, simple bolt connections and welds at elevated temperatures, respectively. The fifth section summarizes past investigations on the behavior of steel beams subject to building fire. This is followed by a review of research on shear tab connections at ambient temperature. In the last section, recent work on the behavior of shear tab beam end framing connections in fire conditions is reviewed.

2.2 ELEVATED-TEMPERATURE PROPERTIES OF STRUCTURAL STEEL

The ability to characterize the elevated-temperature properties of structural steel is a key element for understanding the performance of steel simple shear beam end connections under fire conditions. The properties of structural steel at high temperatures can be drastically different from those at room temperature, and accurate knowledge of these properties is a critical factor in predicting the response of steel structures to fire. Similar to ambient temperature, the mechanical properties of structural steel at high temperatures are also obtained from laboratory testing. A review of past investigations on

the steel mechanical properties at elevated temperatures is summarized and presented in this section.

2.2.1 Testing Methods

In general, steel material mechanical property tests include tension tests, compression tests, Charpy-V Notch tests, and others. Among these, the most widely used are tension coupon tests, which provide basic stress-strain response data used to analyze and design steel structures (Buchanan 2002).

Two types of testing methods are commonly used in tension coupon tests of steel at elevated temperatures: the steady-state test and the transient test.

In a steady-state test, the steel coupon is heated up to a specified temperature without loading or restraint to expansion. Load is then applied while the temperature is held constant. The result of a steady state test is a stress-strain curve at a specified temperature. A steady-state test can be carried out either as displacement or as load controlled. The resulting stress-strain curve can vary somewhat with the displacement or loading rate used in the test.

In a transient test, the steel coupon is loaded to a target engineering stress level at ambient temperature. While holding the stress constant, the temperature is increased until fracture of the coupon occurs. Temperature and strain readings are recorded during the test. After the test, thermal elongation is subtracted from the total strain. The results of a series of transient tests conducted at different stress levels can be converted into temperature dependent stress-strain curves.

The results from these two test methods are usually quite similar, as discussed below. In general, the ultimate strength obtained from the steady-state method is slightly higher than the results obtained from a transient test. A primary reason for differences in the resulting temperature dependent stress-strain curves from these two test methods is the influence of strain rate and creep at high temperatures.

In an actual structure subjected to a fire, neither the temperatures nor the forces on the structure members will be constant. Therefore, some investigations have been done to evaluate which test method simulates the stress and temperature conditions of the material in fire more accurately. Kirby and Preston (1988) compared the two methods by conducting small-scale elevated-temperature tensile tests on grades 43A and 50B structural steel. In their steady-state heating condition tests, a constant strain rate was applied to the coupons over the temperature range of 20-800°C. In the transient heating condition tests, heating rates of 2.5, 5, 10 and 20°C/min were used. The resulting stress-strain curves for the two different methods were compared up to 2-percent strain. Comparing the results from the two conditions, Kirby and Preston concluded that stresses measured in the steady-state tests were somewhat larger than those measured in the transient tests when only small strains are considered. For larger strains, however, the two testing methods produced similar results.

Compared to tension testing, much less information is available in the literature on compression testing of steel at elevated temperatures. This may be due to the substantial complexities and difficulties of compression tests. Therefore, the structural steel properties under compressive loading are not discussed in this research. The assumption is made that structural steel behaves similarly under tensile and compressive loading at elevated temperatures.

The Charpy impact test is another widely used material property test method for metal materials. It is a type of dynamic fracture test that evaluates the ability of metals to absorb energy in the presence of notches before fracturing. As such, Charpy tests are particularly relevant to impact loading, and have limited applications to steel beam end connections under static loading, and thus are not further discussed in this research.

2.2.2 Past Investigations on Structural Steel Properties at Elevated Temperatures

The mechanical properties of structural steel at elevated temperatures of interest include yield strength, tensile strength, modulus of elasticity, proportional limit, ductility,

and others. Similar to ambient temperature, these properties at high temperatures can be obtained from the stress-strain relationships of steel at high temperatures. Considerable data on the elevated-temperature properties of structural steel have been published. A brief review of some past work is presented in this section.

Harmathy and Stanzak (1970) presented elevated-temperature properties of two structural steels (ASTM A36 and CSA G40.12) and a prestressing steel (ASTM A421) up to 1200°F from steady-state tensile tests. Stress-strain curves up to 12-percent strain for the two types of steel were obtained from these tests (Figure 2.1). Harmathy and Stanzak evaluated ultimate and yield strength of these steels from the stress-strain relationships, and also examined the elongation and reduction in area of the tested steels.

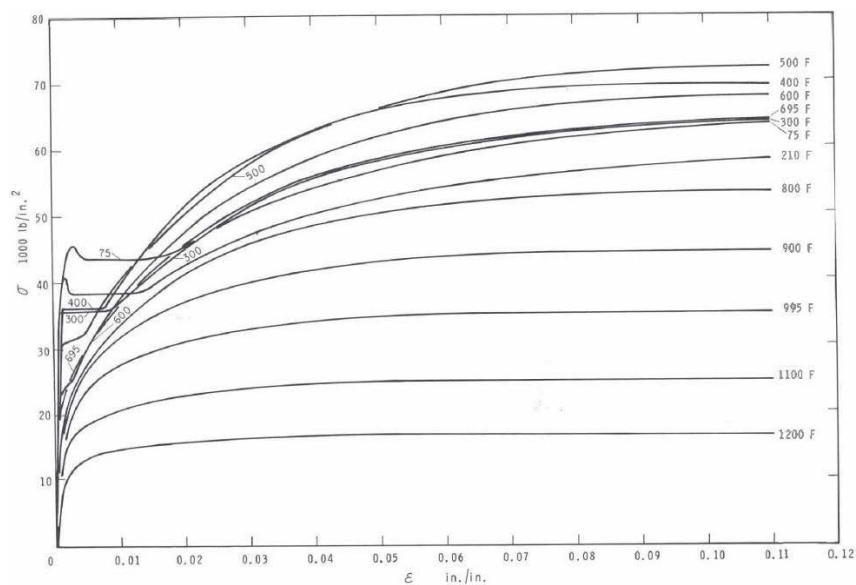


Figure 2.1 Stress-strain curves for an ASTM A36 steel (Harmathy and Stanzak 1970)

Cooke (1988) presented data on the mechanical properties at elevated temperatures of hot-rolled structural steel used in buildings, and discussed the physical meanings of these properties. These properties include Poisson's ratio, thermal expansion and phase transformation, stress-strain relationships and elastic modulus. He concluded

that a Poisson's ratio of 0.3 and coefficient of linear thermal expansion of $14 \times 10^{-6}/^{\circ}\text{C}$ are generally acceptable for fire analyses. He also discussed the importance of developing a material model for stress-strain curves for a range of temperatures.

Kirby and Preston (1988) tested Grade 43A and Grade 50B steel up to 900°C using both the steady-state and transient methods to provide elevated-temperature data for structural fire engineering applications. Figure 2.2 shows an example of strain-temperature curves for Grade 43A steel obtained from their transient tests. Stress-strain relationships can be further derived from the results.

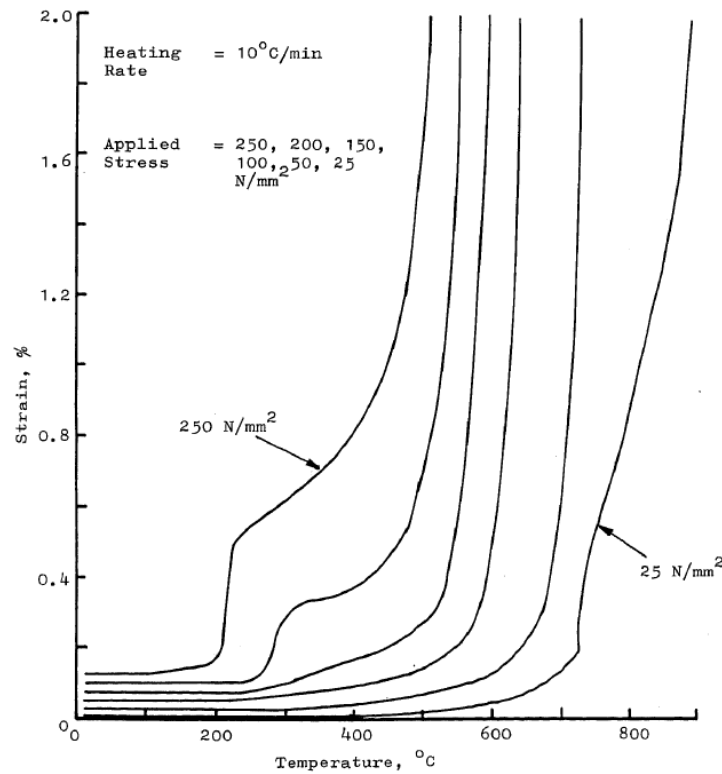


Figure 2.2 Strain-temperature curves of Grade 43A steel (Kirby and Preston 1988)

Li et al (2003) conducted steady-state tests up to 700°C to examine high-temperature properties of two kinds of widely used constructional steel in China: 16Mn

steel and 20MnTiB steel. The properties they obtained from the tests include yield strength, tensile strength, modulus of elasticity, elongation, and thermal expansion coefficient. Based on the tested data, they also developed formulas for prediction of the properties of tested steel at elevated temperatures.

Chen and Young (2005) presented stress-strain curves of stainless steel at elevated temperatures up to 1000°C from results of both steady-state and transient tensile tests. Their testing equipment is shown in Figure 2.3. By resetting the extensometer, they successfully captured the stress-strain curves beyond the 10-percent strain limit of the extensometer (Figure 2.4). They obtained stainless steel properties including elastic modulus, yield strength at different strain levels, ultimate strength, ultimate strain and thermal elongation, and they also developed a unified equation for these properties at elevated temperatures.

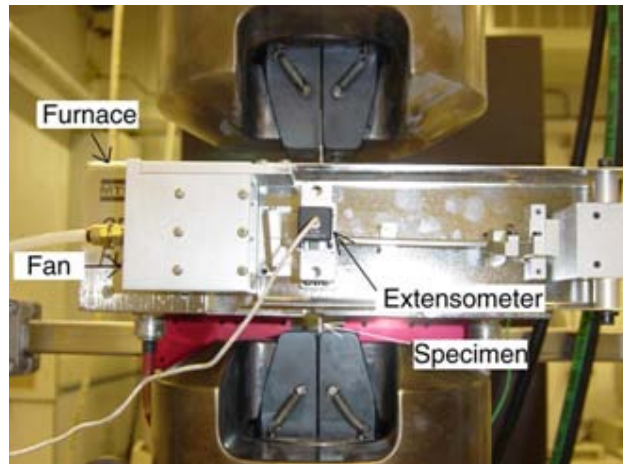


Figure 2.3 Chen and Young's testing device (Chen and Young 2005)

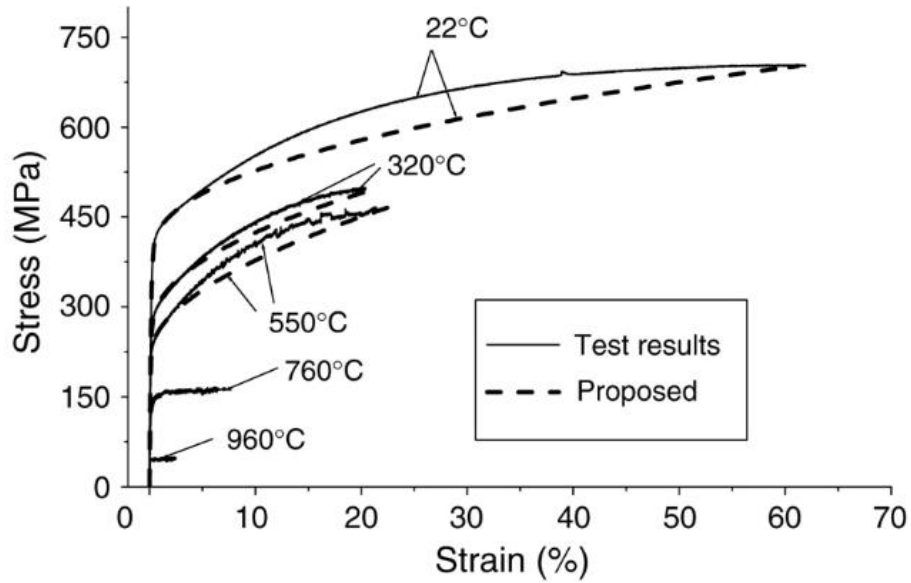


Figure 2.4 Stress-strain curves of stainless steel type EN 1.4301 at elevated temperatures (Chen and Young 2005)

NIST (2005) analyzed mechanical properties of structural steel recovered from the WTC site at ambient temperature and high temperatures. NIST characterized the high-temperature tensile behavior of steel specimens collected from 15 different steel members: three perimeter columns, four core columns, three truss components, and five truss seats. Figure 2.5 is an example of typical high-temperature tensile stress-strain curves from a wide-flange core column in the fire and impact zone of WTC 1. The tested properties were then used for the modeling of structural response of the towers to WTC fire.

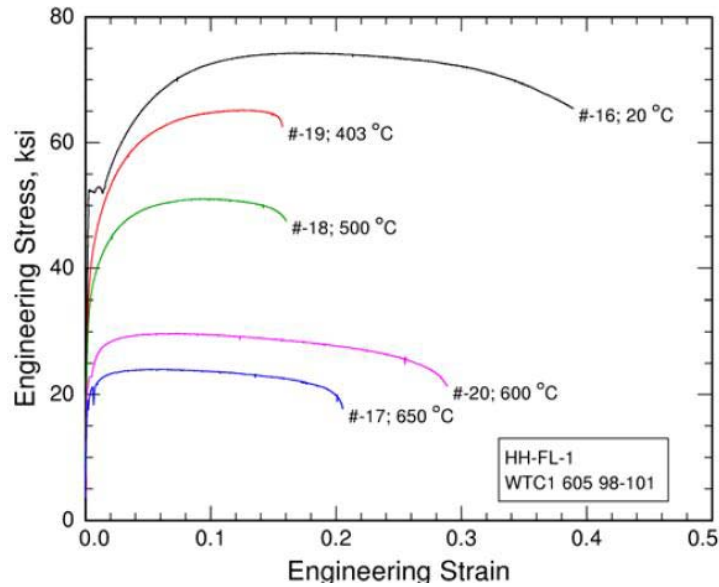


Figure 2.5 Typical high temperature stress-strain curves for specimen from near the fire and impact zone of WTC 1 (NIST 2005)

Outinen (2006) carried out tensile tests to study the behavior of mechanical properties of different steel grades at and after elevated temperatures using both steady-state and transient methods. The testing equipment Outinen used is shown in Figure 2.6. Outinen’s test results were presented with a comparison to the Eurocode 3 (2006). Most of the results of the steel he tested agreed with Eurocode 3 quite well, while the yield strength reduction factors of the cold-formed material were clearly higher than those given in Eurocode 3. He also mentioned that the mechanical properties after cooling largely returned to the nominal values of the steel that had never been heated.

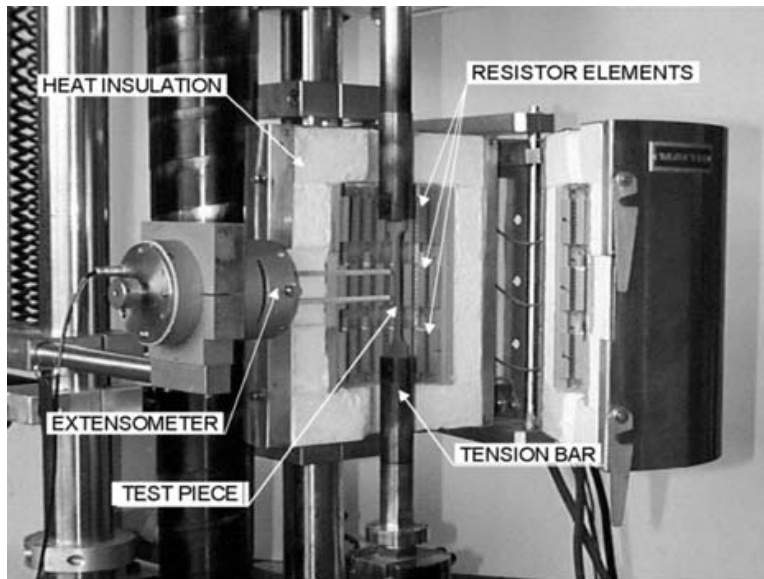


Figure 2.6 Outinen's high temperature tensile testing device (Qutinen 2006)

Yu (2006) tested Grade 50 structural steel at elevated temperatures up to 800°C using the steady-state method with two loading rates. He obtained stress-strain curves of the steel up to 10-percent strain (Figure 2.7). He also examined static yielding behavior of the steel at different temperatures.

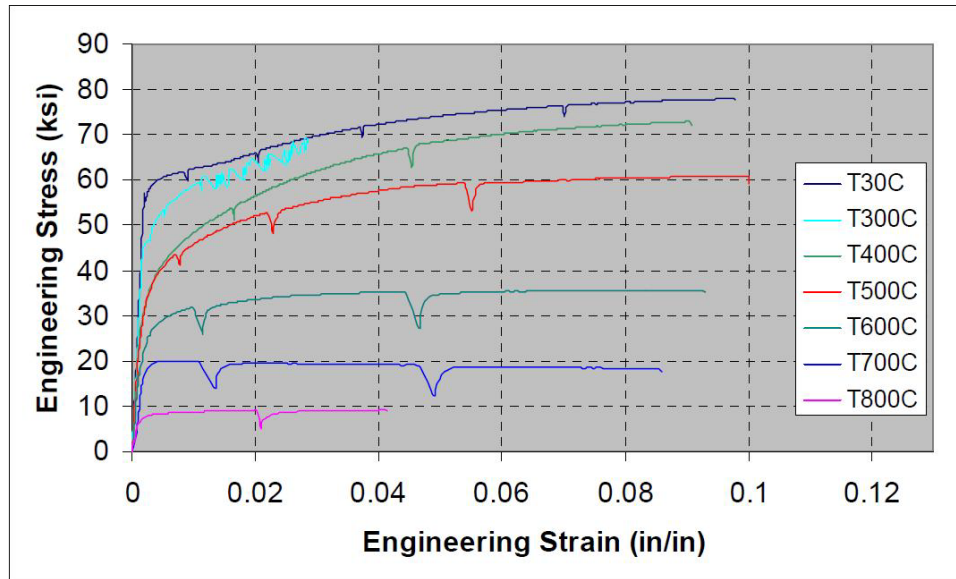


Figure 2.7 Stress-strain curves of Grade 50 steel at elevated temperatures under loading rate of 0.1 in/min (Yu 2006)

2.2.3 General Observations

From previous research conducted on structural steel properties at elevated temperatures, it can be observed that in general the key mechanical properties of steel including yield strength, ultimate tensile strength and modulus of elasticity all decrease with temperature increase. In addition, the reduction rates of strength and modulus vary significantly in different temperature ranges. At temperatures lower than 400°C, the reduction is relatively small while at higher temperatures, the material degradation is remarkably more significant. Further, it can also be observed that at different temperatures the shapes of stress-strain curves are also quite different. For most structural steels, with temperature increase the yield plateau gradually disappears, and the strain-hardening portion of the stress-strain curve shortens significantly, which makes the curve more similar to an elastic-perfectly plastic curve.

2.2.4 Variation of Yield Strength, Tensile Strength and Modulus with Temperature

2.2.4.1 Definition of yield strength

For structural metals, it is usually difficult to precisely define yielding due to the wide variety of stress–strain curves exhibited by real materials. Therefore, there are several possible ways to define yielding (Dieter 1986). These are described below.

Proportionality limit: the highest stress for which the stress-strain curve is linear. Below the proportional limit, the slope of the linear stress-strain curve is the elastic modulus of the material.

Elastic limit: The lowest stress at which permanent deformation can be measured. Beyond the elastic limit, permanent deformation will occur. In a material test, this requires a load-unload procedure.

Upper yield point and lower yield point: At ambient temperature, some structural steels exhibit an upper yield point before dropping rapidly to a lower yield point.

Offset yield point: When a yield point is not easily specified based on the shape of the stress-strain curve an offset yield point can be defined. It is the stress that corresponds to the point of intersection of a stress-strain curve and a line parallel to the linear portion of the curve. The value for the offset is commonly set at 0.2 or 0.5-percent of the strain for structural metals. As discussed above, the yield plateau will disappear when steel is exposed to high temperatures, and thus it is not feasible to find an elastic-plastic transition point on the high-temperature stress-strain curves. Consequently, many previous researchers have used the offset yield point method for the definition of yield strength of structural steel exposed to high temperatures.

Yield strength can be also defined as the stress at a specific strain. This method also has been widely used for defining yield strength of metal at elevated temperatures. For example, Eurocode 3 (2006) takes the stress at 2-percent strain as the yield strength of carbon steel at elevated temperatures.

2.2.4.2 Strength and Modulus Reduction with Temperature

Steel properties at elevated temperatures obtained from stress-strain curves can be presented in the plots of strength versus temperature or modulus of elasticity versus temperature. Figure 2.8 shows the variation of ultimate and yield strength of ASTM A36 steel with temperature tested by Harmathy and Stanzak (1970), in which the 0.2-percent offset yield strength was used.

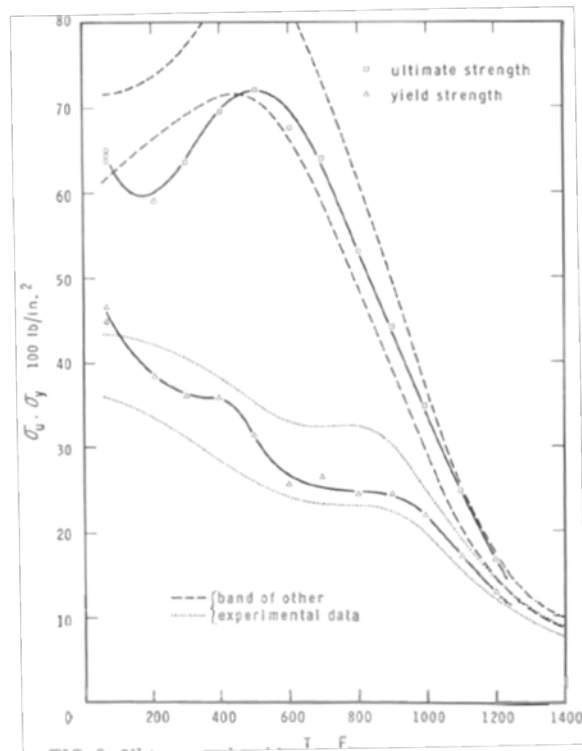


Figure 2.8 Ultimate and yield strengths of an ASTM A36 steel (Harmathy and Stanzak 1970)

Kirby and Preston (1988) conducted elevated-temperature tests on steel BS 4360 and Grade 50B. Test results were presented as strength at different strains (0.2-percent, 1-percent, 2-percent, 5-percent) versus temperature, and one of their results is shown in

Figure 2.9. It is clear from the figure that different strength definitions give different strength variations with temperature.

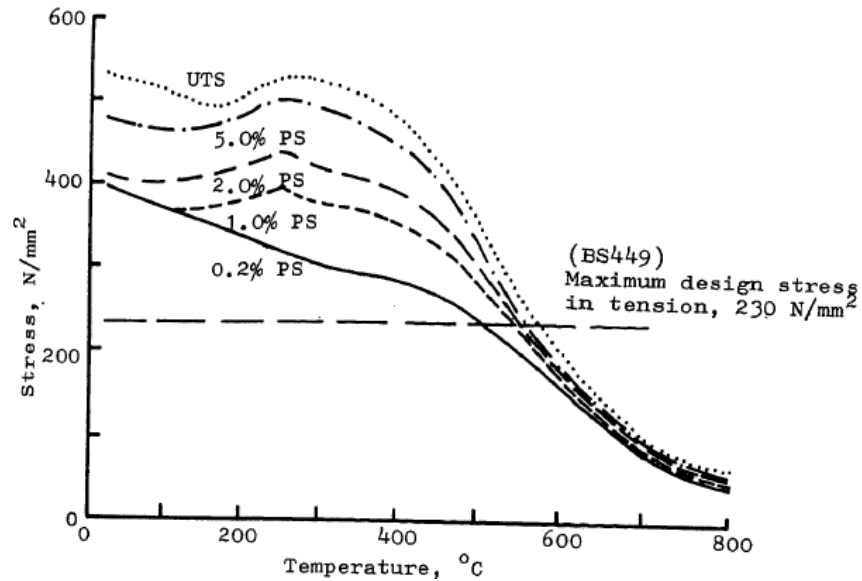


Figure 2.9 Elevated-temperature strength properties of a typical BS 4360: Grade 50B structural steel derived from steady-state tests (Kirby and Preston 1988)

Strength and modulus of structural steel at elevated temperatures can be normalized by the corresponding properties at ambient temperature, and expressed as a reduction factor. Yu (2006) summarized the reduction factors of yield strength (Figure 2.10), tensile strength (Figure 2.11) and modulus of elasticity (Figure 2.12) of different types of steel based on data from standards and previous investigations.

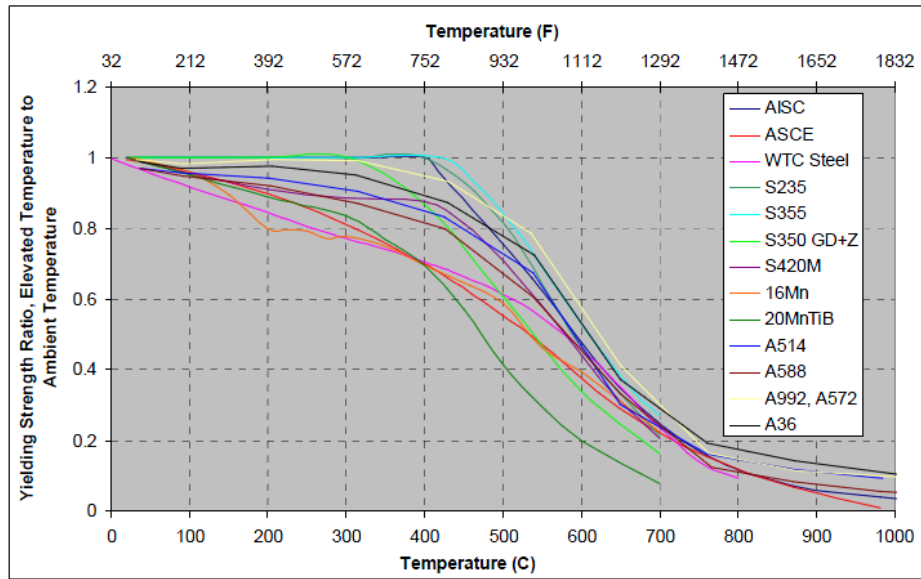


Figure 2.10 Yield strength ratio at elevated temperatures of different structural steels (Yu 2006)

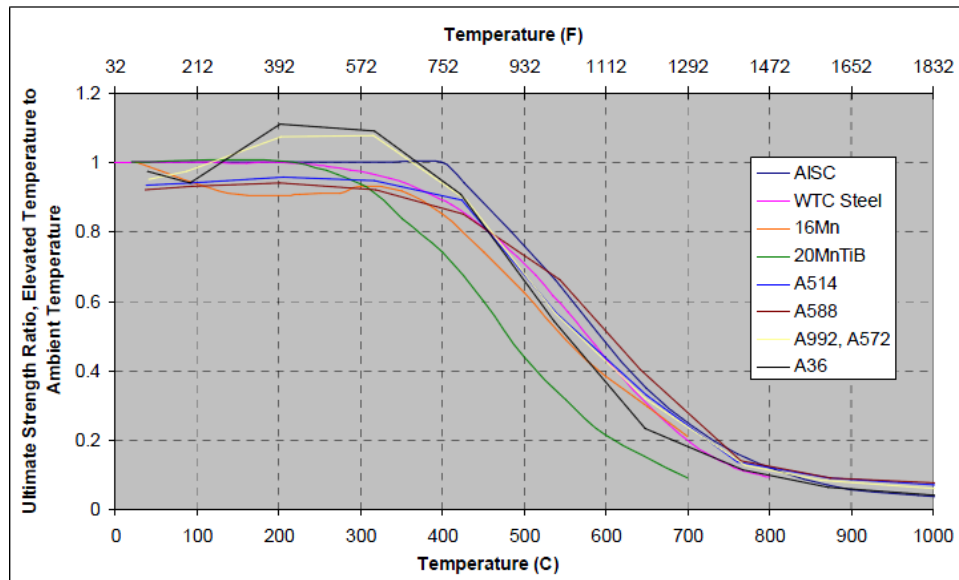


Figure 2.11 Ultimate strength ratios at elevated temperatures of different structural steels (Yu 2006)

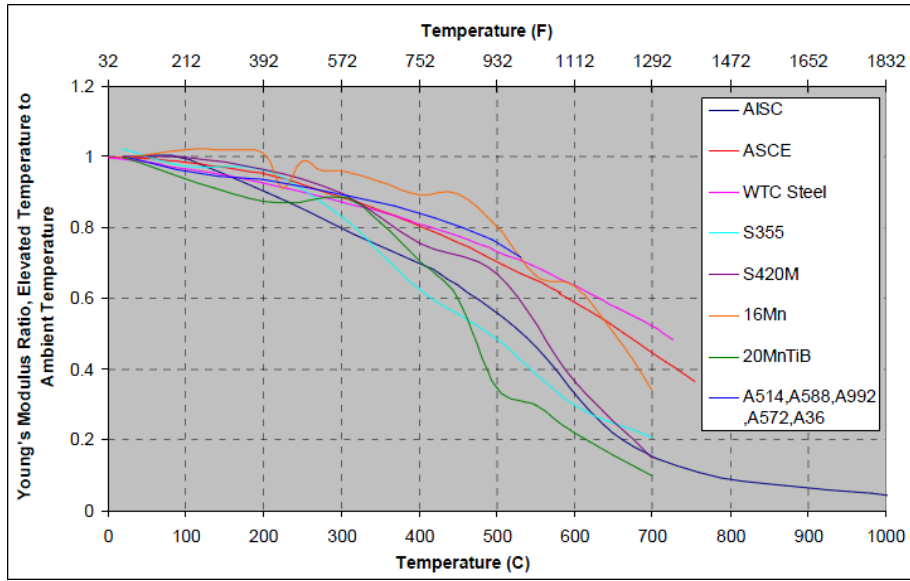


Figure 2.12 Young's modulus ratio at elevated temperatures of different structural steels (Yu 2006)

In addition, equations were also developed to predict the variation of these mechanical properties of structural steel with temperature. For example, Li et al (2003) derived formulas from their test results that can be used to predict the behavior of 16Mn steel and 20MnTiB steel using the least-squares fitting method. Equations 2.1 to 2.3 are examples of their formulas for yield strength, ultimate strength and modulus of elasticity of 16Mn steel.

$$\frac{f_{yT}}{f_y} = -3 \times 10^{-9} \times T^3 + 2 \times 10^{-6} \times T^2 - 0.0013 \times T + 1.0413 \quad (2.1)$$

$$\frac{f_{uT}}{f_u} = -1 \times 10^{-9} \times T^3 - 1 \times 10^{-6} \times T^2 + 0.0002 \times T + 0.9499 \quad (2.2)$$

$$\frac{E_T}{E} = -3 \times 10^{-9} \times T^3 + 1 \times 10^{-6} \times T^2 - 0.0003 \times T + 1.022 \quad (2.3)$$

2.2.4.3 Code Recommendations

Tilt and Both (1991) reviewed various options for stress-strain relationships of steel at elevated temperatures, which are suggested in various European countries as a basis for the calculation of behavior of fire exposed structural steel. These data sources include: European Convention for Constructional Steelwork (ECCS); RILEM; British Steel Corporation (BSC); Ruhr-University-BOCHUM/KRUPP; Braunschweig University of Technology; ARBED-Recherches; CRIF/University of Liege; Institute de Recherches de la Siderugie Francaise. After a systematic comparison, Tilt and Both proposed to use the data of BSC (Kirby and Preston 1988) as a set of “European” stress-strain relationships, and defined the stress level at 2-percent strain as the yield strength of structural steel at elevated temperatures. They also proposed to describe the stress-strain curves by means of a relatively simple mathematical model. They considered a more exact model for stress-strain curves that accounted for strain-hardening effects for the temperatures below 400°C. All of these proposals were finally adopted in Eurocode 3. Reduction factors of yield strength and modulus of elasticity at elevated temperatures up to 1000°C given in Eurocode 3 (2006) are listed in Table 2.1. Further, according to Eurocode 3, the tensile strength of steel at elevated temperature is taken equal to the yield strength.

Table 2.1 Yield strength and modulus of elasticity reduction factors (Eurocode 3 2006)

Temperature (°C)	Yield Strength	Young's modulus
20	1.0	1.0
100	1.0	1.0
200	1.0	0.9
300	1.0	0.8
400	1.0	0.7
500	0.78	0.6
600	0.47	0.31
700	0.23	0.13
800	0.11	0.09
900	0.06	0.0675
1000	0.04	0.045

It can be observed from the reduction factors of Eurocode 3 that the yield strength of structural steel starts to decrease at temperatures above 400°C, while the modulus of elasticity starts to drop at temperatures beyond 200°C. Appendix 4 of the AISC Specification on *Structural Design for Fire Conditions* (2005) adopted the reduction factors for the properties of structural steel at elevated temperatures from Eurocode 3.

2.2.5 Analytical Expressions for Stress-strain Relationships at Elevated Temperatures

Analytical expressions have been proposed to model the stress-strain behavior of structural steel at both ambient and elevated temperatures. These models can be grouped into three major categories: multi-linear (Lie 1992), combination of linear and smooth curves (Swift 1946, Anderberg 1988, Twilt and Both 1991, Gayle et al 2005), and power-law forms (Osgood 1932, Ramberg and Osgood 1943, Hill 1944, Hollomon 1945, Voce 1948, Morrison 1966, Adams and Beese 1974).

Eurocode 3 (2006) has simple equations to predict the stress-strain curves for carbon steel at elevated temperatures using a combination of linear and nonlinear curves. The fundamental basis for these equations is that at elevated temperatures, stress-strain curves for carbon steel can be divided into four parts. The first portion is linear where the strain ε is less than the proportional limit strain $\varepsilon_{p,T}$:

$$\text{When } \varepsilon \leq \varepsilon_{p,T} \quad \sigma = \varepsilon E_{a,T} \quad (2.4)$$

where,

σ = stress

ε = strain

$E_{a,T}$ = tangent modulus at temperature T

The second portion is a curve at strains between the proportional limit and 2-percent strain, and can be expressed as:

$$\text{When } \varepsilon_{p,T} \leq \varepsilon \leq \varepsilon_{y,T} = 0.02 \quad \sigma = f_{p,T} - c + \frac{b}{a} [a^2 - (\varepsilon_{y,T} - \varepsilon)^2]^{0.5} \quad (2.5)$$

$$a = [(\varepsilon_{y,T} - \varepsilon_{p,T}) \left(\varepsilon_{y,T} - \varepsilon_{p,T} + \frac{c}{E_{a,T}} \right)]^{0.5} \quad (2.6)$$

$$b = [c(\varepsilon_{y,T} - \varepsilon_{p,T})E_{a,T} + c^2]^{0.5} \quad (2.7)$$

$$c = \frac{(f_{y,T} - f_{p,T})^2}{(\varepsilon_{y,T} - \varepsilon_{p,T})E_{a,T} - 2(f_{y,T} - f_{p,T})} \quad (2.8)$$

where,

$f_{p,T}$ = proportional limit at temperature T

$f_{y,T}$ = effective yield strength at temperature T

$\varepsilon_{y,T}$ = yield strain at temperature T

The third portion is a horizontal line at strains between 2-percent and a limiting strain which is defined at 15-percent:

$$\text{When } 0.02 = \varepsilon_{y,T} \leq \varepsilon \leq \varepsilon_{t,T} = 0.15 \quad \sigma = f_{y,T} \quad (2.9)$$

where,

$\varepsilon_{t,T}$ = limiting strain for yield strength

The last portion is a decreasing line at strains from 15-percent to 20-percent, where stress drops to zero:

$$\text{When } 0.15 = \varepsilon_{t,T} \leq \varepsilon \leq \varepsilon_{u,T} = 0.2 \quad \sigma = f_{y,T} \left(1 - \frac{\varepsilon - \varepsilon_{t,T}}{\varepsilon_{u,T} - \varepsilon_{t,T}}\right) \quad (2.10)$$

where,

$\varepsilon_{u,T}$ = ultimate strain

In Annex A of Eurocode 3 (2006), for temperatures below 400°C, an alternative expression for stress-strain relationships including strain-hardening is provided. In this option:

$$\text{When } 0.02 < \varepsilon < 0.04 \quad \sigma = 50(f_{u,T} - f_{y,T})\varepsilon + 2f_{y,T} - f_{u,T} \quad (2.11)$$

$$\text{When } 0.04 < \varepsilon < 0.15 \quad \sigma = f_{u,T} \quad (2.12)$$

$$\text{When } 0.15 < \varepsilon < 0.20 \quad \sigma = f_{u,T}[1 - 20(\varepsilon - 0.15)] \quad (2.13)$$

$$\text{When } \varepsilon \geq 0.20 \quad \sigma = 0 \quad (2.14)$$

where,

$f_{u,T}$ is the ultimate strength at elevated temperature, allowing for strain-hardening.

The ultimate strength at elevated temperatures, allowing for strain-hardening can be determined as:

$$\text{When } T < 300^\circ\text{C} \quad f_{u,T} = 1.25f_{y,T} \quad (2.15)$$

$$\text{When } 300^\circ\text{C} \leq T < 400^\circ\text{C} \quad f_{u,T} = f_{y,T}(2 - 0.0025T) \quad (2.16)$$

$$\text{When } T \geq 400^\circ\text{C} \quad f_{u,T} = f_{y,T} \quad (2.17)$$

It should be noted that using this method, the stress-strain curves must be divided into sections and appropriate equations need to be used to the specific sections. This might be improved by using a continuous power-law form expression to represent the entire stress-strain curve. A widely used and accepted continuous stress-strain expression is the Ramberg and Osgood equation (Equation 2.18) (Ramberg and Osgood 1943). It is commonly used for representing the stress-strain curves of metals that do not have a clear yield point. Therefore, it can be used for structural steel at high temperatures, in which the yield plateau no longer exists.

$$\sigma = \frac{(E-E_p)\varepsilon}{[1 + \left| \frac{(E-E_p)\varepsilon^n}{\sigma_0} \right|]^{1/n}} + E_p \varepsilon \quad (2.18)$$

where,

E_p = plastic modulus

σ_0 = a reference plastic stress

n = shape parameter of the stress-strain curve

Poh (1997) pointed out that the Ramberg and Osgood equation (Equation 2.18) may not be able to represent the stress-strain curves of intermediate temperatures at which neither the yield plateau nor the strain-hardening can be neglected. Poh proposed and developed a single continuous equation (Equation 2.19) that can be fitted in a stress-strain curve in one expression, and can be used for all temperature ranges.

$$\sigma = \frac{\varepsilon}{|\varepsilon|} [g(\varepsilon) + h(\varepsilon)] \quad (2.19)$$

where, the first part $g(\varepsilon)$ is a function representing the elastic-perfect plastic portion of the stress-strain curve. The end of the first part then transfers gradually to the second part, $h(\varepsilon)$, which gives a smooth strain-hardening curve.

2.2.6 Creep Behavior of Structural Steel at High Temperatures

Creep is generally defined as time and rate dependent stress-strain response. At ambient temperature, the stress-strain response of structural steel shows only a mild dependence on loading rate. Yield stress variations on the order of 10-percent are possible as loading rates vary (Galambos 1998). Although showing mild rate dependence, steel shows virtually no creep strain at ambient temperatures, and creep effects are normally neglected in the analysis and design of steel structure. However, as temperatures increase, steel exhibits increasingly significant creep effects.

Creep tests on materials are commonly conducted by subjecting the material to constant stress and temperature, and then measuring strain as a function of time. A typical creep strain versus time curve is shown in Figure 2.13. This curve is often divided into the three phases of primary, secondary and tertiary creep. In the primary stage, the curve

is nonlinear and typically exhibits a decreasing creep strain rate with increase in time. In the secondary stage, the creep strain rate is constant, and this stage is often referred to as steady-state creep. In the tertiary stage, the creep strain rate increases with time. For steel, the shape of the curve and the magnitude of the creep strain are highly dependent on temperature and stress level.

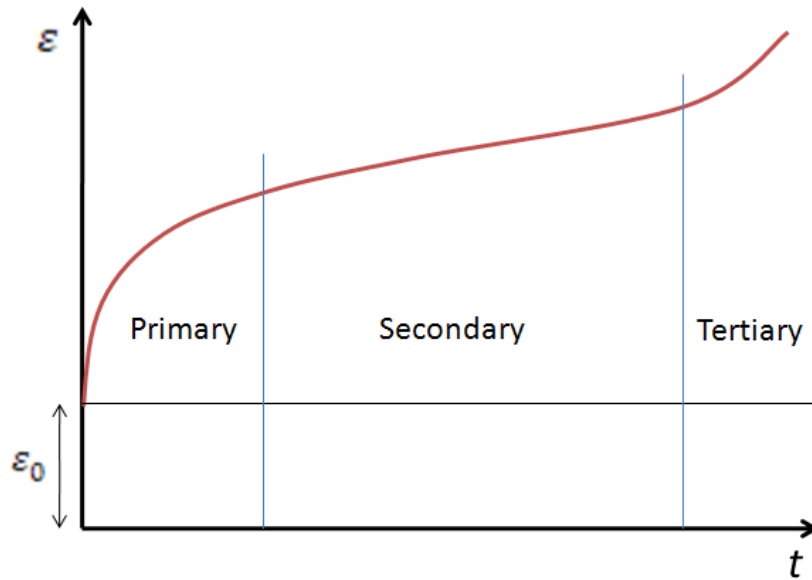


Figure 2.13 A typical creep strain versus time curve

Short-term creep behavior of structure steel at high temperatures has not been thoroughly studied, and only quite limited data can be found in the literature. Harmathy (1967, 1970) appears to be one of the first investigators who attempted at developing creep formulas for structural steel subjected to fire exposure. Harmathy proposed a creep model based on experiments on several structural and prestressing steels including ASTM A36 and CSA G40.12. His model attempts to predict creep strains in both the primary and secondary stages of creep. Later on Plen (1975) developed a simplified creep model with a parabolic and linear representation of the primary and secondary stages of creep, respectively. Harmathy's and Plen's models appear to be the best-known creep

models in the structural fire community and have been widely referred to by researchers in this field. Among other investigators who studied the creep behavior of structural steel are Knight et al (1971), Fujimoto et al (1980 and 1981), Williams-Leir (1983), Fields and Fields (1989 and 1991), and Luecke et al (2005). NIST (2008) highlights the fact that even though there is considerable experimental creep data available for different steels, these data are from tests conducted on steels used in power generation and industrial applications. In general, specimens were exposed to low stresses for long durations in elevated-temperature tests. However, for structural fire engineering applications, structural steel is normally under high stresses and high temperatures during the short period of fire exposure, which may be on the order of minutes to several hours.

As noted earlier, only limited test data is available on the creep behavior of structural steel at high temperatures for structural fire engineering applications. An example of the available experimental creep data is the work by Kelly and Sha (1999). They conducted creep tensile tests on two fire-resistant (FR) structural steels and S275 steel at high temperatures. It was observed that the FR steel exhibited considerably better creep performance than the S275. Figure 2.14 shows tested creep curves of the three types of steel at 600°C. Compared to the typical creep curve (Figure 2.13), it appears that the curves obtained by Kelly and Sha do not clearly exhibit the tertiary stage for the time period considered in the test.

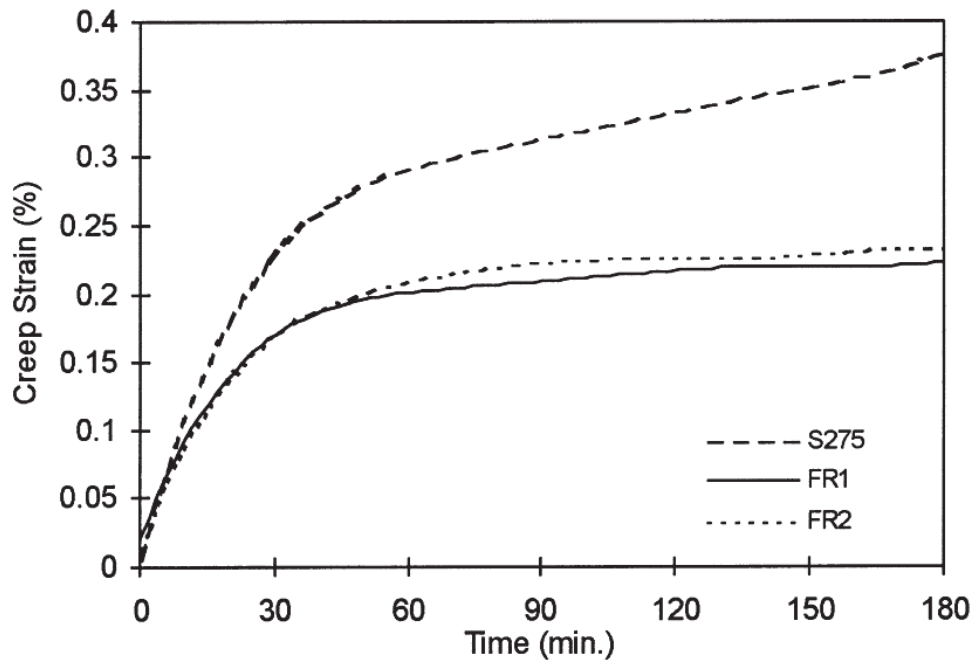


Figure 2.14 Creep curves for the three steels at 600°C (Kelly and Sha 1999)

It should be noted that in most of current investigations in structural fire engineering reported in the literature, creep is not usually modeled explicitly.

2.2.7 Summary

From this literature review, it is observed that various shapes of high-temperature stress-strain curves and different reduction ratios for strength and modulus of structural steel were reported by previous researchers. This variability in test results and design recommendations may be related to variability in materials, test methods and definitions of yield strength.

In this research, investigation on the performance of steel simple shear beam end framing connections in fire requires modeling of elevated temperature stress-strain properties of structural steel. Although several past studies have examined elevated-temperature properties of structural steel, little data is available on ASTM A992 steel, the most common grade of structural steel currently used for wide flange shapes in the US.

Therefore, test data of ASTM A992 steel at elevated temperatures is desired. In addition, it is also important to determine if the available analytical expressions in current codes and standards are appropriate for ASTM A992 steel in terms of strength and modulus variation, as well as stress-strain relationships at elevated temperatures. These questions will be addressed in Chapter 3 of this dissertation.

2.3 ELEVATED-TEMPERATURE PROPERTIES OF STRUCTURAL BOLTS

Behavior of structural bolts at elevated temperatures is another key factor that affects beam end framing connection performance in fire. In steel connections, structural bolts act as an important link between connection components. In general, structural bolts are made of high-strength steel, which contains different alloys and is subjected to different heat treatments compared to structural steel and hence behaves differently at elevated temperatures. In this section, a brief review of the past work on bolt strength at elevated temperatures is presented.

2.3.1 Test Methods

Similar to ambient temperature, the strength of structural bolts at elevated temperatures can be determined from bolt shear fracture tests and bolt tension fracture tests. If the stress-strain relationship is desired, small-scale tension coupon tests can be conducted at elevated temperatures on material samples machined from high-strength bolts.

In addition, hardness tests can be conducted on bolts to provide an estimate of tensile strength. Hardness tests can provide an economical and convenient way to assess the residual strength of bolts after a fire.

2.3.2 Code Recommendations

In Annex D of Eurocode 3 (2006), strength reduction factors of structural bolts at elevated temperatures up to 1000°C are listed (Table 2.2). Eurocode 3 recommends that

the same reduction factors can be used for both tension and shear loading of bolts. From this table, it can be observed that in Eurocode 3, bolt strength is assumed to decrease at temperatures of 100°C and above, and reduces to zero when 1000°C is reached.

Table 2.2 Bolts strength reduction factors (Eurocode 3 2006)

Temperature (°C)	Bolt Strength Reduction Factor
20	1.0
100	0.968
200	0.935
300	0.903
400	0.775
500	0.55
600	0.22
700	0.1
800	0.067
900	0.033
1000	0

2.3.3 Past Investigations

Investigations and information on the properties of structural bolts at elevated temperatures reported in the literature are quite limited. A few key previous studies are reviewed below.

Kirby (1995) conducted an experimental investigation on the behavior of high-strength Grade 8.8 bolts at elevated temperatures. Both tensile and double shear capacity of Grade 8.8 bolts at elevated temperatures were obtained in this research (Figure 2.15). Kirby observed that in both tests, bolts showed a marked loss in strength between 300°C and 700°C. Compared to the reduction factors of hot rolled structural steel at elevated temperatures, high-strength bolts show higher temperature sensitivity, due to a different

heat treatment procedure used during manufacturing. The residual hardness of Grade 8.8 bolts subjected to heating was also examined by Kirby for post-fire investigation purposes (Figure 2.16).

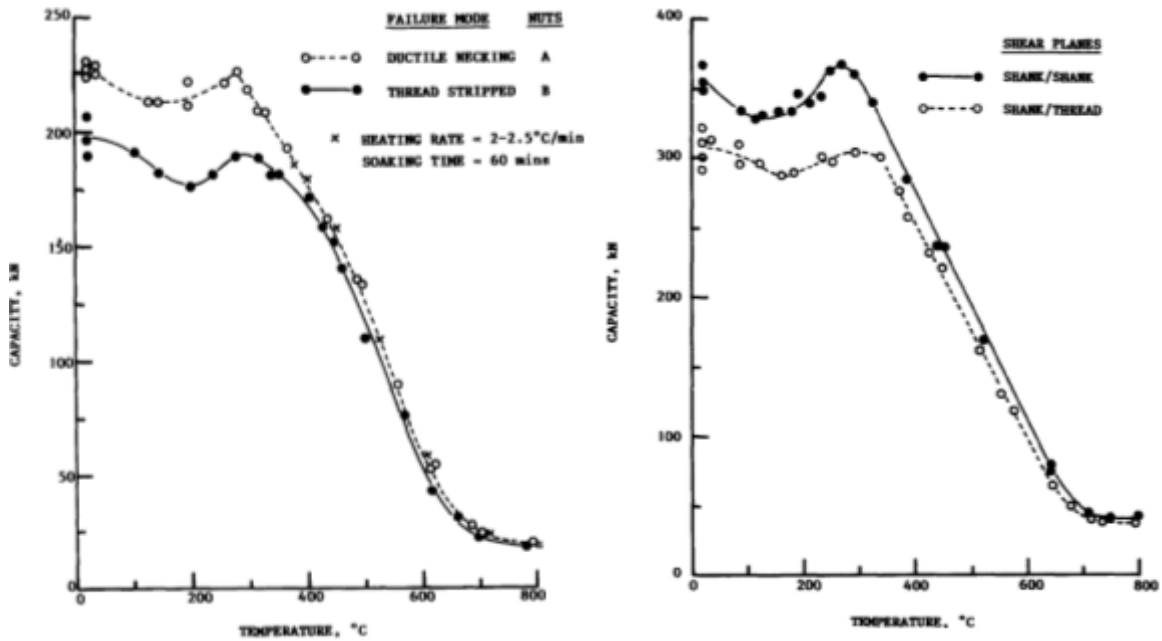


Figure 2.15 Tensile capacity (left) and double shear capacity (right) of Grade 8.8 bolts at elevated temperatures (Kirby 1995)

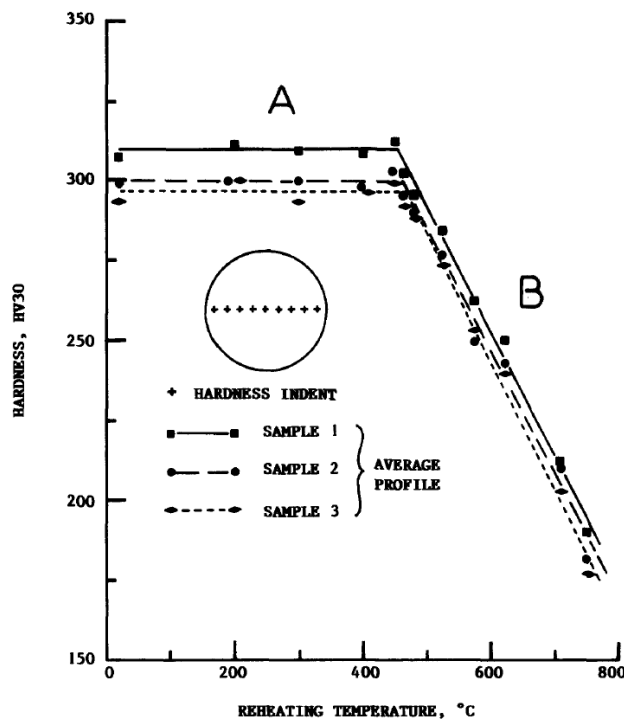


Figure 2.16 Hardness change with different heating temperatures (Kirby 1995)

Li et al (2001) tested elevated-temperature properties of high-strength steel 20MnTib, which is widely used in structural bolts in China. They conducted small scale steady-state tension tests, and obtained mechanical properties of the high-strength steel at different temperatures.

Yu (2006) studied the behavior of ASTM bolts under double shear loading at elevated temperatures. He obtained shear capacities of ASTM A325 and A490 bolts at temperatures up to 800°C. His testing setup is shown in Figure 2.17. Figure 2.18 shows the normalized shear capacities of ASTM A325 and A490 bolts at elevated temperatures. By comparing his test data with Kirby's results, Yu found that in terms of ambient temperature strength, Grade 8.8 high strength bolts are equivalent to A325 bolts. At elevated temperatures, the normalized shear capacities of A490 bolts behave similarly to Grade 8.8 bolts, while A325 bolts behave differently compared to Grade 8.8.

In addition, Yu investigated residual shear capacity of A325 and A490 bolts after exposure to temperatures up to 800°C by conducting shear tests and hardness tests after heating and cooling of the bolts. He obtained the residual shear capacities of both types of bolts (Figure 2.19 and Figure 2.20). Yu's data showed that bolts that were heated above about 400°C to 500°C and subsequently cooled suffered a permanent loss of strength. He also studied the effects of heating time and cooling rate on the bolt residual shear capacity and concluded that the effects are not significant.



Figure 2.17 Yu's bolt shear test setup (Yu 2006)

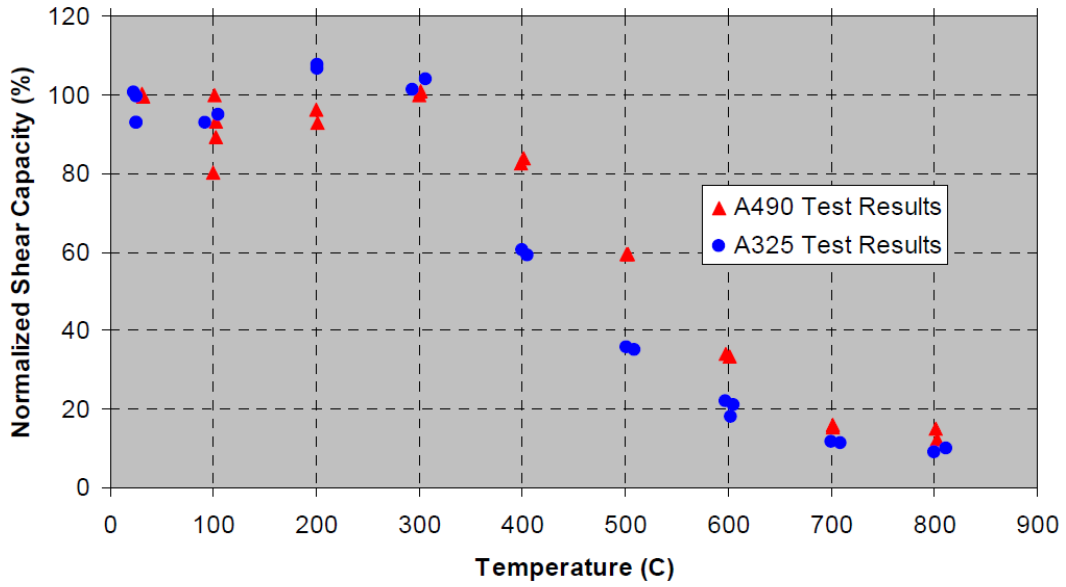


Figure 2.18 Normalized shear capacity of A325 and A490 bolts at different temperatures (Yu 2006)

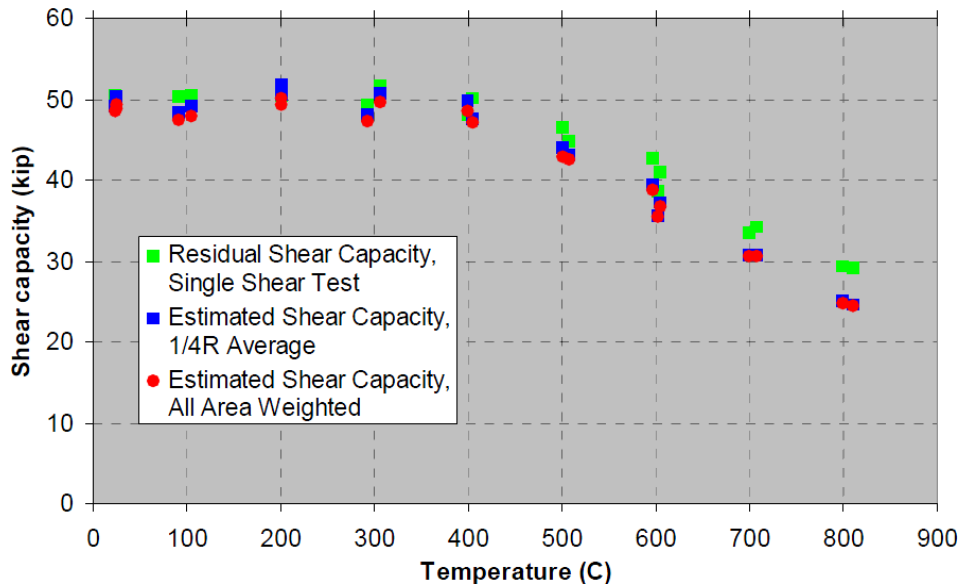


Figure 2.19 Residual shear capacity of A325 bolts (Yu 2006)

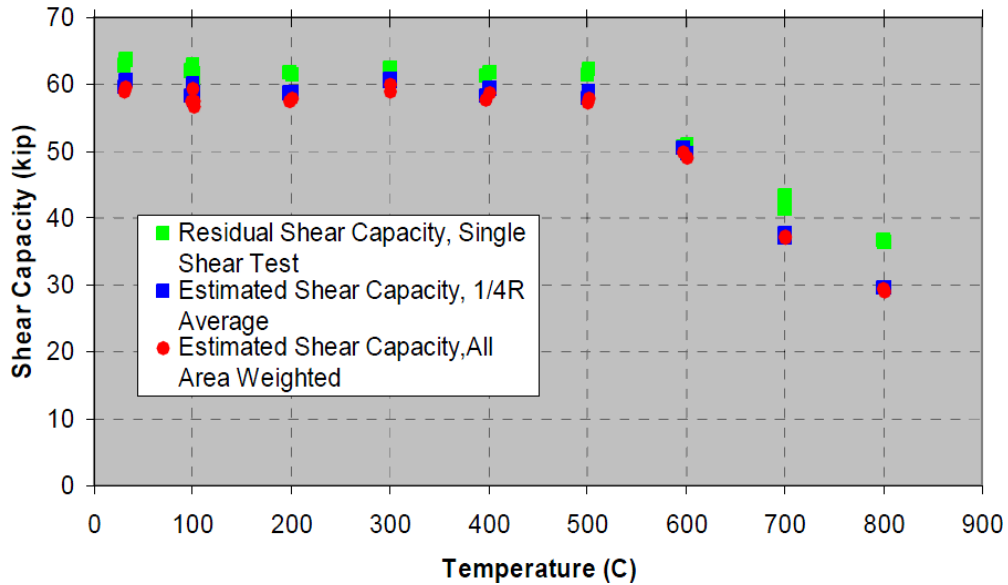


Figure 2.20 Residual shear capacity of A490 bolts (Yu 2006)

In addition to the literature noted above, a few other investigators also studied the behavior of structural bolts in fire conditions. Sakumoto (1993) tested the strength of fire resistant bolts at elevated temperature and after heating and cooling. Gonzalez and Lange (2008) studied the behavior of Grade 10.9 high-strength bolts under fire conditions. Hanus et al (2010) tested Grade 8.8 high-strength bolts under heating and cooling conditions. Lou et al (2010) tested both Grade 8.8 and 10.9 both at elevated temperatures. Figure 2.21 shows the strength reduction factors of different bolts tested by these investigators in comparison with the Eurocode recommendations at elevated temperatures. Figure 2.22 shows the residual strength reduction factors of structural bolts after heating.

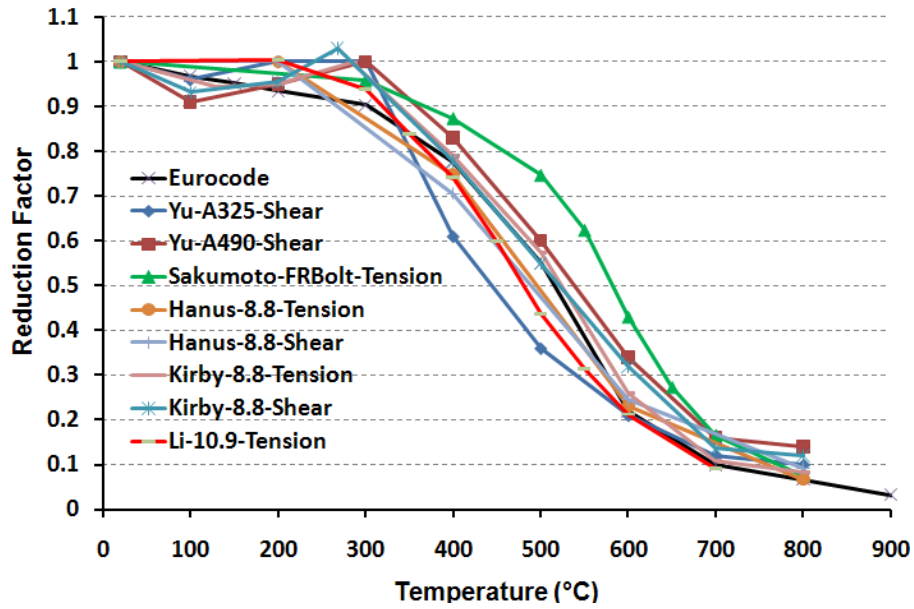


Figure 2.21 Strength reduction factors of different structural bolts at elevated temperatures

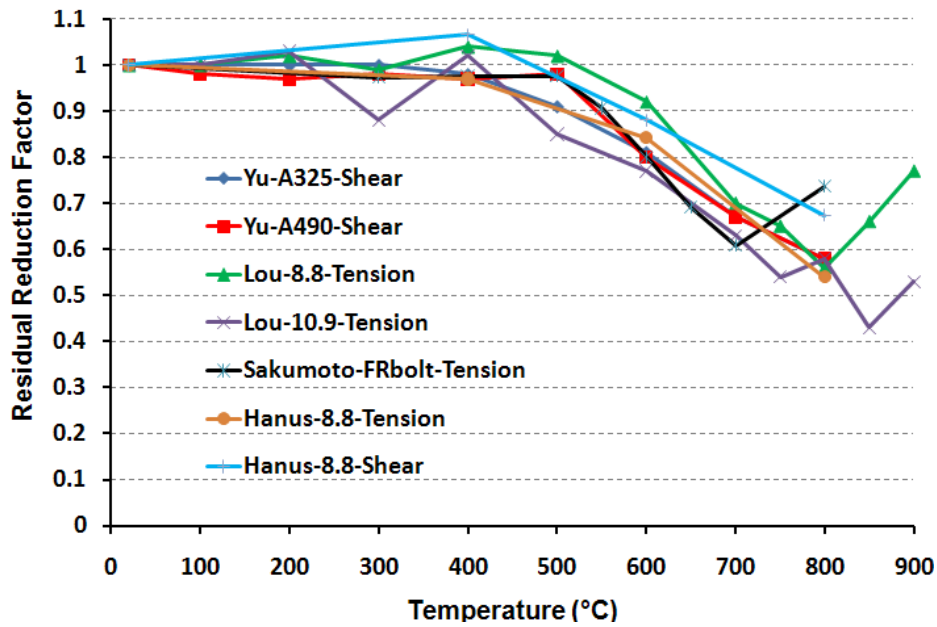


Figure 2.22 Residual strength reduction factors of different structural bolts after heating

2.3.4 General Observations

It can be observed from the limited previous research that the strength of structural bolts reduces significantly at elevated temperature. The strength reduction factors appear similar for shear and tension. From Figure 2.21, it appears that the Eurocode 3 bolt strength reduction factors fit the available experimental data reasonably well. It can also be observed that bolts suffer somewhat greater loss of strength at elevated temperature compared to structural steel. For example, according to Eurocode 3, the strength reduction factors for structural steel at 500°C, 600°C and 700°C are 0.78, 0.47 and 0.23 respectively. The corresponding strength reduction factors for bolts in Eurocode 3 at 500°C, 600°C and 700°C are 0.55, 0.22 and 0.10, respectively. The available experimental data also clearly shows that bolts experience a permanent loss of strength after heating above about 400-500°C followed by subsequent cooling.

2.4 SIMPLE BOLTED CONNECTIONS AT ELEVATED TEMPERATURES

In addition to testing structural bolts, Yu (2006) also studied the behavior of simple bolted connections at elevated temperatures. He tested the slip load capacity, bearing capacity and block shear capacity of simple bolted connections at elevated temperatures. An example of a block shear failure of a twin-bolt connection at 800°C tested by Yu is shown in Figure 2.23. The corresponding reduction factors were obtained from these tests. Besides strength reduction, Yu also observed and reported significant pretension loss in slip-critical bolted connections with temperature increase. A design approach of bolted connections under fire conditions was proposed, by taking into account the strength reductions of connection components.



Figure 2.23 Block shear connection failure at 800°C (Yu 2006)

2.5 ELEVATED-TEMPERATURE PROPERTIES OF WELDS

Welds are another important component in steel beam end framing connections. It can be expected that the strength of welds also reduces with temperature increase. However, there have been very few studies of weld strength at elevated temperature. Nevertheless, a few related previous studies can be found in literatures (Latham and Kirby 1993, and Hanus and Franssen 2010), and welds strength reduction factors at elevated temperatures are also given in Annex D of Eurocode 3 (2006) (Table 2.3). It is also recommended that the reduction factors listed in Table 2.3 should be used for fillet welds.

Table 2.3 Welds strength reduction factors (Eurocode 3 2006)

Temperature (°C)	Weld Strength Reduction Factor
20	1.0
100	1.0
200	1.0
300	1.0
400	0.876
500	0.627
600	0.378
700	0.13
800	0.074
900	0.018
1000	0

2.6 STEEL BEAMS IN FIRE CONDITIONS

As discussed earlier, the strength and stiffness of structural steel reduces at high temperatures, and this can cause large deformations in a steel beams subjected to fire. The behavior of steel beams in fire can be influenced by a number of factors, including the effect of beam end connections and beam end restraint. Restraint at the beam ends can result in large thermally induced forces in the beam, and as discussed in Chapter 1, can also permit the development of catenary action. Several past key experimental, numerical and analytical studies on the behavior of steel beams subjected to elevated temperatures are reviewed in this section.

2.6.1 Beam Tests

Steel beam behavior was studied extensively in the Cardington fire tests (1998, 2003). In these tests, an entire full-scale steel structure was studied under various fire exposures. These tests allowed examination of the behavior of steel beams in fire, when

the beams are part of a complete structural system. In the test structure, the steel beams were connected to the concrete floor slab with shear connectors to allow the development of composite action. In most of the Cardington tests, the steel beams were not protected with fireproofing or other types of insulation. The temperature was measured at different locations on the steel beams, and vertical displacements were measured as well during the tests. From these tests, it was observed that the bottom flanges mostly have the highest temperature in the beams. It was also found that steel beams can experience quite large deflections in fire, and even without protection, steel beams can survive in a fairly large compartment fire.

Liu et al (2002) conducted an experimental investigation on steel beams in fire. In this research, the experimental program was designed to study the effect of beam end restraint and catenary action. Figure 2.24 shows Liu's test frame and electrical furnace. Test beams were connected to test columns by two types of connections: flush end plate connections and web cleat (double angle) connections. Horizontal restraint stiffness could be changed by varying boundary supports of the supporting columns. The columns and the top flanges of the test beams were insulated by a ceramic fiber blanket. The experimental program included 20 fire tests on steel beams. Three main load ratios (0.3, 0.5 and 0.7) and three levels of axial restraint (8kN/mm, 35kN/mm and 62kN/mm) were used in this investigation. During the tests, gas temperature in the furnace was controlled to closely follow the ISO834 standard fire temperature curve. Temperature distribution in the beam was obtained by measuring temperatures on the beam bottom flange, web and top flange. Beam deflections were also measured. The effects of connections on beam behavior were studied as well by comparing moment-temperature curves of the two types of connections for different load ratios. In addition, the effects of axial restraint were examined by studying axial force-temperature behavior for different levels of axial stiffness. From all these test results, the researcher made the following conclusions: connection restraint can increase fire resistance of a steel beam by reducing mid-span moment during fire conditions. Catenary action was much more noticeable in end-plate

moment connections than web-cleat shear connections. Catenary action is more significant in the condition of lower load levels, higher axial restraint and larger deflection.

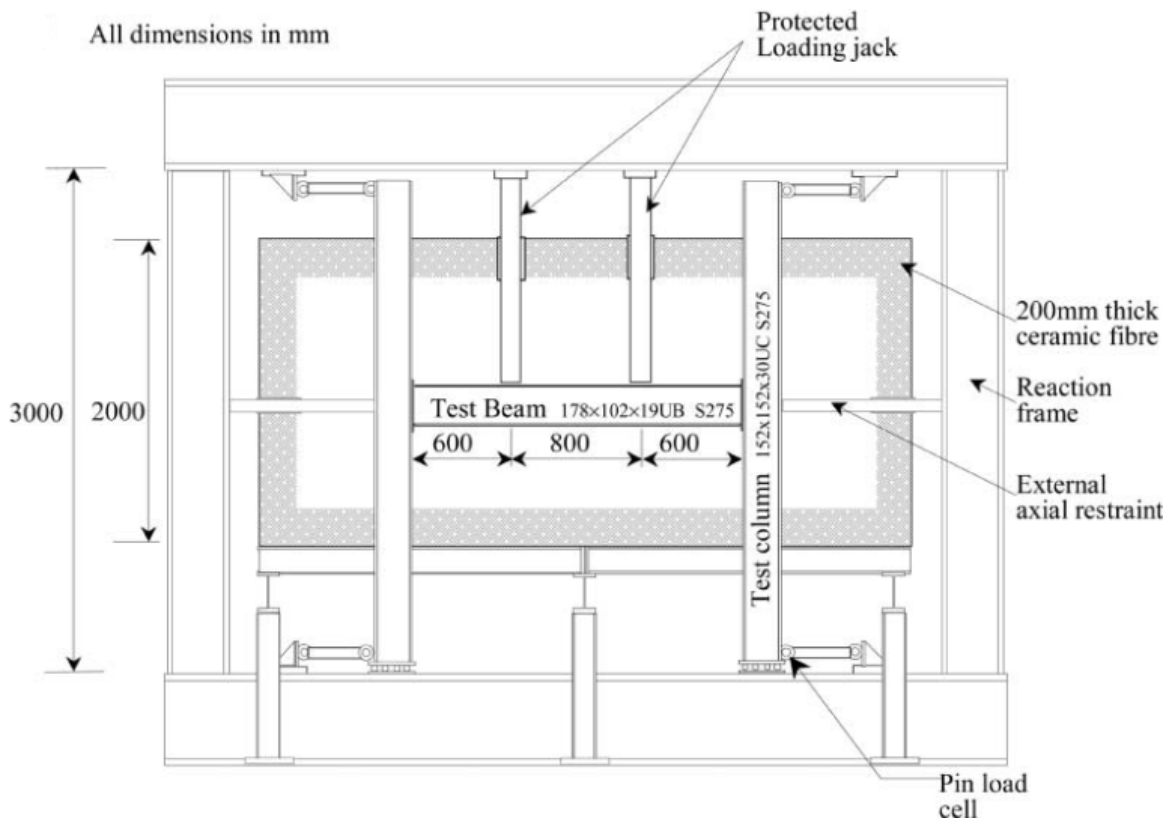


Figure 2.24 Liu's test setup (Liu et al 2002)

Mesquita et al (2005) examined the lateral torsional buckling performance of laterally unrestrained steel beams at high temperatures. The beams tested in this research had no axial restraint at the beam ends. Transient tests were conducted, so that critical temperatures were determined for beams with different effective lengths.

In 2007, Li and Guo (2007) studied the behavior of restrained steel beams subjected to heating and cooling by conducting two full scale beam tests. The setup of Li's test is shown in Figure 2.25. Beam end connections used in this research were

moment connections, namely, welded flange plate connections. Two tests with different beam end horizontal restraints were carried out in this study. Ceramic blankets were used to cover the top flanges of the test beams in order to simulate the insulating effects resulting from concrete slabs on the steel beams in real buildings. Two concentrated loads with the load ratio of 0.7 were applied and maintained symmetrically on the restrained beams by two jacks. Thermocouples, displacement transducers and strain gauges were arranged at different locations on the beams. During the fire tests, beams temperature and displacements at different locations were recorded. The fire was turned off after about 20 minutes of heating, and the air in the furnace cooled down naturally to ambient temperature. The axial forces in the beam were estimated by measuring beam end horizontal displacements. From the results of this experimental investigation, the researchers concluded that the behavior of the restrained beams exposed to fire can be quite different from that of isolated beams. During heating, due to the axial restraint to thermal expansion, an axial compression force is produced initially, followed by an axial tension force due to catenary action that occurred with an increase in beam deflection. The stiffness of the axial restraint has an impact on the axial forces in the restrained beams. The researchers also observed large increases in tensile force in restrained beams and little recovery of vertical deflections during the cooling phase of the fire.

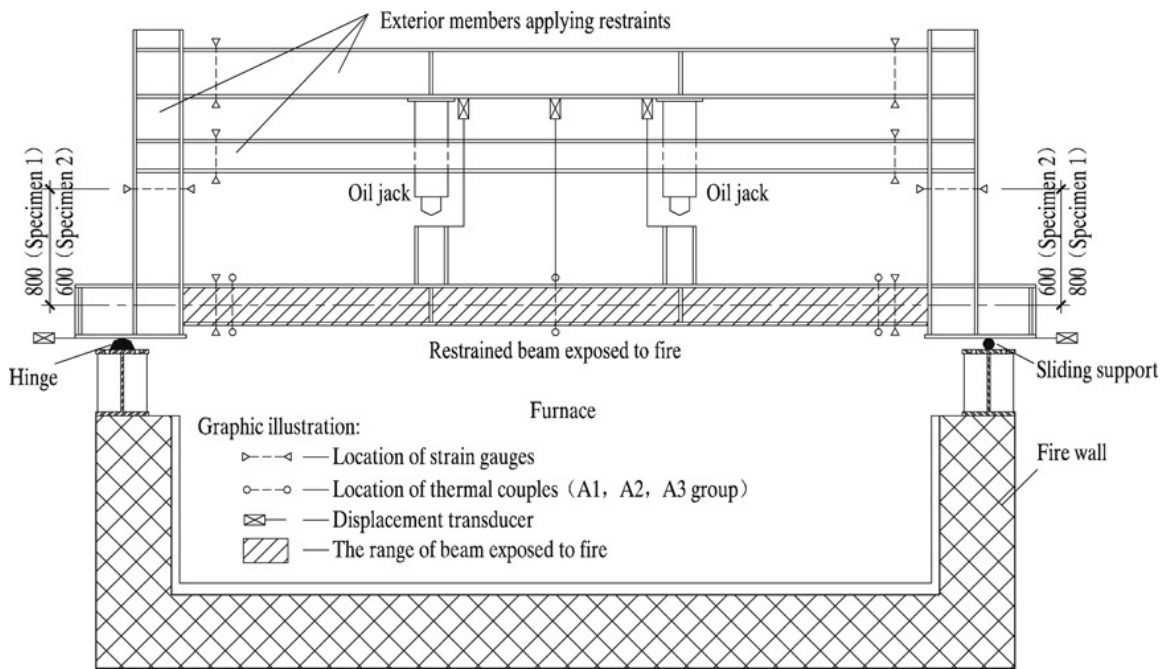


Figure 2.25 *Li's test setup and arrangement of instruments (Li and Guo 2007)*

Dharma and Tan (2007) conducted an experimental program to study the rotational capacity of steel I-beams under fire conditions. They examined the effects of different parameters including temperature, flange slenderness, web slenderness and effective length. From the tests, they observed considerable reduction in the rotational capacity of beams at elevated temperatures.

Tan and Qian (2008) studied the behavior of simply supported steel plate girders subjected to shear loading at elevated temperatures. They conducted twelve steady-state beam tests at three constant temperature levels of 400°C, 550°C and 670°C. In their test system, axial restraints were applied to the beams to simulate the thermal restraint effects of adjacent cooler parts of a steel-framed structure in fire. From these tests, the researchers obtained the ultimate shear capacities of the steel girders at different temperatures, and they also studied the out-of-plane deflection response of these slender section steel girders at high temperatures. A conclusion was made that the restraint to

thermal expansion reduced the ultimate shear capacity of the plate girder web panel compared with unrestrained plate girders, and the restraint effects appeared to be more significant with larger web plate slenderness (d_w/t_w).

2.6.2 Numerical Modeling

Numerical modeling, for example finite element (FE) analysis is another widely used method in investigations of steel beam performance in fire. Modeling of steel structure behavior in fire includes thermal behavior modeling and structural behavior modeling. A fairly large number of past investigations can be found in the literature. Some important previous numerical studies on steel beam fire performance reviewed by the author of this dissertation includes Burgess et al (1990), Liu (1996), Bailey et al (1996), Yin and Wang (2003), Vila Real et al (2003), Buchanan et al (2004), Tan and Huang (2005), Mesquita et al (2005), Li et al (2006), Dharma and Tan (2007) etc.

In these previous studies, the finite element programs used for analysis of steel beam behavior in fire conditions included SAFIR (Franssen 2005), FEMFAN (Tan et al 2002), MSC.MARC, ANSYS and ABAQUS. It was noted that finite element models using beam, shell and solid elements can be used for the analysis of global beam behavior. However, to accurately capture the beam behavior at local areas such as connections and to capture local buckling an FE model with shell or solid elements is required.

2.6.3 Analytical Investigations and Design Equations

In addition to the experimental and numerical approaches, analytical methods have also been widely used to understand steel beam behavior in fire conditions and to develop simplified design equations and procedures. It should be noted that Eurocode 3 (2006) provides design equations to calculate the beam moment resistance and the beam lateral torsional buckling resistance for both uniform and non-uniform temperature distribution conditions. However, these equations are derived from similar concepts of

beam behavior at ambient temperature, with reduction of steel properties at elevated temperatures included. Therefore, beam large deflection, catenary action, and the influence of beam end connections are not considered in these equations. In recent years, some investigators have explored approaches to include these effects.

El-Rimawi et al (1997) provided a simple analysis approach to study the influence of connection stiffness on the behavior of steel beams in fire. This approach was based on a secant stiffness approach, and was validated by experimental data. Different parameters were examined in this study, including connection temperature, beam span and beam depth. The investigators concluded that the behavior of the beam in fire significantly depends on the bending stiffness and resistance of the supporting structure.

Yin and Wang (2005) developed a simplified hand calculation method to analyze beam catenary effects. In this investigation, some assumptions on the beam's deflection profile and interaction between axial force and bending moment were made to simplify the problem. Two beam loading conditions including uniform load and point load were considered. Different levels of axial restraint as well as rotational restraint at the beam ends were also studied. Later on, Yin developed a similar approach in studying steel beams with non-uniform temperature distribution. Hand calculation equations were obtained and results were validated by finite element modeling. From the results of this research, by knowing the stiffness of the supports at the beam boundaries, one can calculate the internal forces in the beam under catenary action in a fire. The authors proposed that this approach can be adopted as the basis of a future design calculation method.

2.6.4 General Observations

As discussed above, it has been widely recognized that the behavior of steel beams in fire conditions is remarkably different with that at ambient temperature. Some general observations from the literature described in this section can be made:

1. Steel beams lose strength and stiffness in fire, and can experience large vertical deflections at high temperatures. Beam catenary action can develop in fire conditions if the beam end supports can develop the needed reactions that accompany catenary action.
2. Beam catenary action can help steel beams survive fire loading, but imposes large axial tension and large rotation demands at the beam ends.
3. During the heating stage of a fire, due to thermal expansion, large axial compression can develop in a steel beam with axial restraint at its ends.
4. During the cooling stage of a fire, large axial tension can develop in a steel beam due to thermal contraction.

Previous research has clearly shown that large axial forces, both tension and compression, develop in steel beams during the heating and cooling stages of a fire, and these forces have to be transferred to adjacent structures through beam end framing connections. Therefore, sufficient strength and deformation capacity is required at beam end connections to prevent connection failure.

2.7 SHEAR TAB CONNECTIONS

2.7.1 Shear Tab Connections at Ambient Temperature

As described in Chapter 1, the shear tab connection is one of the most widely used simple beam end framing connections in the US, and is designed to resist the shear at the ends of floor beams at ambient temperature. In addition, the connection needs to provide sufficient rotation capacity to allow the beam to reach its plastic moment capacity. The requirement for both strength and ductility has led to numerous analytical and experimental studies of shear tab connections at ambient temperature. A brief summary of previous studies of shear tab connections at ambient temperature is presented below.

Early work by Lipson (1968) examined shear tab beam end framing connections by doing a series of tests at the University of British Columbia in Canada. The goals of

the research were to examine the behavior of the connections under working loads, to evaluate the rotational capacity of the connections, to obtain a consistent factor of safety, and to determine if the connections should be classified as flexible or rigid. Two types of experiments were conducted. In the first type, specimens were subjected to pure bending moment, and in the second type a combined shear and moment loading were applied. Lipson identified three failure modes: tensile yielding of the plate, weld rupture, and vertical tear out of the bottom bolt. Significant deformations of the bolt holes were also observed. The connections were classified as partially restrained connections with characteristics of both flexible and rigid connections.

Richard et al (1980) created a series of finite element models of shear tab connections and conducted a series of bolt shear tests. From their models, a beam line concept was developed. The beam line is an equation defining the relationship between the end moment and the end rotation of a single span beam subjected to a uniformly distributed load. The beam line utilized assumed linear beam response action and nonlinear connection behavior to find the moment–rotation relationship for shear tab connections. Five full scale beam tests were performed to establish the validity of the beam line. The researchers also proposed a design procedure based on connections attaching to a rigid support with standard bolt holes. Rotational ductility was provided by limiting the thickness of shear tabs to ensure the development of adequate plate bearing deformations prior to the development of any brittle limit states.

Astaneh-Asl et al (1989) did not quite agree with the simple test methods widely used in previous studies for connection investigations, and emphasized that, for beam end shear connections, shear effects should be studied realistically. They developed a test procedure to examine the connection behavior under combined moment, shear and rotation. The test setup consisted of a beam and a short column. A shear tab was welded to the column outer flange. A cantilever beam was connected to the shear tab through bolts. Load was applied on the beam's top flange through an actuator placed near the support to provide shear, and another actuator placed near the cantilever end of the beam

to provide rotation. They proposed that this new test approach can determine the behavior of shear tab connections under loading conditions representing the actual behavior of a beam in a steel structure. By doing fifteen full-scale tests in which connections with three, five, seven and nine A325 and A490 bolts were tested, they concluded the possible failure modes of these connections and developed a method to predict the strength capacity of shear tab connections. They also developed a design procedure for sizing the shear tab, welds and bolts. They concluded that 6 limit states should be considered for design of shear tab connections.

1. Yielding of gross area of plate,
2. Bearing yielding of bolt holes in the plate and beam web,
3. Bearing tear out of bolts in the plate and beam web,
4. Shear fracture of the net area of plate,
5. Fracture of bolts,
6. Fracture of welds.

For each failure mode, a design formula was suggested. The design procedure was developed to ensure the ductile failure modes will occur first. The recommended design approach was adopted into the AISC 2nd Edition Manual (AISC 1993) and still forms the basis for shear tab design in current U.S. practice.

Metzger (2006) studied the behavior of steel shear tab beam end connection by doing several real scale beam tests. The test setup consisted of the test beam, supporting column, free end support beam, loading support frame, and lateral bracing frames. The hydraulic rams were placed in two separate loading frames which were bolted to the reaction floor. An additional testing frame was placed between the loading frames to provide support for lateral bracing. Load was applied to the test beam at nominal third points by two hydraulic rams. The test beam was attached to the column flange with a shear tab connection. The other end of the test beam was supported by a roller on a load cell supported by a beam bolted to the reaction floor (Figure 2.26). Connections containing three, four, five and seven rows of bolts were tested. The experimental results

were compared to the predicted strengths determined according to the procedure in the AISC 13th Edition Manual (AISC 2006), and showed a significantly higher value. This indicated that the predictions of AISC Manual on the ultimate strength of shear tab connections are conservative.

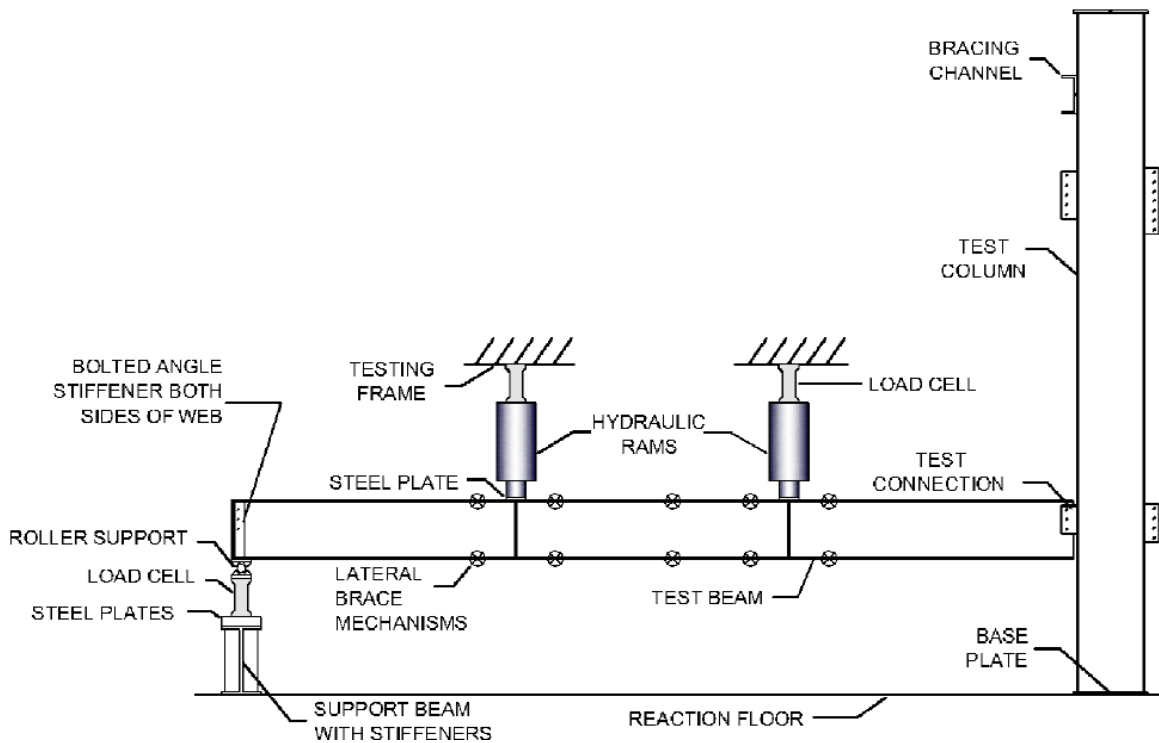


Figure 2.26 Setup of Metzger's shear tab connection test (Metzger 2006)

Ashakul (2004) developed finite element models using ABAQUS to evaluate the design models of shear tab connections. He conducted model verifications, and evaluated some control parameters, including the effect of the distance between the face of the column and the bolts (referred to as the “a-distance”), plate thickness, plate material, and the position of a connection with respect to a beam neutral axis. His results showed that bolt shear rupture strength of a connection is not a function of the a-distance. He also observed that plate materials and thicknesses that do not satisfy ductility criteria can

result in connections with significant horizontal forces at the bolts. These horizontal forces reduce the shear strength of the bolt group and create a moment that must be considered in design. The magnitude of the force depends on the location of the bolts with respect to the beam neutral axis. He also proposed a new design model for bolted shear tab connections.

From the previous work described above, it may be concluded that the behavior of shear tab beam end framing connections at ambient temperature has been studied quite extensively. Connection performance and limit states have been studied both in experiments and by finite element analysis, and design procedures are well developed. With this knowledge and understanding, further research regarding to the behavior of connections at elevated temperatures can be discussed.

2.7.2 Shear Tab Connections in Fire Conditions

As discussed in Section 2.6, large axial forces and rotations can be generated at steel beam ends when subjected to fire. These force and rotation demands raise concerns about the performance and safety of beam end framing connections in fire. In recent years, a significant number of investigations have been conducted on the behavior of beam end connections in fire. Some early work includes Lawson (1990), Liu (1994, 1996, 1998, 1999, 2002), Al-Jabri et al (1996, 1998), El-Rimawi et al (1997, 1999), Leston-Jones et al (1997), El-Housseiny (1998), Simones da Silva (2001, 2004), Spyrou et al (2002), Yu et al (2008) and Santiago et al (2003, 2004, 2009). Much of this research has been on steel beam-to-girder and on moment resisting beam-to-column connections in fire. Fewer previous studies have focused on simple shear connections, of the types widely used in steel structures in US. In this section, the limited previous work conducted on shear tab connections in fire conditions is summarized.

The fire tests in the Cardington laboratory (Wald et al 2004) showed that during the heating phase of a fire, the temperature of the connections is lower compared to the beam. In the cooling phase of the fire, the temperature of the connections is higher. That

is, connections cooled more slowly than the beams. The shear tabs had higher temperatures compared to the bolts, and the temperature of lower bolts was higher than upper ones. The elongations of the holes in the beam webs and shear tabs due to the associated large connection rotations were observed in the tests.

Two tests of shear tab connections (also referred to as fin plate connections) were conducted by Ticha and Wald (2005). It was observed from the two tests that the failure modes of the connections were bolt shear fractures during the cooling stage at the temperature of about 725°C.

Wald and Ticha (Sarraj 2007) conducted a transient fire test on a steel beam with shear tab connections at the Czech Technical University in 2005. A three-bolt shear tab connection was assembled using fully threaded Grade 8.8 high strength bolts with a 3 meter-long IPE 160 beam. The loads were applied by two hydraulic jacks 0.25 meter from the beam ends. The furnace gas temperature was controlled to follow the Cardington fire test for the heating and cooling stages and reached a temperature as high as 1200°C. Temperatures at different locations on the beam, and deflections at the loading points were recorded during the test. From the test, it was observed that the weld showed no sign of failure or fracture, while most of the bolts were sheared off completely (Figure 2.27). Some of the bolts were embedded into the web or shear tab holes, implying large forces acting on the bolts along the longitudinal direction of the beam. The bolt holes in the beam web were distorted significantly and local buckling occurred in the beam web near both beam ends.

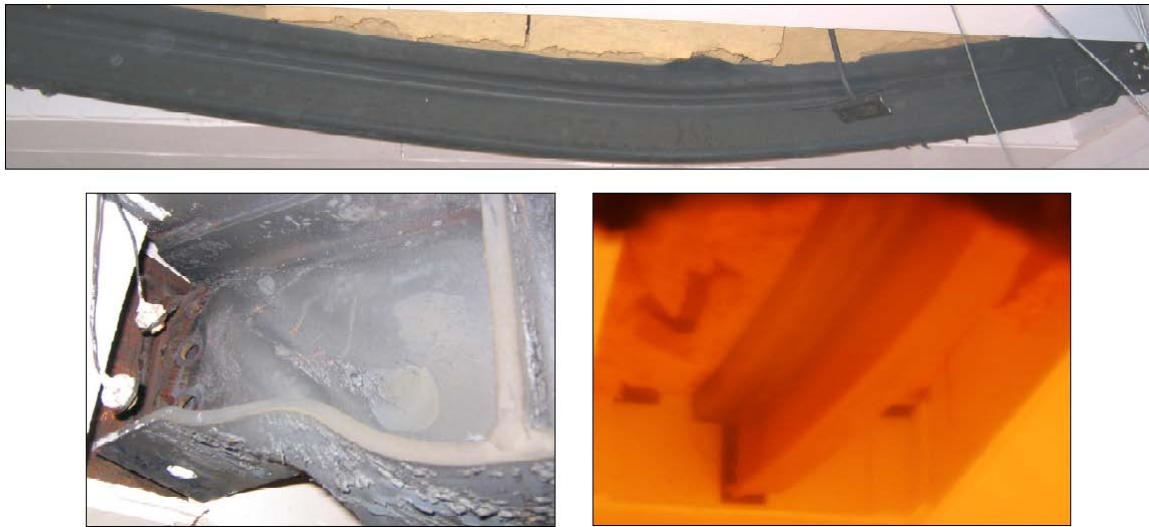


Figure 2.27 Wald and Ticha's fin plate connection test (Sarraj 2007)

The structure fire engineering research group at the University of Sheffield has done a series of research investigations on shear tab connections, including finite element modeling and elevated-temperature tests.

Using the FEA package ABAQUS/Standard, Sarraj (2007) developed an advanced three-dimensional finite element model to study the behavior of shear tab connections in fire. Solid element and detailed modeling was performed for all connection components including bolts, nuts, shear tab and beam. Contact interaction was incorporated in the models to simulate the bolt shearing and bearing behavior in shear tab connections. The model also included geometric and material non-linearity. Comparing with existing experimental results, Sarraj's model successfully simulated the behavior of shear tab connections under both ambient temperature and fire conditions. Using the proposed models to conduct some parametric studies, Sarraj concluded that the horizontal tying force resistance of shear tab connections was almost equal to their vertical shear capacity. He observed that the inclination of the tying force has a large influence on the failure mode above 550°C. He also concluded the most damaging action on shear tab connections is excessive rotation rather than uniform tension or shear. In addition, Sarraj

also developed a simplified component model approach by modeling spring elements representing each connection component (Figure 2.28). Taking into account bolt shearing, shear tab bearing, web bearing and friction, this component model showed the capability of simulating the connection behavior with reasonable accuracy and significantly reduced computational cost compared to the detailed finite element model.

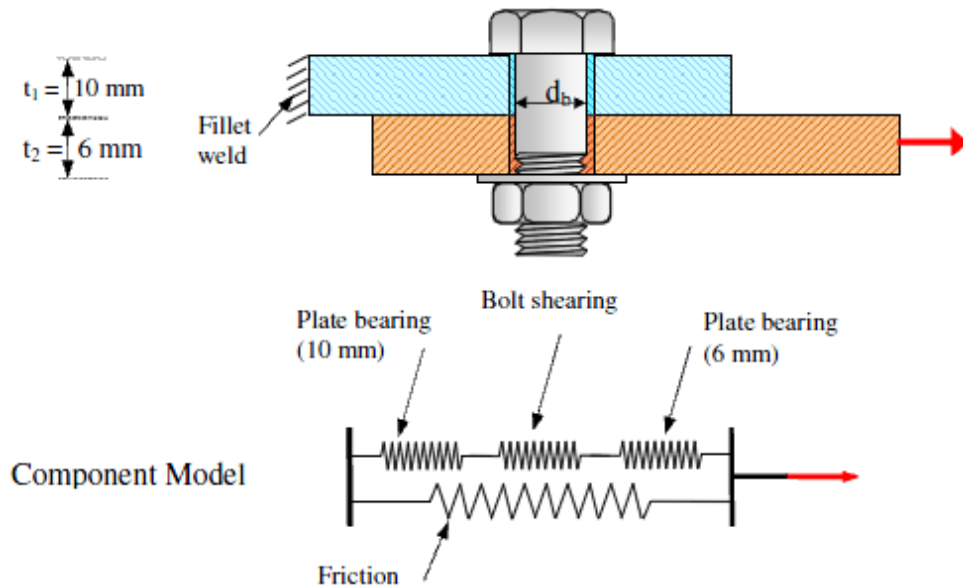


Figure 2.28 Lap joint component model (Sarraj 2007)

Yu et al (2008) conducted steady-state experiments on shear tab connections at elevated temperatures. Their test setup (Figure 2.29) consisted of a short column and a short beam. The beam was attached to the column by a shear tab connection. The whole setup was assembled into an electrical furnace. The loading device was located outside of the furnace, and connected with the beam end through a hole in the furnace wall. By pulling the load jack, a combined shear and tension were applied to test connections, and failure conditions were reached for all tests. Different rotations, corresponding to the ratio of applied shear and tension, were applied by changing the furnace bar angles. Fourteen full-scale shear tab connections were tested under different loading angles and different

temperatures. The results showed that the shear capacity of the bolts reduced faster than other components with an increasing temperature. From this observation, they concluded that bolt shear fracture tends to govern the failure of shear tab beam end connections at high temperatures and proposed higher strength bolts could be used to enhance the whole connection capacity in fire conditions. A modified Sarraj's component model taking into account the contact between column flange and beam bottom flange under a large rotation was proposed in this research and showed a good agreement with test results.

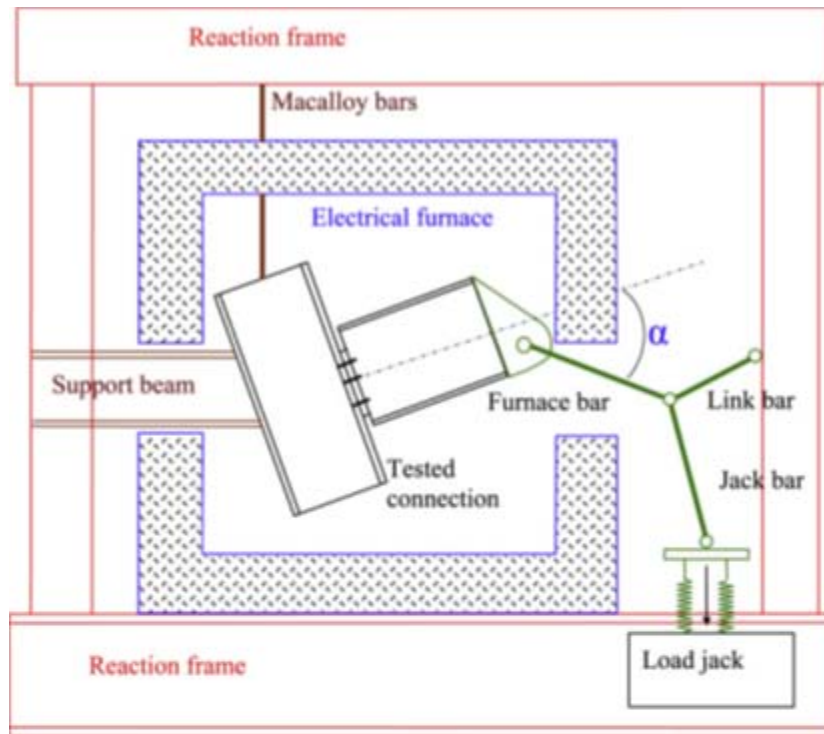


Figure 2.29 Setup used in Yu's connection test (Yu et al 2008)

More recently, Garlock and Selamet (2010) examined the effect of heating and cooling rates on the steel shear tab connections using finite element analysis. They modeled the concrete slab using a spring element and performed uncoupled thermo-mechanical analysis. As a conclusion, they demonstrated that heating and cooling rates affect the beam stress distribution, peak temperatures, and peak displacements, but not the peak beam axial force. They also concluded that large tensile forces in the connections are created in the cooling phase, and can lead to connection failure.

Other than the studies reviewed above, Rahman et al (2004) performed finite element analysis on the behavior of shear tab connections in fire conditions using ANSYS. Temperatures of the standard fire exposure were used in this study. LaMalva et al (2009) conducted a failure analysis on the shear connections in the floor system of WTC building 5 using an ABAQUS finite element model. A conclusion was made by the researchers that the connection failed due to the large rotations and prying actions at high temperature.

2.8 SUMMARY

As discussed in this chapter, it has been recognized that the connection force and deformation demands in fire conditions is significantly different than those at ambient temperature. An assessment of previous related research shows a limited number of investigations on the behavior of simple shear beam end framing connections at elevated temperatures. This previous research has identified the difficulty in predicting the force and deformation demands on connections during the heating and cooling phases of a fire as well as the difficulty in predicting connection stiffness, strength and ductility under these demands. Therefore, there is a need to gain an improved understanding of the behavior of the simple shear beam end framing connections in fire conditions.

Based on the review of previous research, several keys areas were identified where additional information or study is needed to better understand the behavior of beams and beam end simple framing connections in fire. These include the following:

1. Accurate mechanical properties of ASTM A992 structural steel at elevated temperatures, in particular, stress-strain relationships in the full strain range are needed.
2. The agreement of tested A992 steel mechanical properties with current code recommendations and analytical approaches need to be determined.
3. Creep behavior of A992 steel needs to be better understood.
4. Accurate modeling of steel simple shear beam end framing connections in fire using tested material properties is needed.
5. Forces and deformation demands on beam end simple shear connections in fire during both heating and cooling stages requires further study.
6. Improved methods to predict the stiffness, strength and deformation capacities of beam end simple shear connections under fire conditions are needed.
7. Failure modes of simple shear beam end connections in fire conditions need to be better identified.
8. Important parameters that can potentially affect the performance of steel simple shear beam end connections in fire need to be more understood.
9. Additional experimental data on the behavior of steel simple beam end connections is needed to improve understanding and for validation of models.

The research reported in the remainder of this dissertation is intended to contribute in several of the areas listed above.

CHAPTER 3

Elevated Temperature Properties of ASTM A992 Steel

3.1 OVERVIEW

To study the behavior of steel beam end framing connections in fire, it is important to be able to understand and predict the behavior of the beam itself in fire. This, in turn, requires knowledge of the mechanical properties of structural steel at elevated temperatures. For simplified predictions of beam response under fire conditions, simplified material models are often used. These simplified models require information on the yield strength, tensile strength and modulus of elasticity of steel at elevated temperatures. Advanced analysis methods, for instance, finite element analyses, require a more complete description of the elevated temperature mechanical properties of steel, including data on the shape of the entire stress-strain curve as well as information on time dependent effects such as strain rate effects and creep.

Although several previous studies have examined elevated-temperature properties of structural steel, there are some important gaps in the experimental database. Specifically, little data is available on ASTM A992 steel, the most common grade of structural steel currently used for wide flange shapes in the US. Furthermore, past studies have not adequately examined the important role of strain rates in tension testing at elevated temperatures.

This chapter presents results of a study on the elevated temperature properties of ASTM A992 steel. Full stress-strain curves for this grade of steel at elevated temperatures up to 900°C are presented here with a description of the testing procedure and equipment. The important mechanical properties of structural steel, such as the yield strength, elastic modulus, tensile strength and ultimate strain, were obtained from the stress-strain curves. Results are compared with elevated temperature properties specified by Eurocode 3 (2006) and by the AISC Specification (2005). This chapter also presents observations on the effects of crosshead displacement rate in tension tests at elevated

temperatures. Test results for crosshead rates of 0.01 and 0.1 inch/min are presented. The static yielding behavior of A992 steel under elevated temperatures (300°C and above) was also studied.

3.2 EXPERIMENTS

3.2.1 Equipment

A 22-kip capacity MTS 810 test frame with water cooled grips was used to conduct these tension tests, and an MTS Model 653 furnace (Figure 3.1) was used as the heating device. The furnace generates heat using electrical coils, and is separated into upper, middle and lower heating zones that can be individually controlled using an MTS Model 409.83 temperature controller. Three thermocouples are located inside the furnace to measure the furnace air temperature. In addition, three thermocouples were used to measure the surface temperature of the specimen at different locations along the gage length of the coupon. An MTS Model 632.54E-11 air-cooled high temperature extensometer with 1 inch gauge length (with limit strain of -10-percent to +10-percent) was used for measurement of strain.

3.2.2 Specimens

All specimens were cut from the web of a single ASTM W30×99 girder made from ASTM A992 structural steel. The dimensions of the specimens, in accordance with ASTM Standard A370 (ASTM 2008), are shown in Figure 3.2. The cross sectional area of each coupon is approximately 0.25 inch². A coupon specimen during heating and loading within the furnace is shown in Figure 3.3.

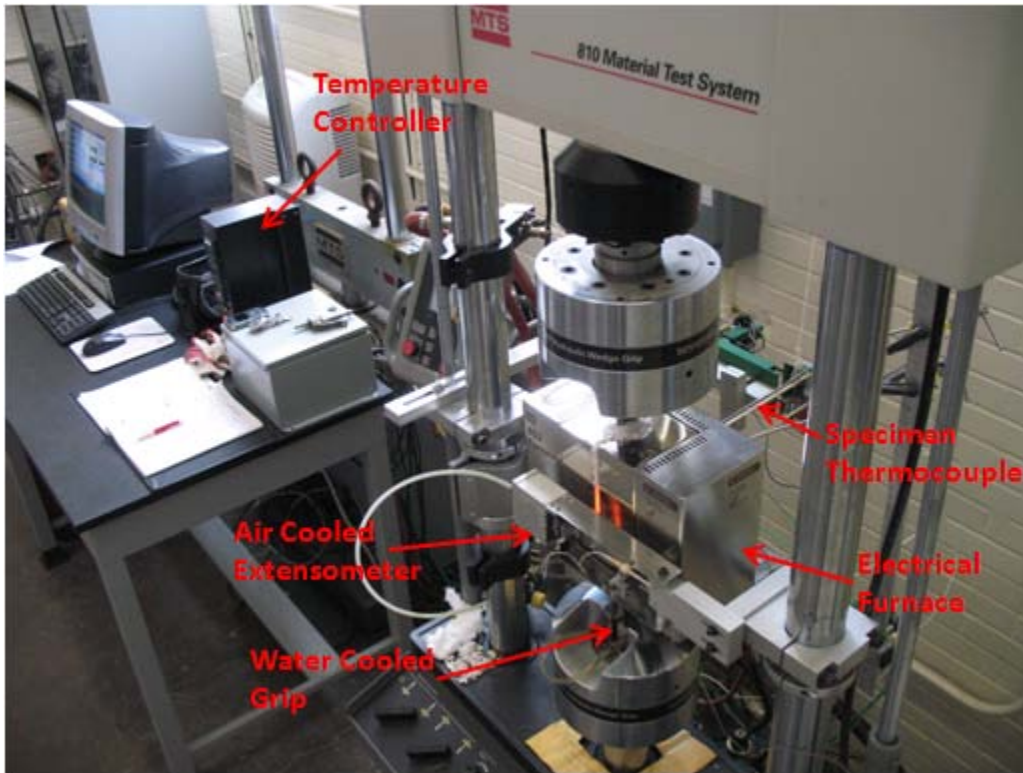


Figure 3.1 Testing equipment

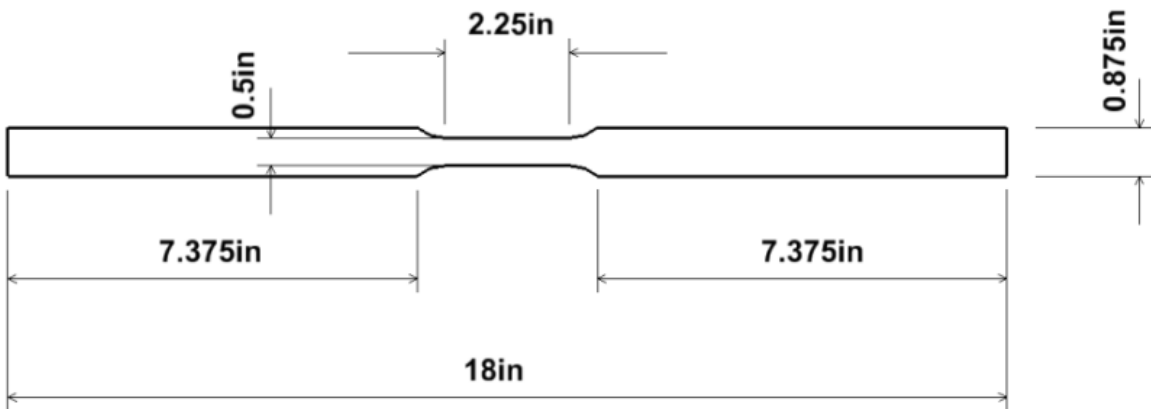


Figure 3.2 High temperature testing coupon specimen

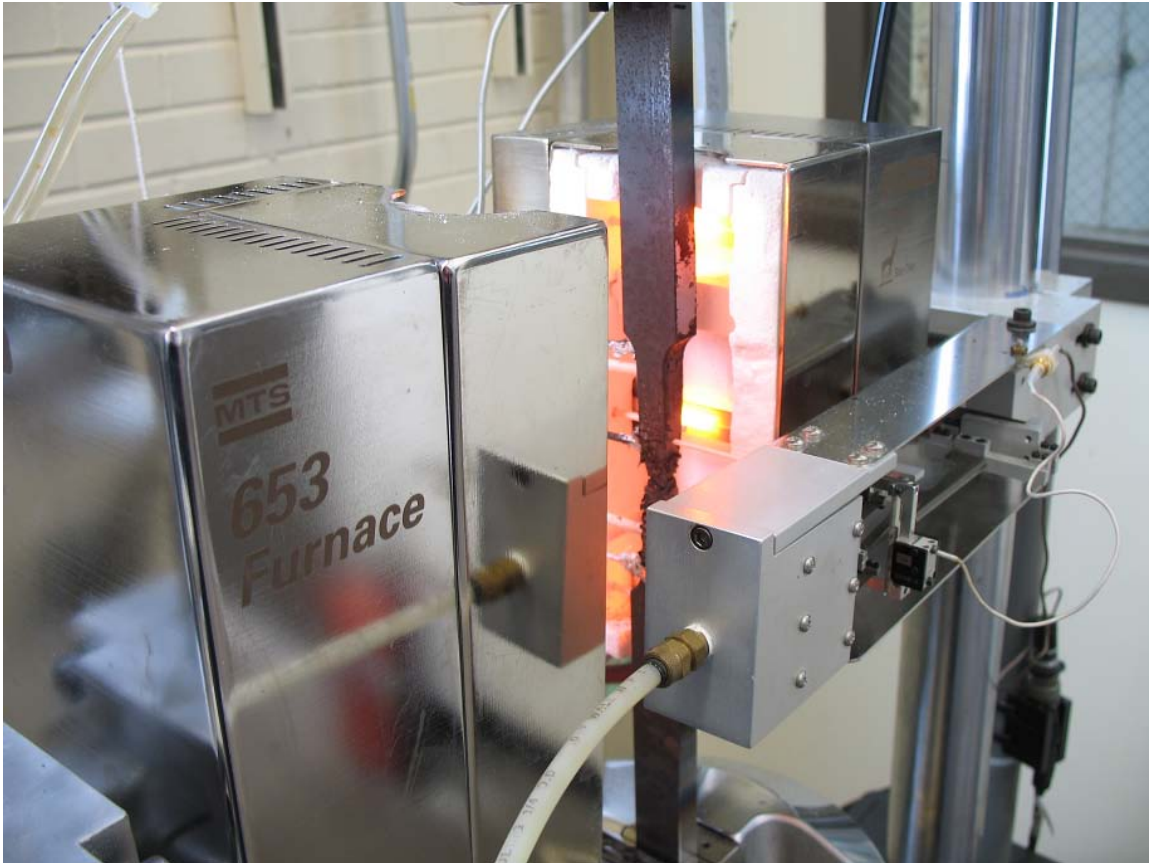


Figure 3.3 Coupon specimen in the furnace during a test (furnace is normally closed during test).

3.2.3 Loading Control and Measurement

The loading applied to the specimen was controlled and recorded by the load cell in the MTS test machine. In this research, the stress refers to the engineering stress, which is equal to the measured load divided by the measured initial cross-section area of the coupon's reduced section.

3.2.4 Temperature Control and Measurement

Temperature measurement is a critical factor in elevated temperature testing. To obtain mechanical properties at a target temperature, a uniform temperature distribution

over the gage length of the steel coupon is needed. In this study, three stick thermocouples were used to measure the surface temperature of the specimen at different locations along the gage length of the coupon (Figure 3.4).

It should be noted that considerable experience in elevated-temperature coupon testing was required before repeatable results were obtained. The investigator initially encountered significant difficulties in controlling the temperature of the coupons. It was found that a uniform air temperature in the three zones of the furnace resulted in a significant variation in steel temperature over the gage length of the coupon. These problems were exacerbated as the coupon lengthened during testing and moved through different temperature zones in the furnace. Consequently, considerable trial-and-error experimentation was required before developing furnace control techniques that resulted in uniform steel temperatures over the height of the gage section and throughout the duration of a test.

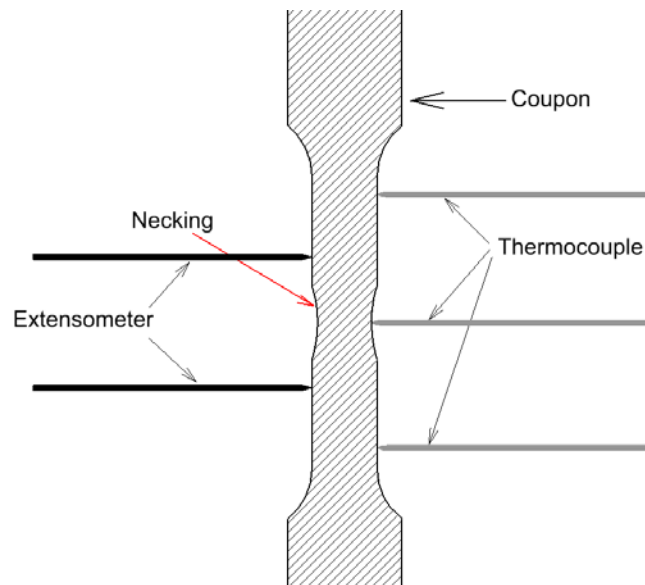


Figure 3.4 Strain and temperature measurement

3.2.5 Strain Measurement

In this study, the strain refers to engineering strain, based on the initial 1-inch gage length of the extensometer. In order to capture the entire stress-strain relationship, the extensometer was reset when it approached the 10-percent limit during the tests. However, a modification was made on the measured strain for each resetting due to the reason explained below.

Without resetting, the measured strain can be expressed as:

$$\varepsilon = \frac{l-l_0}{l_0} \quad (3.1)$$

where, l_0 is the initial gage length of the extensometer (1 inch). Strain at the moment of resetting is:

$$\varepsilon_{reset} = \frac{l_{reset}-l_0}{l_0} \quad (3.2)$$

Where, l_{reset} is the measured length when resetting occurs. After each resetting, l_{reset} reduces to l_0 . As can be noted from Figure 3.5, with each resetting, a part of the initially measured length (red lines in the figure) moves outside of the new gage length, and the strain of this part is not included in the subsequent strain measurement. Therefore, after each resetting, a modification factor of l_{reset}/l_0 should be applied to the new measured strain, assuming the elongation of the steel coupon is uniform along the length of the reduced section. In this study, the extensometer had a 10-percent strain limit, so $l_{reset}=1.1 \times l_0$, assuming each resetting occurs when strain limit is reached. Consequently, with the modification, the strain obtained from this study should be expressed as:

$$\text{When } \varepsilon < 0.1 \quad \varepsilon = \varepsilon_{read} \quad (3.3)$$

$$\text{When } \varepsilon > 0.1 \quad \varepsilon = 0.1 + \sum (1.1)^n \varepsilon_n \quad (3.4)$$

Where, n is resetting times, ε_n is strain measured after n th resetting.

In addition, it should be noted that the above expression can only be used before necking occurs, when uniform elongation can be assumed to occur along coupon's length. After necking occurs, the elongation of the coupon localizes to the necking area, and the strain now measured by the extensometer can be directly used as engineering

strain without any modification. However, it is important that the necking location be within the gage length of the extensometer during the test, otherwise significant strain can be missed. It should be pointed out that considerable testing difficulties exist due to the reason that necking location at elevated temperatures is hard to predict, and this has to be solved by repeating tests several times.

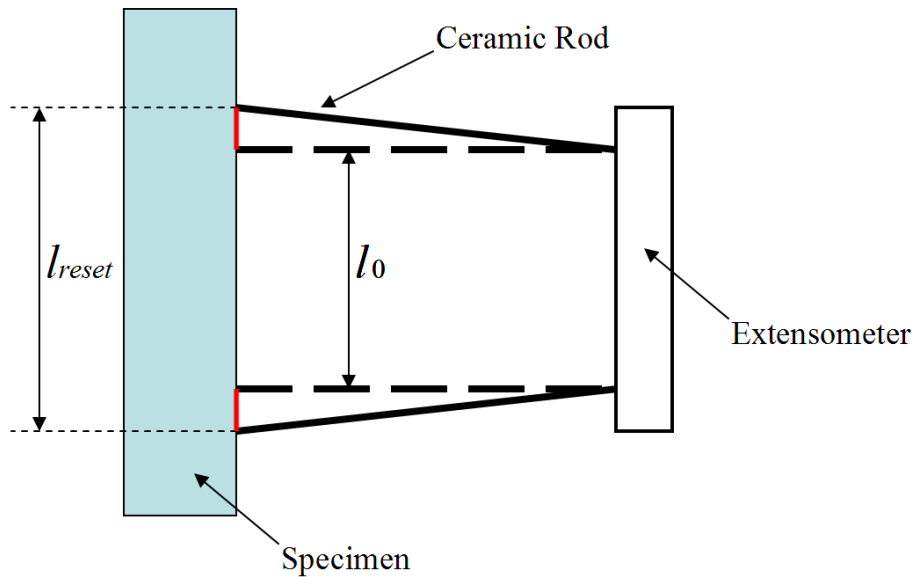


Figure 3.5 Strain measurement with resetting extensometer

The investigator also initially experienced difficulties in the use of the high temperature extensometer, which often slipped during the course of a test. The extensometer contacts the coupon through ceramic rods, which extend outside of the furnace. A trial-and-error process was required to establish the proper tip profile and contact pressure for the ceramic rods to prevent slip. Experimentation and experience were needed to develop techniques for resetting the extensometer each time at its 10-percent strain limit, while minimizing overall errors in the strain measurement.

3.2.6 Testing Procedure

All tests were thermal steady-state tests, in which the specimens were heated up to a specified temperature and then loaded until failure while maintaining the same temperature. During the initial heating process, the load was maintained at zero to allow free expansion of the specimen.

Besides being thermal steady state, all tests were displacement-controlled, in which crosshead displacement rates were maintained at a constant value throughout a test. Specifically, two crosshead displacement rates were used: 0.01 inch/min (slow test), and 0.1 inch/min (fast test). Coupon temperatures from 20°C to 900°C were studied at each displacement rate. In addition, static yielding behavior was investigated for slow tests in the temperature range of 300°C to 800°C, in which the crosshead movement was suspended for 30 and 3 minutes respectively to obtain static yielding behavior.

Testing steel coupons at elevated temperature introduces a number of experimental difficulties that are not encountered in ambient temperature testing. Specialized equipment is needed, as well as considerable care and experience is required in temperature control and strain measurement techniques. The need for specialized equipment, specialized test techniques and the need for considerable experience likely contributes to the paucity of elevated temperature stress-strain data for structural steel.

3.3 TEST RESULTS

Table 3.1 summarizes the key data from the tests. The necking and elongation of the coupons are shown in Figure 3.6 and the cross sections of the coupons at fracture are shown in Figure 3.7. It can be observed that at temperatures of 800°C and 900°C, the necking shows a trend of distributing more along the length of the coupon's reduced section. Coupons tested at 300°C exhibited a characteristic blue color after the testing. Coupons tested at very high temperatures, above about 700°C, exhibited a black and very rough surface appearance. Fractures surfaces in coupons tested at lower temperatures exhibited sharp corners at failure locations.

Table 3.1 Summary of test results

Temp (°C)	Loading Rate (in/min)	0.2% Offset Yield Strength (ksi)	Tensile Strength (ksi)	Elastic Modulus (ksi)	Final Elongation (%)	Stress Drop in 3 Min Load Pause (ksi)	Stress Drop in 30 Min Load Pause (ksi)
20	0.01	62.2	75.2	30890	56	N/A	N/A
	0.1	63.3	76.8	29120	49		
100	0.01	59.3	72.2	28127	47	N/A	N/A
	0.1	58.9	71.5	30382	47		
200	0.01	58.8	76.0	31571	42	N/A	N/A
	0.1	58.1	73.5	26900	42		
300	0.01	45.8	78.2	24912	47	4.7	5.3
	0.1	48.2	76.6	24832	43		
400	0.01	43.2	69.2	23978	43	5.3	8.6
	0.1	43.1	67.8	26083	41		
500	0.01	36.9	48.0	20329	38	6.9	12.7
	0.1	37.1	51.6	18126	38		
600	0.01	24.8	28.2	14125	49	6.9	11.9
	0.1	27.7	32.0	15253	52		
700	0.01	12.7	13.1	13923	71	4.4	7.4
	0.1	16.3	16.9	12531	79		
800	0.01	5.4	5.8	5432	110	3.4	5.0
	0.1	7.8	8.8	6535	100		
900	0.01	3.9	4.6	2935	41	N/A	N/A
	0.1	6.5	7.0	3818	36		



Figure 3.6 Coupons from elevated temperature tests - elongation



Figure 3.7 Coupons from elevated temperature tests - fracture section

3.3.1 Stress–Strain Curves

The complete stress-strain curves measured at each temperature, from the start of loading to the fracture of the coupon, are shown in Figure 3.8 and Figure 3.9 at crosshead displacement rates of 0.01 inch/min and 0.1 inch/min, respectively. As illustrated by these curves, the tensile strength increases compared to the room temperature coupon, at temperatures of 200°C to 300°C. At higher temperatures, progressive strength loss can be clearly observed. Another important property, ductility, as measured by the final elongation of the coupon (Figure 3.12), exhibits a small reduction up to 500°C, then increases in the range of 600°C to 800°C, and then reduces again at 900°C. On the other hand, ductility, as measured by the strain at which the tensile strength is developed, shows a dramatic decrease with increasing temperature (Figure 3.13). For example, the strain at the development of the tensile strength, for a crosshead rate of 0.1 inch/min, is 14-percent at 20°C, 9-percent at 500°C and 1-percent at 800°C.

Since understanding of the behavior of structural steel during the initial loading stage is crucial in structural design, the measured stress-strain curves in the range of zero to 10-percent strain are plotted in Figure 3.10 and Figure 3.11. As observed in previous tests reported in the literature, this data indicates that the fundamental shape of the stress-strain curve changes as temperature increases. At temperatures above about 200°C to 300°C, the steel no longer exhibits a yield plateau, and shows significant nonlinearity at low levels of stress and strain. As described above, the strain at which the maximum engineering stress (tensile strength) is developed decreases rapidly as temperature increases, and the stress-strain curve subsequently shows a long, gradual decline. At ambient temperature, the initial portion of the stress-strain curve is often modeled using a simple elastic-plastic approximation in which the response is linear-elastic up to yield, and then follows a plateau. Simple elastic-plastic stress-strain models may be less appropriate at elevated temperatures due to early nonlinearity. This early nonlinearity may be particularly significant when considering stability phenomena, wherein stiffness is a critical material property.

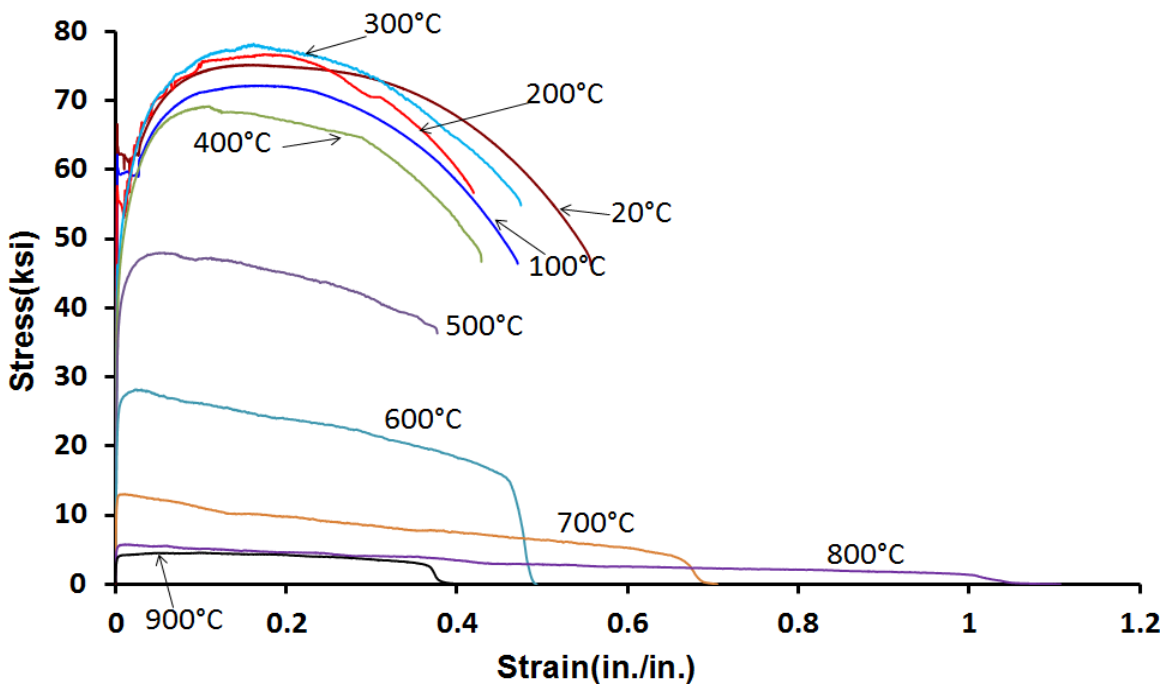


Figure 3.8 Complete stress-strain curves at elevated temperatures – 0.01 inch/min

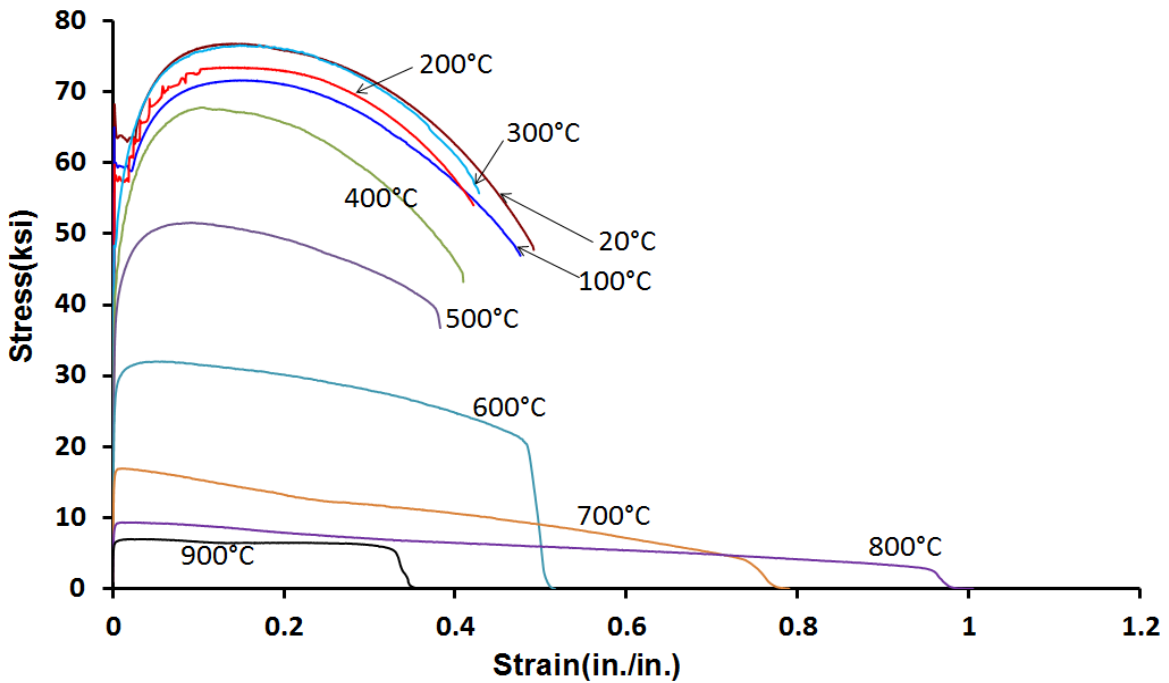


Figure 3.9 Complete stress-strain curves at elevated temperatures – 0.1 inch/min

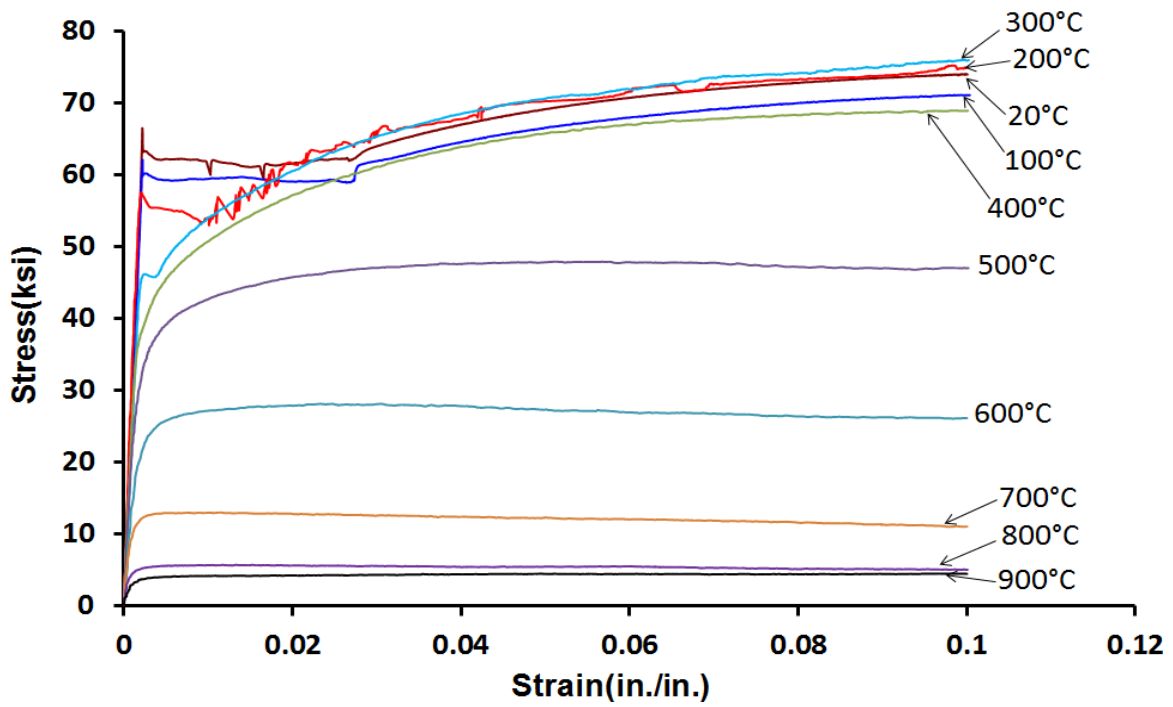


Figure 3.10 Stress-strain curves up to 10% strain – 0.01 inch/min

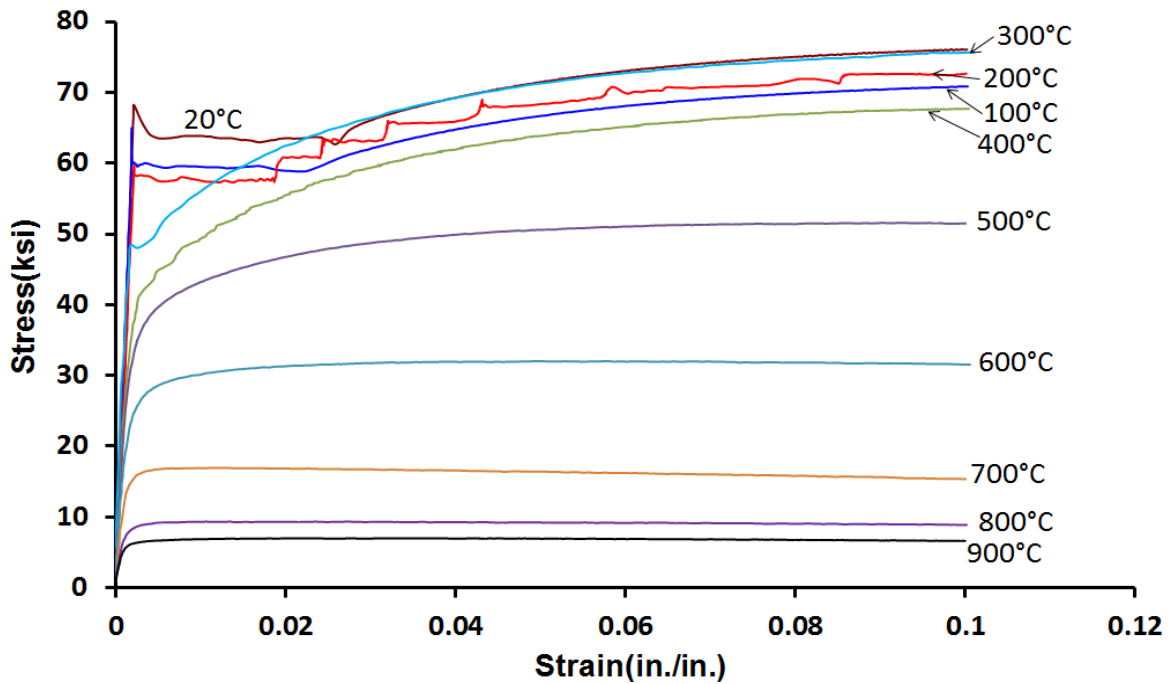


Figure 3.11 Stress-strain curves up to 10% strain – 0.1 inch/min

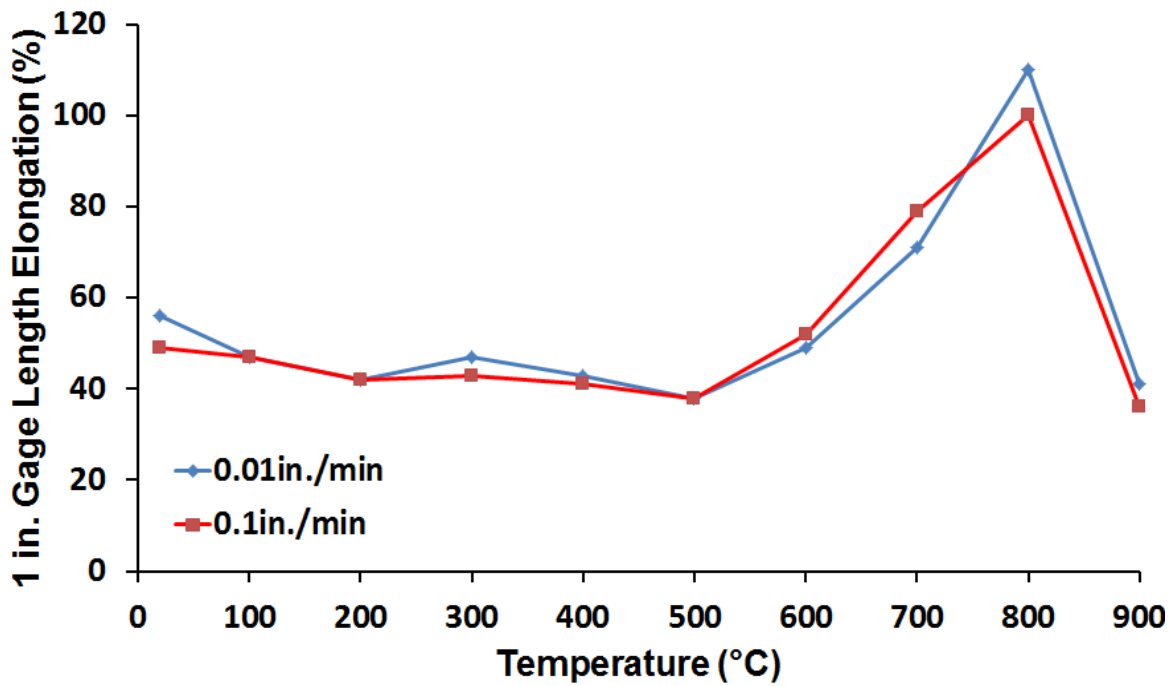


Figure 3.12 Final elongations of tested coupons

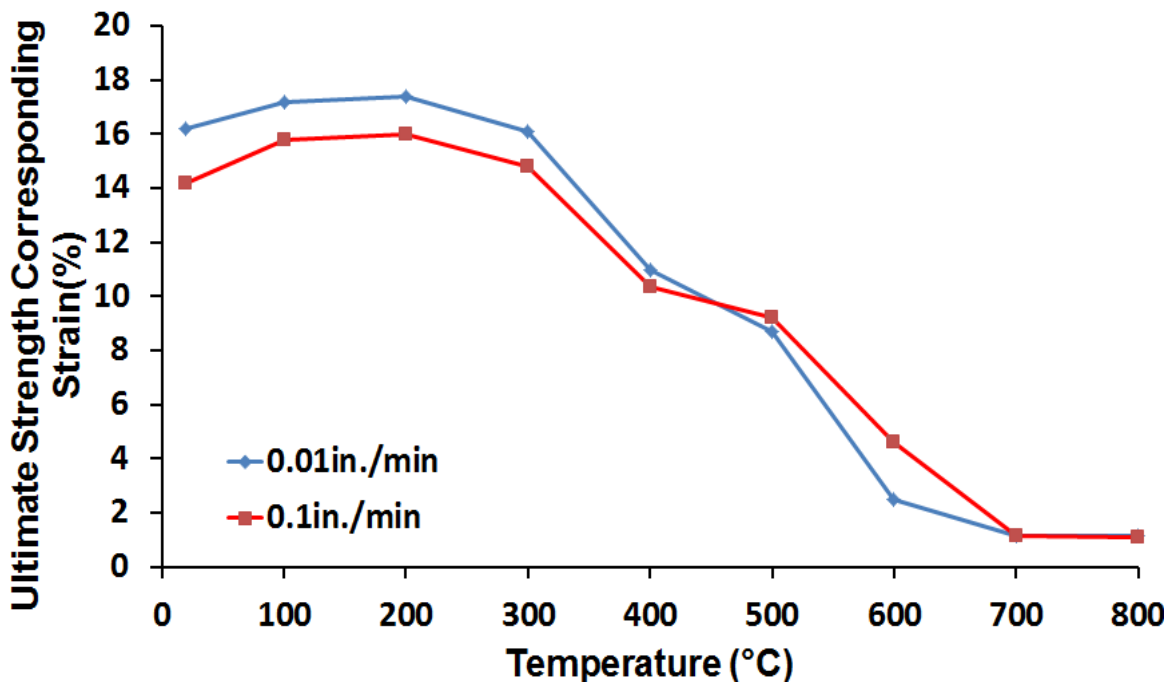


Figure 3.13 Strain at the ultimate tensile strength

A phenomenon observed at 200°C, for both displacement rates, was that the stress-strain curve was not smooth in the strain hardening range, but rather exhibited a number of sudden stress jumps. At first, this was believed to be slipping of the extensometer. However, this effect was observed repeatedly in tests at 200°C, and thus did not appear to be experimental error. A review of the literature suggests this may be a metallurgical phenomenon known as “Portevin-LeChatelier effect” (Dieter 1986).

3.3.2 Analysis of Experimental Data

Eurocode 3 (2006) has simple equations to predict stress-strain curves for carbon steel at elevated temperatures. These equations (discussed in Chapter 2) divide stress-strain curves into four sections, and include both rising and descending portions of the stress-strain curves.

In Figure 3.15 through Figure 3.18, stress-strain curves from tests are compared against corresponding ones predicted by the Eurocode 3 at 400°C, 500°C, 600°C, 700°C and 800°C, respectively. At 400°C, 500°C and 600°C, it can be seen that at strains smaller than 15-percent the Eurocode’s simplified stress-strain relationships match the test data quite well. At temperatures of 700°C and 800°C where loading rates have significant effects, the Eurocode’s simplified stress-strain relationships lie in between the data of slow and fast loading. For all temperatures considered, strains larger than 15-percent, the Eurocode model displays a faster stress drop and a smaller total elongation and ductility. It should be noted that the typical shapes of the stress-strain model of Eurocode are similar for all temperatures higher than 400°C, while as discussed in Section 3.3.1, the actual curves obtained from test vary with temperature significantly.

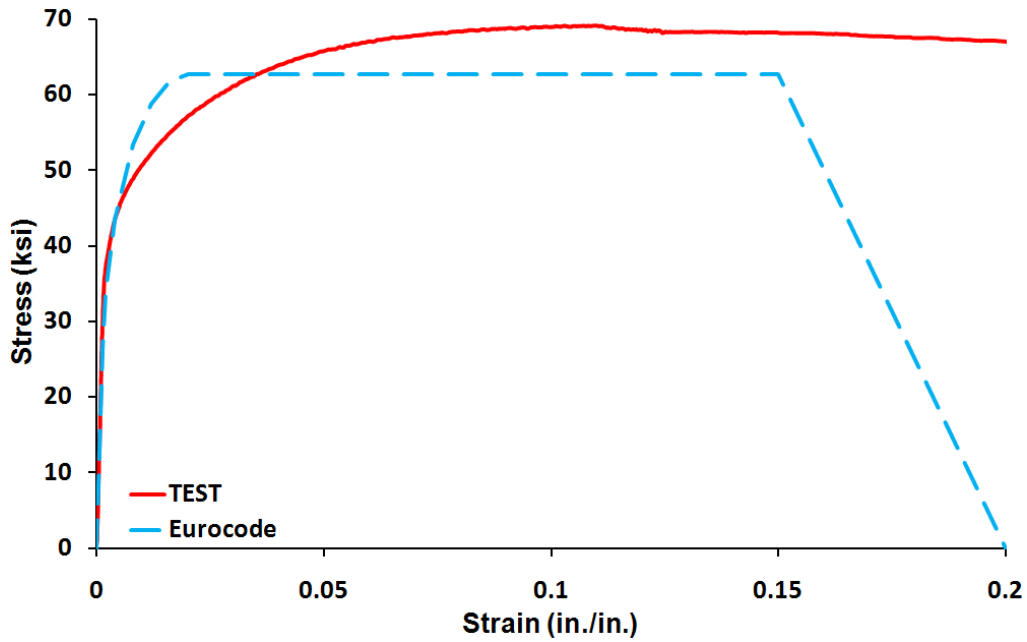


*Figure 3.14 Stress-strain curve comparison between test data and Eurocode 3 - 400°C
- 0.1 inch/min*

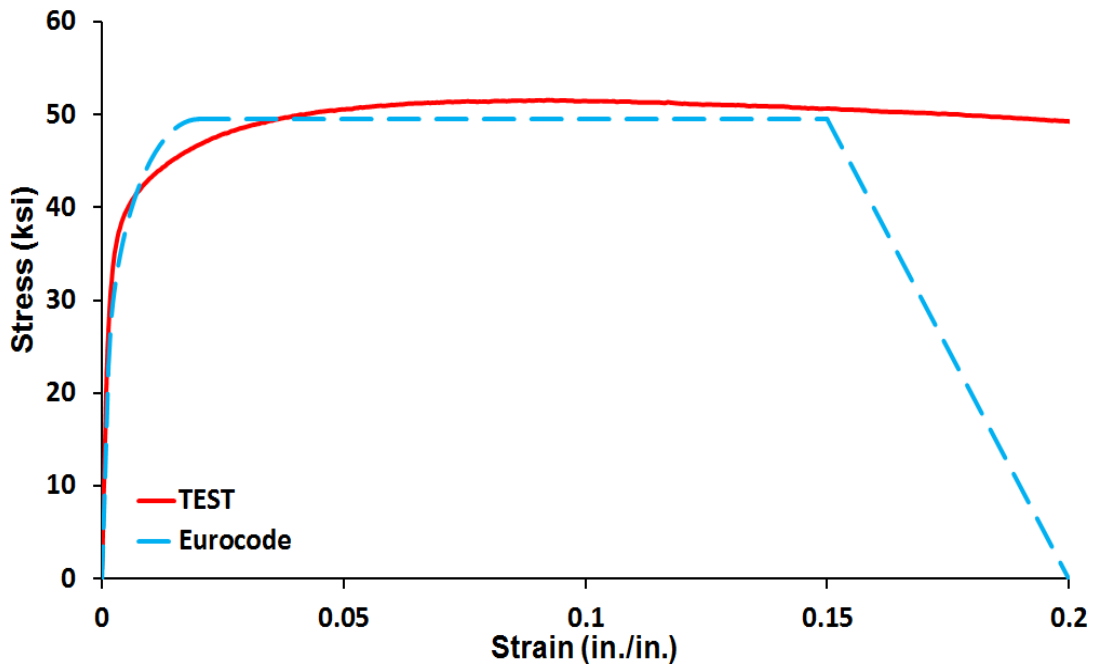


*Figure 3.15 Stress-strain curve comparison between test data and Eurocode 3 - 500°C
- 0.1 inch/min*

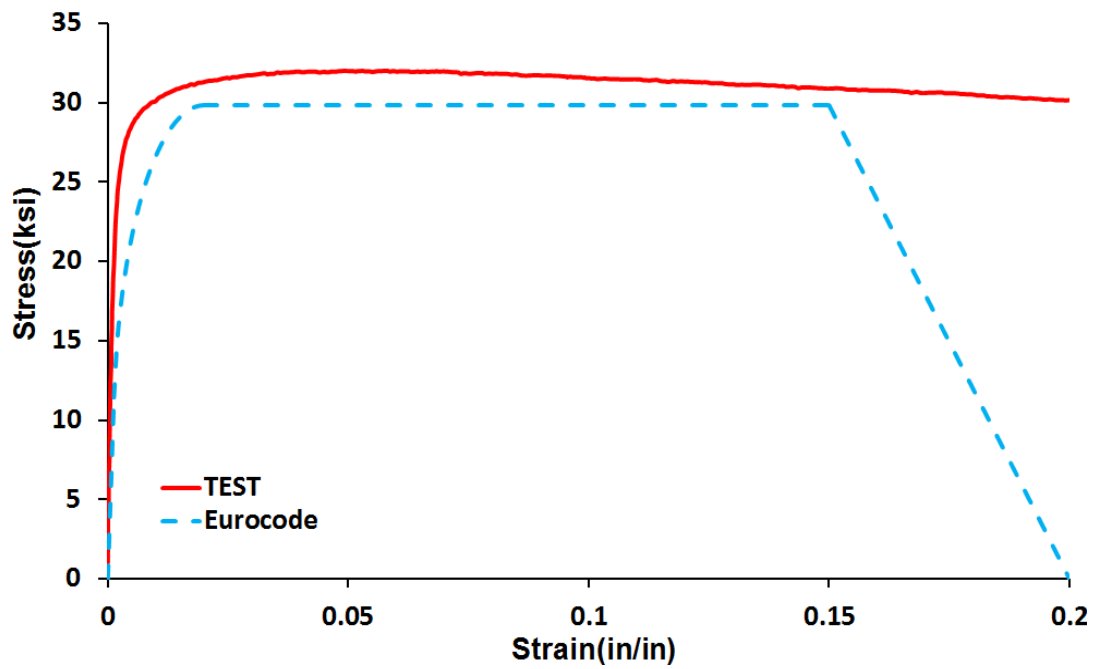


Figure 3.16 Stress-strain curve comparison between test data and Eurocode 3 - 600°C
- 0.1 inch/min

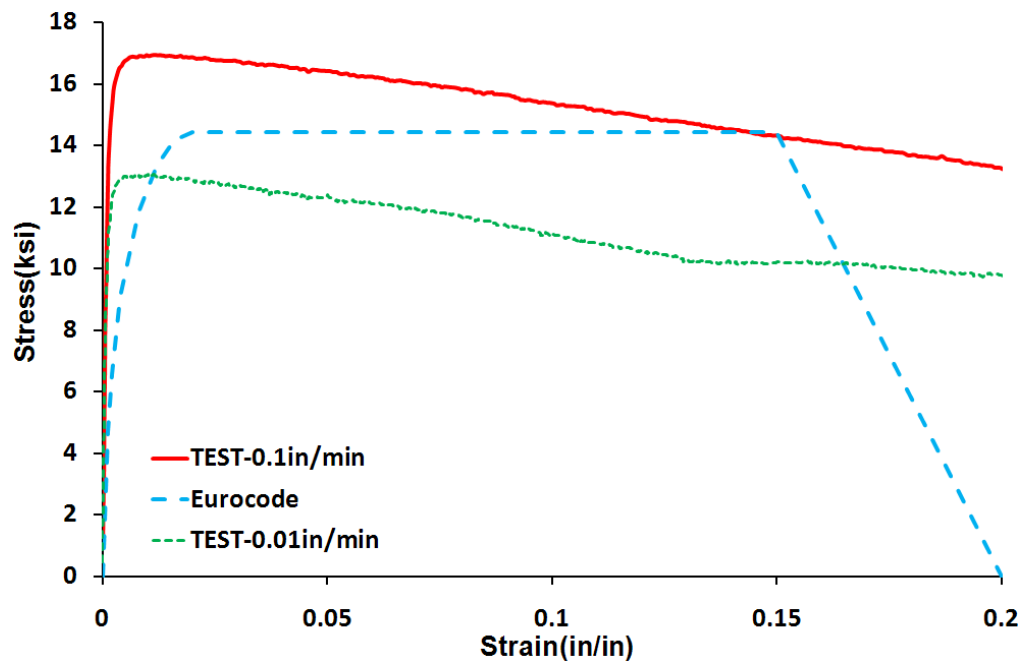


Figure 3.17 Stress-strain curve comparison between test data and Eurocode 3 - 700°C

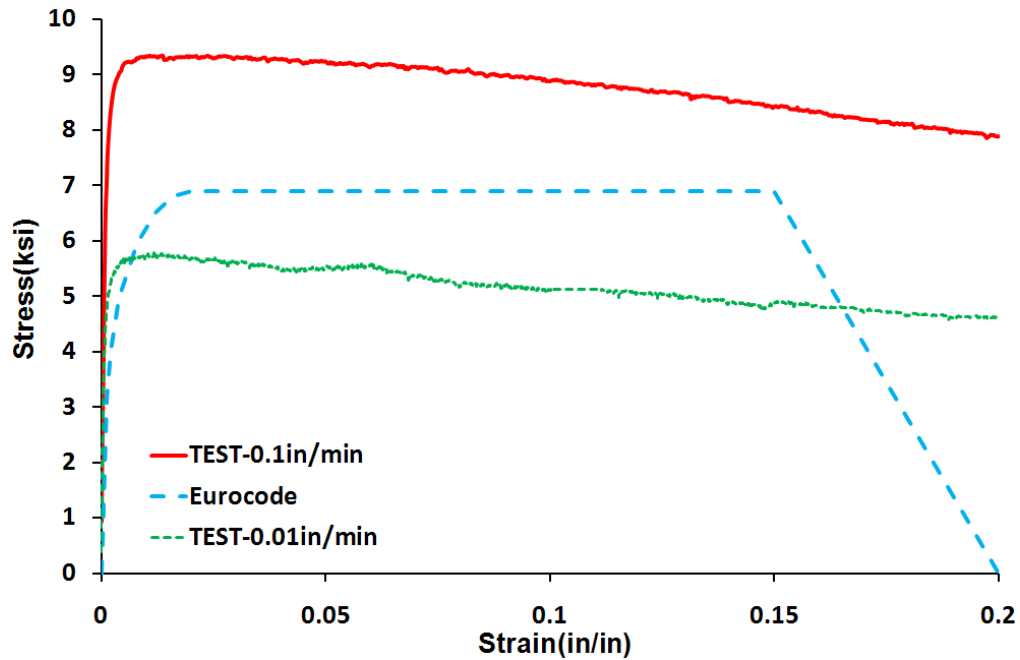


Figure 3.18 Stress-strain curve comparison between test data and Eurocode 3 - 800°C

3.3.3 Yield Strength

Yield strength reduction factors based on data collected in these tests are plotted in Figure 3.19 through Figure 3.21, and compared to reduction factors defined by Eurocode 3 (2006) and by AISC (2005). The yield strength reduction factor is defined as the yield strength at elevated temperature divided by the yield strength at ambient temperature.

At temperatures above approximately 200°C to 300°C, steel does not exhibit a well-defined yield plateau. Consequently, defining yield strength becomes more subjective at elevated temperatures than at ambient temperature. For steels that do not exhibit a yield plateau, the 0.2-percent offset yield strength definition is widely used and is specified by ASTM E21 (ASTM 2005) for defining the yield strength of metals at elevated temperatures. With this method, yield strength is defined as the stress at the intersection of the stress-strain curve and the proportional line off-set by 0.2-percent strain. The reduction factors of 0.2-percent offset yield strength obtained from

displacement rates of 0.01 and 0.1 inch/min tests are compared with the Eurocode 3 and AISC reduction factors in Figure 3.19. It can clearly be seen that, from 100°C to 500°C, the yield strength from tests at both crosshead rates are significantly lower than the values specified by Eurocode 3 and the AISC specification.

The 0.5-percent yield strength definition is also sometimes used and defined as the stress value at 0.5-percent strain. Figure 3.20 shows a comparison of the reduction factor of 0.5-percent yield strength obtained from tests at both displacement rates with the Eurocode 3 and AISC specification. Again, test results gave significant lower values from 100°C to 500°C.

Based on Tilt and Both (1991), it appears that the structural steel yield strengths at elevated temperatures used in Eurocode 3 were obtained from British Steel Corporation data (Kirby and Preston 1988), in which yield strength was defined as the stress at 2-percent total strain. Figure 3.21 shows a comparison of the reduction factor of 2-percent yield strength obtained from tests at both loading rates with the Eurocode 3 and AISC specification. It can be seen that all curves agree well.

As is clear from these figures, the yield strength of steel at elevated temperatures up to about 600°C is highly dependent on the manner in which yield strength is defined. It appears that Eurocode 3 and AISC have chosen to define yield strength as the stress at 2-percent total strain. However, little was found in the literature to support this definition of yield strength for structural-fire engineering design of steel structures. The most appropriate definition of elevated-temperature yield stress ultimately lies in how these values are used in design formulae, and further investigation and discussion of this issue appears justified.

Another questionable assumption regarding yield strength is that both Eurocode 3 and AISC specification consider a yield strength reduction factor of 1.0 for structural steel in the temperature range of 20 to 400°C. This simply implies that in structural design for fire safety, designers can assume no reduction in steel strength up to 400°C. However, as can be seen in Figure 3.22, in which stress-strain curves of ASTM A992 steel are compared at ambient temperature and 400°C, this assumption may lead to un-

conservative predictions for structural fire design applications. Therefore, further research seems necessary to investigate the most appropriate yield strength reduction factors for structural fire engineering applications.

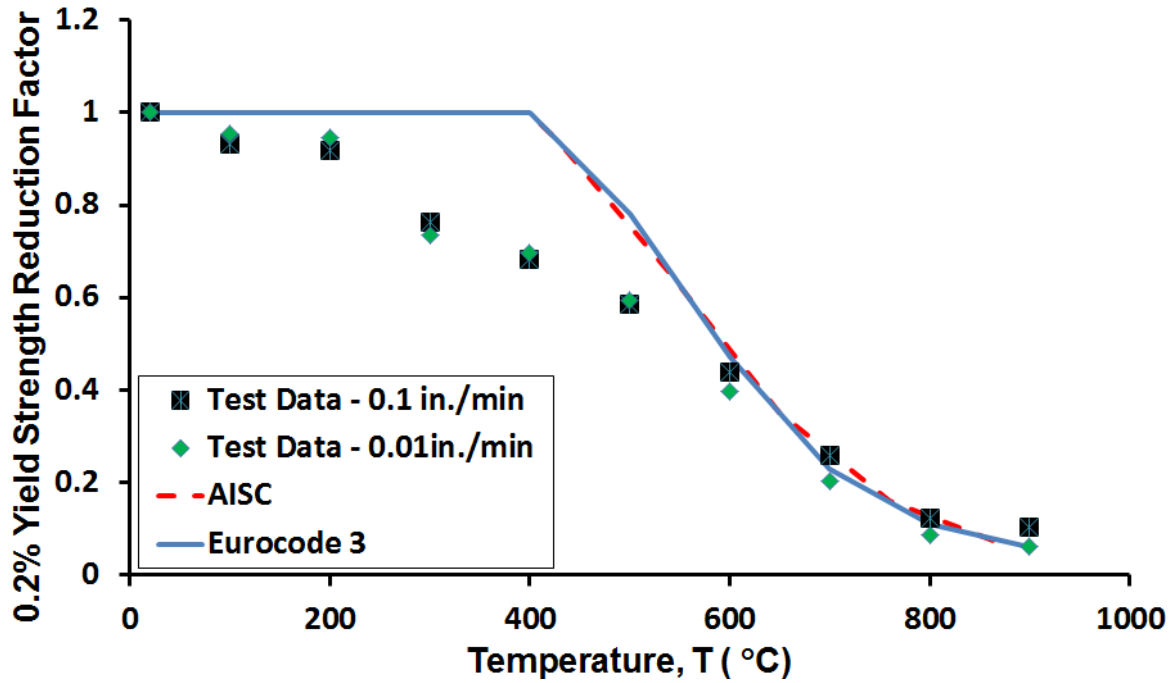


Figure 3.19 0.2-percent offset yield strength reduction factor

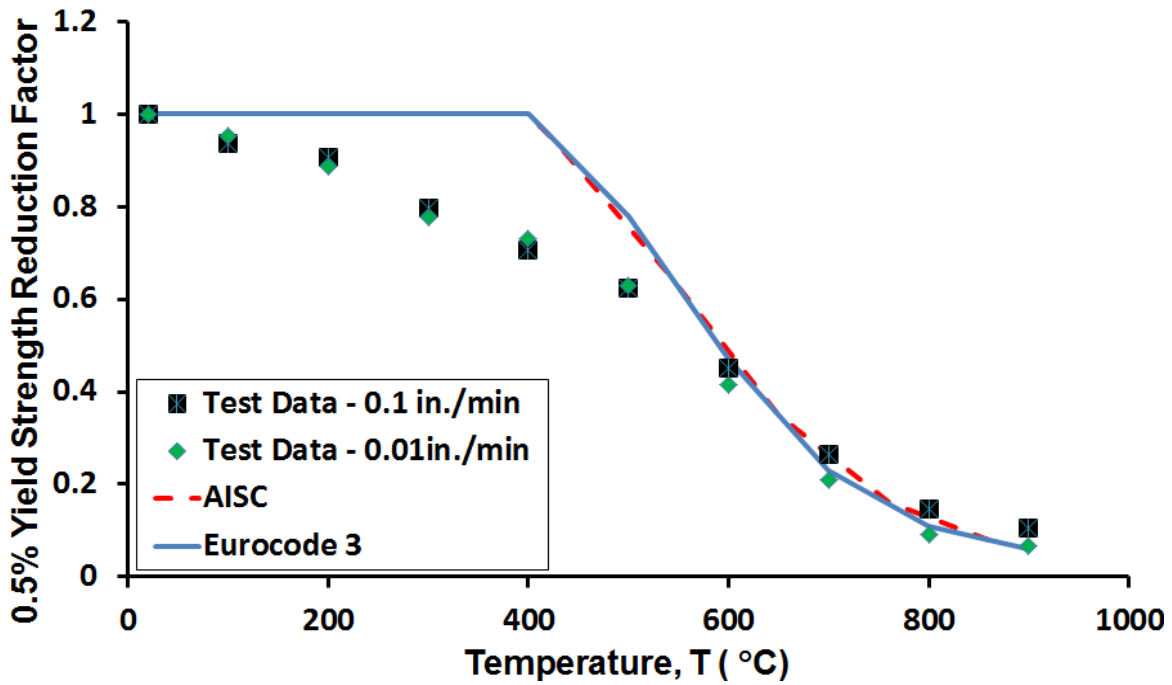


Figure 3.20 0.5-percent yield strength reduction factor

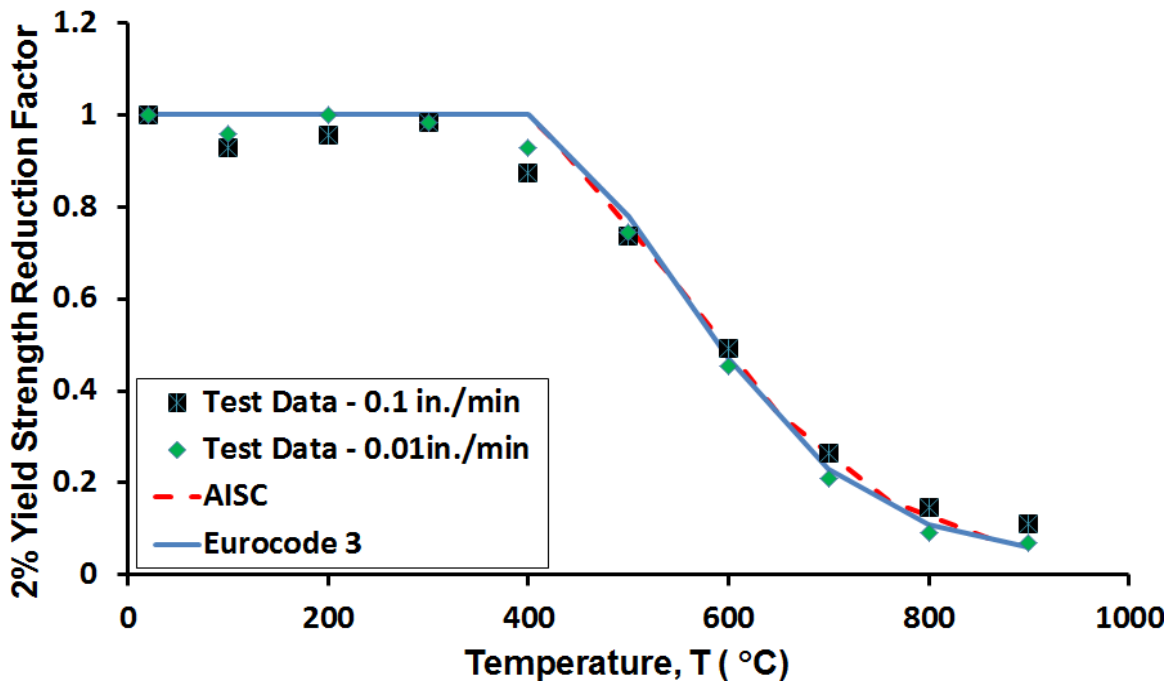


Figure 3.21 2-percent yield strength reduction factor

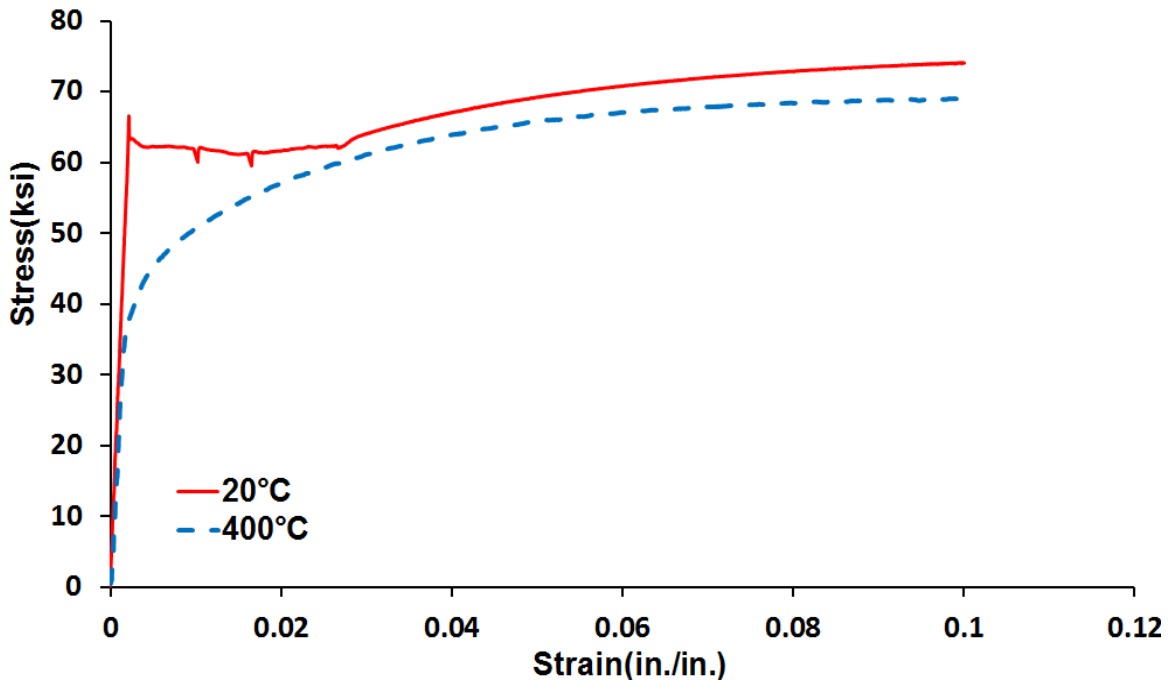


Figure 3.22 Stress-strain curves compared at temperatures 20°C and 400°C

3.3.4 Tensile Strength

The reduction factor for tensile strength, obtained at both displacement rates, is also compared with the corresponding values in Eurocode 3 and the AISC specification in Figure 3.23. In this figure, the tensile strength reduction factor is defined as the tensile strength measured at elevated temperature divided by the yield strength measured at ambient temperature. The data is presented in this manner as this is how the tensile strength reduction factor is defined in the AISC Specification (2005). For temperatures at and above 400°C, both Eurocode 3 and AISC take the elevated-temperature tensile strength equal to the elevated-temperature yield strength. Thus, at temperatures at and above 400°C, steel has an effective yield ratio (F_y/F_u) equal to 1.0. High yield ratios can contribute to non-ductile behavior of steel structures, as there is little margin between

yield and fracture. Whether this is a factor in the fire performance of steel structures may require further investigation.

Finally, Figure 3.24 shows the tensile strength reduction factor from these tests, where the reduction factor is defined as tensile strength measured at elevated temperature divided by the tensile strength measured at ambient temperature. This is a more conventional definition of tensile strength reduction factor. The reduction factor obtained from these tests are also shown in Table 3.2.

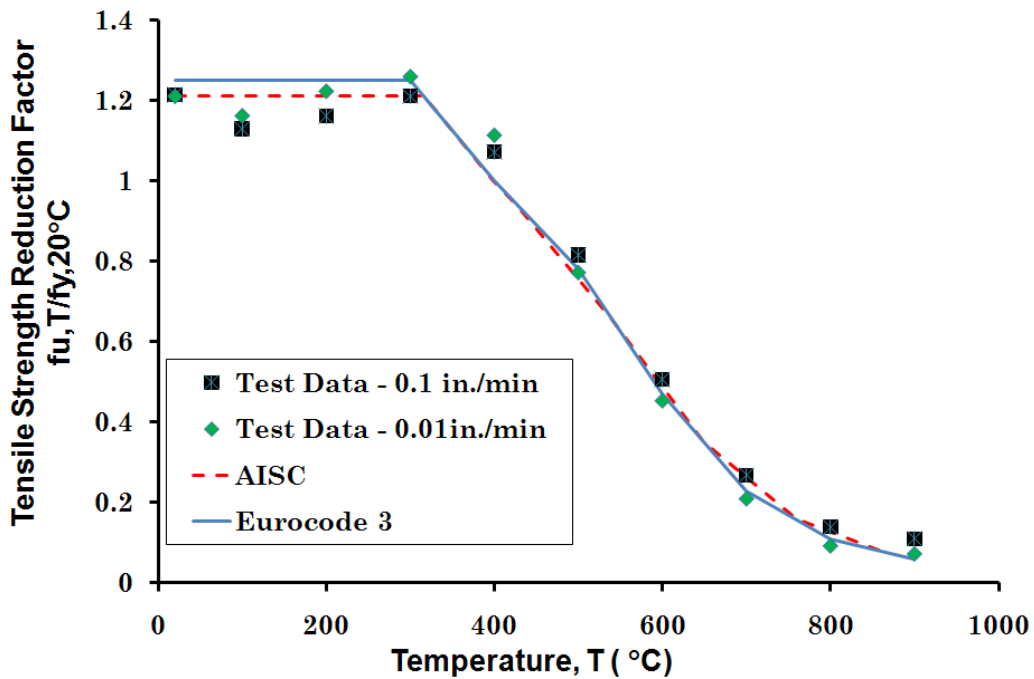


Figure 3.23 Tensile strength reduction factor $f_{u,T}/f_{y,20}$

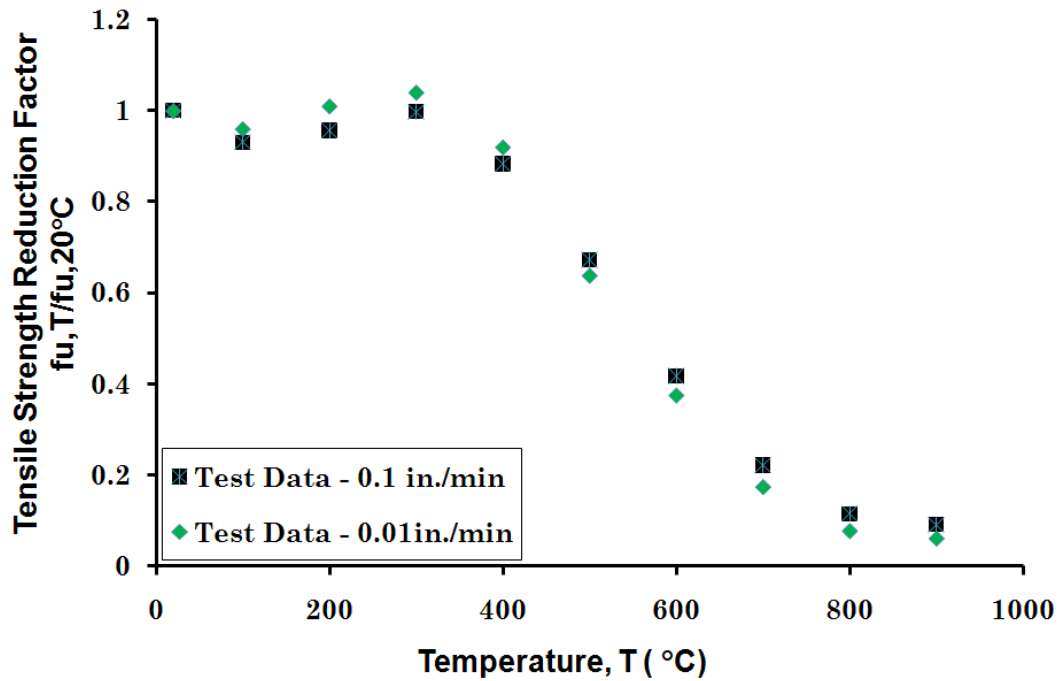


Figure 3.24 Tensile strength reduction factor $f_{u,T}/f_{u,20}$

Table 3.2 Tested tensile strength reduction factor

Temperature (°C)		20	100	200	300	400	500	600	700	800	900
Reduction Factor	0.01 in/min	1.00	0.96	1.01	1.04	0.92	0.64	0.37	0.17	0.08	0.06
	0.1 in/min	1.00	0.93	0.96	1.00	0.88	0.67	0.42	0.22	0.11	0.09

3.3.5 Elastic Modulus

The elastic modulus was determined by monitoring the slope of the initial linear elastic portion of the stress–strain curves. Compared to Eurocode 3 and the AISC specification in Figure 3.25, the test results show an overall good agreement.

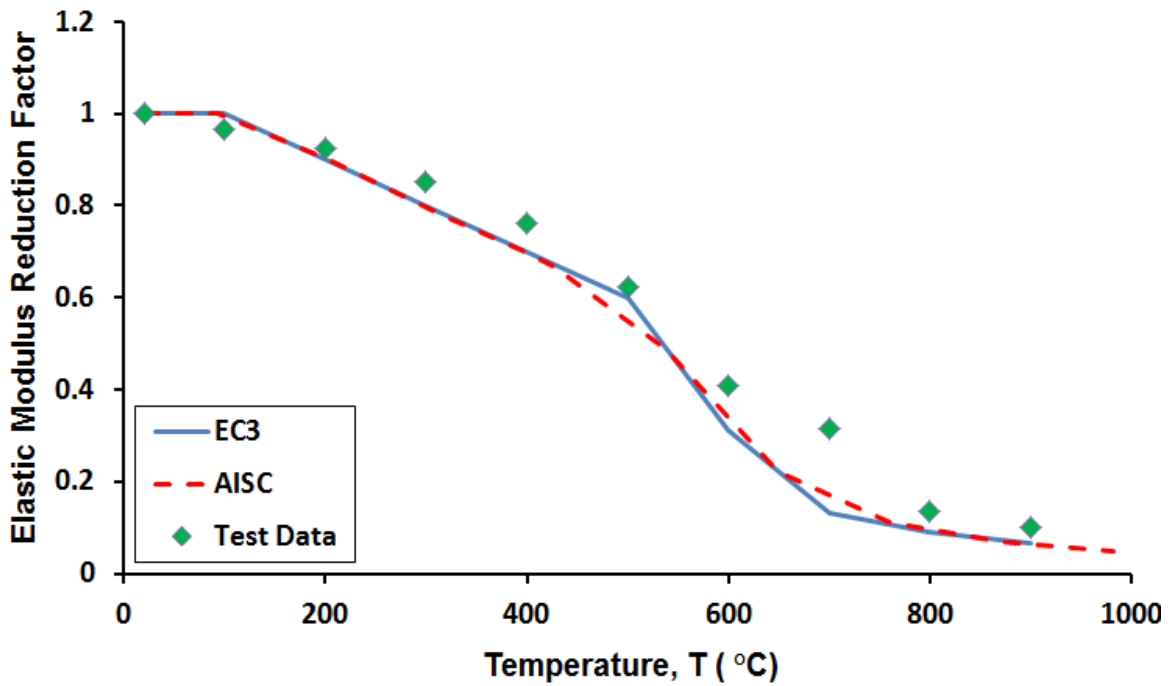


Figure 3.25 Elastic modulus reduction factor

3.3.6 Proportional Limit

The proportional limit was determined by monitoring the highest stress at which the curve in a stress-strain diagram is a straight line. At room temperature, the proportional limit is about same as the yield strength. However, at high temperatures, proportional limits are usually lower than yield strength due to early nonlinearity. The proportional limit is an important property for structural steel at elevated temperatures when considering stability phenomena, since the tangent modulus reduces rapidly after exceeding the proportional limit.

In this study, the test results match well with Eurocode 3 over most of the temperature range (Figure 3.26).

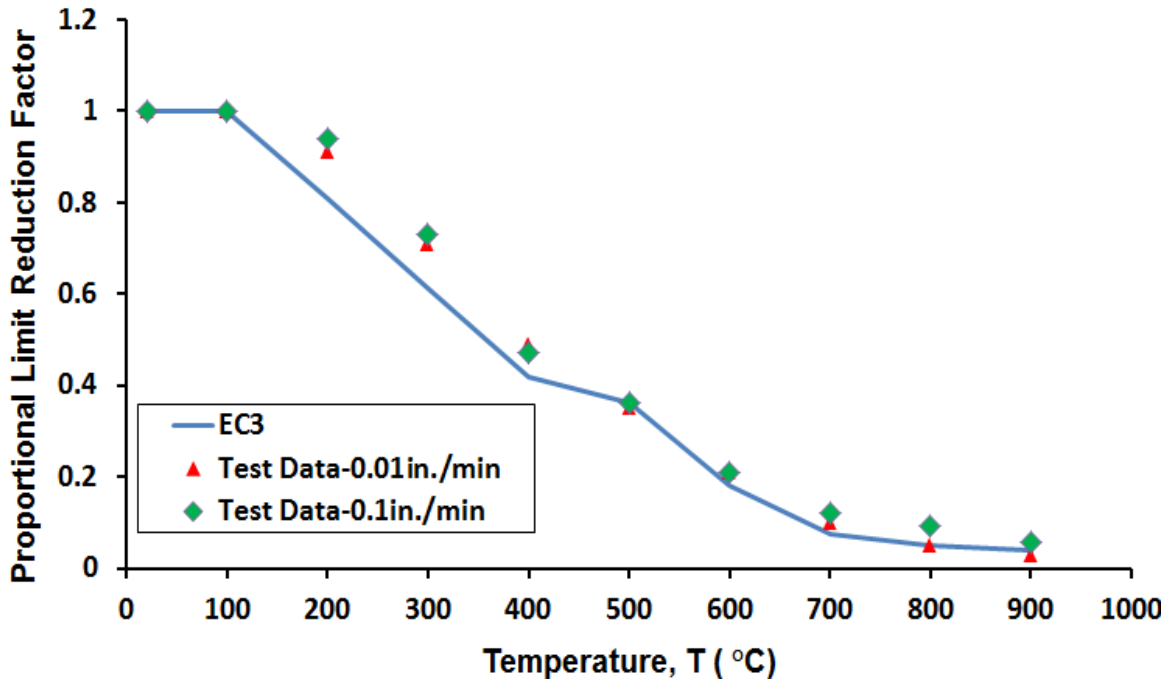


Figure 3.26 Proportional limit reduction factor

3.3.7 Effect of Crosshead Displacement Rates

Loading rate can have a significant effect on the measured stress-strain curves of structural steel, and this effect appears to be more pronounced at elevated temperatures. Figure 3.27 shows the comparison of stress-strain curves for crosshead displacement rates of 0.01 and 0.1 inch/min at temperatures from 600°C to 800°C. At these temperatures, the displacement rate of 0.1 inch/min results in yield and tensile strengths 30-40-percent higher than those obtained at 0.01 inch/min. This data suggests the importance of controlling and reporting loading rates in elevated temperature tests on structural steel materials, members and connections, and in considering rate effects in overall analysis and design of steel structures for fire conditions.

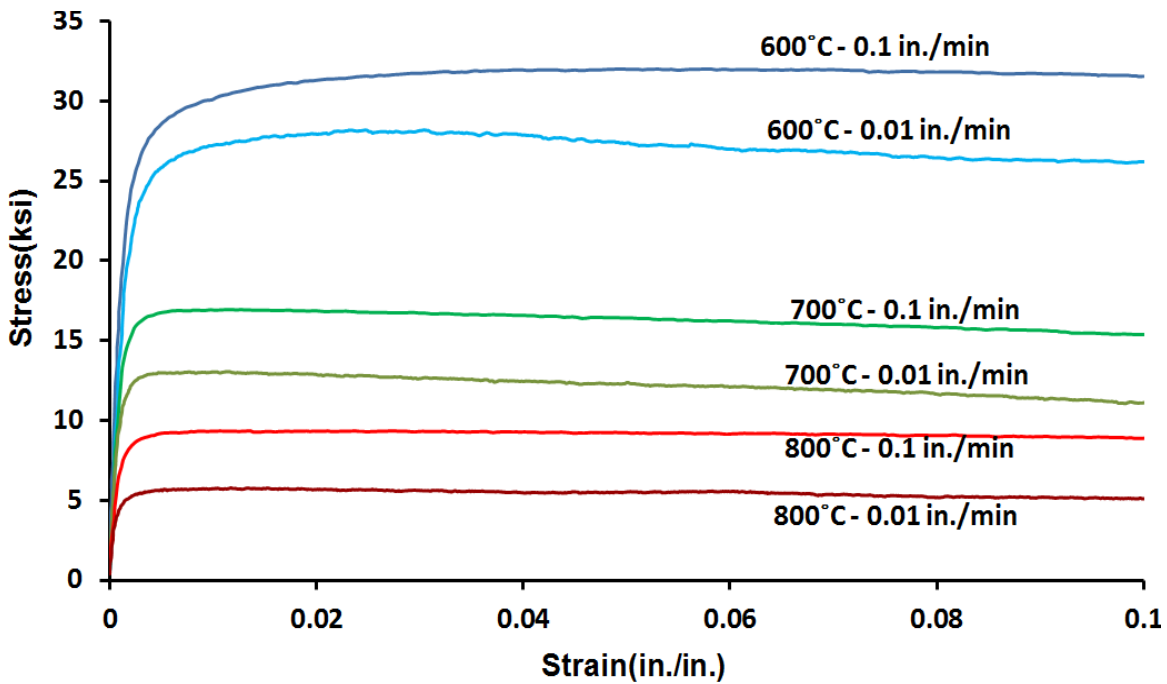


Figure 3.27 Stress-strain curves compared at two different crosshead rates

3.3.8 Static Yield Stress

In ambient temperature testing, static yield stress values are often measured in coupon tests to provide a zero-strain rate evaluation of yield stress. Static yield values are useful in research for comparing member and material tests at comparable strain rates (SSRC 1987) and are useful in the development of design rules that properly account for loading rate effects (Beedle and Tall 1960). Static yield stress values at ambient temperature are obtained by stopping the machine crossheads and holding the crossheads at a fixed displacement for 3 to 5 minutes, and then reading the value of stress. In these elevated-temperature tests, the static stress-strain relationship was examined by suspending crosshead movement for about 30 and 3 minutes in the slow tests (0.01 inch/min) at different temperatures. The resulting stress-strain curves are shown in Figure 3.28. Compared with dynamic yielding, static yielding produced significantly lower values of steel strength at high temperatures. At 800°C, the steel strength almost dropped

to 0 after a 30 minute crosshead hold. The significant difference between static and dynamic yielding reflects the influence of creep at high temperatures. Interestingly, at 300°C such static yielding behavior tests increased the tensile strength of structural steel, which may be due to strain aging phenomenon at that temperature. The data in Figure 3.28 further illustrate the importance of rate effects on the effective strength of steel at elevated temperature and the influence of creep. These factors are often neglected in describing the high temperature stress-strain response of structural steel, but appear to be very important phenomena that merit further investigation.

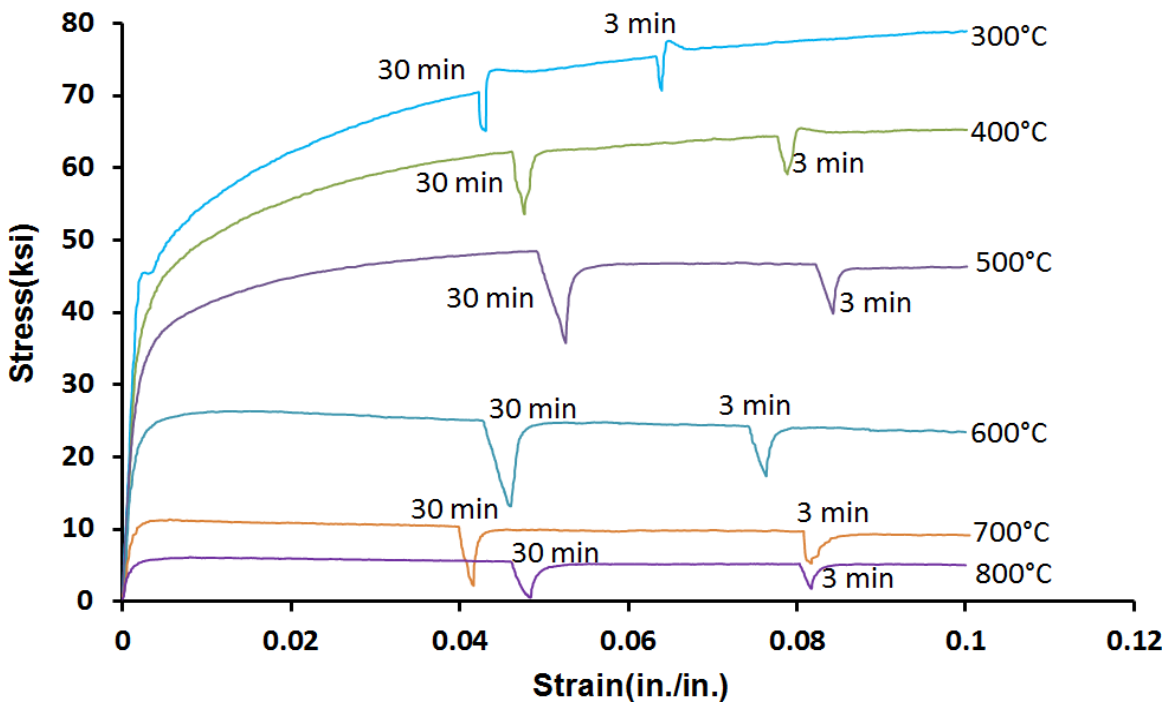


Figure 3.28 Static yield phenomenon at elevated temperatures for ASTM A992 steel

To evaluate the significance of creep further, data in Figure 3.28 will be presented in the form of a stress relaxation curve. A representative result from the static yield test at 700°C and for a crosshead displacement hold of 30 min is shown in Figure 3.29. This figure shows the relaxation in stress versus time response. To be more specific, a steel coupon was heated to 700°C and then loaded to a stress of about 10 ksi. Loading was

then stopped, the strain was then held constant for a period of 30 min, and the relaxation in stress was measured. As indicated by the data in Figure 3.29, the steel exhibited a quite large relaxation of stress (from about 10 to 2 ksi), indicating a considerable influence of creep on the material response.

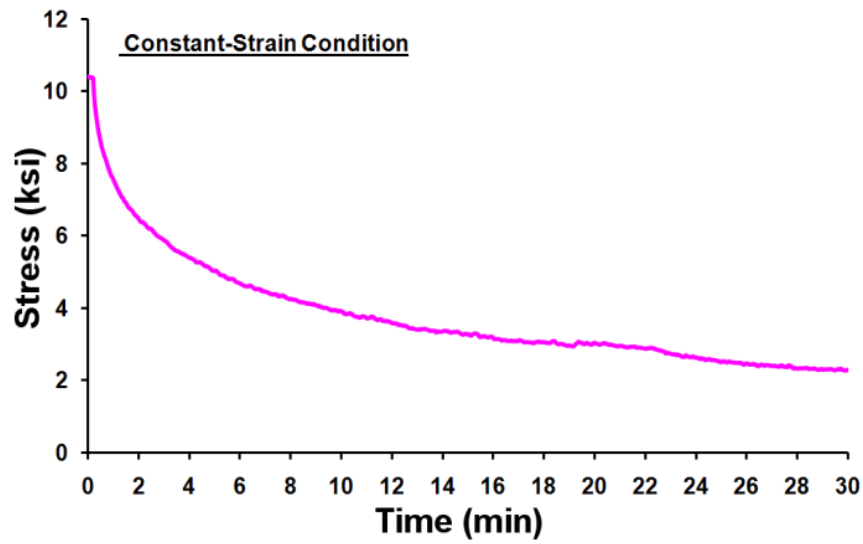


Figure 3.29 Stress relaxation test for ASTM A992 steel at 700°C

3.4 CONCLUSIONS

Results of an experimental program on the material properties of ASTM A992 structural steel at elevated temperatures have been presented in this chapter. Steady state tension coupon tests were conducted at temperatures up to 900°C. Full stress-strain curves at elevated temperatures were obtained. The yield strength, tensile strength, elastic modulus and proportional limit obtained from the tests were compared with values specified by Eurocode 3 and the AISC Specification. The measured values of yield strength agree well with Eurocode 3 and AISC, when yield strength is defined as the stress at 2-percent strain. However, for more conventional definitions of yield strength, such as the 0.2-percent offset yield strength, the agreement is poor. The yield strength of steel at elevated temperatures up to about 600°C is highly dependent on the manner in

which yield strength is defined, and the justification for the definition of yield stress adopted by Eurocode 3 and by AISC is unclear.

The effects of displacement loading rates of 0.1 and 0.01 inch/min on steel strength were compared and static yielding behavior was also investigated in this study. It is shown that the displacement rate has a large impact on the steel strength at elevated temperatures, especially at temperatures higher than 600°C. Further work is needed to fully characterize the time dependent effects on the elevated-temperature stress-strain response of structural steel.

As discussed earlier, an accurate stress-strain model is a key factor to simulate the structure behavior using finite element analysis. Therefore, for the FE models developed in later chapters of this dissertation, the stress-strain relationships used are mostly simplified from the test data, and the Eurocode model is only used when tested properties are not available. Further, although loading rate has a large impact on the test results due to creep effect of structural steel at high temperature, the FE models in this study will not include this time dependent material property, as this is beyond the scope of this investigation. However, reasonable loading rate is still considered. In this study the material properties will be used in the FE models are from the data of the 0.1 inch/min test, as this represents a reasonable loading rate in a structure-fire test.

CHAPTER 4

Development of Finite Element Models

4.1 OVERVIEW

As part of this research program, the behavior of beam end framing connections in fire was studied by experiments and by finite element (FE) models. This chapter describes in detail the development of three dimensional FE models for predicting the thermal and structural behavior of steel beam and beam end framing connections in fire. The capabilities and limitations of the models are then evaluated by comparison with experimental data reported in the literature. Further evaluation of the FE models are made by comparison with the experiments on beam end connections described in Chapter 5. The FE models were used to conduct a series of parametric studies on the behavior of beam end framing connections in fire, as described in Chapter 6.

The ABAQUS (Version 6.7) FE package was utilized to simulate the thermal and structural behavior of restrained steel beams subjected to heating and cooling. ABAQUS was also used to develop detailed models of the beam end connections. ABAQUS was used both for heat transfer analysis and for structural analysis. For heat transfer, ABAQUS is capable of modeling convective and radiative heat transfer at the interface of the fire environment and the surface of a structural member, and conductive heat transfer within the member. Temperature dependent thermal properties can be incorporated in the analysis. For structural analysis, ABAQUS is capable of modeling material and geometric nonlinearities and can incorporate temperature dependent material properties.

4.2 OVERALL APPROACH FOR THERMAL-STRUCTURAL ANALYSIS

The analysis of a member subjected to fire consists of two sequential analysis steps: (1) thermal analysis (heat transfer analysis), and (2) structural analysis. The heat

transfer analysis is conducted first to obtain temperature distributions within the structure as a function of time during the course of a specified fire event, where the fire is normally characterized in terms of a gas temperature versus time relationship. Details of the FE heat transfer analysis are described in Section 4.3 below.

Once the heat transfer analysis is completed, the temperatures computed within the member are then used in the structural analysis to compute the structural response of the member under the action of the internal time varying temperatures and any specified external loads. The details of the FE structural model are described in Section 4.4.

In the analysis approach used herein, the heat transfer analysis is uncoupled from the structural analysis. This approach assumes that the structural analysis has no effect on the heat transfer analysis. This simplification may introduce errors in some situations. For example, if the structural analysis predicts large movement of a member, the member may move closer or farther from the fire and thereby affect heat transfer to the member. However, in most practical situations, it is believed that an uncoupled heat transfer and structural analysis provide reasonable results.

4.3 THERMAL ANALYSIS OF STEEL BEAMS IN FIRE

4.3.1 Heat Transfer Mechanisms

For structure-fire problems, three key modes of heat transfer must be modeled. These are convection and radiation at the interface of the fire environment and the surface of the structural member, and conduction within the member. These modes of heat transfer are briefly reviewed below. Further background can be found in standard texts on heat transfer (see for example, Incropera et al 2007), and in Buchanan (2002). Figure 4.1 qualitatively illustrates the heat transfer mechanism involved in structure-fire problems.

4.3.1.1 Conduction

Conduction is the mechanism for heat transfer in solid materials. Conductive heat transfer is governed by Fourier's law, which in one-dimension can be written as Equation 4.1:

$$\dot{q}'' = -k \frac{dT}{dx} \quad (4.1)$$

In this equation, \dot{q}'' is heat flux (heat energy per unit time per unit area), k is the thermal conductivity of the material, and T is the temperature. The quantity dT/dx is the temperature gradient in the solid.

Fourier's law combined with heat balance in a solid can be used to derive the heat diffusion equation, which governs transient heat conduction. The three dimensional heat diffusion equation can be written in the form of Equation 4.2:

$$\frac{\partial T}{\partial t} = \frac{k}{\rho c} \nabla^2 T = \frac{k}{\rho c} \left(\frac{\partial^2 T}{\partial x^2} + \frac{\partial^2 T}{\partial y^2} + \frac{\partial^2 T}{\partial z^2} \right) \quad (4.2)$$

In this equation, T is temperature, t is time, k is thermal conductivity, ρ is density, and c is specific heat. In general, the values of k , ρ and c are temperature dependent.

4.3.1.2 Convection

Convection is transfer of heat at the interface of a fluid and a solid. In structure-fire problems, convective heat transfer occurs at the interface of the hot fire gases and the surface of a solid, or at the interface of cool air and a solid (for portions of a member not exposed to hot gases). The basic equation for convection heat transfer is given by Equation 4.5:

$$\dot{q}'' = h(T_\infty - T_s) \quad (4.5)$$

Where \dot{q}'' is heat flux at the fluid-solid interface, T_∞ is the fluid temperature, T_s is the material surface temperature, and h is the convective heat transfer coefficient. For the components exposed to fire, T_∞ is taken as the gas temperature T_f . For portions of members not exposed to hot gases (for example, the unexposed side of a beam), T_∞ is normally taken as ambient temperature. The convective heat transfer coefficient h is

typically estimated to be in the range of 25 to 35 W/m²K for the surface exposed to the fire and in the range of 5 to 10 W/m²K for surfaces not exposed to fire (Franssen et al 2009).

4.3.1.3 Radiation

Radiation is defined as heat transfer by electromagnetic waves. Radiation is normally the dominant mode of heat transfer between the fire environment and the surface of a structural member (Buchanan 2002).

The radiant heat flux that is incident on a surface exposed to fire is given by:

$$\dot{q}'' = \varphi \varepsilon_e \sigma T^4 \quad (4.6)$$

where, φ is the configuration factor, σ is the Stefan-Boltzmann constant which is equal to 5.67×10^{-8} W/m²K⁴, ε_e is the emissivity of the emitting surface and T is the absolute temperature of the emitting surface in K.

In structure-fire heat transfer analysis, it is often assumed that combustion fire gases are the primary source of radiant emissions and that the hot gases are in close contact with the structural members (so that $\varphi=1$). The net heat flux transferred to the surface of the structural member by radiation from the hot gases can then be expressed as follows:

$$\dot{q}'' = \varepsilon_r \sigma (T_f^4 - T_s^4) \quad (4.7)$$

In this equation, T_f is the fire gas temperature (K), T_s is the temperature of the surface of the structural member, and ε_r is the resultant emissivity between the fire gases and the surface of the structural member. The resultant emissivity can be expressed as follows:

$$\varepsilon_r = \frac{\varepsilon_1 \varepsilon_2}{\varepsilon_1 + \varepsilon_2 - \varepsilon_1 \varepsilon_2} \quad (4.8)$$

where ε_1 is the emissivity of the fire gases and ε_2 is the emissivity of the surface of the structural member. Values of ε_r in the range of 0.7 to 0.8 are typically suggested for bare

steel (Franssen et al 2009). A value of ε_r equal to 0.8 was used for the heat transfer analysis in this dissertation.

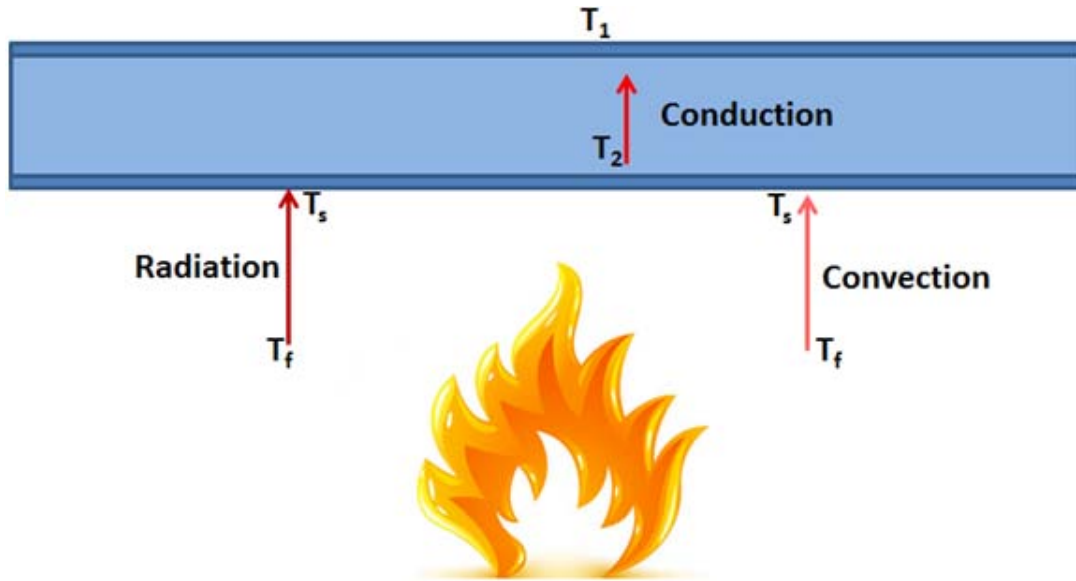


Figure 4.1 Three heat transfer mechanisms involved in structure-fire problems

4.3.2 Analysis

In the heat transfer analyses, fire conditions are modeled as a hot gas in contact with the structural member. Therefore, the fire environment is represented by a gas temperature (T_f) versus time curve. From the gas temperature, the convective and radiative heat flux entering the surface of the member is computed from Equations 4.5 and 4.7 above. The heat flux at the surface then serves as a boundary condition for solving the heat diffusion equation (Equation 4.2) for transient heat conduction in the member. In carrying out the conduction analysis, temperature dependent material properties are used. In all of the analyses, the initial (ambient) temperature is taken as 20°C.

4.3.3 Element Selection

ABAQUS provides several types of element for FE analysis such as solid elements, shell elements, beam elements, membrane elements and truss elements. In this study, a 3-D element (DCC3D8), defined as an eight-node convection/diffusion brick element, was employed for heat transfer analysis of steel members as well as for insulation (fireproofing) on the steel members, when present (Figure 4.2). A conduction contact surface was established at the interface of the steel and the insulation material.

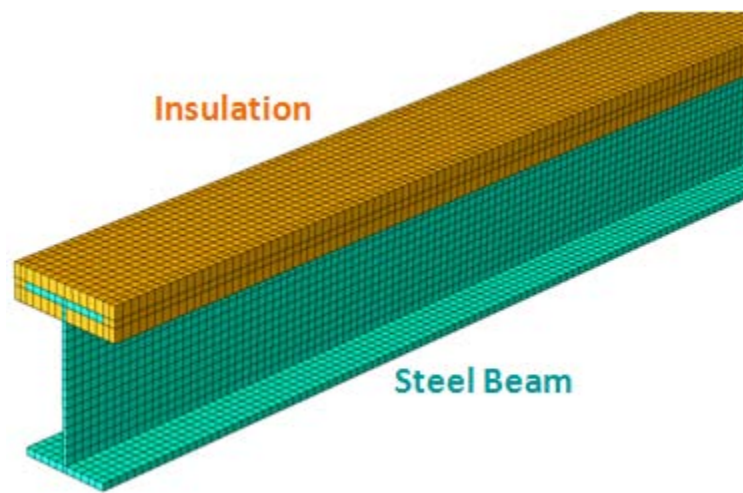


Figure 4.2 Heat transfer FE model of steel beam and insulation

4.3.4 Thermal Properties of Steel

The thermal properties of steel are temperature dependent parameters. In this study, the thermal properties given by the Eurocode 3 (2006) were used.

The thermal conductivity of steel, k (W/mK), can be determined by the following equations:

$$k = \begin{cases} 54 - 3.33 \times 10^{-2} T & \text{for } 20^{\circ}\text{C} < T < 800^{\circ}\text{C} \\ 27.3 & \text{for } 800^{\circ}\text{C} < T < 1200^{\circ}\text{C} \end{cases} \quad (4.9)$$

Or by the following table:

Table 4.1 Thermal conductivity of structural steel (Eurocode 3 2006)

Temperature (°C)	20	100	200	300	400	500	600	700	800	900	1000
Conductivity (W/mK)	53.3	50.7	47.3	44.0	40.7	37.4	34.0	30.7	27.3	27.3	27.3

The thermal conductivity of steel varies with temperature as shown in Figure 4.3, reducing linearly from 53.3 W/mK at 20°C to 27.3 W/mK at 800°C, and then keeping constant up to 1200°C.

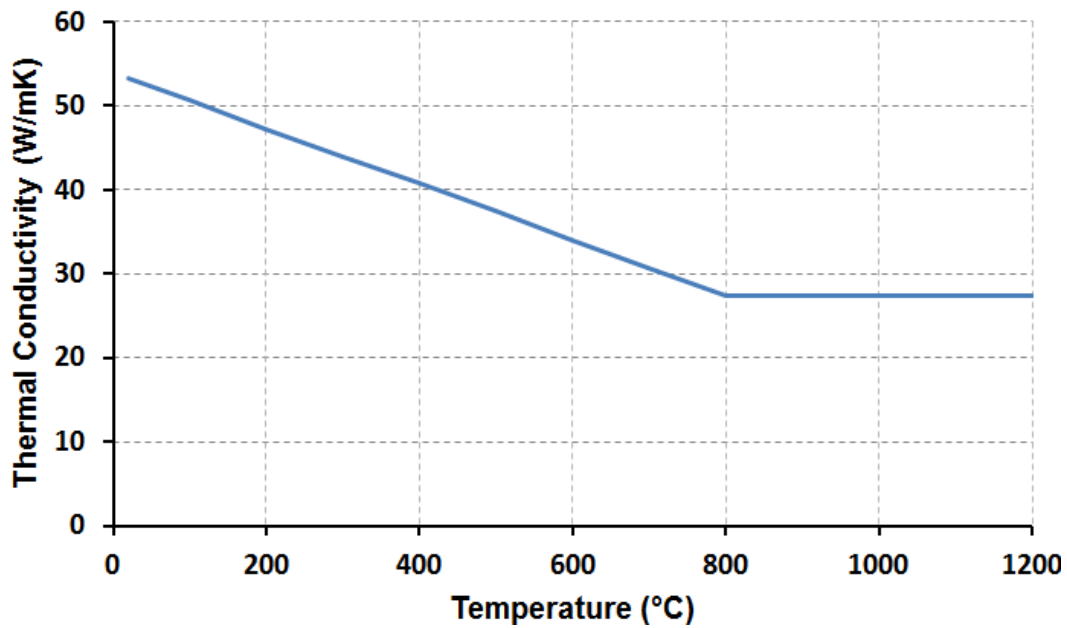


Figure 4.3 Thermal conductivity of carbon steel as a function of the temperature (Eurocode 3 2006)

Specific heat capacity is the amount of heat required to raise the temperature of a unit mass of material by one degree, with units of J/kgK. The variation of specific heat of steel with temperature is defined in Eurocode 3 and can be illustrated by Figure 4.4. A peak in specific heat occurs at about 730°C, corresponding to a phase change that occurs in carbon steel at this temperature.

The density of steel was taken as $\rho = 7850 \text{ kg/m}^3$ in this calculation, remaining essentially constant with temperature.

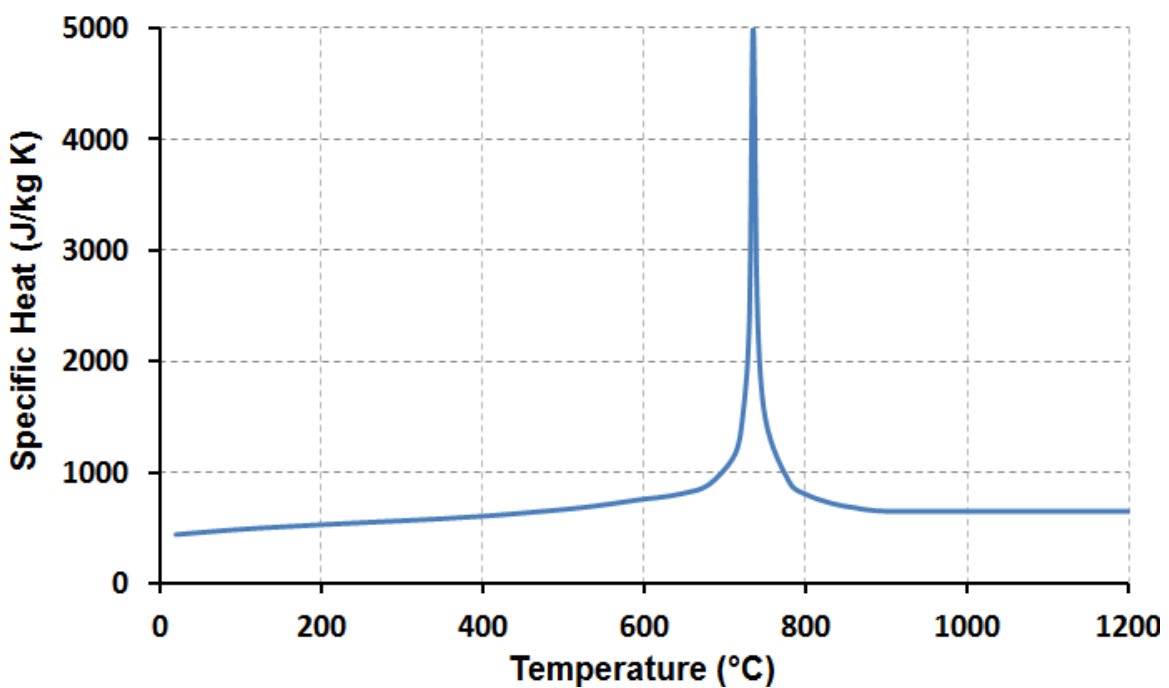


Figure 4.4 Specific heat of carbon steel as a function of the temperature (Eurocode 3 2006)

4.3.5 Thermal Expansion of Steel

The thermal expansion strain (ε_{th}) of steel is given by Equation 4.11 (Eurocode 3 2006):

$$\varepsilon_{th} = \begin{cases} -2.416 \times 10^{-4} + 1.2 \times 10^{-5} T + 0.4 \times 10^{-8} T^2 & \text{for } T \leq 750^\circ\text{C} \\ 0.011 & \text{for } 750^\circ\text{C} < T \leq 860^\circ\text{C} \\ -0.0062 + 2 \times 10^{-5} T & \text{for } T > 860^\circ\text{C} \end{cases} \quad (4.10)$$

A graphical representation of thermal elongation ($\Delta l/l$) of steel at different temperatures is shown in Figure 4.5. The step change in the temperature range 750°C-860°C is due to a phase change in the steel.

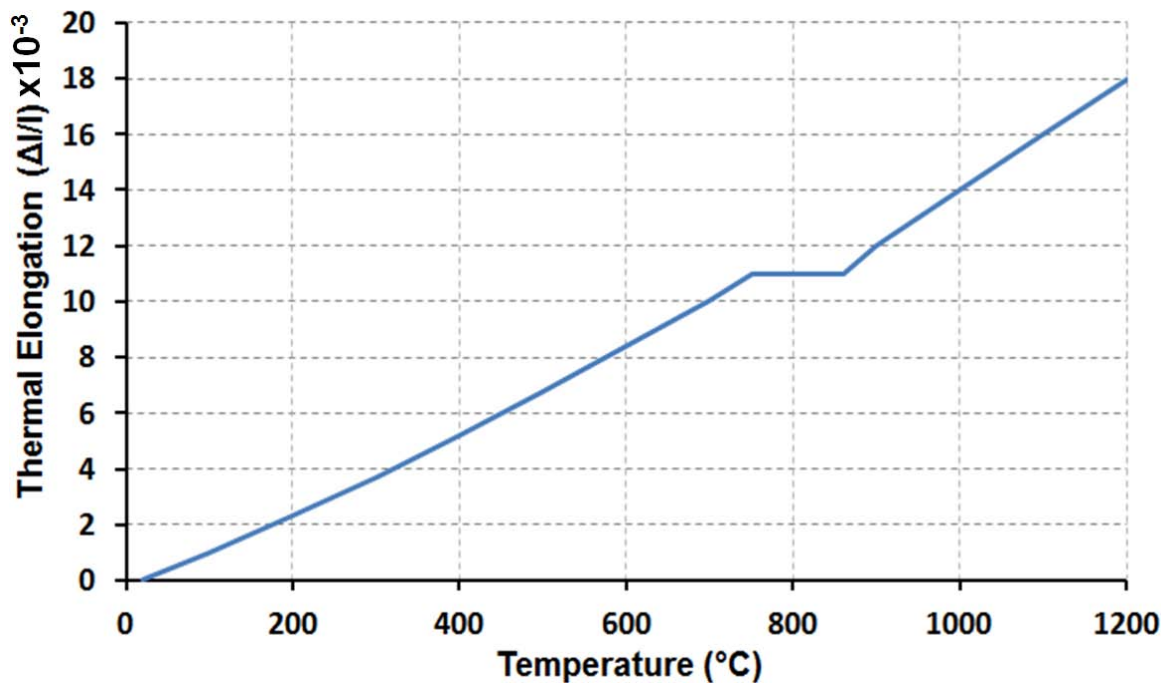


Figure 4.5 Thermal elongation of carbon steel as a function of the temperature (Eurocode 3 2006)

4.3.6 Thermal Properties of Insulation Materials

Like steel, the thermal properties of insulation materials, such as thermal conductivity and specific heat, and even density are temperature dependent. However, very little data is available in the literature on temperature dependent thermal properties

of commercially available insulation materials used for fire protection of steel. Typical properties of common insulation materials used for fire protection of steel are available in the literature, and are listed in Table 4.2.

Table 4.2 Density and thermal conductivity of different insulation materials (ECCS 1995)

Material	Density (kg/m ³)	Thermal Conductivity (W/mK)	Specific Heat (J/kgK)
Sprayed mineral fiber	300	0.12	1200
Perlite or vermiculite plaster	350	0.12	1200
Fiber-silicate board	600	0.15	1200
Gypsum plaster	800	0.2	1700
Compressed fiber board	150	0.2	1200

4.3.7 Heat Transfer FE Model Evaluation

The capabilities and limitations of the heat transfer FE model was evaluated by comparing with experimental data reported in the literature. In this section, two well documented steel beam fire tests were chosen to evaluate the FE model, and these are tests reported by Li and Guo (2007) and by Liu et al (2002). In conducting the FE analysis for comparison with experimental measurements, the thermal properties of steel given in Section 4.3.4 were used. For the properties of the ceramic fiber insulation used in these tests, the properties recommended by Lee et al (2006) were used: thermal conductivity = 0.12 W/mK, specific heat = 1130 J/kgK and density = 128 kg/m³. A resultant emissivity of 0.8 was used at bare steel surfaces, and a value of 0.3 (assumed) was used at the surface of insulation. A convective heat transfer coefficient of 25 W/m²K was used.

4.3.7.1 Model Evaluation by Experimental Data of Li and Guo

Li and Guo (2007) reported data from two experiments studying the behavior of restrained steel beams subjected to heating and cooling. Their test setup is shown in Figure 2.25. The results of both steel beam tests were used for comparison with the developed FE models.

Their tested beams were made of Q235B steel. Through material tests, the average yield strength of Q235B steel was obtained as 271 MPa. The beam-to-column connections of these two specimens were moment resisting connections. The difference between their two tests was that the beam end axial stiffness of test 1 (39.5 kN/mm) was less than test 2 (68.3 kN/mm), so a larger internal axial force was produced in specimen 2 due to the larger restraint stiffness. The top flanges of the steel beams were wrapped with ceramic fiber blankets, for which the thicknesses were 3 mm and 10 mm for specimen 1 and specimen 2, respectively. Two concentrated loads were applied symmetrically on the beams by two jacks. The loads were applied and kept constant after reaching 130 kN, and the fire was then ignited in the furnace. With temperature increase, the deflection of the beam increased. When the deflection of the beams reached about 1/16 of their spans, the fire was turned off and the temperature in the furnace began to decrease. Thermocouples were installed in the top flange (TF) and bottom flange (BF), as well as in the web.

According to the test data, two FE beam models were developed. Transient heat transfer analyses were then conducted with the measured furnace temperature used as the gas temperature input to the model. Figure 4.6 shows one example of the temperature distribution contour on the cross-section of the FE beam model for specimen 1 during heating. It can be observed in the figure that the bottom flange has the highest temperature, while the temperature in the top flange is lower due to the protection of the ceramic fiber blanket. From the analyses, nodal temperature histories were monitored and obtained at the corresponding locations where the thermocouples were installed in the tests. Figure 4.7 to Figure 4.10 show the temperature-time responses of the FE analyses

in comparison with the experimental results of the two tests. In general, the FE models agree well with the experimental data in both the heating and cooling stages of the tests.

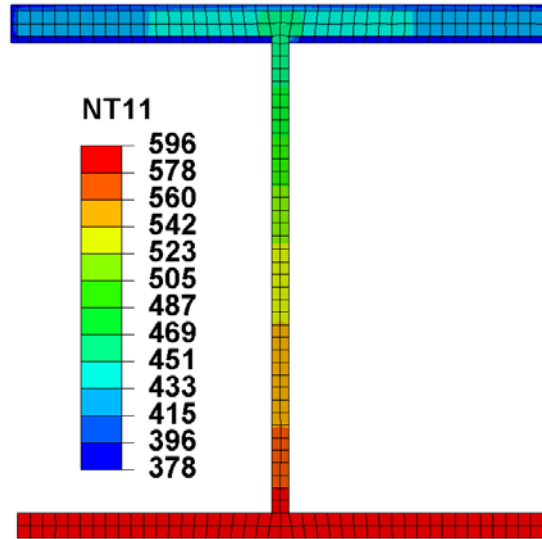


Figure 4.6 Temperature (°C) distribution on the cross-section of Li's beam during heating obtained by FE model

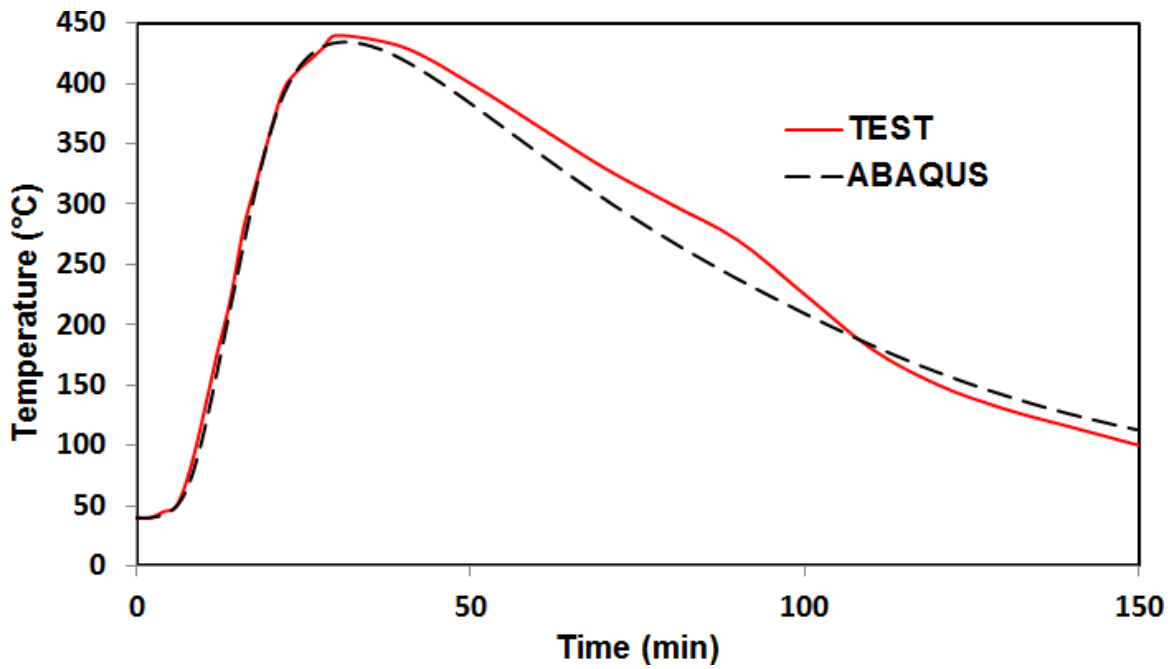


Figure 4.7 Temperature-time comparison between FEA and Li's test (TF 1)

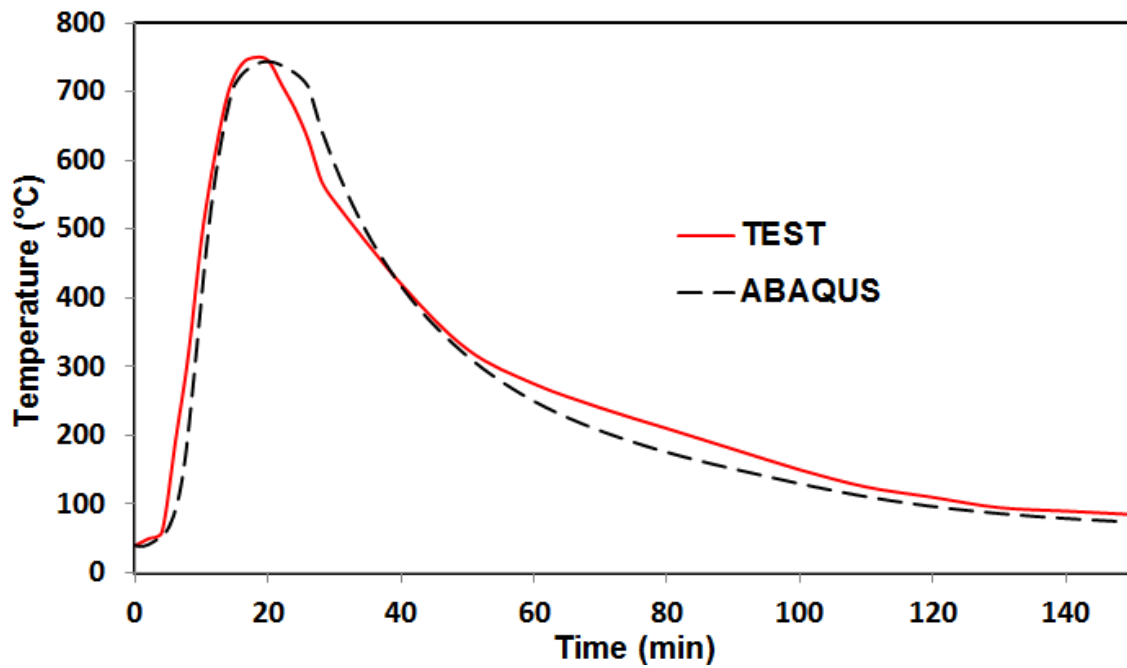


Figure 4.8 Temperature-time comparison between FEA and Li's test (BF 1)

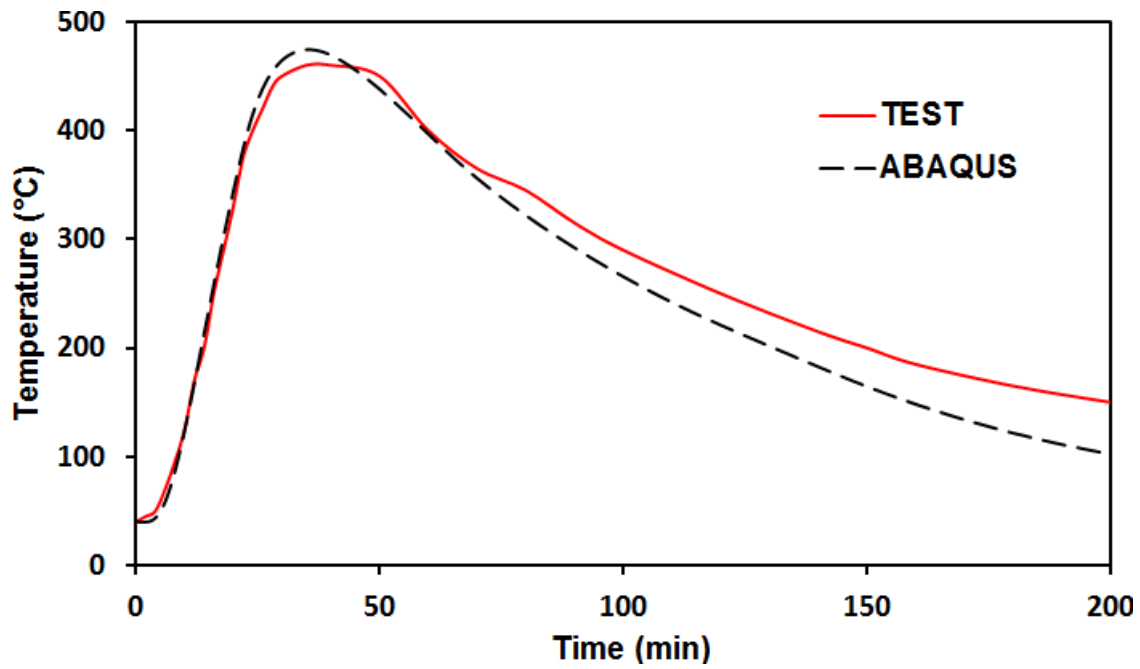


Figure 4.9 Temperature-time comparison between FEA and Li's test (TF 2)

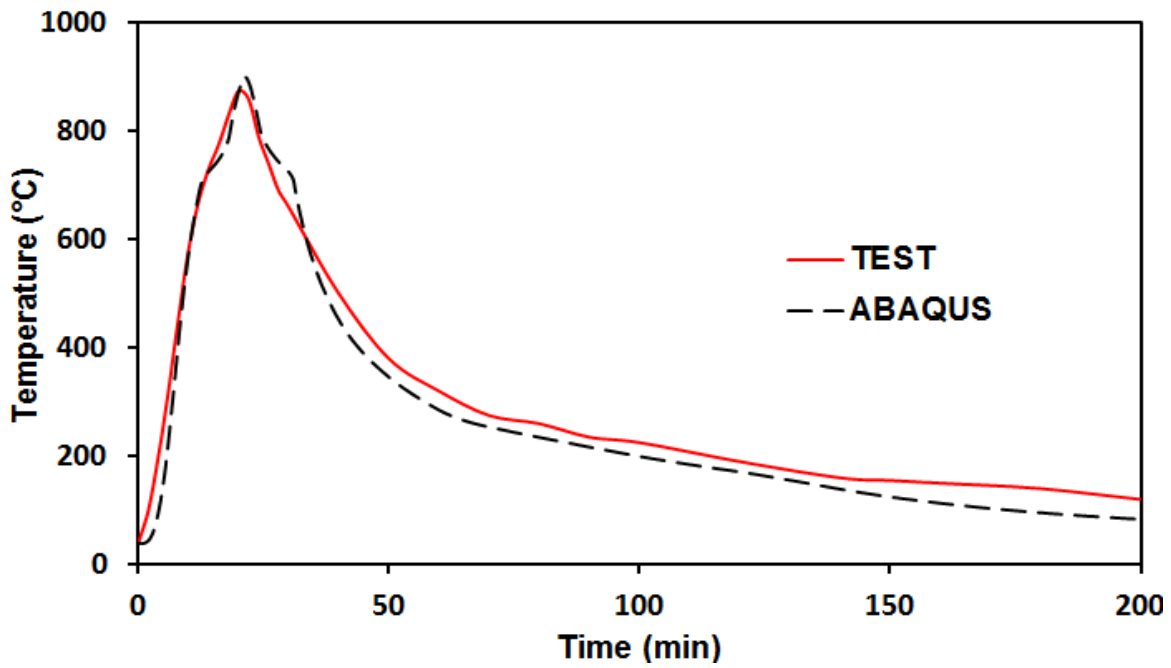


Figure 4.10 Temperature-time comparison between FEA and Li's test (BF 2)

4.3.7.2 Model Evaluation by Experimental Data of Liu et al

Results of FE analyses were also compared to the experimental study of the axially and rotationally restrained steel beams in fire by Liu et al. The test setup was shown in Figure 2.24. A steel beam, a 178×102×19UB (S275) section, was connected to two columns of 152×152×30UC (S275) sections. In order to simulate the insulating effect of the concrete slab, the top flange was also wrapped with 15 mm thick ceramic fiber blanket. The columns, together with the connections were generally fire-protected by the use of 50 mm thick ceramic fiber blankets. Transverse loads were applied to the beam using two independent hydraulic jacks connected to the top member of the reaction frame surrounding the furnace. The connections between the beam and the columns were flush end-plate connections. By using additional struts spanning between the columns of the test frame and the columns of the reaction frame, a test beam axial end stiffness of 62 kN/mm was achieved. An 80 kN jack load was calculated as the capacity of this beam at ambient temperature, and the test with load ratio of 0.5 was selected to compare with FE analyses. In the test, the gas temperature in the furnace was increased after the target loading was applied. Heat transfer FE analysis was conducted for comparison with the experimental data.

Figure 4.11 (a) and (b) illustrate examples of the temperature distribution contour on the cross-section of the beam during heating and cooling, respectively, as predicted by the FE analysis. As with the previous of Li's test, the top flange has significantly lower temperature than the web and bottom flange during the heating process due to the protection of the ceramic blanket. On the other hand, during cooling the top flange can have higher temperatures than the web and the bottom flange because the ceramic blanket insulation slows cooling of the top flange. Figure 4.12 through Figure 4.14 show the temperature-time responses of the FE model in comparison with the experimental results at the corresponding locations of the beam cross-section. In general, the FE model predictions are quite close to the measured temperatures.

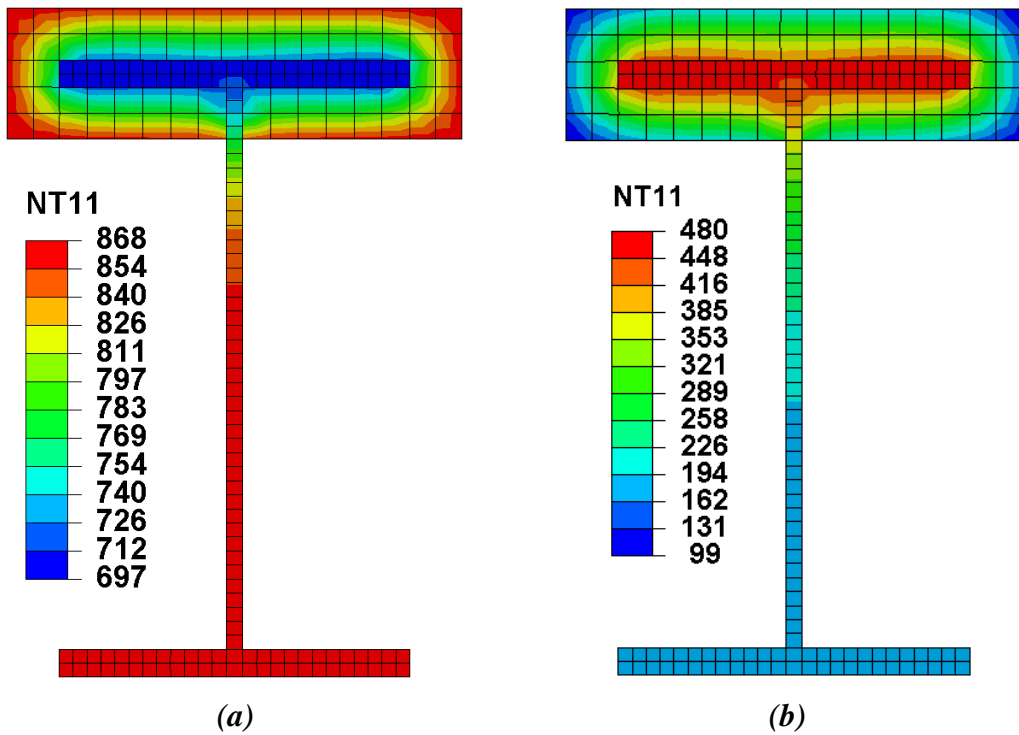


Figure 4.11 Modeled temperature ($^{\circ}\text{C}$) on Liu's beam during heating (a) & cooling (b)

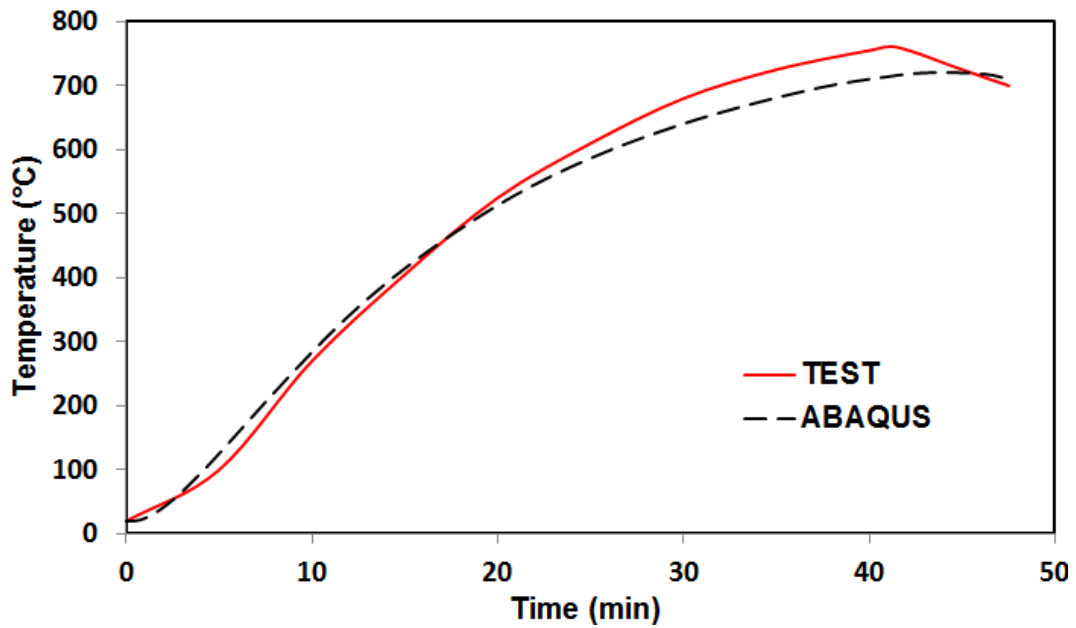


Figure 4.12 Temperature-time comparison between FEA and Liu's test (TF)

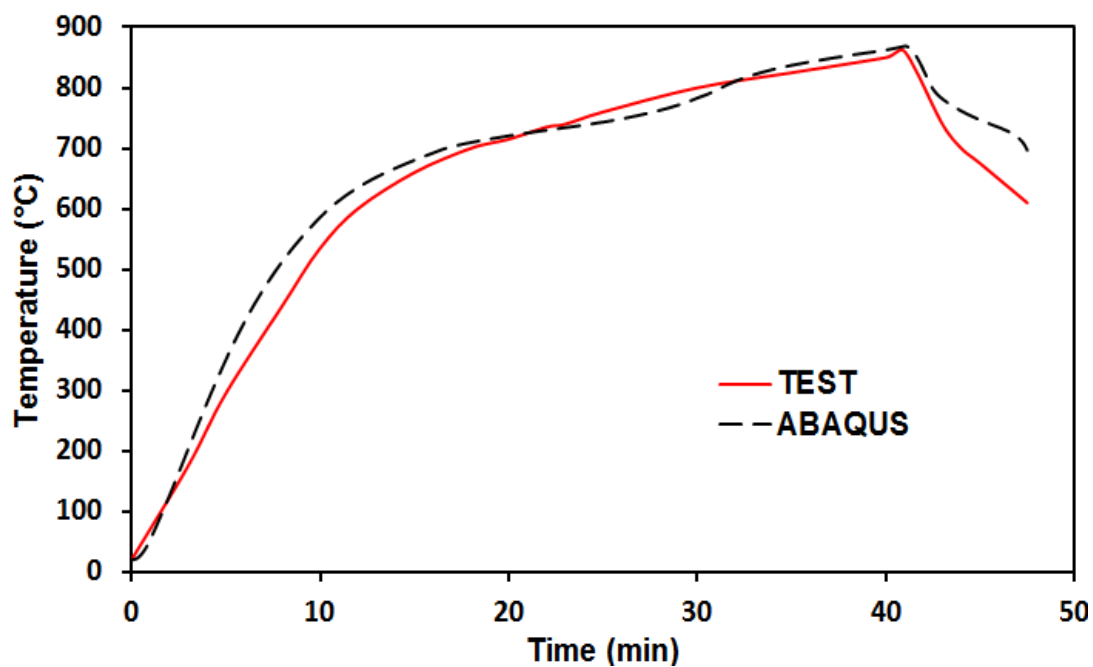


Figure 4.13 Temperature-time comparison between FEA and Liu's test (BF)

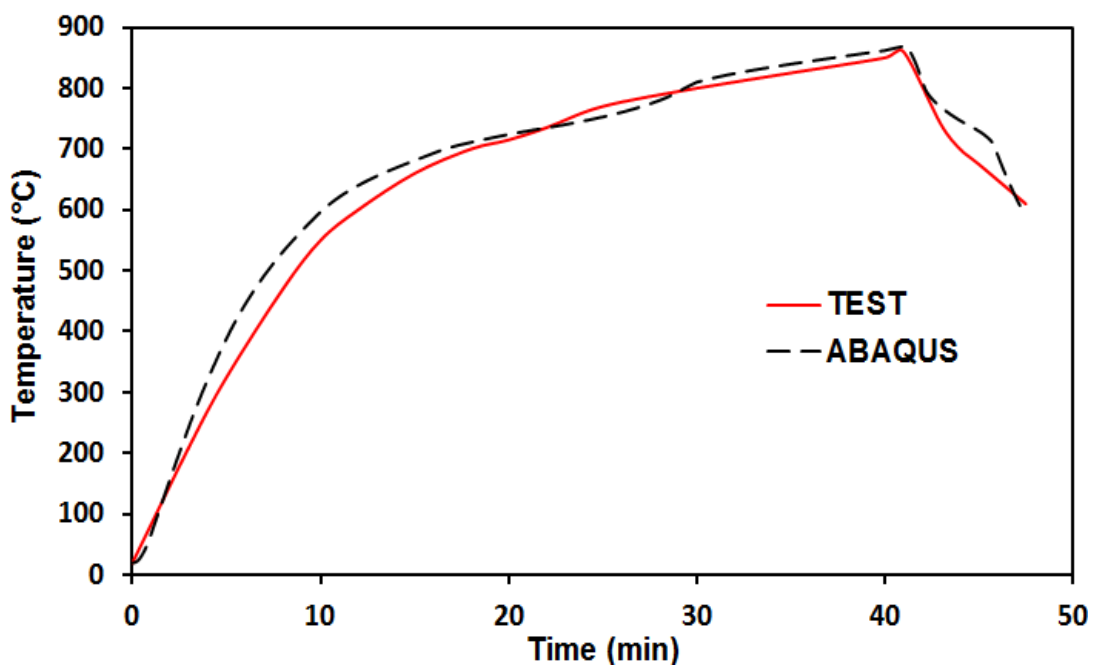


Figure 4.14 Temperature-time comparison between FEA and Liu's test (web)

4.3.8 Observations

From the thermal analysis conducted above, as discussed in this section, the FE analysis results agree reasonably well with the experimental results. The ability to predict the experimentally measured temperatures using ABAQUS depends on a number of factors, including the assumed mechanism of heat transfer between the fire environment and the surface of the member, the assumed heat transfer coefficients at the surface of the member (resultant emissivity and convective heat transfer coefficients), the assumed thermal properties of the steel and the assumed thermal properties of the insulation. A recent study (Subramanian 2008) has shown that for insulated steel members exposed to fire, the predicted steel temperatures are most sensitive to the assumed thermal properties of the insulation. The thermal properties of steel are well known, so these introduce little error in the results. The predicted temperatures are also much less sensitive to the assumed heat transfer coefficients at the surface of the member. Consequently, if reasonably accurate data is available on the thermal properties of insulation, the temperature of steel members in fire can be predicted with the modeling techniques described above. It is also noted that in this study the FE heat transfer model showed a quite high convergence rate with increasing mesh refinement. The temperature change along the thickness of steel member is small so that there is no need to use a large number of elements through the steel thickness.

4.4 STRUCTURAL ANALYSIS OF STEEL BEAMS IN FIRE

The main purpose of the structural analyses conducted in this research is to simulate the deformations of the beam and the deformations and forces at the beam end connections due to the thermal effect of a fire and external loading. Temperatures obtained from a corresponding transient heat transfer analyses can be used as input temperatures for the structural analysis, or temperatures can be input independently for the structural analysis.

Nonlinear structural analyses were conducted including large-displacement effects and material non-linearity. The default Newton-Raphson algorithm in ABAQUS was used to perform iteration calculations. Thus, the solutions were usually obtained as a series of time increments, with iterations to obtain equilibrium within each time increment. Automatic time increment schemes were used, and the increment sizes are based on computational efficiency in ABAQUS. The analysis outputs include complete histories of stresses and strains for the steel elements, and displacements and reaction forces at nodal positions.

4.4.1 Element Selection

In the structural analyses on ABAQUS, the meshes (number, location and size of elements) are identical to those used in heat transfer analyses, but with different element types. To keep in line with the previous thermal analysis, a linear element was also used in structural analysis. In this research, a three-dimensional solid brick element (C3D8R) was chosen. The C3D8R is defined as a three-dimensional, hexahedral eight-node linear brick, reduced integration with hourglass control solid element. This element has good performance in calculating displacement, and it works quite well when large element distortion exists (Shi and Zhou 2006). Insulation has little effect on structural behavior of steel member, so modeling of insulation material is not needed in the structural analyses.

4.4.2 Material Properties

As previously discussed, high-temperature mechanical properties of structural steel are dependent on the type of steel and are still under investigation by a number of researchers. In the selected previous steel beam tests for the FE model validation, steel material properties at elevated temperatures were not reported by the investigators. Therefore, in this model validation study, reduction factors of structural steel recommended by Eurocode 3 (2006) were considered.

Material nonlinearity was considered using the von Mises yield criterion, which is the default option adopted by ABAQUS. Hardening was modeled by an isotropic hardening rule. The constitutive rule of the isotropic hardening material was modeled by a multi-linear rule and the high-temperature (above 400°C) steel stress-strain relationship was assumed to be elastic-perfectly plastic, as shown in Figure 4.15. The variation in material property on the cross-section and residual stresses arising from the steel manufacturing process and fabrication process were not accounted for in the model. Thermal creep effects also were not considered. This material model was adopted to evaluate how well experimentally measured response could be predicted with a relatively simple material model.

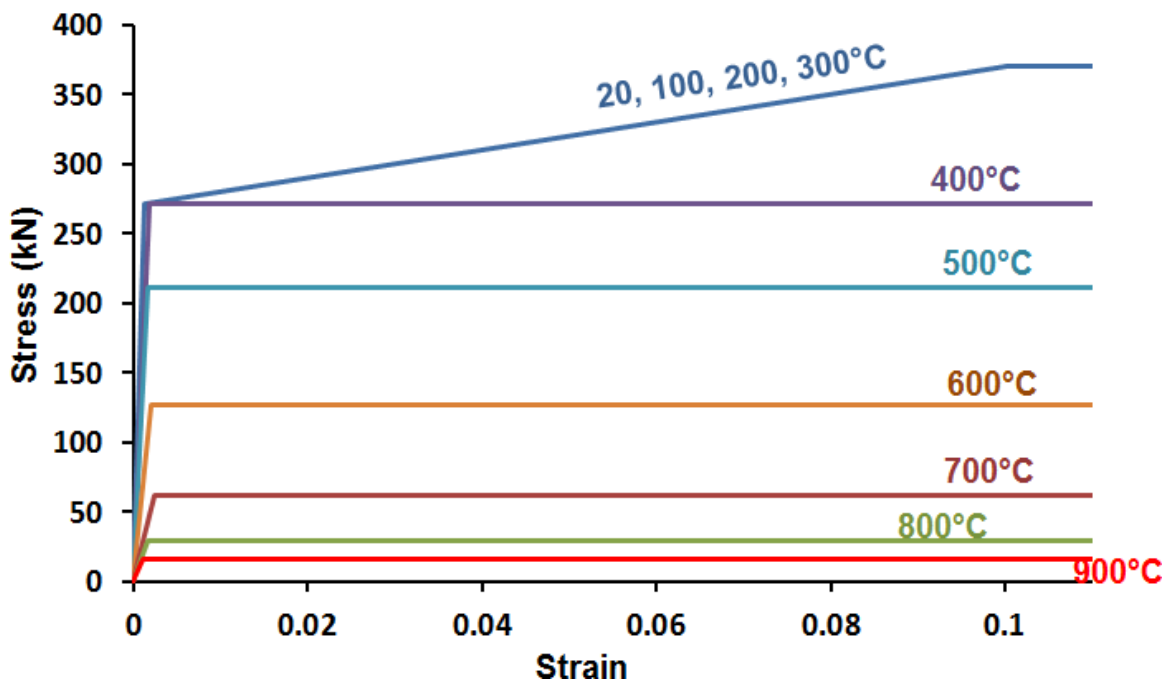


Figure 4.15 Steel properties used in FE model of Li and Guo's test

In ABAQUS, the definition of nonlinear uniaxial material response requires the use of the true stress-strain relationship. This can be determined from the engineering

stress-strain relationship using Equation 4.11 and 4.12 (Hosford 2010). Hence, the stress and strain values used in the FE models of this study were converted to true stress and true strain from these two equations.

$$\sigma_{True} = \sigma_{Eng}(1 + \varepsilon_{Eng}) \quad (4.11)$$

$$\varepsilon_{True} = \ln(1 + \varepsilon_{Eng}) \quad (4.12)$$

$$\sigma_{True} = \text{True Stress}$$

$$\sigma_{Eng} = \text{Engineering Stress}$$

$$\varepsilon_{True} = \text{True Strain}$$

$$\varepsilon_{Eng} = \text{Engineering Strain}$$

4.4.3 Geometric Nonlinearity

Geometric nonlinearity was considered in all analyses by a large displacement formulation. ABAQUS adopts a large strain formulation for 3-D solid elements by default. When the optional parameter “NLGEOM” is activated, the locations of all nodes are updated after each analysis step. The “NLGEOM” was activated for all analyses so that local instability and large deformation effects could be captured. No initial imperfection was introduced in the analyses.

4.4.4 Boundary and Load Conditions

In the selected experimental studies in the literature, the tested beams were connected to column frames, which provided horizontal axial restraint. The beam-column connections were endplate bolted connections, which provided large moment resistances. Therefore, in the FE structural analyses, rotations at the end of the beams were prohibited, but the horizontal movements were allowed by modeling spring connectors with the same amount of stiffness that the columns provide to the beam in the axial direction. Loads were applied on multiple nodes to prevent local failure.

4.4.5 Model Evaluation

4.4.5.1 Model Evaluation by Experimental Data of Li and Guo

Beam fire tests by Li and Guo (2006) were selected to evaluate the FE structural models. Transient structural analyses were conducted using the temperature-time history output obtained from the previous heat transfer analyses described in Section 4.3. Figure 4.16 and Figure 4.17 show the deflection-time responses of the FE models in comparison with Li and Guo's experimental results. Test results in the referenced paper only provided beam deflections during the heating stage of the tests that lasted about 20 minutes, and it is clear from the figures that in this time period the FE analysis results matched quite well with the experimental data. From the further analyses of the FE models, it can be observed that during cooling (after 20 minutes in the figures), the deflections of the beams recovered by only a small amount.

Figure 4.18 and Figure 4.19 illustrate the axial force versus time responses of the FE simulations in comparison with the experimental results. The axial force in the beam was initially compression and increased with temperature increase due to restrained thermal expansion. With further temperature increase, the axial compressive force decreased and turned into tensile force, reflecting the softening of the beam and the apparent development of catenary action. The tensile force in the beam increased significantly during the cooling phase of the test. From the two figures, it can be seen that during the heating stage, the FE models predicted the experimental results quite well. However, the beam axial force predicted by the FE model deviated considerably from the experimental results during the cooling phase. The FE models predicted lower values in both cases. One possible reason for this difference is that the beam end stiffness probably varied during the tests due to large horizontal deformations. The beam end axial forces for the tests were obtained from the measured horizontal displacements of the beam end multiplied by the end stiffness, which was assumed to be a constant by the investigators

of the referenced paper. Consequently, there is some uncertainty in the experimental data, since the beam end axial forces were not directly measured in the tests.

The final deflected shape of the modeled beam obtained by FE analysis is compared with a photo of the beam after testing in Figure 4.20. It can be seen that the large beam deformation was captured by FE model reasonably well.

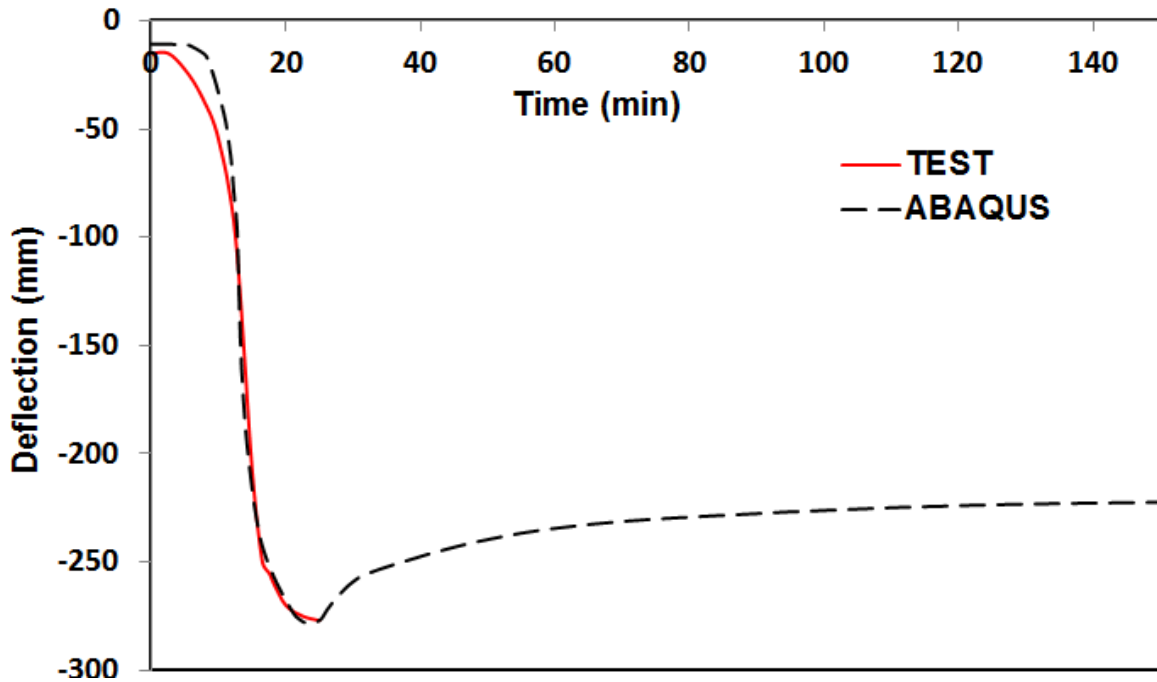


Figure 4.16 Deflection-time comparison between FEA and Li's test (test 1)

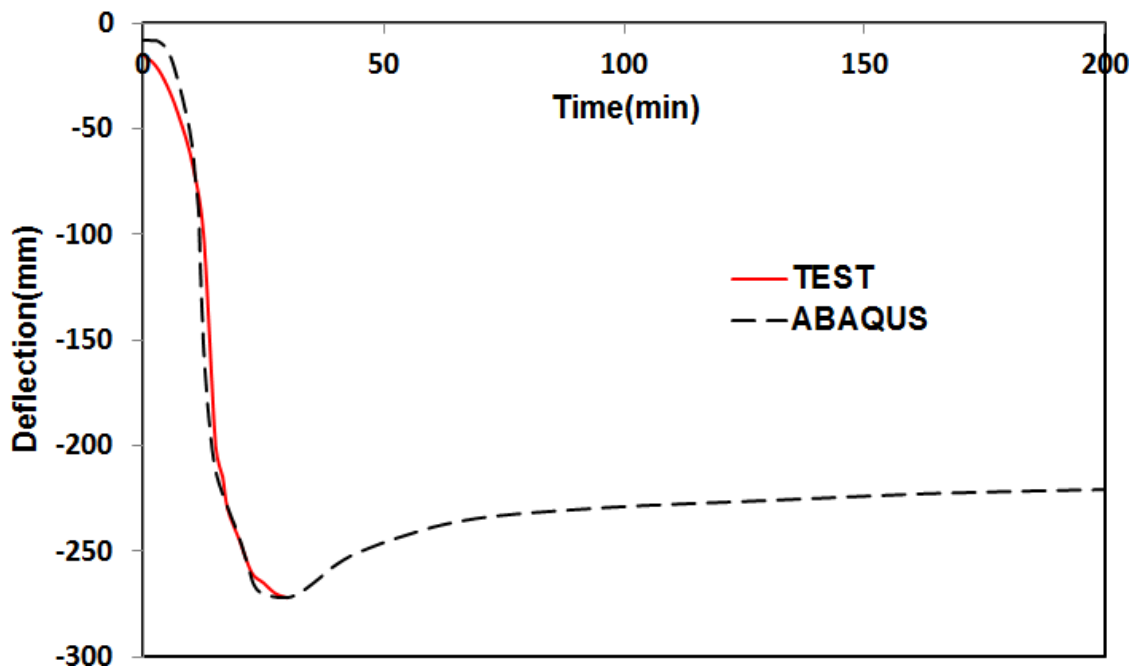


Figure 4.17 Deflection-time comparison between FEA and Li's test (test 2)

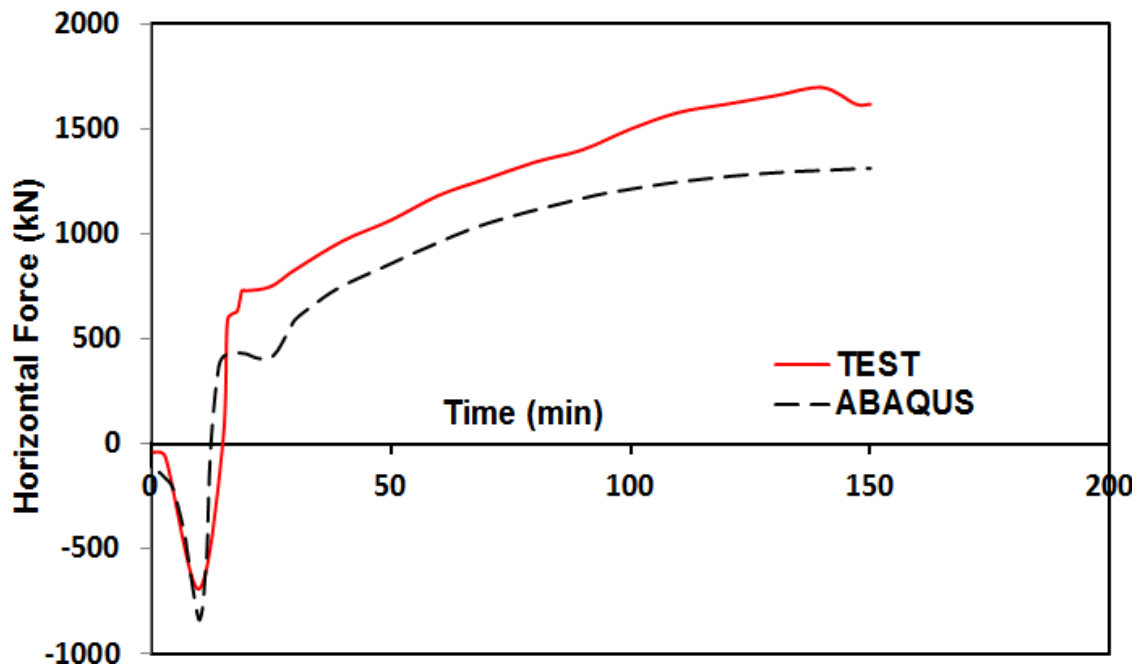


Figure 4.18 Axial force-time comparison between FEA and Li's test (test 1)

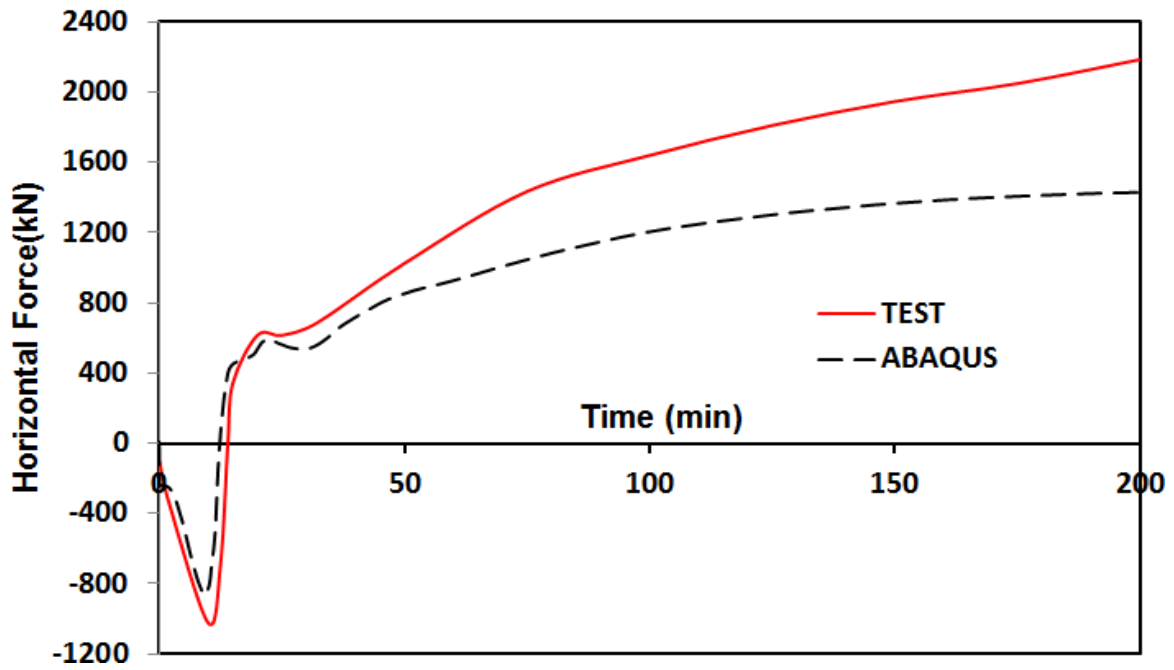


Figure 4.19 Axial force-time comparison between FEA and Li's test (test 2)



Figure 4.20 Beam deflection shape of fire test and FEA

4.4.5.2 Model Evaluation by Experimental Data of Liu et al

Beam tests by Liu et al (2002) were also used to evaluate the FE structural model. Figure 4.21 shows the comparison of the FE model with Liu's experimental results in a plot of bottom flange temperature versus beam mid-span deflection. From the figure it can be observed that before the bottom flange temperature reached approximately 700°C, the mid-span deflection of the beam increased linearly with the temperature, while above 700°C, the beam "run-away" (rapid increase in deflection) occurs. Beyond this point, catenary action was observed, which generated axial tension in the beam (Figure 4.22). Comparison of the FE model with test results on the response of axial force versus bottom flange temperature is shown in Figure 4.22. In this figure, the FE analysis results are shifted towards the left compared to the test data. This phenomenon may be due to inaccuracy in modeling the stiffness of the beam end support. From the test data, it can be seen that a significant increase of beam axial force did not occur until the beam reached about 200°C. This might be because during the early stages of the heating in the test, firm contact between the components of the beam end connections did not form. When the temperature reached about 200°C, with considerable amount of thermal expansion in the beam, the components of beam end connections had full contact with each other, and the full stiffness of the connections were achieved.

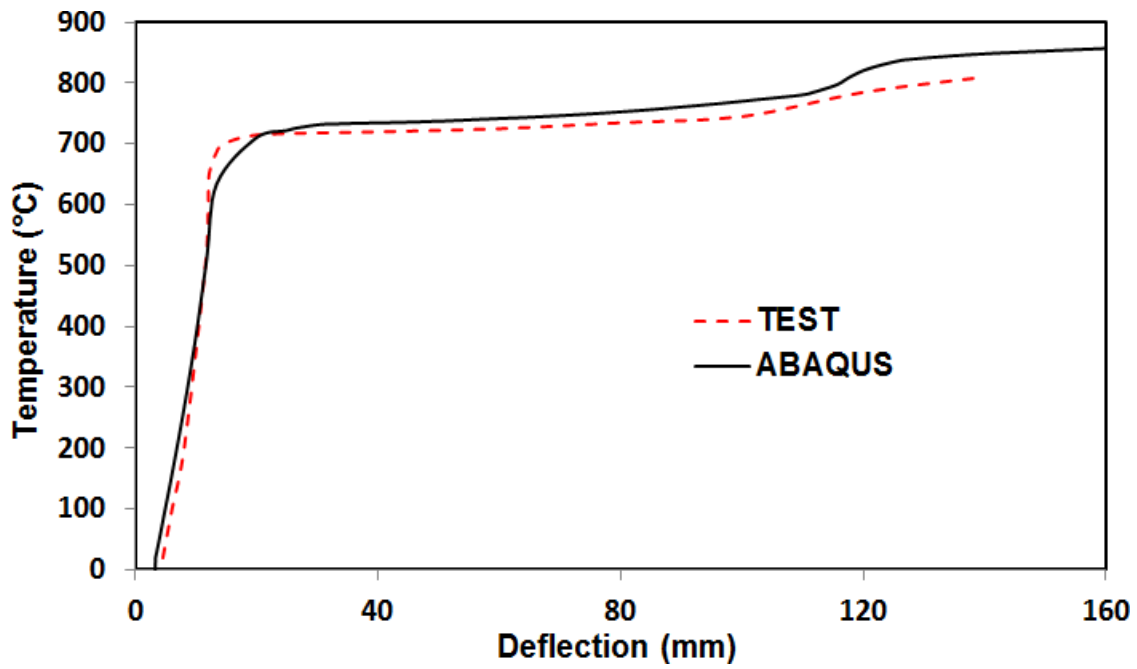


Figure 4.21 Bottom flange temperature - mid span deflection response (FEA vs. Liu's test)

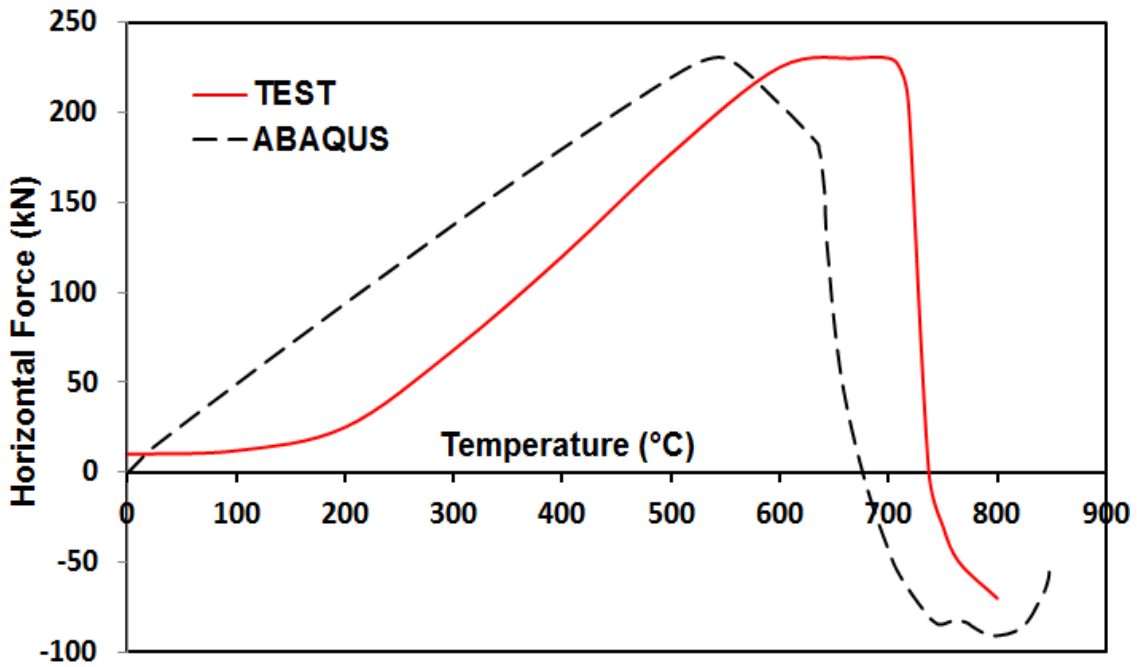


Figure 4.22 Beam axial force - temperature response (FEA vs. Liu's test)

4.4.6 Observations

From the structural model evaluation, it is observed that the structural response of beams at elevated temperatures predicted by ABAQUS compared reasonably well with the experimental data from two previous research investigations. Although accurate elevated-temperature material properties were not available and a simplified material model was used, the structural performance of the modeled members was reasonably well predicted. Using simplified beam end boundary conditions in the models, it was found that the beam deformations predicted by the FE model match the test results significantly better than the simulation of beam end axial forces, in which obvious discrepancies exist. This may suggest that the performance of beam end connection in fire has larger impact on beam forces than beam deformations. Therefore, to obtain realistic beam end stiffness and capture forces at beam end accurately, modeling of beam end connection is essential in some way.

4.5 FE MODELING OF SIMPLE SHEAR CONNECTIONS AT AMBIENT TEMPERATURE

4.5.1 Brief Description

The detailed modeling of the bolted connections can introduce a number of modeling difficulties and complexities that are not encountered in global structural modeling. It involves contact problems between the bolt shank and the edge of the bolt hole and the plate, contact between the bolt head and the plate, contact between the nut and the plate, and contact between the plates (Figure 4.23). The contact areas of concern are generally in the vicinity of high stress. Therefore, to accurately capture the stress behavior in the region around the bolt holes where failures would probably initiate, an intensive mapped meshing is made in the vicinity of the holes and for the bolts as shown in Figure 4.24. It is recommended by the ABAQUS User's Manual (2007) that linear elements should be used for contact behavior modeling. Therefore, the C3D8R element and C3D8I element (three-dimensional, hexahedral eight-node linear brick, incompatible

modes solid element), were used throughout the connection models. The incompatible modes in the C3D8I element improve the bending behavior of the model if bending occurs.

To make the analysis accurately represent the real conditions, the bolt holes were modeled 1/16 inch larger than the bolt shank diameters, which were assumed to be unthreaded. The hexagonal shape bolt heads and nuts were modeled as cylinders for simplicity. Since there should be no relative movement between the bolt shank and the nut, a tie constraint function was used to model the contact between the bolt shank and the nut. Surface-to-surface contact with a small-sliding option was used for all other contact surfaces. In the tangential direction, a friction coefficient of 0.35 was used and hard contact was applied in the normal direction for all contact pairs. In the first analysis step before initial contact develops, each bolt was restrained from movement using temporary boundary conditions, and then in the later steps the temporary boundary conditions were released and all bolts were freed of any restraints as contact was then already established.

Simulating the contact behavior between the parts of shear connections is difficult to achieve. Difficulties arise because some special arrangements are needed to bring the connection parts into initial contact. First, the mesh should be fine enough for the parts both on the master surface and on the slave surface. Second, temporary boundary conditions need to be assigned to the parts that have no external restraint. Lastly, load needs to be applied slowly until initial contact is established.

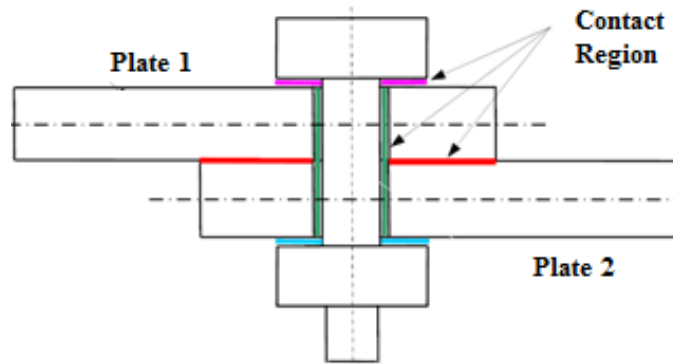


Figure 4.23 Layout of bolted connection model

4.5.2 FE Model Convergence Study

The computational time needed to run an analysis depends, among other factors, on the number and order of elements. Using more elements can improve accuracy but will also increase computational time. Consequently, the model with the minimum number of element consistent with adequate accuracy is needed to minimize the computational time. Hence, convergence studies were conducted by creating several models with different mesh sizes and comparing the resulting stresses and deformations.

A model of bolt bearing on a plate was used to study the influence of the mesh density on the accuracy of calculated displacements and stresses. The number of elements was varied from 50 to 3250 in this convergence study. For each case, the same locations were examined, and the stresses and displacements were plotted against the number of elements, as shown in Figure 4.25 and Figure 4.26. It was concluded that with about 1300 elements in the model the stress and displacements converged with sufficient accuracy. Therefore, this mesh pattern for the model was used throughout the FE analyses in this study.

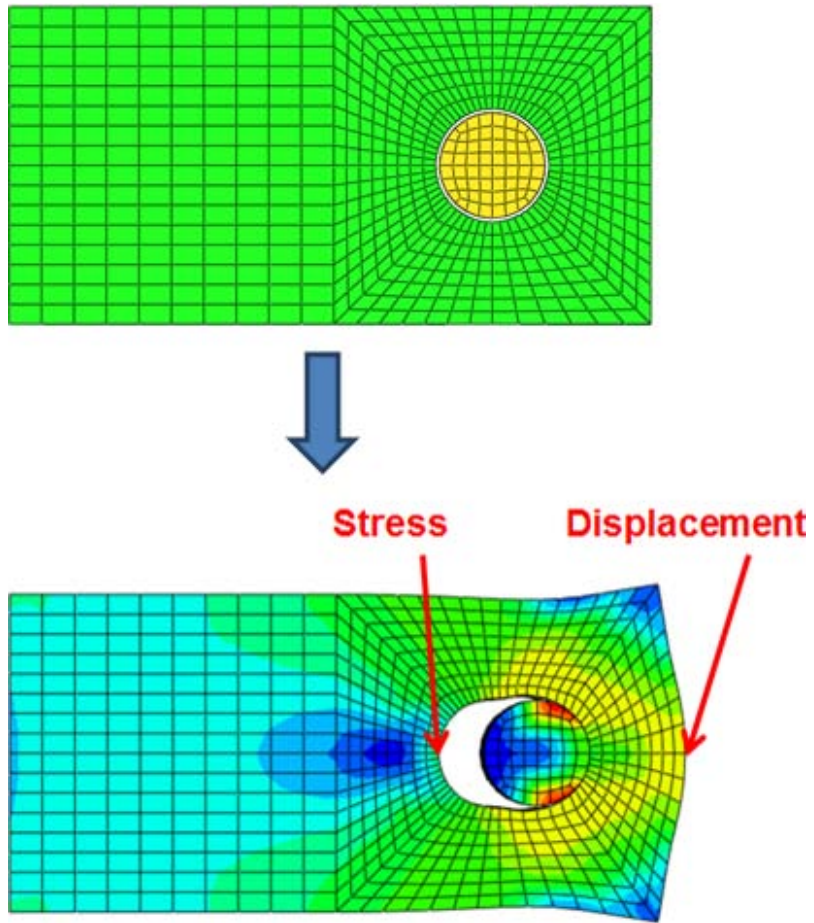


Figure 4.24 Mesh of FE model for convergence study

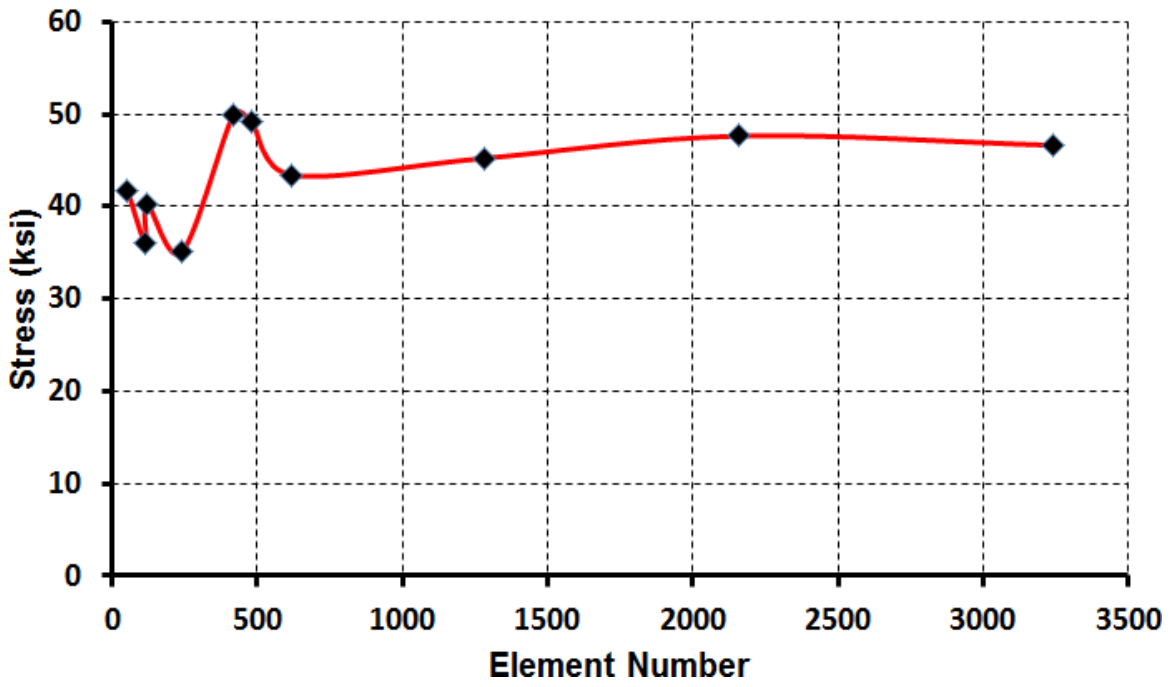


Figure 4.25 Convergence study on stress

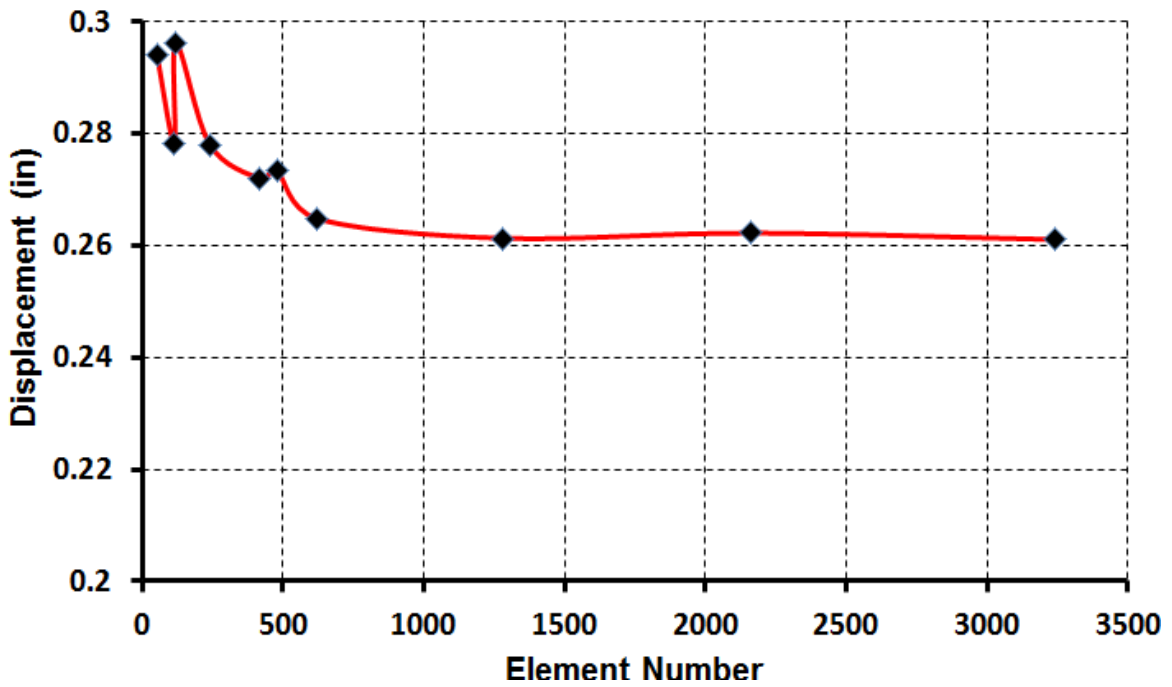


Figure 4.26 Convergence study on displacement

4.5.3 Evaluation of FE Model for A Simple Bolted Connection

An FE model was developed and compared to the experimental study results of simple steel lap joints by Richard et al (1980).

The test specimen dimensions are shown in Figure 4.27. The plates in the lap joint specimen were of two different thicknesses, 1/2 inch and 3/8 inch. Both plates were made of ASTM A36 steel. A 3/4 inch diameter ASTM A325 high strength bolt was installed in over-sides holes with a diameter of 13/16 inch.

Since Richard did not report the properties of the steel used in the tests, ASTM A36 steel mechanical properties tested in Ferguson Lab by the investigator was then applied in the FE model. The yield strength of the tested A36 steel was about 46 ksi and the ultimate strength was about 65 ksi. Figure 4.28 shows the stress-strain relationship of the tested A36 steel, along with the simplified stress-strain model used in the FE analysis. The yield strength and ultimate strength of the A325 bolt used in this analysis was taken as 100 ksi and 120 ksi, respectively. A simplified tri-linear stress-strain relationship for the bolt was used in the FE model (Figure 4.29).

A 3-D FE model for this lap joint was then created and analyzed (Figure 4.30). A comparison of the FE analysis results with test data for the load-deflection curve indicates an overall good agreement, with some discrepancy only in the elastic range (Figure 4.31).

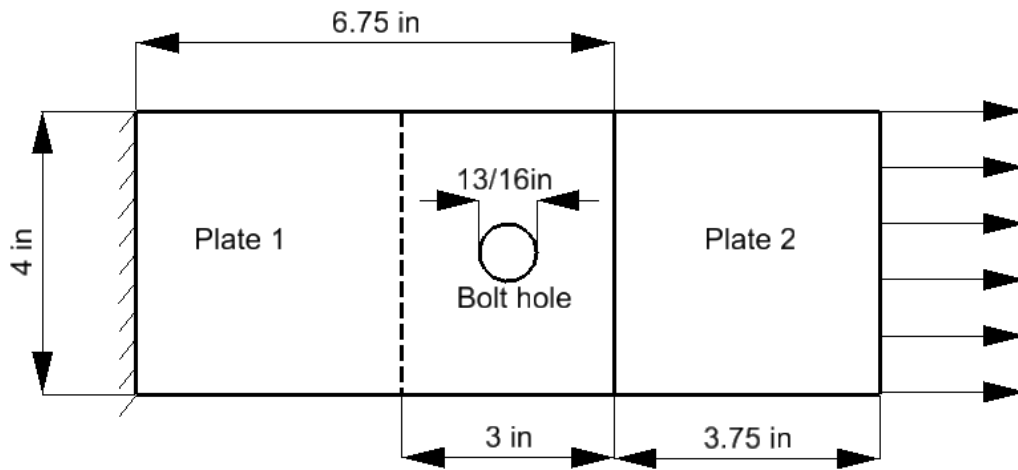


Figure 4.27 Geometry and dimensions of steel lap joint used in Richard's test

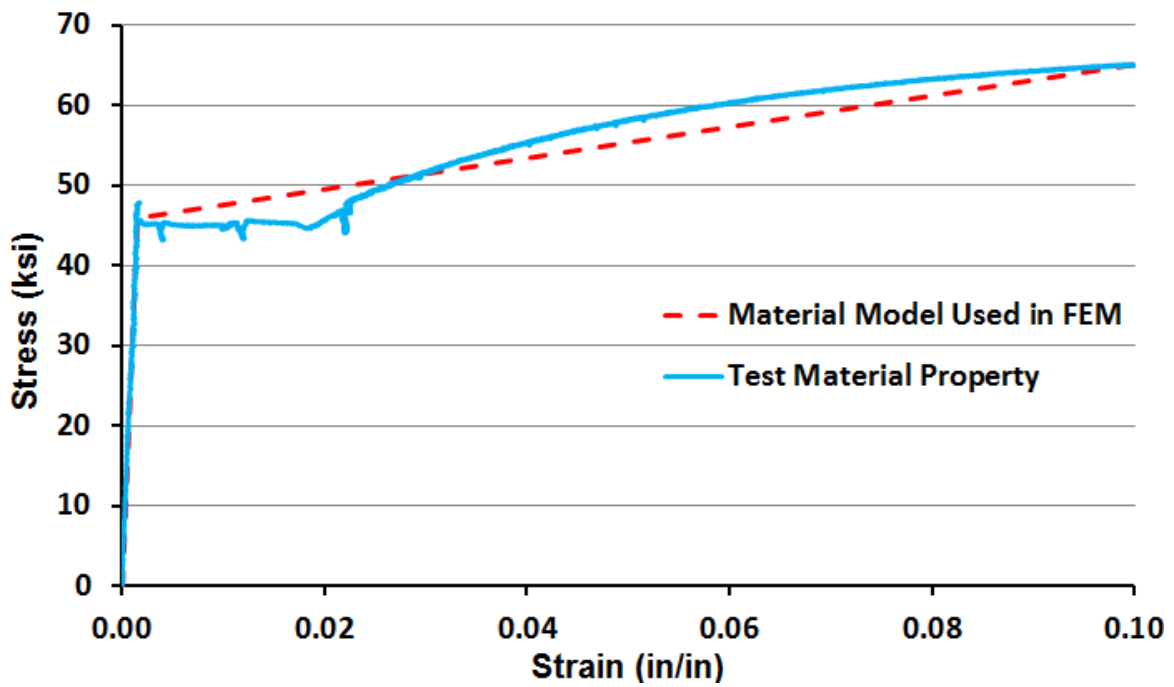


Figure 4.28 Stress-strain curve of ASTM A36 steel

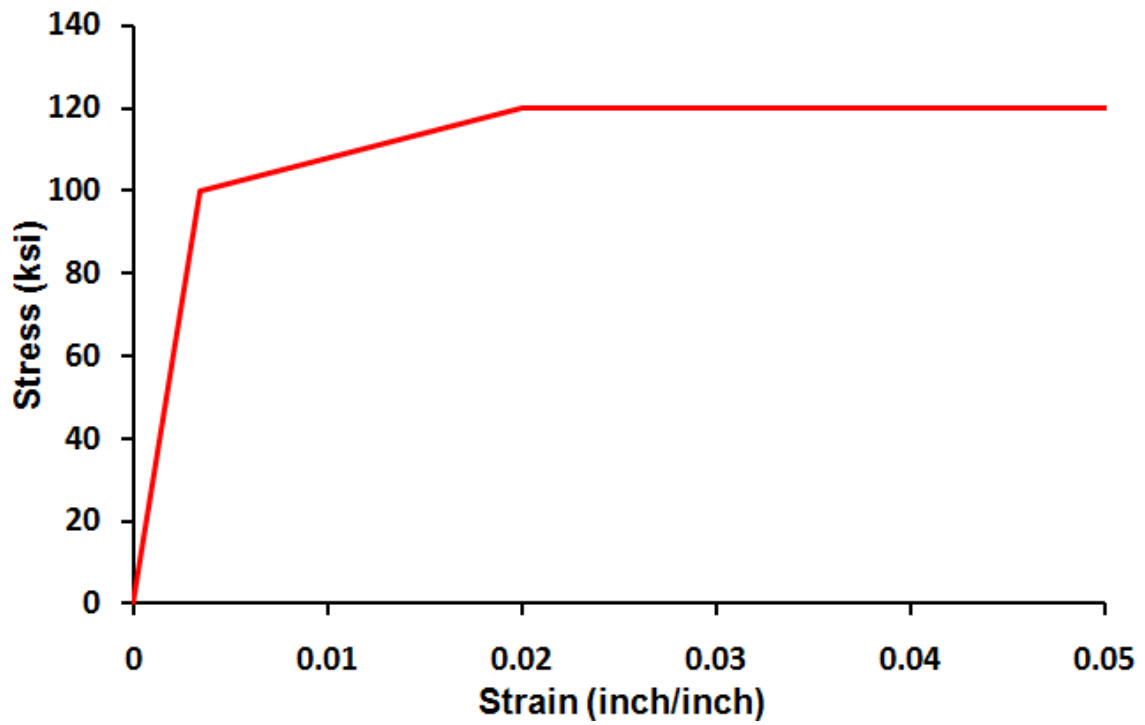


Figure 4.29 Stress-strain relationship of A325 Bolt used in FE model

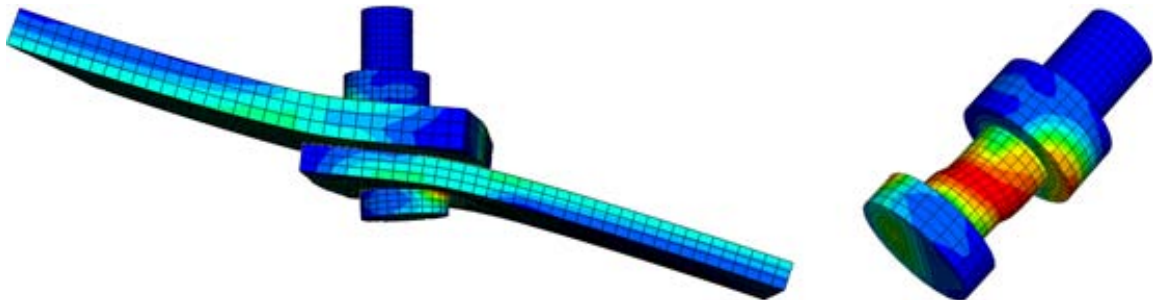


Figure 4.30 Deformations and stress contours of FE model of steel lap joint

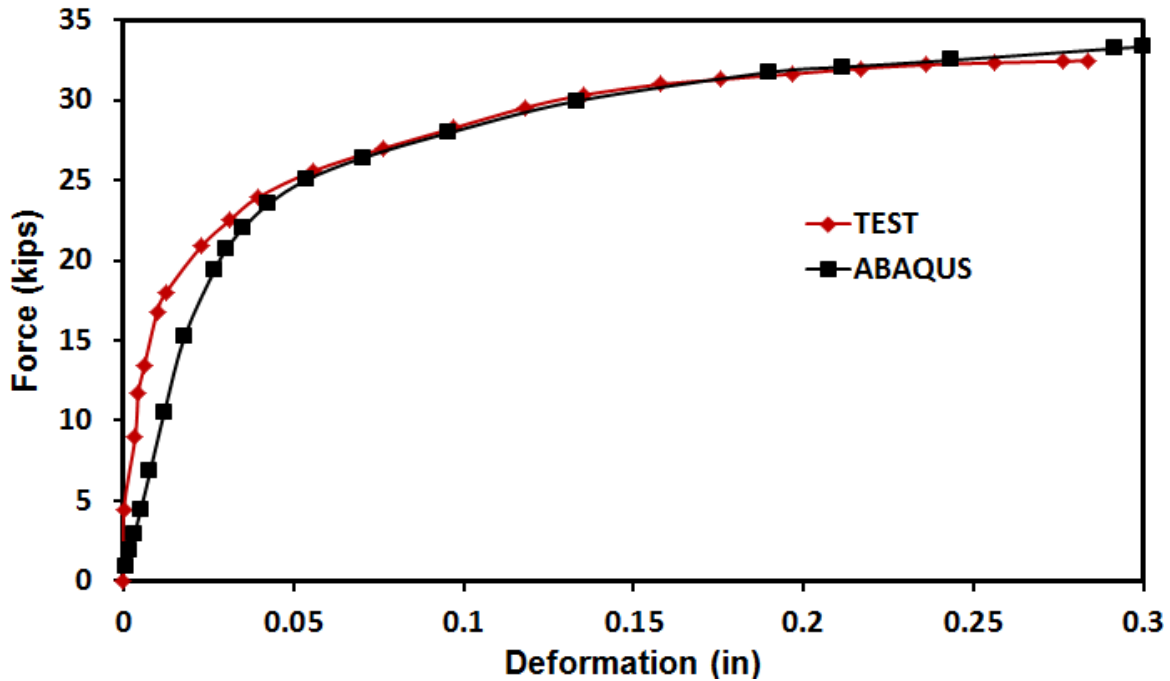


Figure 4.31 Load-deflection comparison between FEA and Richard's test

4.5.4 Evaluation of the FE model for A Beam and Connection

Metzger (2006) conducted real scale beam tests to study the behavior of steel simple shear connections. The test beam was attached to a column flange at one end with a shear tab connection, and the other end of the test beam was supported by a roller on a load cell supported by a beam bolted to the reaction floor. Loads were applied to the test beam at nominal third points by two hydraulic rams (see Figure 2.26).

Steel used for the test beams and test columns was specified as ASTM A992 and steel used for the shear tabs was specified as ASTM A572 Gr. 50. Both A992 and A572 Gr. 50 have a specified minimum yield strength of 50 ksi. All bolts were 3/4 inch ASTM A325-N. The shear tabs were welded to the column flanges using E70 electrodes. Metzger also reported all the material properties used in these tests by conducting coupon

tensile tests and bolt shear tests (Metzger 2006), and these material properties were used in the FE model.

Three-bolt shear tab connection and five-bolt shear tab connection tests were chosen for the model evaluation. Both shear tabs used in the tests were 3/8 inch thick. Figure 4.32 gives the dimension of the test specimens and Figure 4.33 shows the FE mesh of the shear tabs and beam ends for both tests. A fixed boundary condition was used to simulate the fillet weld between the shear tab and supporting column. Consequently, the welds were not explicitly modeled.

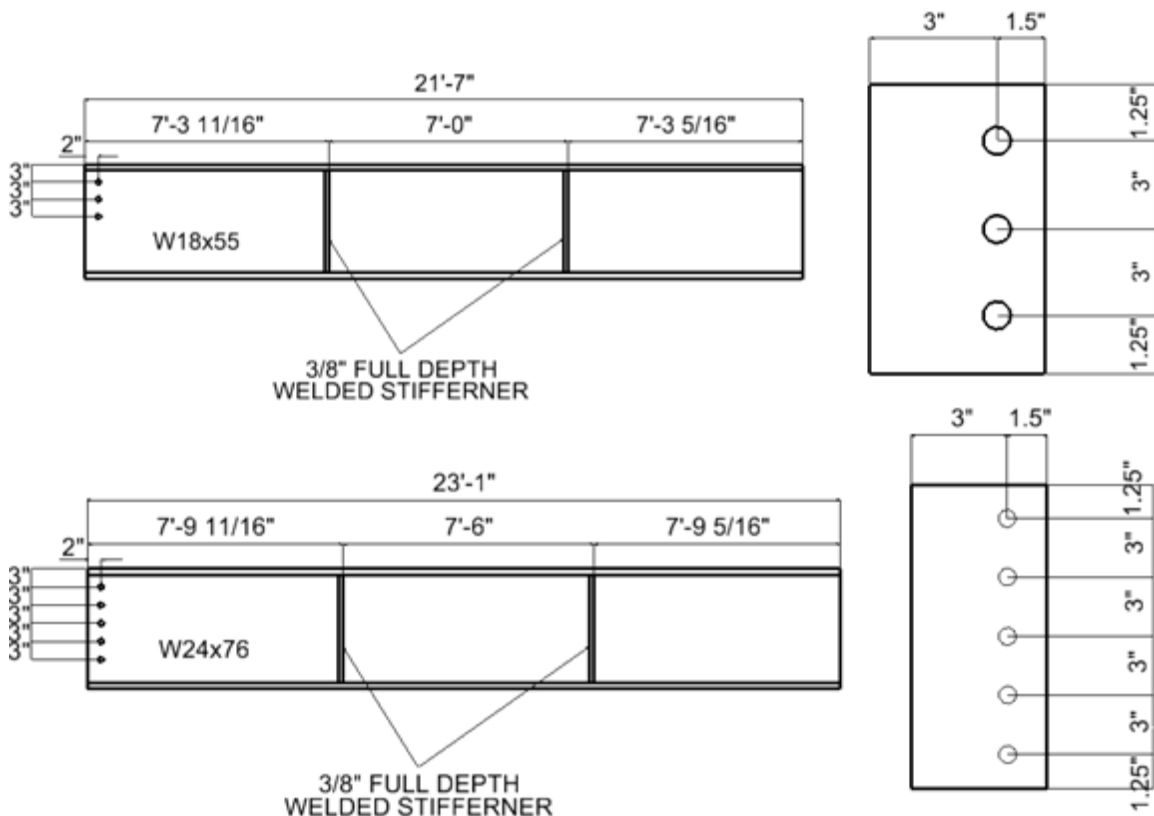


Figure 4.32 Dimensions of Metzger's shear tabs and test beams (Not in scale)

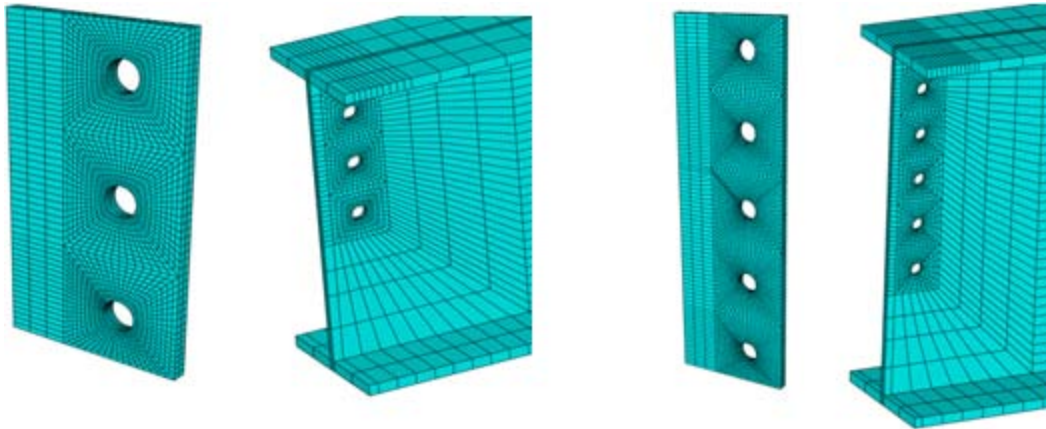


Figure 4.33 FE mesh of shear tabs and beam ends of Metzger's test

FE analyses were then performed for these two models. The deformed shapes and von Mises stress contours are shown in Figure 4.34. The analyses showed that the middle bolts acted as the center of rotation, whereas the top holes underwent large deformations and the top bolts bear toward the outer edge of the beam webs. In contrast, the bottom bolts bear in the opposite direction. The failure modes of these two tests were reported as bolt shear fracture failure, which appeared as large shear deformations in the FE bolt models.

Figure 4.35 shows load-rotation responses of the FE analyses together with the experimental load-rotation curves for both simulations. In general, the FE analyses results matched the experimental data of Metzger's test with reasonable accuracy.

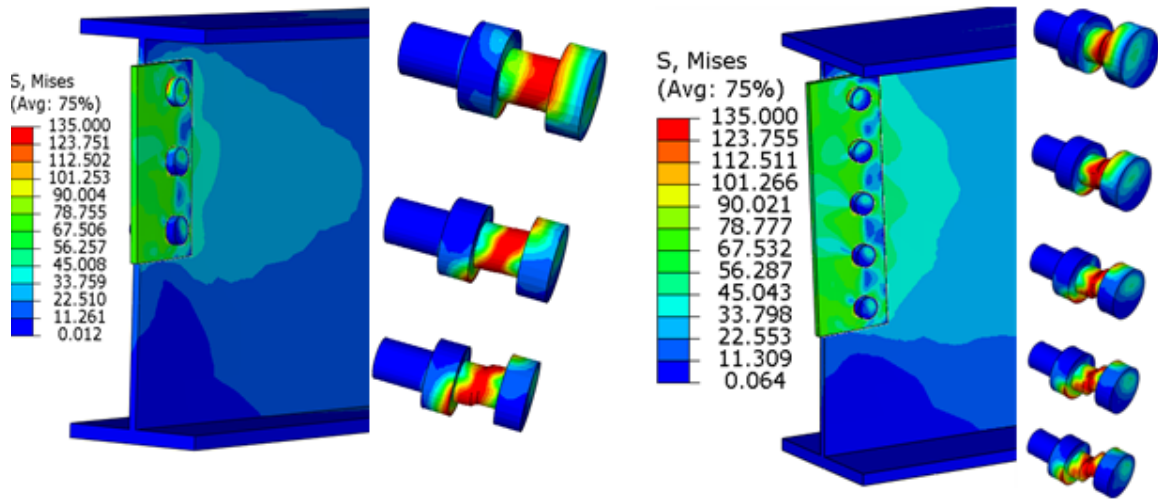


Figure 4.34 Deformations and stress contours of connection FE model of Metzger's test

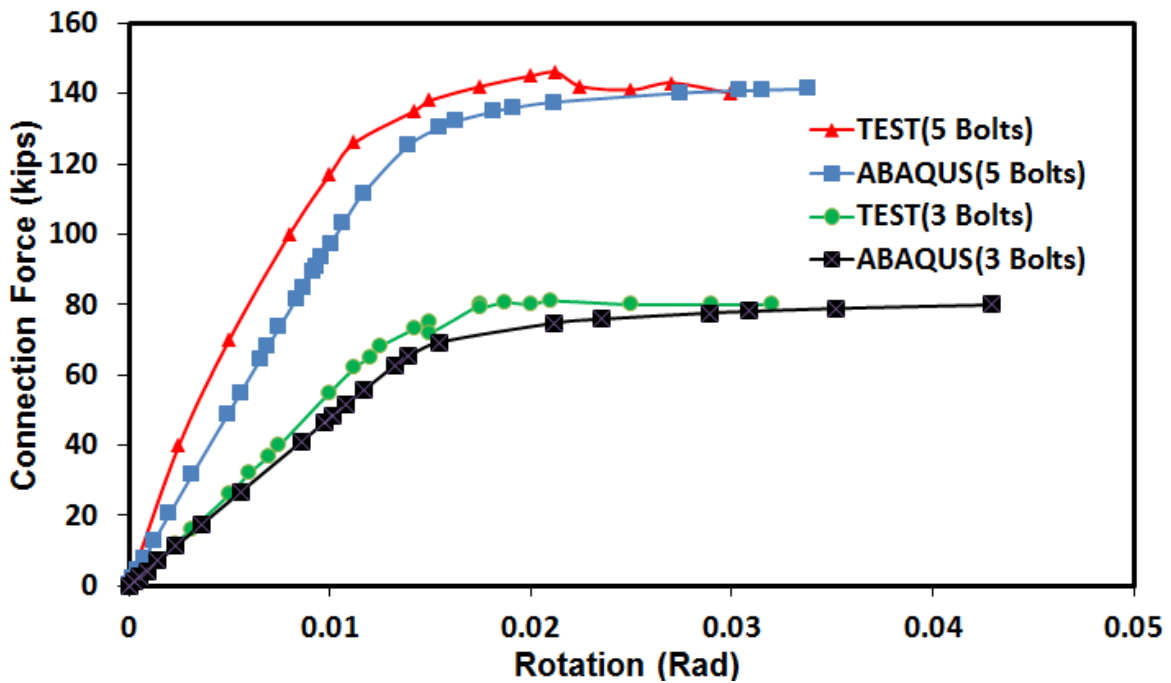


Figure 4.35 Load-rotation comparison between FEA and Metzger's test

4.5.5 Observations

As discussed above, modeling the contact interaction between the parts of a bolted steel connection poses a number of challenges. The simulation results are sensitive to the meshing patterns and element numbers. Numerical convergence difficulty is usually the major modeling issue, and it can be overcome by mesh refinement and proper boundary conditions. It was observed that if the material properties are accurately modeled, the FE analysis results show reasonably good agreement with the corresponding test results, in terms of force-deformation relationships and peak force. A major limitation of the FE model developed for this research, however, is that fracture is not modeled. The ultimate failure mode for steel connections is typically fracture of a connection element. Ultimate failure modes can include bolt shear fracture, tear out failure at a bolt hole, block shear fracture, etc. Thus, the FE model cannot predict the occurrence of first fracture, and cannot predict behavior after the first connection component fractures.

4.6 FE MODELING OF SIMPLE SHEAR CONNECTIONS AT ELEVATED TEMPERATURES

The predictions of the simple shear connection FE model compared reasonably well with test results at ambient temperature, as presented in the previous section. The model was then developed further to study connection performance at elevated temperatures. In the new model, the element type and meshing was still same, but the material properties were changed to temperature dependent variables.

Yu (2006) studied the behavior of simple shear connection components under elevated temperatures by conducting an extensive series of experiments. The single bolt (A325) connection test and twin-bolt (A490) connection test carried out by Yu were chosen for comparison with the FE analysis. Specimen setups and dimensions are shown in Figure 4.36 and Figure 4.37.

In the FE analysis of these tests, all the modeling procedures were kept the same as those used for the ambient temperature models except that elevated temperatures were

applied to the models using a predefined field function in ABAQUS. The properties of the plate steel and bolts at elevated temperatures were tested and reported by Yu. For the plate steel, simplified multi-linear stress-strain curves based on Yu's material test report were used in the FE models (Figure 4.38). Bilinear stress-strain relationships for different temperatures were applied to the bolt models (Figure 4.39). Meshing and deformed shapes of connection models are shown in Figure 4.40 and Figure 4.41, respectively.

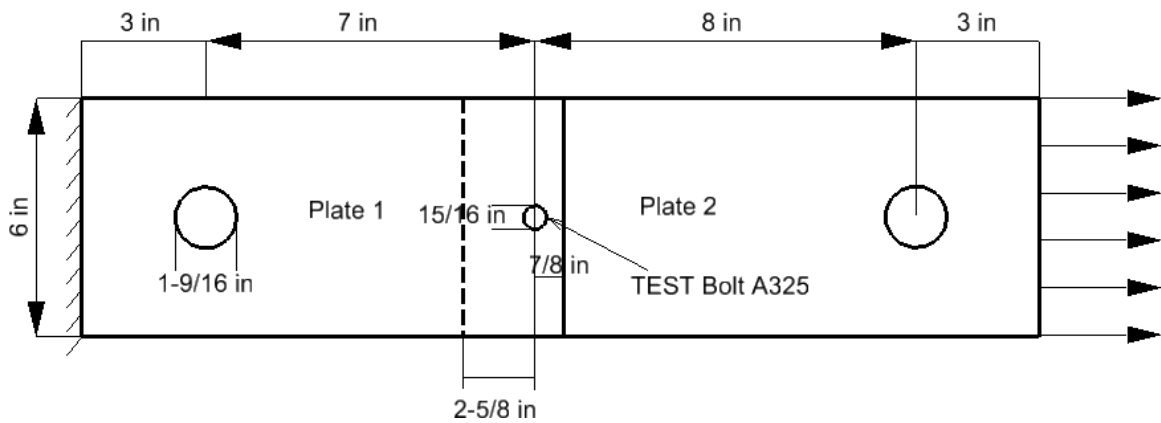


Figure 4.36 Single bolt connection setup and dimensions of Yu's test (Not in scale)

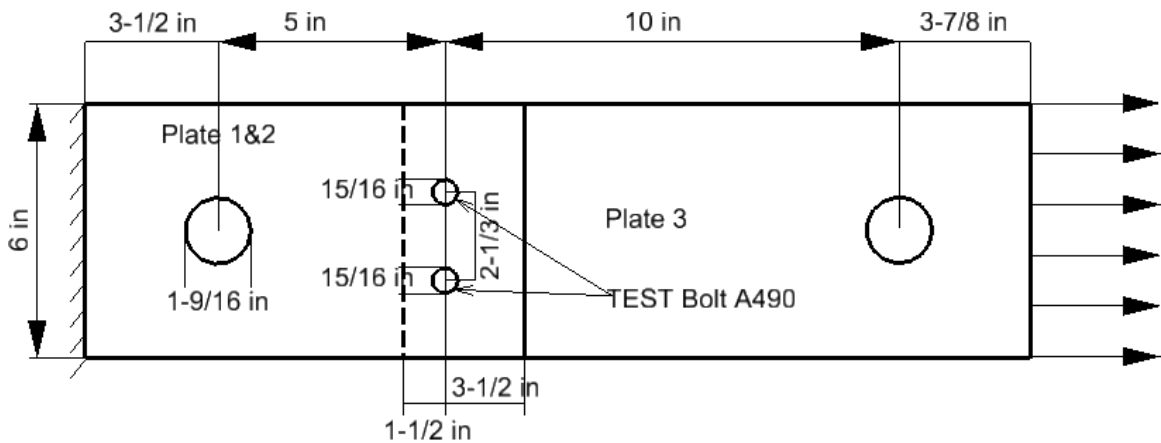


Figure 4.37 Twin-bolt connection setup and dimensions of Yu's test (Not in scale)

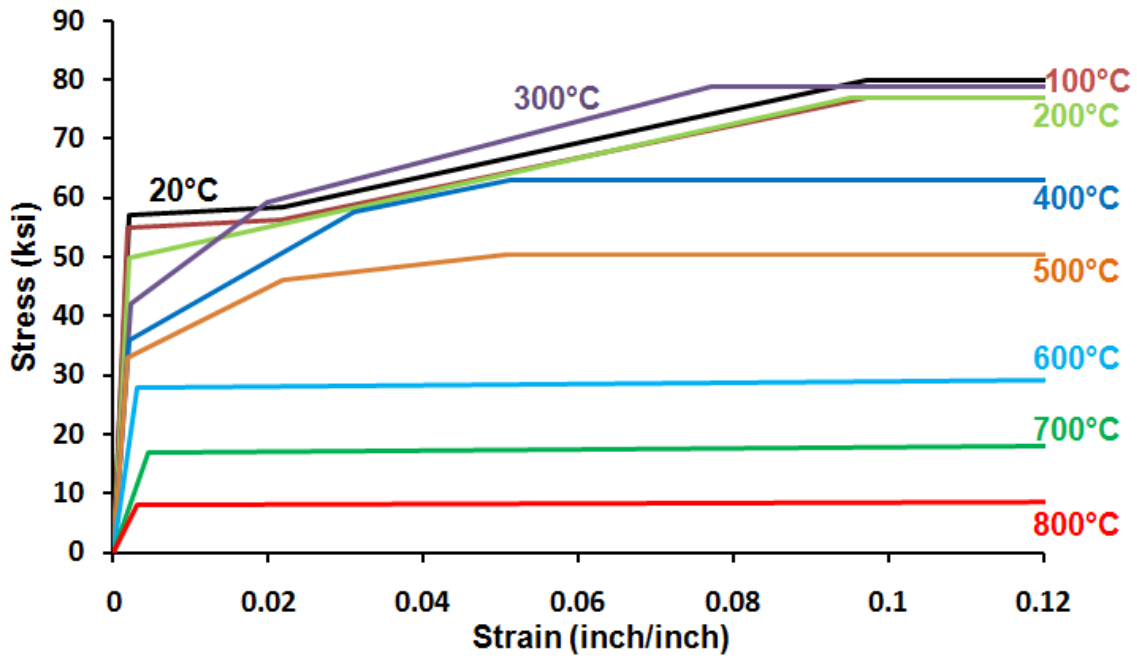


Figure 4.38 FE material model of plate steel at elevated temperatures used in Yu's test

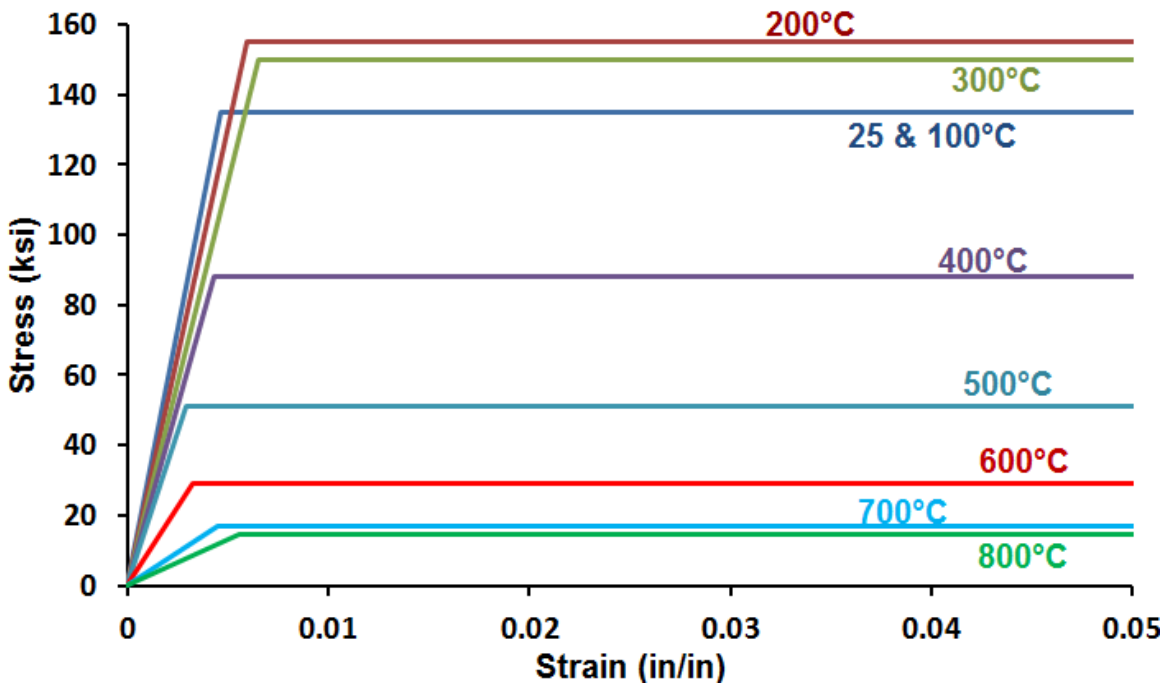


Figure 4.39 FE material model of A325 bolt at elevated temperatures used in Yu's test

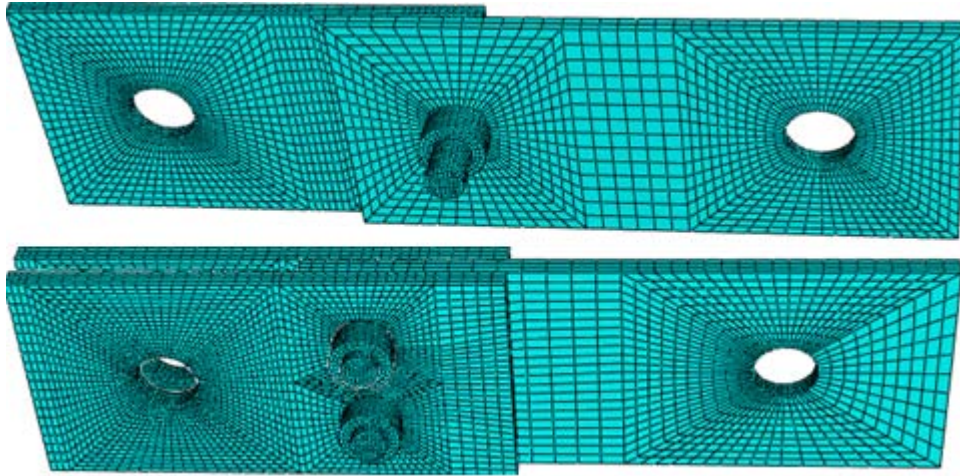


Figure 4.40 FE mesh of single and twin-bolt connection test

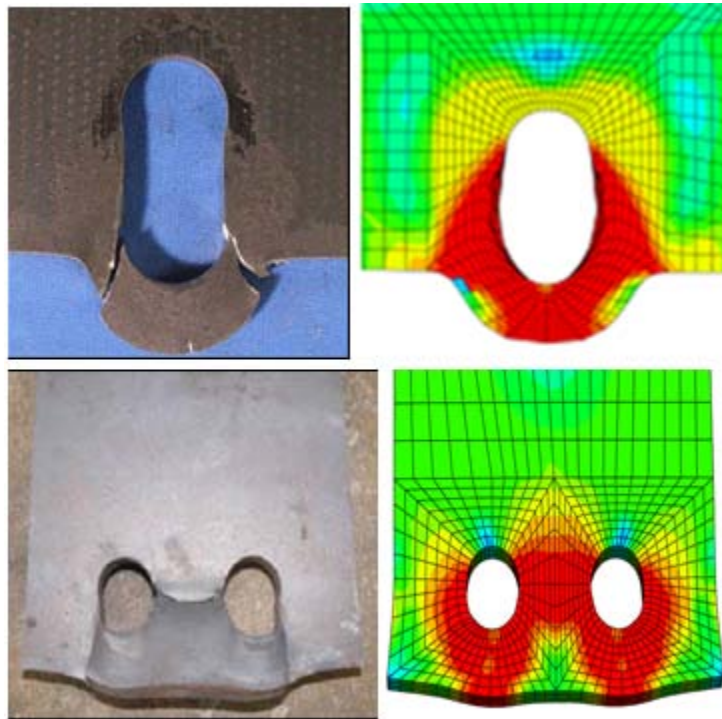


Figure 4.41 Deformations and stress contours of single bolt and twin-bolt connections

Comparisons between the FE analysis and Yu's test results are provided in Figure 4.42 through Figure 4.46. Figure 4.42 and Figure 4.43 show the load-deformation response of the single bolt connections at 300°C and 600°C, respectively. Figure 4.44, Figure 4.45 and Figure 4.46 show the load-deformation response of the twin-bolt connections at 300, 400 and 600°C, respectively. In Yu's test report, an initial flat portion of the curves exist in some connection test results due to initial slip of the bolted connection. However, in all figures of this study, the initial slip curves were removed for the purpose of comparison with the FE analysis results.

From these figures, it can be observed that the FE models captured the load-deformation response of the tests quite well at elevated temperatures for both connection configurations. It should be noted that in Yu's tests, all connections were tested under steady-state and simple loading conditions. To build sufficient confidence on the models, the FE model should be further validated by tests with transient-state heating and more complicated loading conditions.

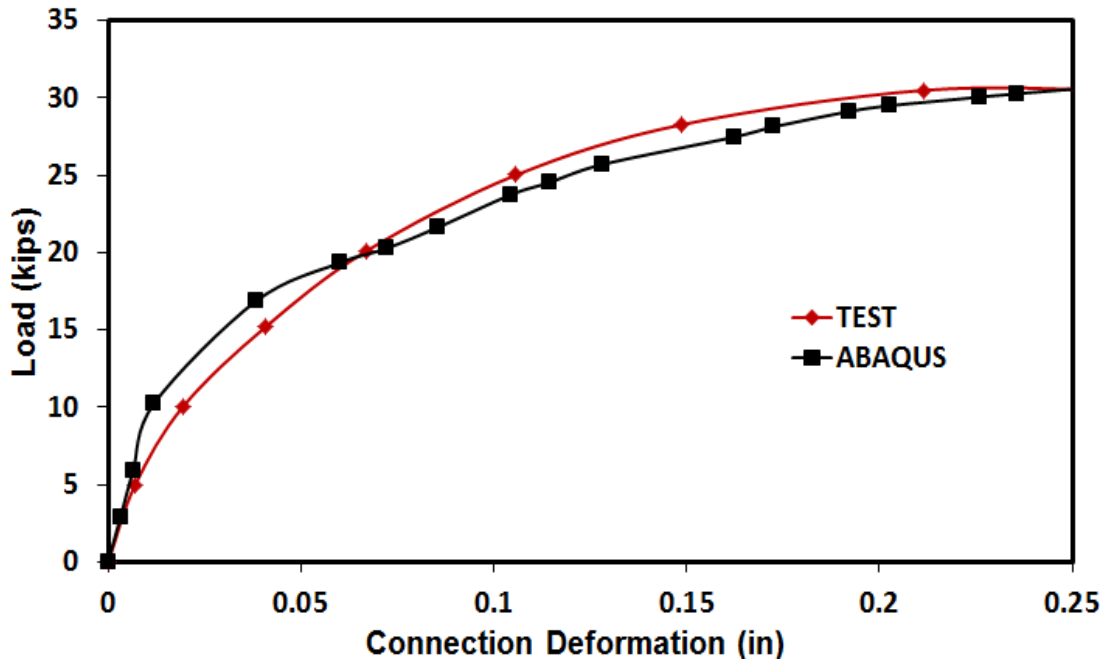


Figure 4.42 Single bolt load-deformation comparison between FEA and test (300°C)

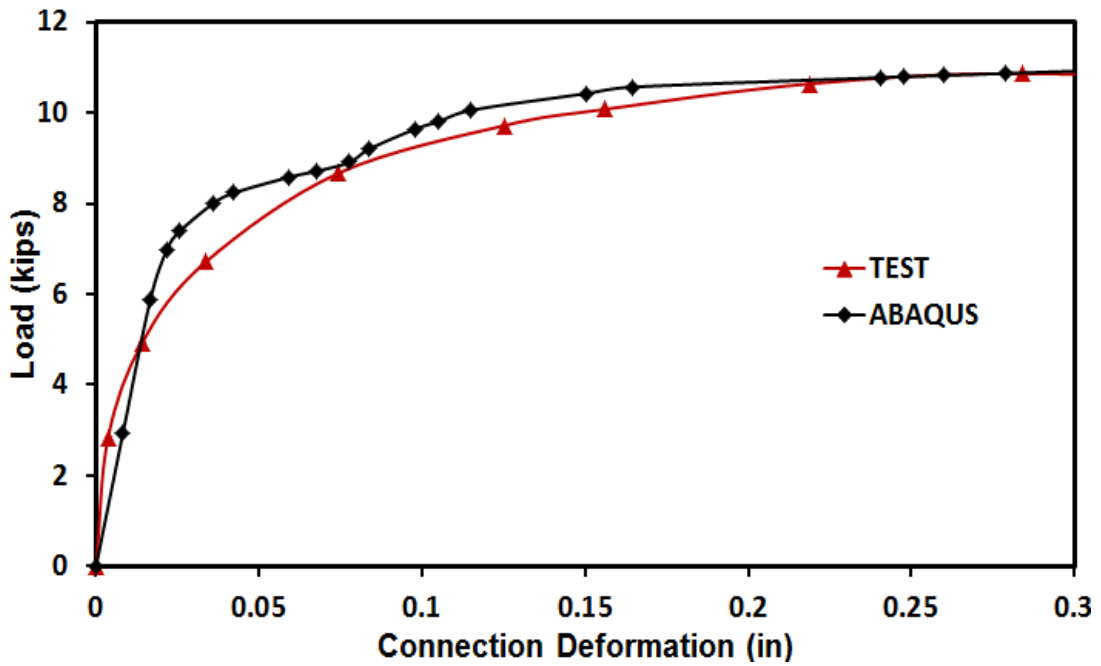


Figure 4.43 Single bolt load-deformation comparison between FEA and test (600°C)

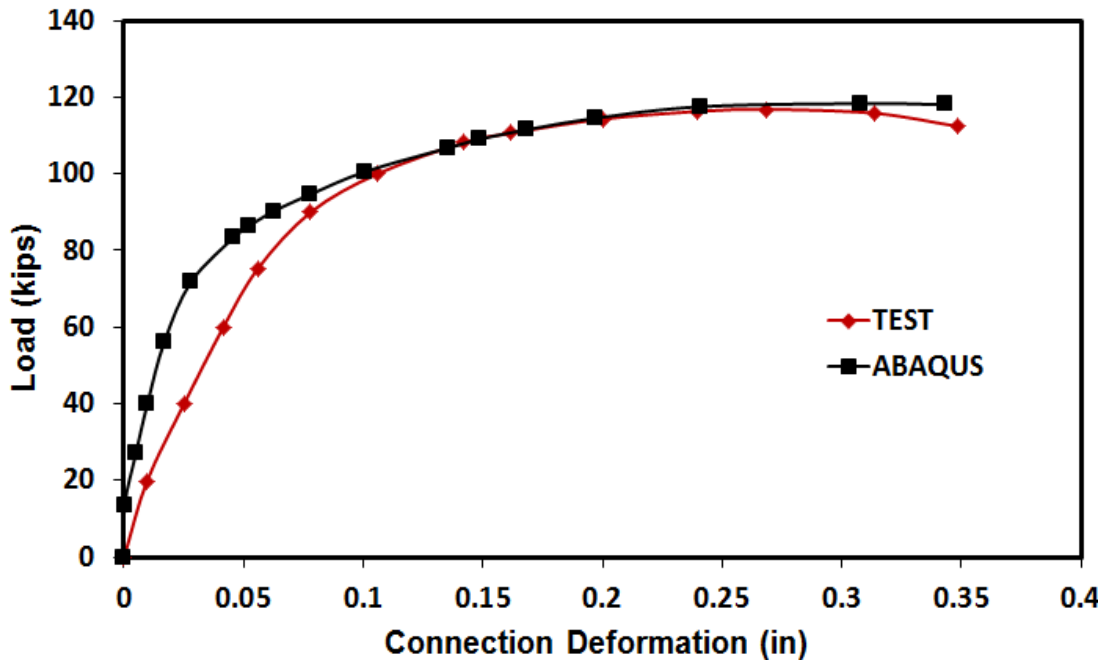


Figure 4.44 Twin-bolt load-deformation comparison between FEA and test (300°C)

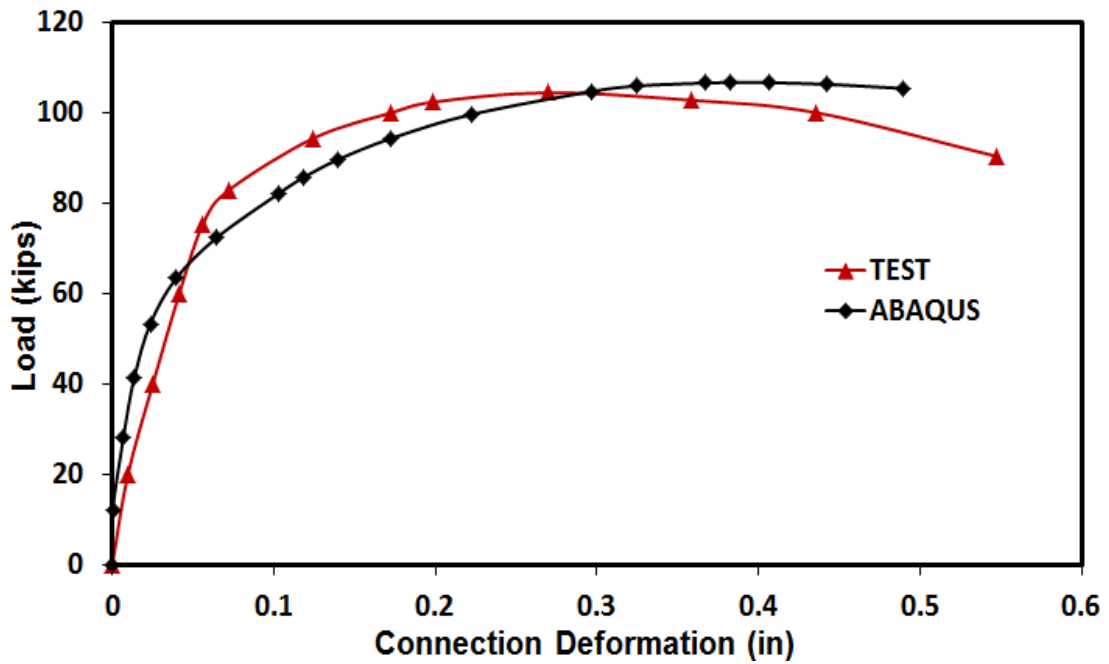


Figure 4.45 Twin-bolt load-deformation comparison between FEA and test (400°C)

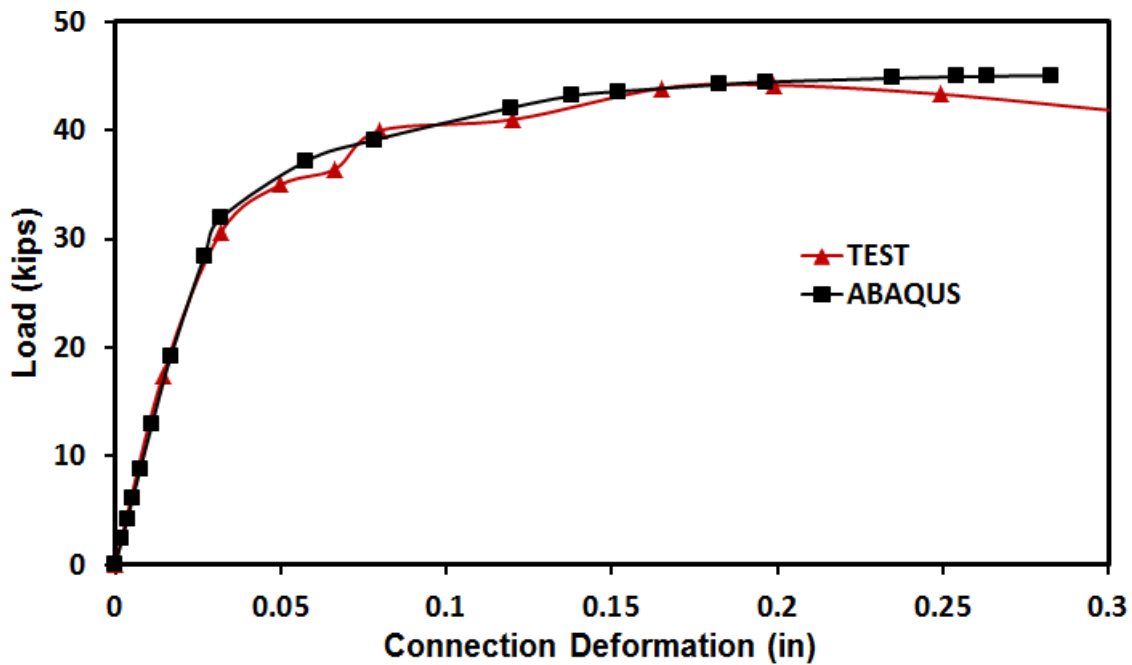


Figure 4.46 Twin-bolt load-deformation comparison between FEA and test (600°C)

4.7 FE MODELING OF SHEAR TAB BEAM END FRAMING CONNECTION IN FIRE

Wald's test (Sarraj 2007) was well documented and therefore was chosen to evaluate the beam end shear tab connection FE analysis model. In 2005, Wald and Ticha conducted a fire test on a steel beam with shear tab connections at the Czech Technical University (Figure 2.27). Three-bolt shear tab connections were assembled using fully threaded 12 mm diameter Grade 8.8 high-strength bolts with 6×60×125 mm shear tabs. The beam was a 3 meter long IPE160, and the loads (60 kN each) were applied by two hydraulic jacks 250 mm from the beam ends. The test beam was laterally restrained by regularly spaced thin steel strips welded to the beam top flange and the test rig. The shear tabs and steel beam were both of Grade S235 steel. The furnace gas temperature was controlled to follow the Cardington fire test no. 7 (Wald et al 2004) record for both heating and cooling stages. The temperatures of the connected beam and the connection

components were monitored and recorded throughout the test via several thermocouples. The deflection of the beam was measured at the load points.

With the given dimensions of Wald's specimen, an FE model was constructed (Figure 4.47). Since elevated-temperature stress-strain data for the steel used in Wald's specimen were not available, nominal values and reduction factors recommended by Eurocode 3 (2006) were applied. For Grade 8.8 high strength bolts, experimental elevated temperature strength values reported by Kirby (1995) were used. Temperatures at different locations on the beam and connections were successfully measured and recorded by Wald. Therefore, no heat transfer analysis was conducted for this simulation, as temperatures recorded in the test were considered as known inputs and were applied to the structural FE model directly.

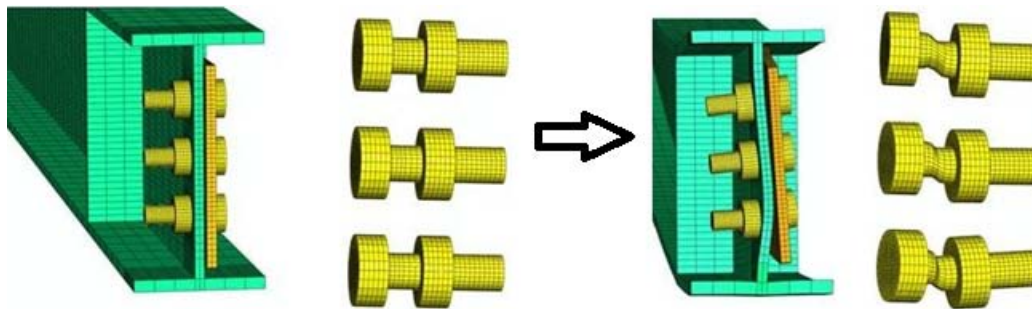


Figure 4.47 FE model of Wald's test specimen

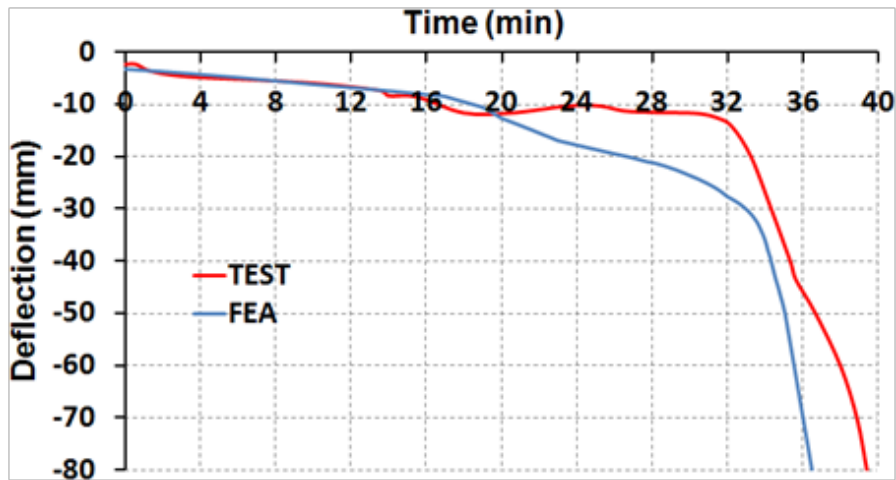


Figure 4.48 Deflection-time comparison between FEA and Wald's test

Figure 4.48 shows the comparison of Wald's test with the FE analysis results for beam deflection versus heating time. It can be observed that the two curves agree reasonably well except for a discrepancy at the "run-away" stage that may be caused by inaccurate material properties or temperature measurements. In addition, it was observed that in Wald's test the main failure mechanism for the shear tab connection was bolts shearing, which was also successfully predicted by the FE analysis. As described earlier, the FE analysis is not capable of explicitly modeling fracture of the bolts. However, bolt fracture was inferred from the model by the occurrence of very large deformations in the bolts.

4.8 OTHER TYPES OF CONNECTIONS

The FE connection model can be further developed to model other types of beam end bolted connections. For instance, using similar modeling technique, 3-D FE models of a double angle bolted connection and a top-seat angle connection are illustrated in Figure 4.49.

The FE model of a top and bottom seat angle connection is compared to the elevated-temperature connection tests by Daryan and Yahyai (2009). In this investigation,

cantilever beam tests were conducted, in which connections were loaded first and then furnace temperature was raised while maintaining a constant load. Comparison of the deformed shape of the connection from the test and FE model is exhibited in Figure 4.50. As shown in the figure, the large connection, prying action on the top bolt and upper angle are clearly simulated. An example of the good agreement between FE analysis and test on temperature - connection rotation response is shown in Figure 4.51. While this current research study is focused on shear tab connections, the comparison of the model with the test on a top and bottom seat connection helps build confidence in the capabilities of the model.

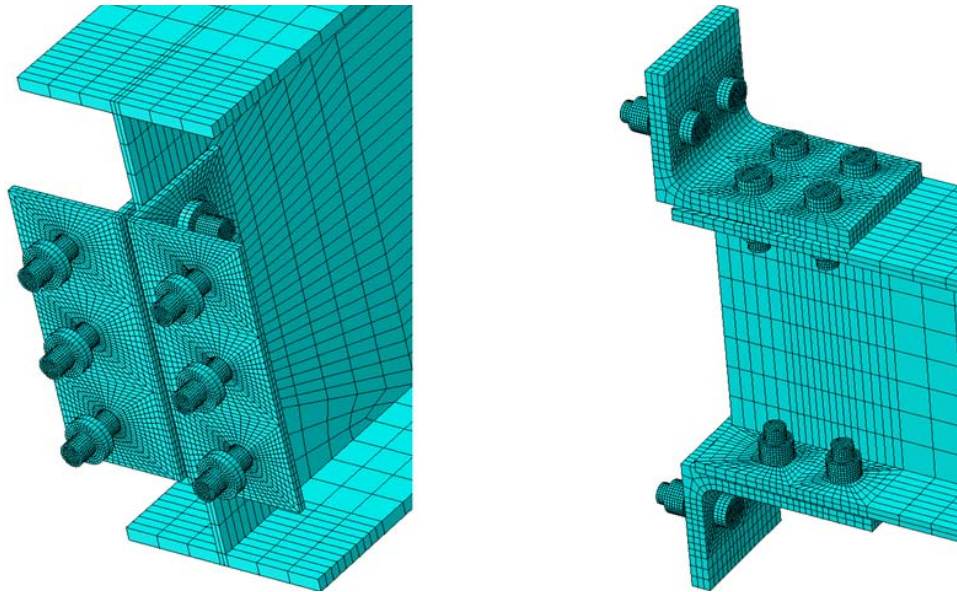


Figure 4.49 FE model of double angle and top-seat angle connection

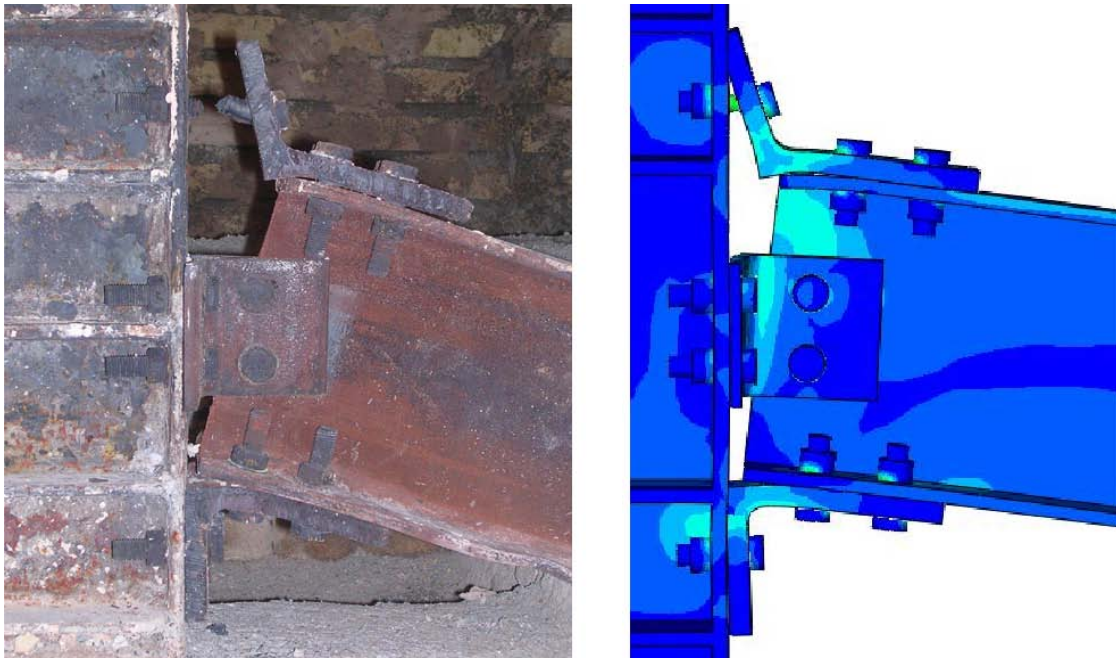


Figure 4.50 Deformations of top and bottom seat angle connection of Daryan's test and FE model

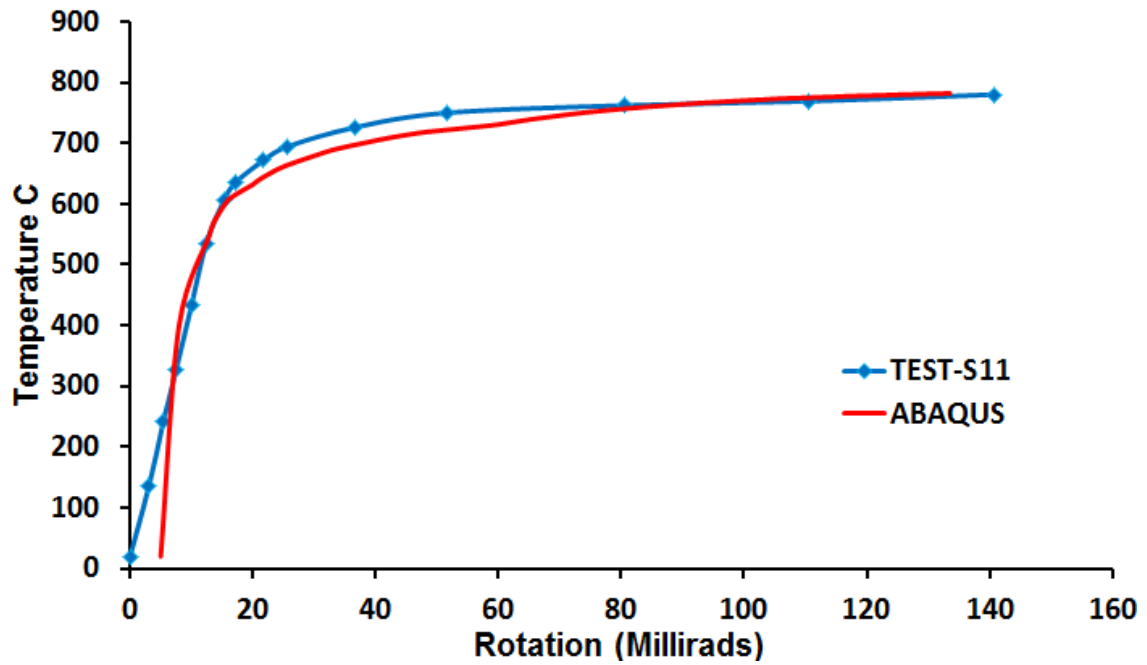


Figure 4.51 Temperature-rotation comparison between FEA and Daryan's test (test 11)

4.9 SUMMARY

In this chapter, the development of an FE heat transfer model and structural model was introduced. The ABAQUS program was used to simulate the thermal and structural behaviors of restrained steel beams in fire conditions. Both the heat transfer and structural models provided predictions that compared well with test results reported in the literature. Further, three-dimensional detailed connection models were developed, incorporating contact, geometric and material nonlinearity to capture steel bolted shear connection behavior under both ambient temperature and elevated temperatures. A convergence study was conducted on the bolted connection model to optimize the meshing pattern and element numbers. The FE model results compared reasonably well with experimental data from tests on connection components and beam-connection assemblies reported in the literature.

The FE modeling techniques developed in this chapter will be subsequently used to model the connection tests reported in Chapter 5 and to conduct parametric studies in Chapter 6.

CHAPTER 5

Shear Tab Connection Tests at Elevated Temperatures

5.1 OVERVIEW

As discussed in Chapters 1 and 2, observations from major building fire events and the Cardington fire tests showed that common failure modes seen in shear tab beam end framing connections subjected to fire are plate bearing failure and bolt shear failure. These connection failures are mainly caused by large axial forces in the beam during the heating and cooling phases of a fire, and large rotations when the beam starts to sag. Therefore, the load and deformation capacities of the connections under axial load and rotation are important factors that influence connection performance in fire.

This chapter describes a series of shear tab connection tests under axial tension and inclined tension (combined tension, shear and rotation) at elevated temperatures. The objectives of these tests were: (1) to gain an improved understanding of the performance of shear tab connections at elevated temperatures; (2) to provide experimental data that can be used for validation of finite element models; and (3) to provide experimental data to assess the ability of simplified design equations to predict elevated temperature connection performance. The loading and temperature conditions imposed on the test specimens were not intended to represent any specific building or fire scenario. Rather, the tests were intended to permit investigation of connection behavior under well-defined thermal conditions and well defined loading conditions that are generally representative of the conditions experienced by a connection during a fire. A primary focus of the experiments was to better understand the key limit states involved in connection response at elevated temperatures. While the experiments represent highly simplified thermal exposures and loading conditions, the intent is to use the experimental results to further

develop modeling approaches that permit the study of connection performance under a much wider range of more realistic conditions.

This chapter first describes the testing facilities and procedures used for these experiments. The results of a series of tests are then described. The measured and observed performance of selected specimens is then compared to the predictions from a finite element model, to better understand the capabilities and limitations of the model. Finally, connection test results are also evaluated using simplified equations provided in the AISC Specification (2005).

5.2 HIGH TEMPERATURE TEST SYSTEM

Two types of elevated-temperature connection tests were performed in this research program: tests on connections under axial tension and tests on connections under inclined tension. The same basic test equipment was used for both types of tests. The following sections describe the test equipment. This is followed by further detailed descriptions of the test specimens.

5.2.1 Loading System

A 550 kip-capacity MTS testing frame with 12 inch stroke was used to conduct these connection tests. Figure 5.1 shows the overall test frame with the furnace and other associated equipment. An MTS controller was used to control the load and/or crosshead displacement of the machine. The specimens were attached to the hydraulic grips of the test machine with 3-inch thick grade 50 steel plates. These plates were designed to work inside the furnace. Compared to the tested specimen, the loading plates were very stiff, and contributed very little to the overall deformations of the specimen.

5.2.2 Heating System

Specimens were heated using an Applied Test Systems (ATS) split box furnace with a 54 inch \times 27 inch \times 17 inch heated enclosure. The furnace uses electrical heating

elements with a 1000°C heating capacity. The furnace is supported by a motor driven lift system that allowed the furnace segments to be moved in and out of place easily. The furnace contains top, middle and bottom sections along the height. In all the connection tests conducted in this research, only top and bottom sections were used to save working space. Furnace temperature is measured by several thermocouples installed on the interior wall, and is controlled by an ATS temperature controller (Figure 5.1). A built-in safety thermocouple is located on the sidewall of the furnace (Figure 5.1) to ensure the temperature in the furnace will not exceed 1000°C.

5.2.3 Cooling System

The hydraulic loading grips for the test machine are not supplied with an internal water cooling system. To prevent the temperature of the top loading grip from being too high, a 44 inch × 26 inch stainless steel sheet was designed above the top of the furnace to block the convective heat (Figure 5.1). Besides a heat shield, the stainless steel sheet was also intended to prevent the hydraulic oil leaks onto the hot surface of the furnace, which can cause a fire. A suspended cooling electrical fan was also used during all tests to cool the upper grips (Figure 5.1). A heating test was conducted before all the connection tests. In this heating test, a steel plate was used as a test specimen and heated up to 700°C. After maintaining this temperature for 30 minutes, the temperature of the top and bottom loading grip and wedges was measured by thermocouples. The wedge was only heated up to 50°C primarily through conduction, and there was little noticeable heating in the grips.

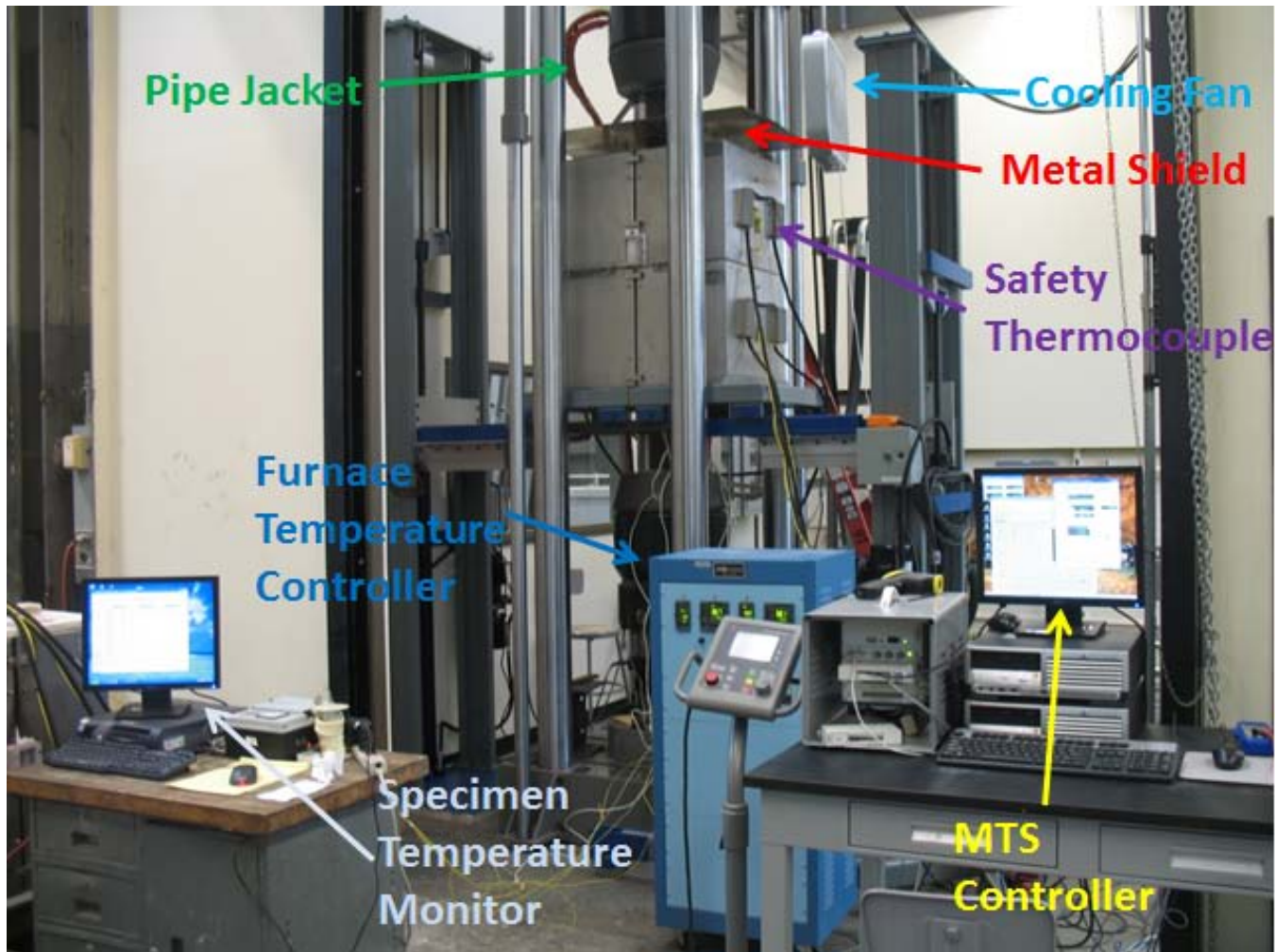


Figure 5.1 Testing facilities

5.3 INSTRUMENTATION

5.3.1 Temperature Measurement

Thermocouples were attached to beam web, shear tab and bolts to measure the surface temperature of the specimens at different locations. Type K thermocouple wires were used inside the furnace. Thermocouples can lose their accuracy after being heated to high temperatures several times, and thus the thermocouples were periodically replaced throughout the test program. From temperature data collected on the beam web, shear tab and bolts (an example is shown in Figure 5.2), it was found that the temperature distribution on the connection specimen was quite uniform. In this figure, it also can be noted that the heating time of the furnace is quite long (more than two hours to reach 400°C). The loading time was in the range of 30 minutes to an hour for all the connection tests.

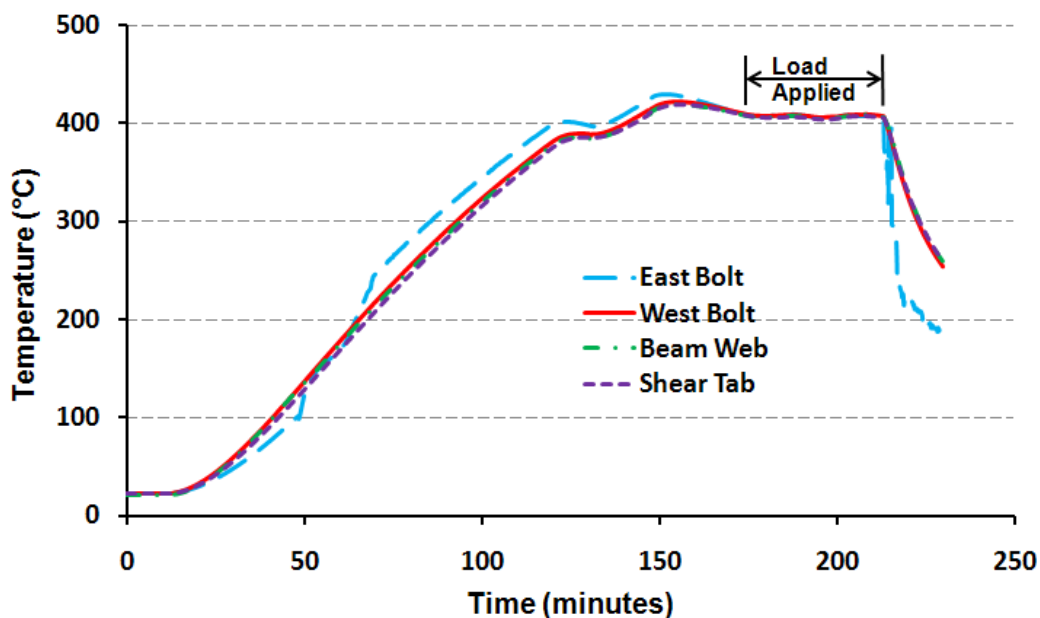


Figure 5.2 Temperatures collected on the different locations of specimen for a 400°C connection test

5.3.2 Load and Displacement Measurement

The load applied on the test specimens were measured using the load cell in the MTS test frame.

The MTS test machine measures and records the vertical displacement of the upper loading head. The displacement of the loading head is referred to as the total displacement in this chapter. For tests in which specimens were subjected to axial tension, the connection base plate displacements were measured by displacement transducers attached on two stainless steel rods extending outside of the furnace (Figure 5.6 (left)). These transducers permitted measurement of the relative displacement of the connection base plates.

For tests in which specimens were subjected to inclined tension, displacements of the connection base plates were measured using linear transducers attached to high temperature resistant wire extending outside of the furnace (Figure 5.6 (right)). These transducers allowed measurement of connection rotations. Labview based software was used for automatic data acquisition.

5.4 TEST SPECIMENS

Test specimens were cut from a W12×26 steel beam, which was made from ASTM A992 (minimum specified $F_y = 50$ ksi) structural steel. All of the W12×26 beam sections came from the same heat of steel. Beam sections were connected to a 3/8 inch-thick shear tab made from A36 structural steel (minimum specified $F_y = 36$ ksi) using three hand tightened A325 structural bolts (minimum specified $F_u = 120$ ksi). 3/4 inch diameter bolts and 1 inch diameter bolts were used in the connections under both loading conditions. All bolts of a given diameter came from the same production lot. Threads were excluded from the shear plane of the bolts. Shear tabs and beam sections were both welded to two thick base plates by 1/4 inch fillet welds using SMAW/shielded metal arc welding with 7018 electrode ($F_y = 50$ ksi). Connection dimensions follow the standard dimension requirements of the AISC Manual (2006) (Figure 5.3 and Figure 5.4). A

limited number of tests were also conducted with sections cut from a W12×40 A992 beam. These were preliminary tests conducted at the start of the experimental program to help develop the test procedures and instrumentation.

In the inclined tension test, the angle between the axis of the connection and the loading direction was 37° (Figure 5.4). To avoid having the specimens striking the wall of the furnace, the beam sections are 2 inch shorter than those used in axial tension tests.

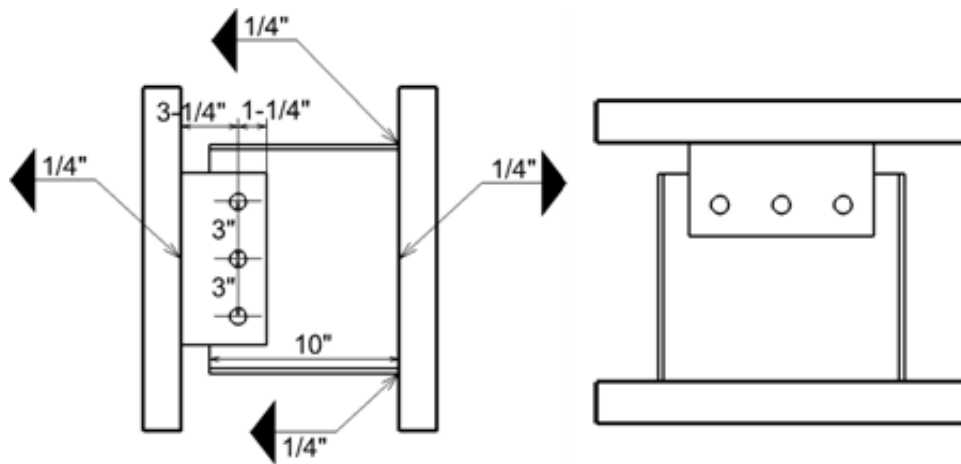


Figure 5.3 Axial tension test specimen dimensions

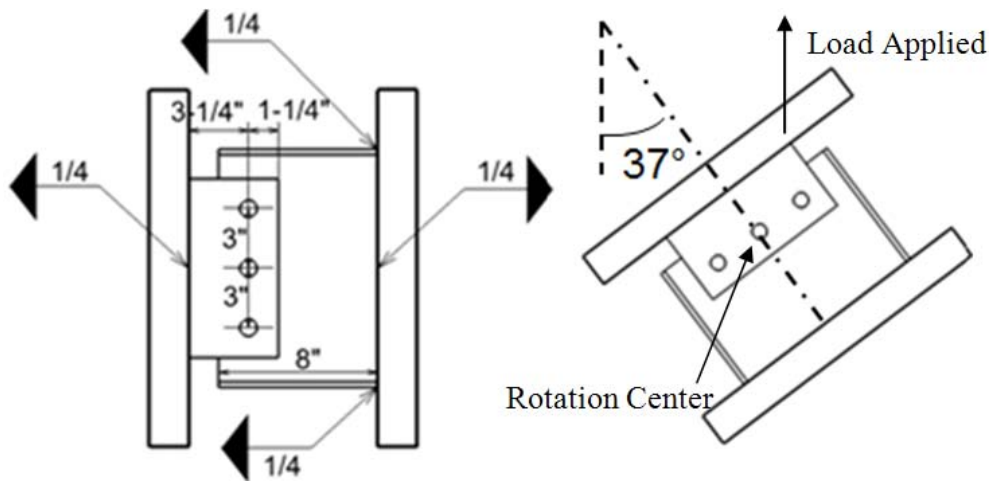


Figure 5.4 Inclined tension test specimen dimensions

Material mechanical properties of connection components at ambient temperature were determined by experiments (Table 5.1). Ambient temperature stress-strain curves of structural steel used in beam section and shear tab are shown in Figure 5.5. It is noted the ambient temperature strength of the structural steel used in W12×26 is quite similar with the A992 steel tested in Chapter 3.

Table 5.1 Measured material properties at ambient temperature

Connection Part	Yield Strength (ksi)	Tensile Strength (ksi)	Final Elongation
W12×40	49.9	75.0	28%
W12×26	58.9	75.1	32%
Shear tab	43.9	65.6	35%
Bolts	Not Measured	139.4	Not measured

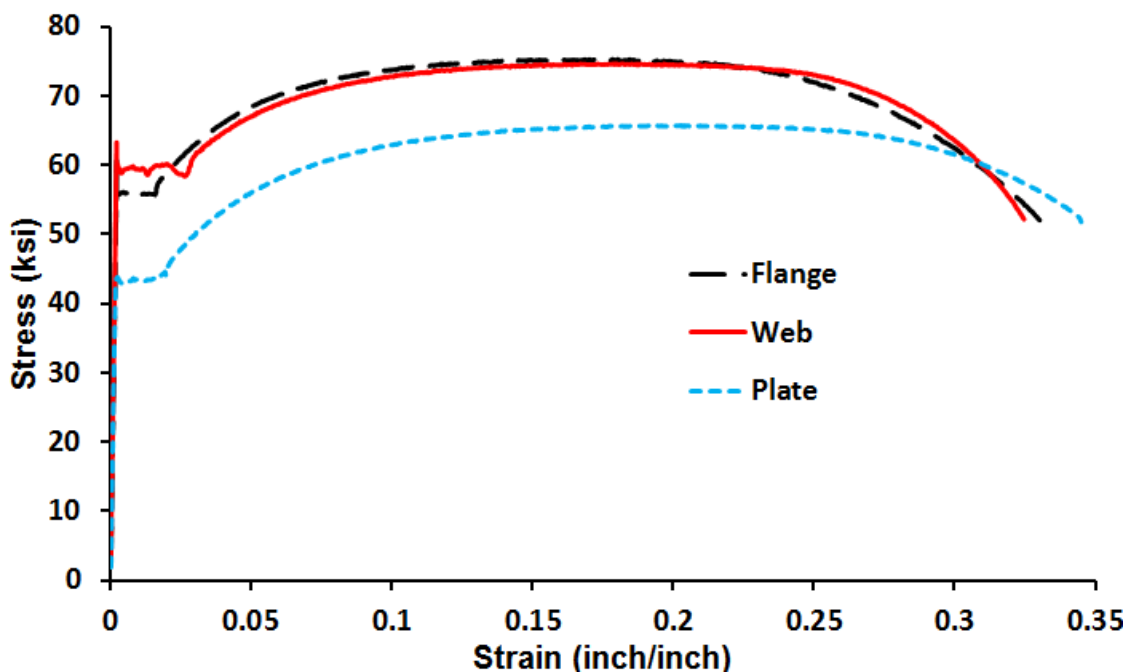


Figure 5.5 Stress-strain curves of steel used in beam and shear tab

5.5 TESTING PROCEDURE

In this study, all tests were thermal steady state tests, in which the specimens were heated up to a target temperature and then loaded to failure while maintaining the same temperature. During the heating process, the load was maintained at zero to allow free expansion of the specimen. Besides being thermal steady state, all tests were displacement-controlled, in which a crosshead displacement rate of 0.05 inch/min was maintained at a constant value throughout a test. To evaluate repeatability of results, selected connection tests were repeated.

5.5.1 Connections under Axial Tension

5.5.1.1 *Connection under Axial Tension at Elevated Temperatures*

For these tests, the specimen is heated to the desired temperature and then loaded under axial tension until failure is achieved (Figure 5.6 (left)). The maximum load during the test is taken as the specimen's tensile capacity at this temperature.

To help develop the testing procedures and instrumentation, preliminary tests were conducted on connection specimens containing W12×40 beam sections at ambient temperature and at 600°C. After building sufficient confidence, connection specimens containing the W12×26 beam section using 3/4 inch diameter A325 bolts were tested at temperatures of 20°C, 400°C, 500°C, 550°C and 700°C. Specimens containing same beam section using 1 inch diameter A325 bolts were tested at temperatures of 20°C, 500°C and 700°C. It was observed that test specimens can experience large rotations after the first failure is achieved, and the specimen can subsequently strike the inside wall of the furnace. Therefore, for connections tested at elevated temperatures using the furnace, loading was stopped after first failure was achieved. However, for connection tests at ambient temperature, loading was continued until the final failure of the connection occurred, which means the beam sections and shear tabs were completely separated from each other.

5.5.1.2 Connections under Axial Tension after Cooling

As described in Chapter 2, previous research has shown that structural bolts can suffer permanent loss of strength after exposure to high temperature and subsequent cooling (Kirby 1995 and Yu 2006). Structural steel, on the other hand, experiences only minor loss of strength after heating and cooling, although more significant strength loss is observed at temperatures of 800 to 1000°C (Lee and Engelhardt 2010). To understand the post-fire behavior of shear tab connections, connections were heated to selected temperatures, cooled to ambient temperature, and then tested to failure.

In these tests, connections with 3/4 inch A325 bolts were initially heated up to 800°C, 900°C and 1000°C, respectively, using an electrical split box furnace with a 48 inch × 14 inch × 14 inch heated enclosure (Figure 5.8). After maintaining the target temperatures for an hour, the furnace was shut down and the connections naturally cooled down to ambient temperature in the furnace. The connections were then installed in the testing machine and loaded under axial tension to final failure.

This study requires understanding of the behavior of structural bolts after exposure to high temperatures. As discussed in Chapter 2, Yu (2006) conducted tests to study the behavior of ASTM A325 structural bolts after exposed to high temperatures. However, Yu did not study the residual strength of A325 bolts after exposed to a temperature higher than 800°C. Therefore, in this research, a similar heating and cooling test procedure was conducted on 3/4 inch A325 structural bolts. The residual strength of the bolts after exposure to temperatures of 800°C, 900°C and 1000°C was investigated using a bolt tensile strength testing device (Figure 5.9). These bolt tests after heating and cooling can provide supportive information in understanding connection behavior after exposed to high temperature, and also helps fill a gap in the previous research on the A325 bolts.

5.5.2 Connections under Inclined Tension

As discussed in Chapters 1 and 2, when exposed to a building fire simple beam end framing connections can be subjected to a combination of shear and axial loading, combined with large rotations. The shear loading is mostly caused by the gravity load of the floor system, which mostly does not change significantly during a fire event. However, the axial force and rotation at the beam ends are highly temperature dependent, and thus can vary considerably during a fire. This complex load condition creates large difficulties in the testing of beam end connections under steady-state thermal conditions, so some simplifications have to be made in the test design. Nevertheless, the complex load that the connection experiences during a fire still needs to be considered and included in such a test.

In this study, specimens were rotated to 37° angle relative to the loading direction. This angle was chosen largely based on geometric constraints of the furnace. The tensile displacement loading was applied off the rotation center of the connection, resulting in a combination of shear, tension and rotation in the connection. During a test, the increase of the applied displacement loading changes the angle between loading direction and the axis of specimen, and thus changes the ratio of shear and axial forces in the connection. Rotations will also change with increasing axial displacements. This loading condition was considered as capturing key elements of the actual loading conditions of the connection in a building fire. In each test, loading was applied until final failure was achieved. Specimens with 3/4 inch and 1 inch diameter A325 bolts were tested at temperatures of 20°C, 400°C, 500°C and 700°C.

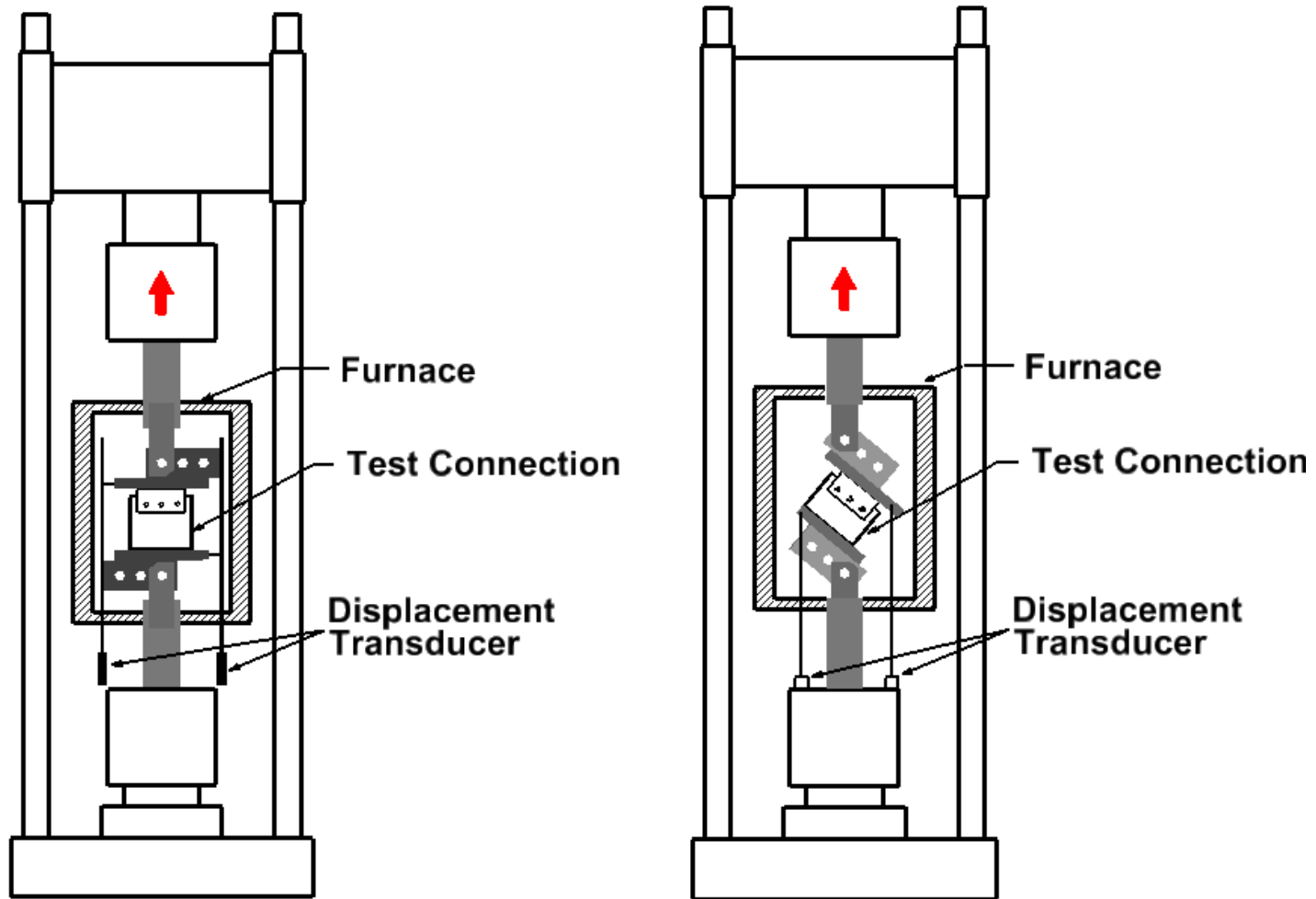


Figure 5.6 Layout of test setup for connections subject to tension (left) and specimens subject to inclined tension (right)



Figure 5.7 Test setup without furnace, for connections subject to tension (left) and specimens subject to inclined tension (right)



Figure 5.8 Furnace used for heating and cooling



Figure 5.9 Testing device for bolt tensile strength

5.6 TEST RESULTS

5.6.1 Connections under Axial Tension at Elevated Temperatures

5.6.1.1 Connections with 3/4 inch A325 bolts

A summary of the test results is given in Table 5.2. Figure 5.10 shows the failure shape of W12×40 preliminary connections after testing at temperatures of 20°C and 600°C. Figure 5.11 through Figure 5.13 show the failure shape of W12×26 connections after testing. At ambient temperature, bearing tear out failure at bolt holes in the beam web was the major failure mode, with little shear deformation observed in the bolts. Significant out-of-plane bending deformations can be observed in the beam web and shear tab. At 400°C, the connection still failed due to tear out of the beam web, but noticeable bolt shear deformation was observed. Further, at higher temperatures (500°C and above) little permanent deformation of the bolt holes was observed after the tests, and connections failed by shear fracture of the bolts. No obvious out-of-plane bending

deformation was observed. For all the connection tests conducted, welds failure was not observed. It should also be noted that in these tests, for the two failure modes discussed above, the fracture failures at different locations of the connection occur simultaneously, and the load on the connection drops to zero level immediately after the fractures occur. The change of failure mode from bearing failure at lower temperatures to bolt shear failure at higher temperatures likely reflect the fact that bolts lose strength at high temperatures at a faster rate than structural steel, as discussed in Chapter 2.

Figure 5.14 shows the load-displacement curves for the W12×26 specimens. A progressive loss of connection strength with increasing temperature can be observed. Moreover, it can be seen that as the temperature increased from 20°C to 400°C, the connection failure mode remained the same (bearing failure) but connection deformation capacity was smaller. This is consistent with the test results on A992 structural steel at elevated temperatures in Chapter 3, which showed reduced material ductility at 400°C.

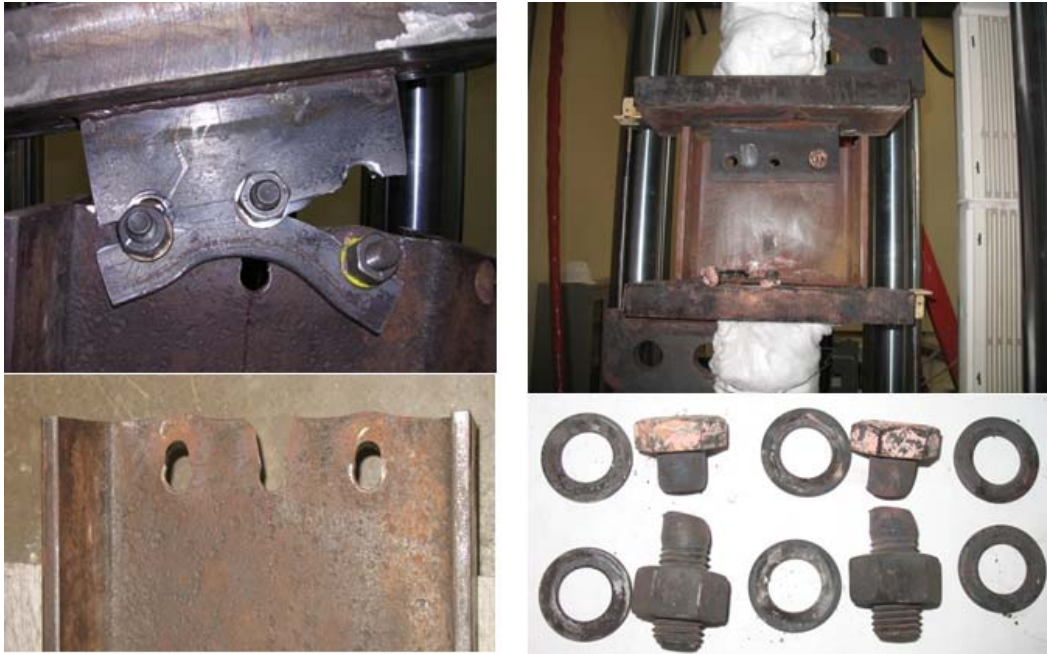


Figure 5.10 Connection failures after axial tension tests at 20°C (left) and 600°C (right) – W12×40



Figure 5.11 Connection failures after axial tension tests at 20°C (left) and 400°C (right) – W12×26 – 3/4 inch A325 bolts



Figure 5.12 Connection failures after axial tension tests at 500°C (left) and 550°C (right) – W12×26 – 3/4 inch A325 bolts



Figure 5.13 Connection failure after axial tension test at 700°C – W12×26 – 3/4 inch A325 bolts

Table 5.2 Test results for connections with 3/4 inch A325 bolts under axial tension

Specimen	Temperature (°C)	Peak Load (kip)	Failure Mode
W12x40	20	109.4	Bearing/Fracture
W12x40	600	20.6	Bolt Shear
W12x26	20	75.3	Bearing
W12x26	20	78.5	Bearing
W12x26	400	70.1	Bearing
W12x26	400	70.3	Bearing
W12x26	500	47.4	Bolt Shear
W12x26	550	33.5	Bolt Shear
W12x26	700	10.8	Bolt Shear

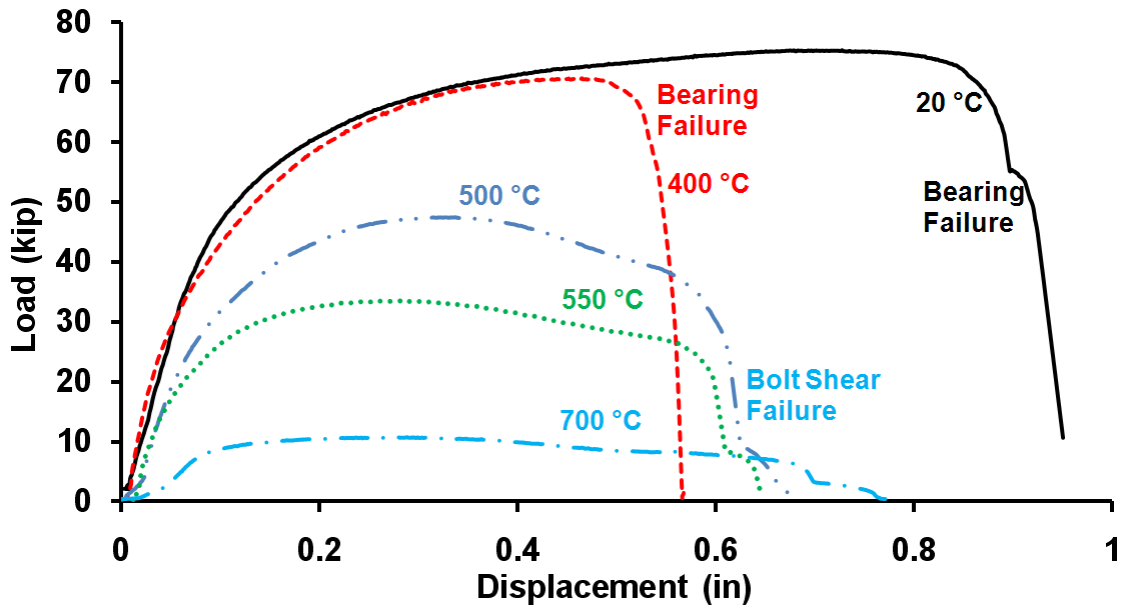


Figure 5.14 Load displacement response of connections with W12x26 beams and 3/4 inch A325 bolts under axial tension

5.6.1.2 Connections with 1 inch A325 bolts

Test results are given in Table 5.3, and the failure shapes of the connections after testing are shown in Figure 5.15. It can be seen that by increasing the bolt size, all of the connections failed by bearing failure at the beam web at all test temperatures. Figure 5.16 shows the load-displacement responses. The connection tested at 500°C exhibited the least ductility among the three. The comparison of load-displacement relationships between connections with 3/4 inch bolt and connections with 1 inch bolt at temperatures of 500°C and 700°C is shown in Figure 5.17. At 500°C, the connection failure modes are different, but the ductility of the two connections is similar. At 700°C, the connection that failed by bearing exhibited significantly larger ductility than the connection that failed by bolt shear fracture.



Figure 5.15 Connection failures after axial tension tests at 20° (top left), 500°C (top right) and 700°C (bottom) – W12×26 – 1 inch A325 bolts

Table 5.3 Test results for connections with 1 inch A325 bolts under axial tension

Temperature (°C)	Peak Load (kip)	Failure Mode
20	74.8	Bearing
500	52.7	Bearing
700	14.9	Bearing

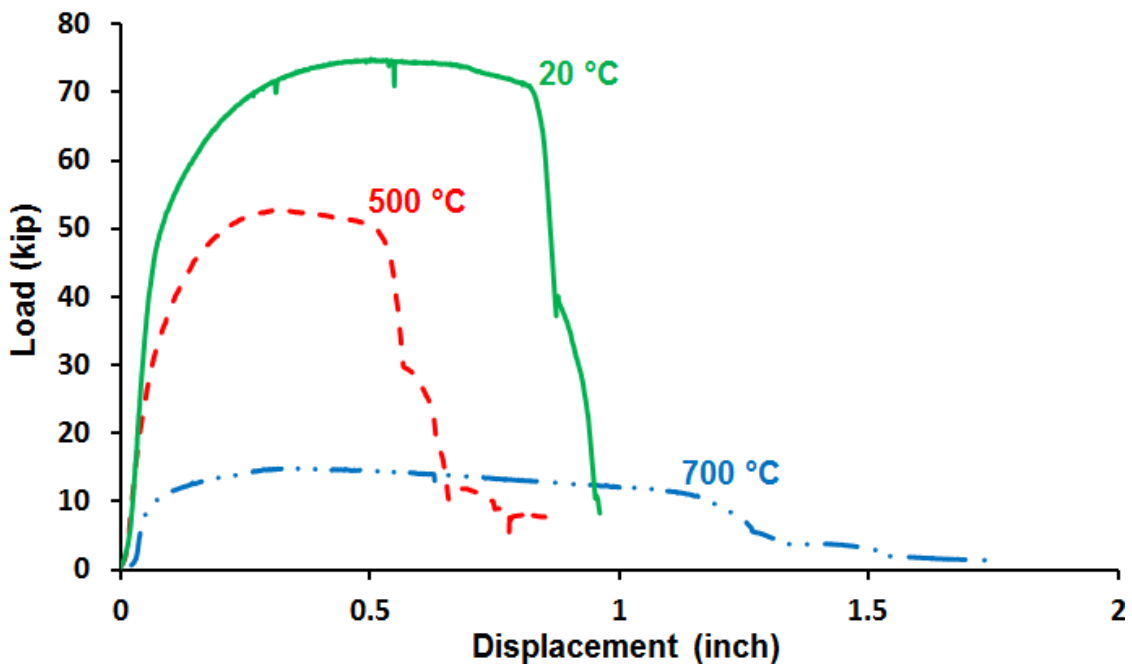


Figure 5.16 Load-displacement response of connections with 1 inch A325 bolts under axial tension

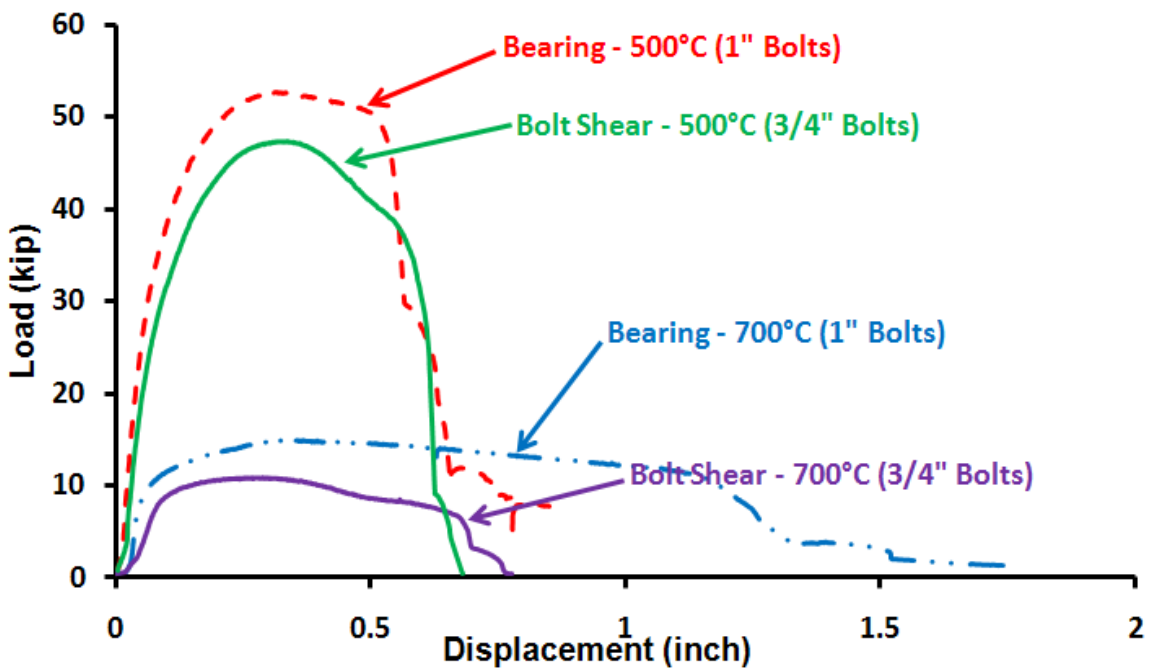


Figure 5.17 Comparison between connections with two bolt sizes

5.6.2 Connections under Axial Tension after Heating and Cooling

A summary of the test results is given in Table 5.4. Figure 5.18 shows a completely cooled specimen taken out from the furnace after being exposed to 900°C. Figure 5.19 shows the failure shape of the connection tested after being exposed to 1000°C.

Compared to the bearing failure mode observed in the unheated connections, after being heated to 800°C and cooling, the connection failure mode changed to bolt shear fracture. This indicates that the structural bolts experienced larger strength reduction than the structural steel of the beam section after being heated to 800°C and cooling down to ambient temperature. However, further testing the connections that were exposed to 900°C and 1000°C led to an interesting finding that the connection failure mode changed back to bearing failure in the beam web. This suggests that, exposed to a temperature at or above 800°C and then cooled down to ambient temperature, the further strength reduction of the bolts is less than the structural steel of the beam. To investigate this, bolt residual tensile strength after being exposed to temperatures of 800°C, 900°C and 1000°C was measured, and the results are shown in Table 5.5. From these tests, the strength reduction factor of 0.59 was obtained for A325 structural bolts after being exposed to 800°C, and this result is in good agreement with Yu's test results (Yu 2006), in which 800°C is the maximum temperature investigated. Interestingly, when exposed to 900°C and 1000°C, the residual strengths of A325 bolts are almost the same as those exposed to 800°C. With Yu's results incorporated, the strength reduction factors for A325 bolts after heating and cooling can be further evaluated to 1000°C, and are shown in Figure 5.21.

The load-displacement response of these connections is shown in Figure 5.22. Based on the discussion above, it can be concluded that compared to the unheated connection, the strength reduction of the connection exposed to 800°C is mainly caused by strength reduction of the bolts. However, compared to the connection exposed to 800°C, further strength reduction of connections exposed to higher temperatures (900°C

and 1000°C) is mainly caused by the strength loss of the structural steel. In addition, compared to the unheated connection there is noticeable ductility loss for connections exposed to heating and cooling.

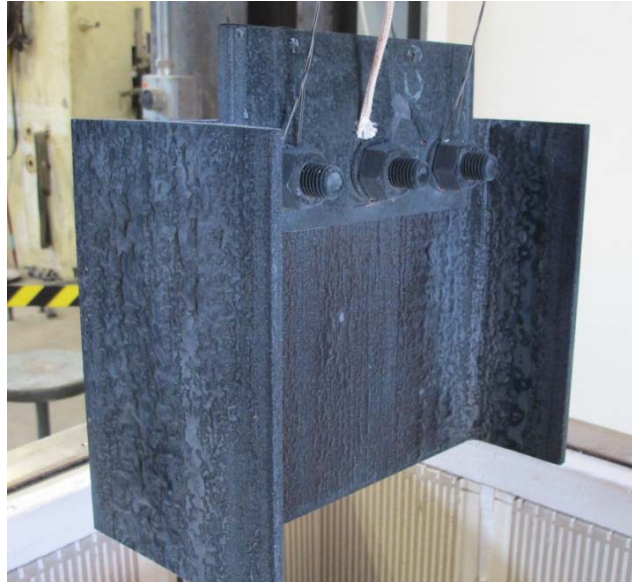


Figure 5.18 Specimen after exposure to 900°C



Figure 5.19 Failure shape of specimen exposed to 1000°C and subsequently cooled and tested



Figure 5.20 Bolts fracture in tensile test after exposure to high temperatures (900°C- left two; 1000°C-right two) and cooling

Table 5.4 Test results for connections with 3/4 inch A325 bolts under axial tension after heating and cooling

Temperature Exposed (°C)	Peak Load (kip)	Failure Mode
800	70.2	Bolt Shear
900	65.8	Bearing
1000	64.0	Bearing

Table 5.5 Residual tensile strength of 3/4 inch A325 bolts after heating and cooling

Temperature Exposed (°C)	Bolt Strength (ksi)
800	83.79
900	83.82
1000	83.73

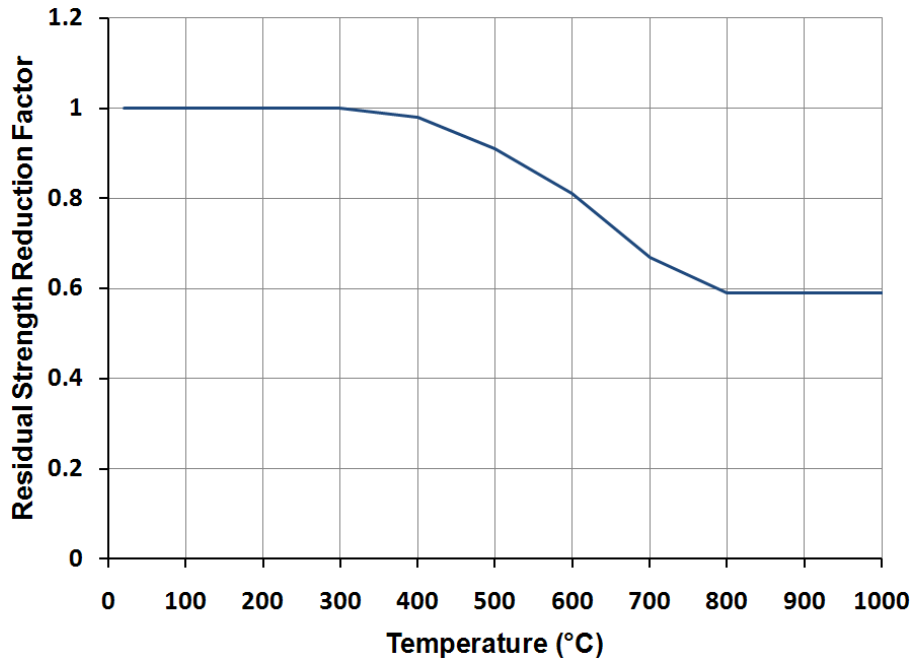


Figure 5.21 Residual Strength Reduction Factor for A325 Bolts after Heating and Cooling

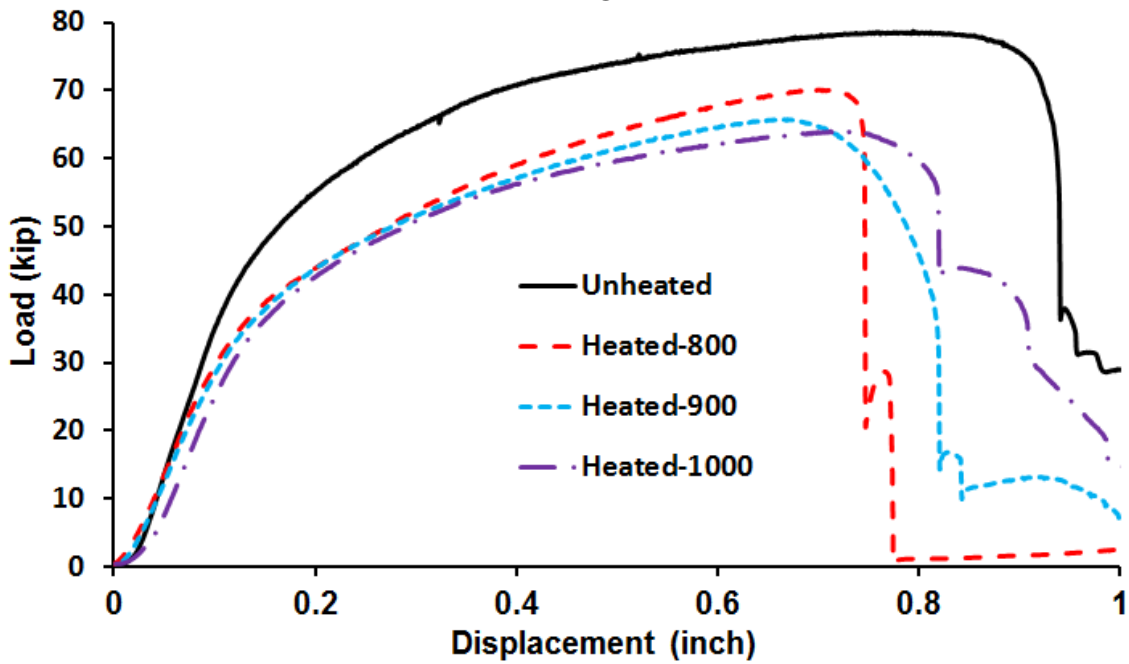


Figure 5.22 Load-displacement response of connections tested in axial tension after heating and cooling

5.6.3 Connections under Inclined Tension at Elevated Temperatures

5.6.3.1 Connection with 3/4 inch A325 bolts

Table 5.6 summarizes the peak loads and failure modes for these connection tests. Figure 5.23 and Figure 5.24 show the failure shapes and deformations of the connections tested at different temperatures. At ambient temperature, the connection failed by bearing failure in the beam web, and the bearing fracture path is in the same direction of the applied load. At temperatures of 400°C and above, connections failed by bolt shear failure. It was observed that in these tests for both failure modes, all the connections were subjected a sequential failure, which means after the first failure (bearing tear out in web or bolt shear fracture) the connection can still take a considerable amount of force until the subsequent failures occur. Relationships of the applied loads and measured connection rotations at elevated temperatures are shown in Figure 5.25. The rotation plotted in this figure is the relative rotations between the two connection end plates: the end plate supporting the shear tab and the end plate supporting the beam. It can be observed that during these tests, the connections experienced large rotations before final failure was reached. Figure 5.26 shows the load-displacement response measured during the tests by the MTS machine.

The connection behavior under combined tension, shear and rotation can be illustrated by the load-rotation curve at 500°C (Figure 5.27). Three sequential bolt shear failures can be observed from this example. The first bolt shear failure occurred after the connection reached its peak load when the connection rotation was relatively small (about 0.05 rad in this test). This was followed by a significant load drop and an increase in connection rotation until the load increased again. The second bolt shear failure occurred when the connection rotation nearly reached 0.1 rad, and then the load decreased to about zero with quite a large increase in rotation. At this point, the third bolt started to pick up load up to the final bolt shear failure. The rotational capacity of this connection at 500°C was on the order of 0.4 rad before final failure was achieved. As described earlier, final

failure is considered to the point where the beam is completely separated from the shear tab.



Figure 5.23 Connection failures after inclined tension tests at 20°C(left) and 400°C (right) – 3/4 inch A325 bolts

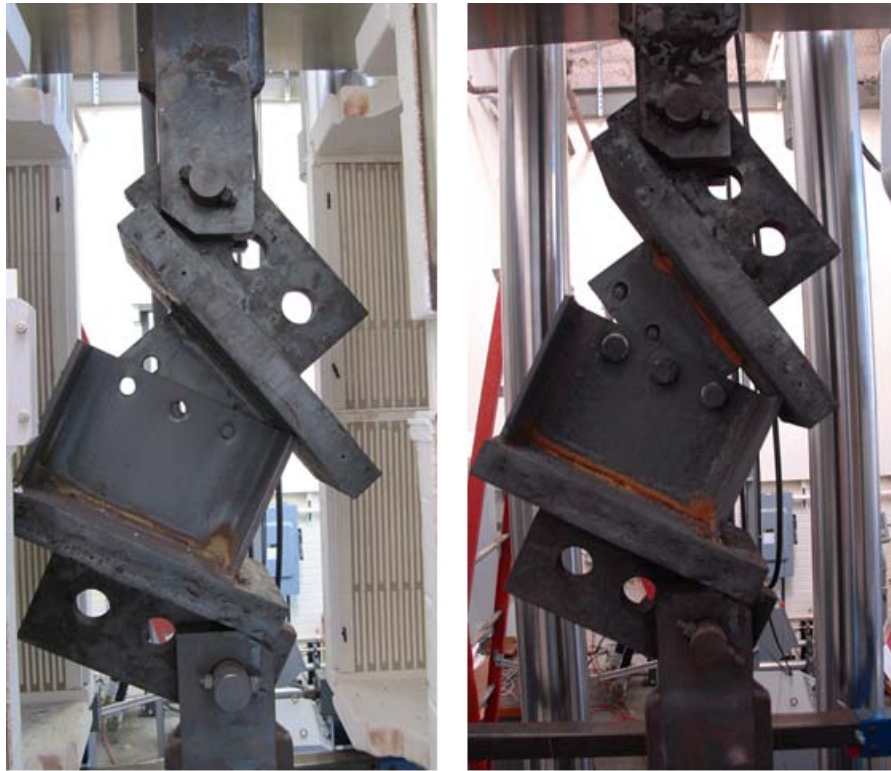


Figure 5.24 Connection failures after inclined tension tests at 500°C (left) and 700°C (right) – 3/4 inch A325 bolts

Table 5.6 Test results for connections with 3/4 inch A325 bolts under inclined tension

Temperature (°C)	Peak Load (kip)	Failure Mode
20	81.3	Bearing
20	80.2	Bearing
400	76.7	Bolt Shear
500	46.2	Bolt Shear
700	10.5	Bolt Shear

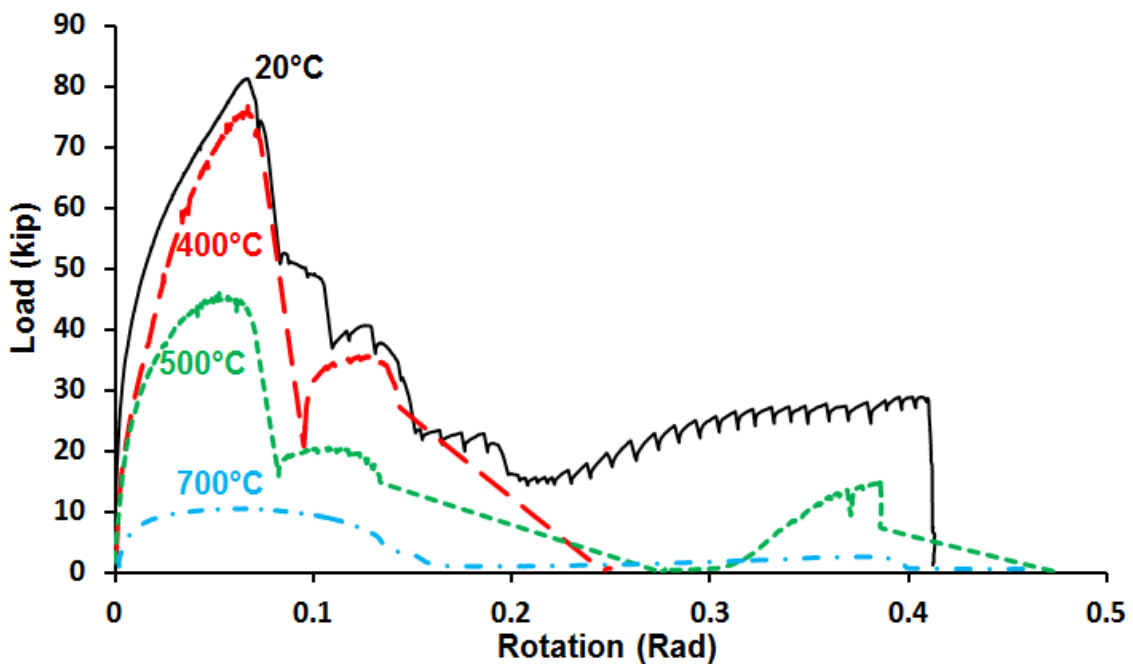


Figure 5.25 Load-rotation response of connections with 3/4 inch A325 bolts under inclined tension

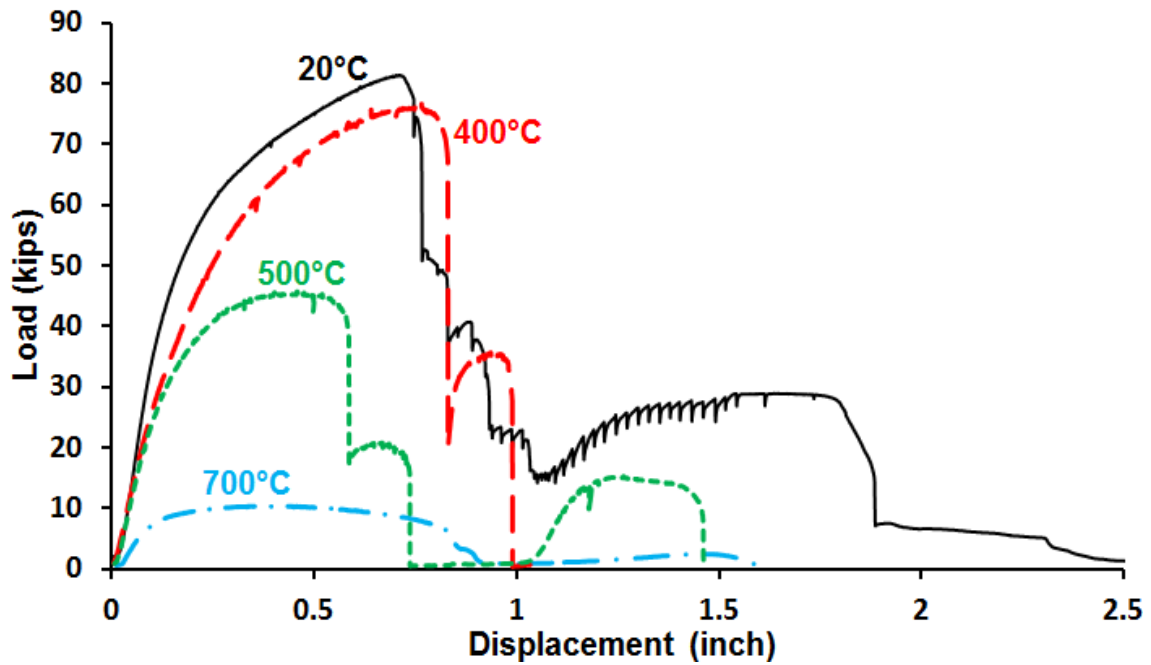


Figure 5.26 Load-displacement response of connections with 3/4 inch A325 bolts under inclined tension

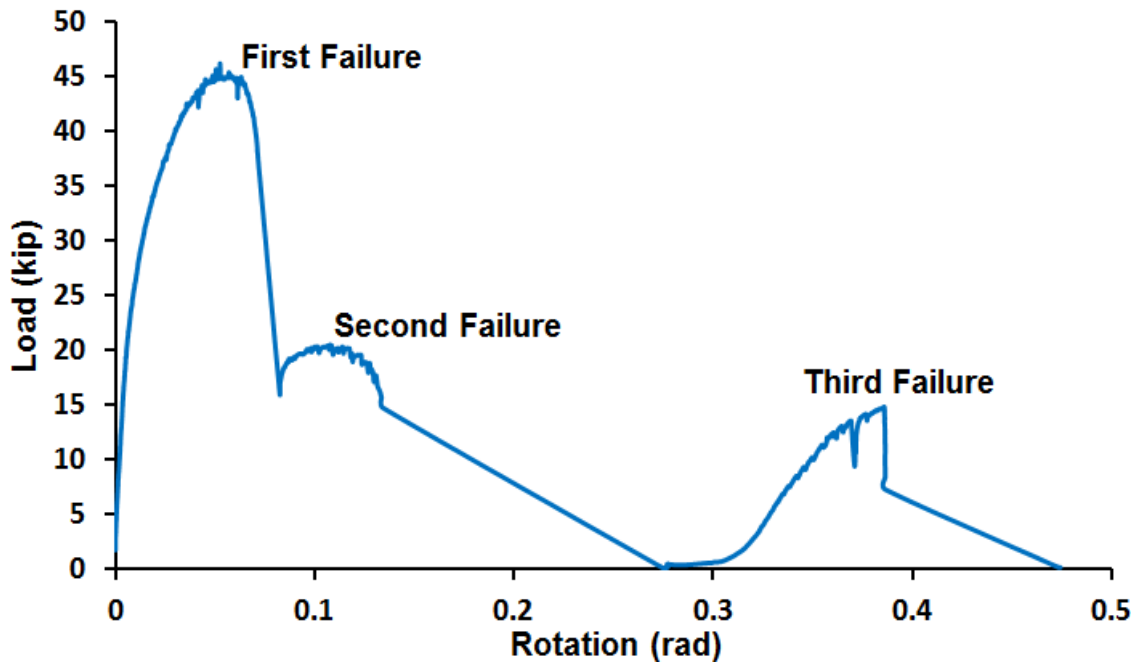


Figure 5.27 Load-Rotation rotation response of connection with 3/4 inch A325 bolts under inclined tension - 500°C

5.6.3.2 Connections with 1 inch A325 bolts

Test results are presented in Table 5.7. Figure 5.28 shows connection failure shapes after testing at temperatures of 400°C and 500°C. It should be noted that for the tests conducted, the connections failed by bearing tear out in the beam web, except for the 700°C test (Figure 5.29) where block shear fracture of the beam web occurred. For this test, connection rotation was quite small. Figure 5.30 and Figure 5.31 shows the load-rotation response and the load-displacement response of the connections. In Figure 5.30, it is observed that the connections that experienced bearing failure also exhibited quite large rotational capacities. It should be noted that the connections with 1 inch bolts also displayed sequential failure behavior, but the fracture failure steps are not as clear as the connections with 3/4 inch bolts, and the load drops (Figure 5.27) are not as pronounced and never reach a zero level before final failure. With a block shear failure mode, the

connection tested at 700°C displayed a large translational deformation capacity, but very little rotational capacity. This phenomenon implies that at this temperature, using bigger or stronger bolts may reduce the connection rotational capacity, and can therefore lead to a more brittle failure when the connection is subjected to large rotation demand.

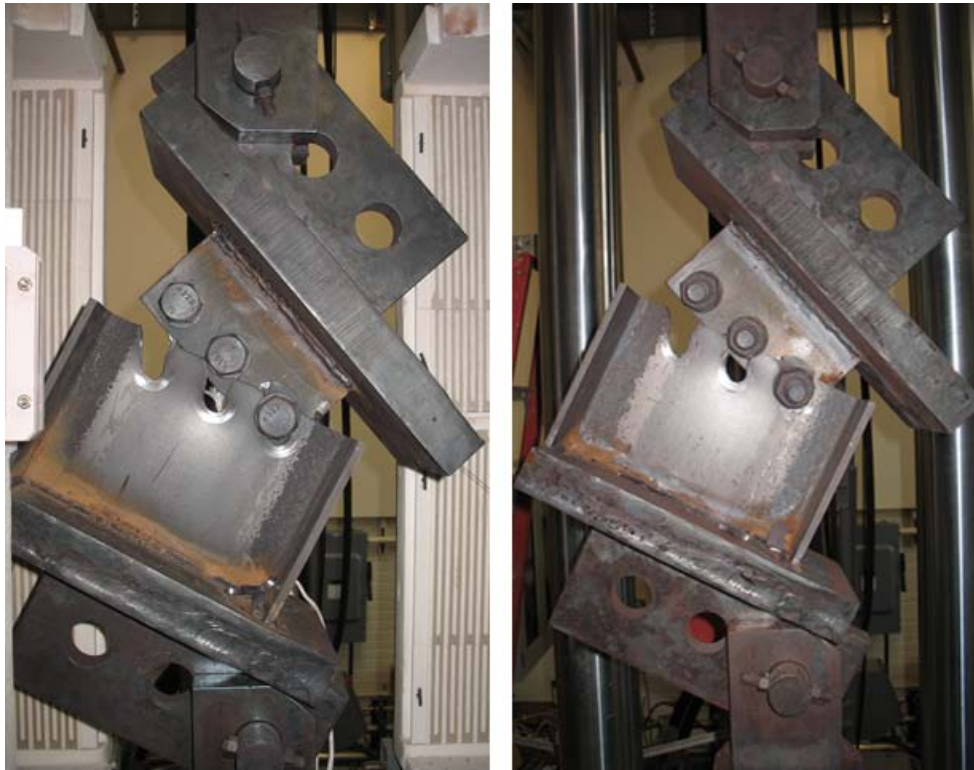


Figure 5.28 Connection failures after inclined tension tests at 400°C (left) and 500°C (right) – 1 inch A325 bolts



Figure 5.29 Connection failure after inclined tension test at 700°C – 1 inch A325 bolts

Table 5.7 Test results for connections with 1 inch A325 bolts under inclined tension

Temperature (°C)	Peak Load (kip)	Failure Mode
400	79.3	Bearing
500	55.5	Bearing
700	15.8	Block Shear

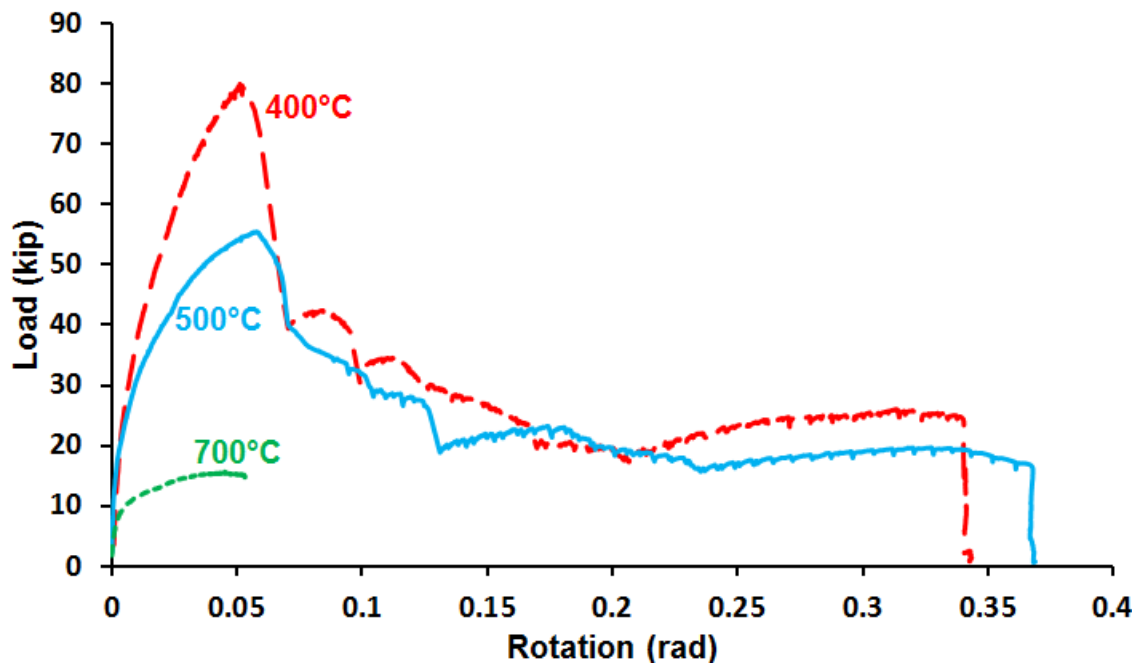


Figure 5.30 Load-rotation response of connections with 1 inch A325 bolts under inclined tension

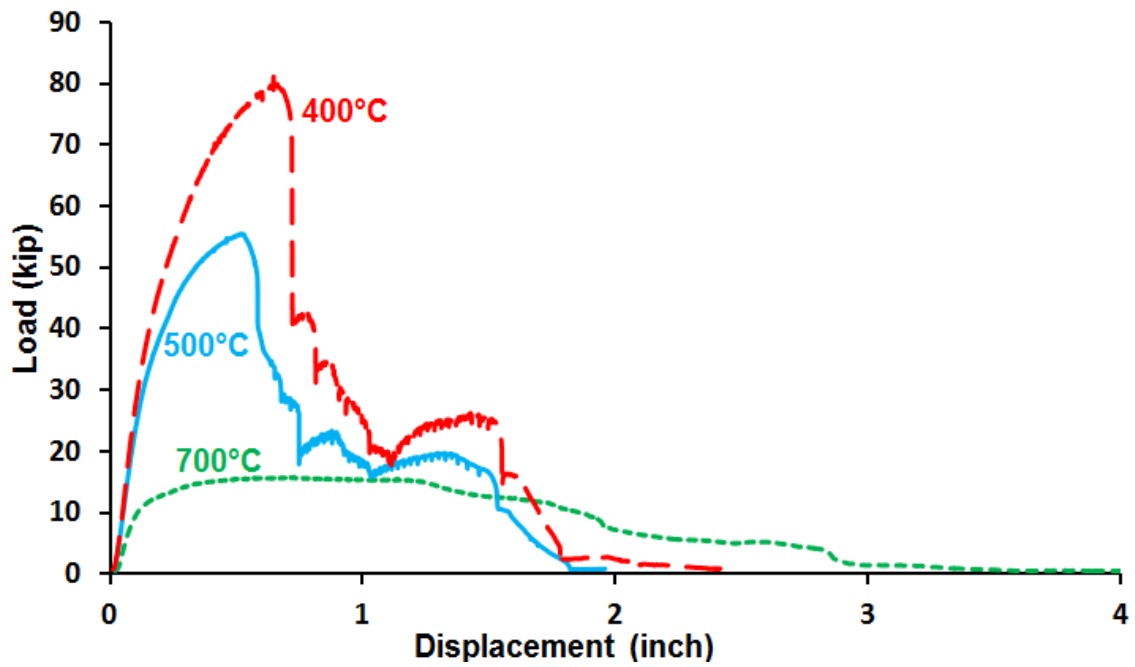


Figure 5.31 Load-displacement response of connections with 1 inch A325 bolts under inclined tension

5.7 COMPARISON OF EXPERIMENTAL DATA WITH FINITE ELEMENT CONNECTION MODELS

In this section, the ABAQUS finite element program (FE) is utilized to perform analysis and simulation of the connection tests described above. A three-dimensional brick element was employed in all the connection components (Figure 5.32 and Figure 5.33). The details of the FE model are given in Chapter 4, in which initial evaluation of the FE model was conducted by comparison with experimental data in the literature. The tests described above were then used for further evaluation of the model.

In this study, to compare with the test results, measured material properties at ambient temperature were employed in the FE model. For elevated temperatures, reduction factors for ASTM A992 structural steel reported in Chapter 3 and reduction factors for A325 structural bolts reported by Yu (2006) were used. In these analyses, steady-state temperature conditions were simulated, and displacements were applied to the base plates. The load-displacement relationships for each connection specimen with 3/4 inch bolts at different temperatures were obtained. Comparisons of the load-displacement response between FE analysis results and test results for W12×40 specimens at ambient temperature and 600°C are shown in Figure 5.34 and Figure 5.35, respectively. Figure 5.36 through Figure 5.42 show the load-displacement response comparisons between the FE analysis results and the test results of W12×26 specimens at different temperatures for the two types of loading conditions. The comparisons between peak loads obtained from FE analysis and measured values from the experiments are shown in Table 5.8.

In general, the FE model predicted the peak connection strength reasonably well. The ability of the FE model to predict the overall load-deformation response of the connections (Figure 5.34 through Figure 5.42) was also reasonably good. However, as mentioned in Chapter 4, one of the shortcomings of the FE model used in this research is that the fracture of the connection components is not explicitly modeled. This limits the

ability of the model to simulate connection behavior after the first fracture occurs. Therefore, the sequential failure behavior of the tested connections at elevated temperatures cannot be captured by the FE analysis.

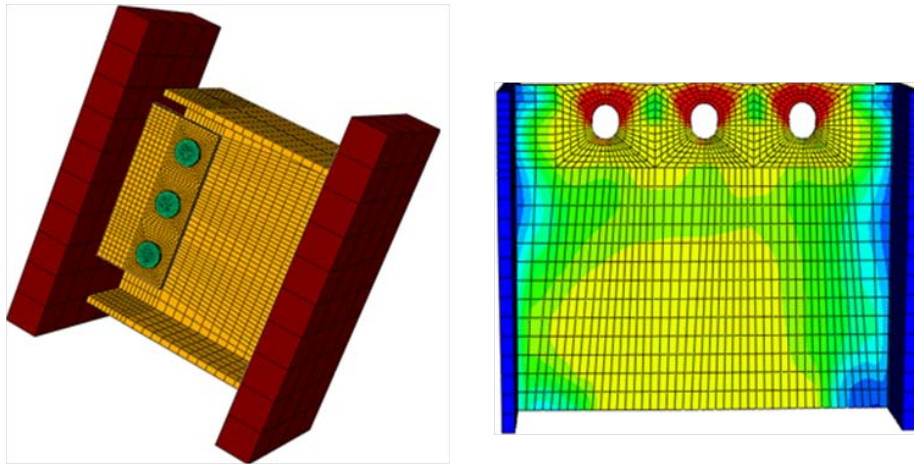


Figure 5.32 Finite element model of connections under axial tension

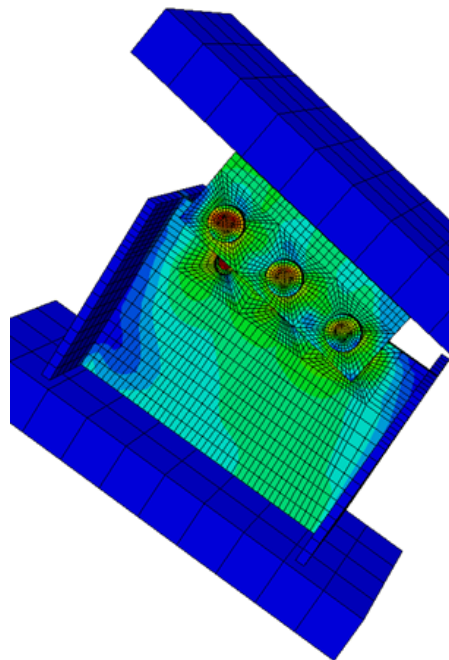


Figure 5.33 Finite element model of connections under inclined tension

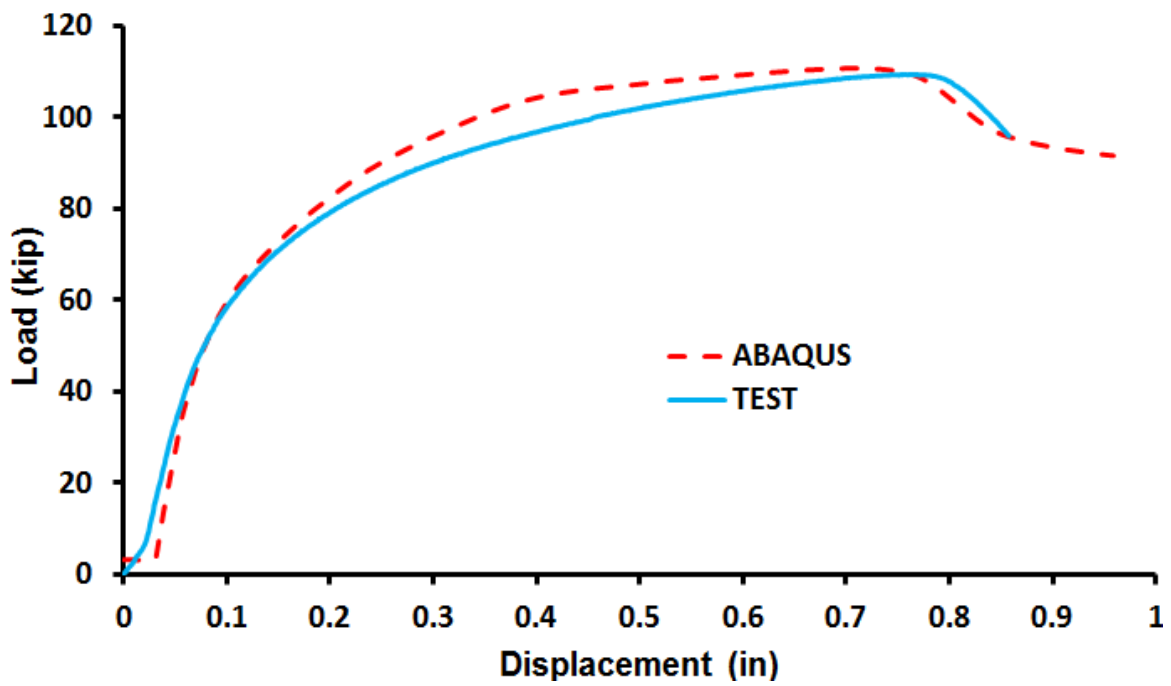


Figure 5.34 Comparison of test result and finite element analysis - 20°C – W12×40

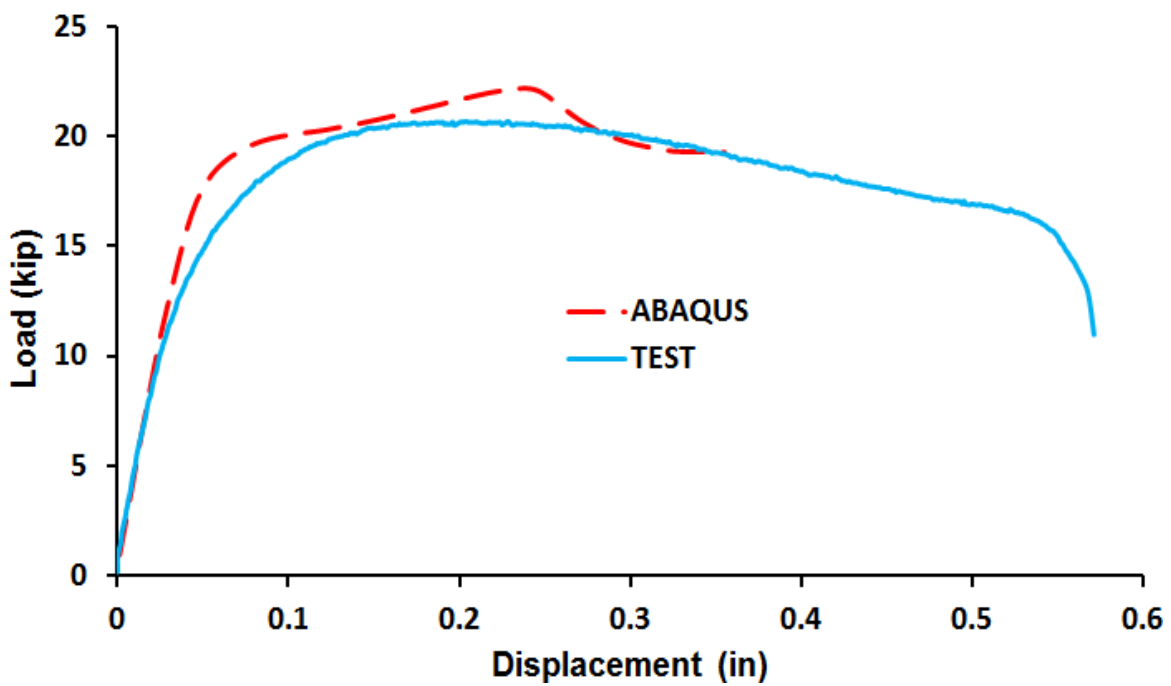


Figure 5.35 Comparison of test result and finite element analysis - 600°C – W12×40

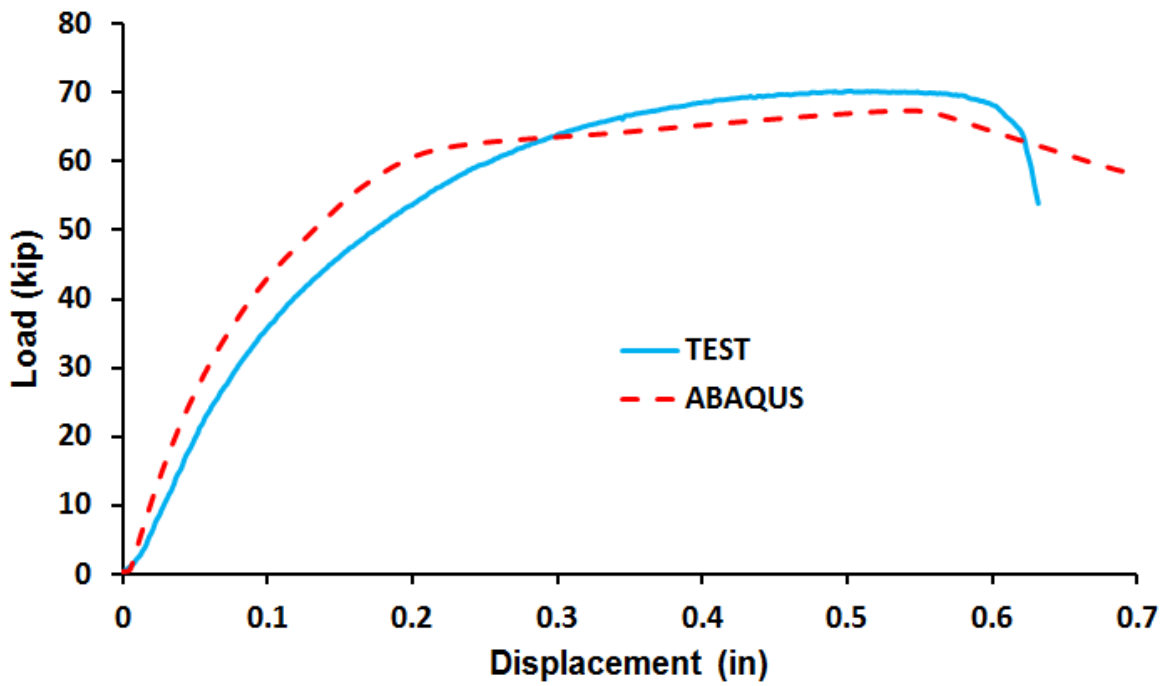


Figure 5.36 Comparison of tension test and finite element analysis - 400°C – W12×26

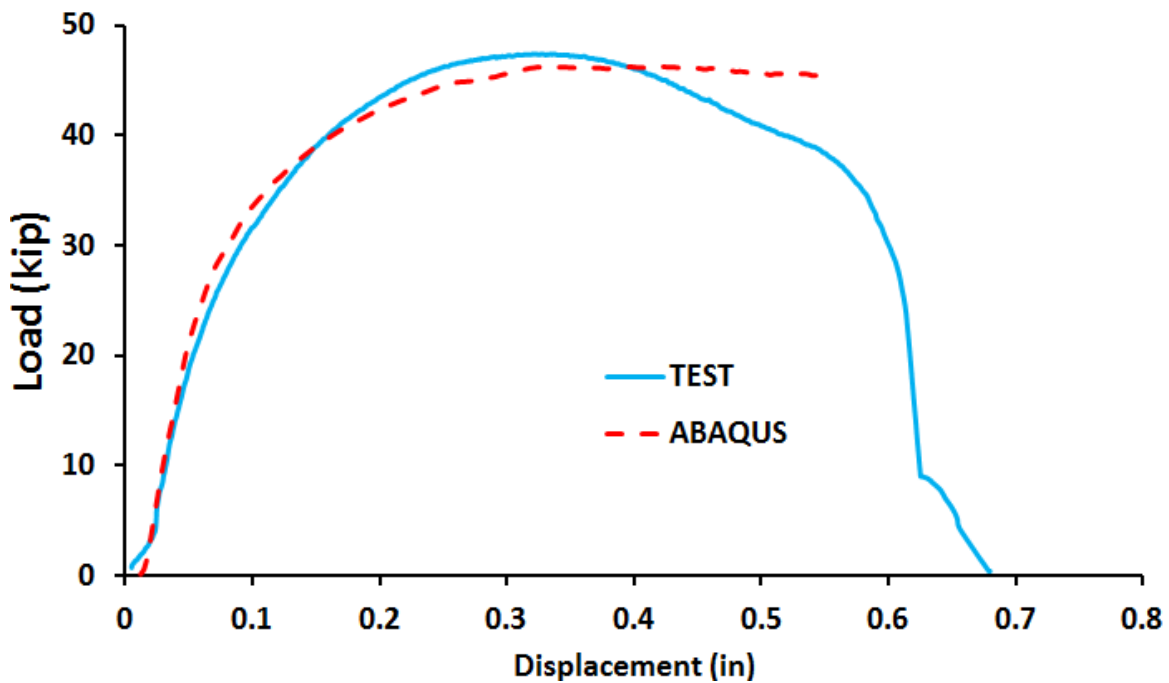


Figure 5.37 Comparison of tension test and finite element analysis - 500°C – W12×26

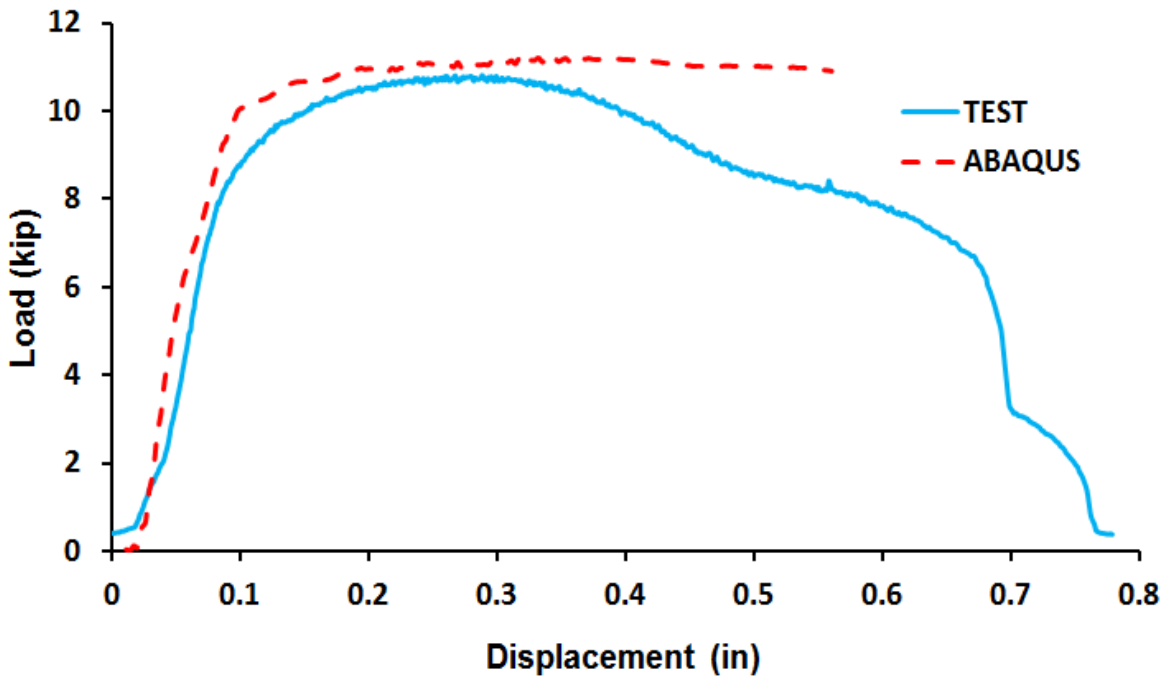


Figure 5.38 Comparison of tension test and finite element analysis - 700°C – W12×26

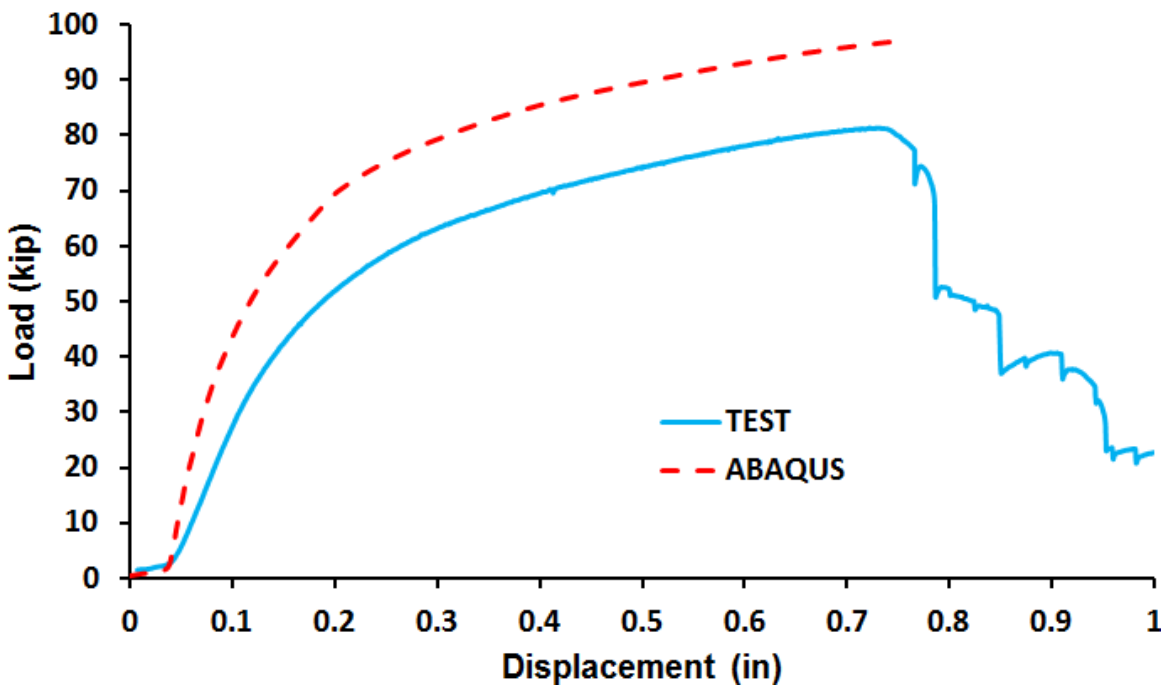


Figure 5.39 Comparison of inclined tension test and finite element analysis - 20°C

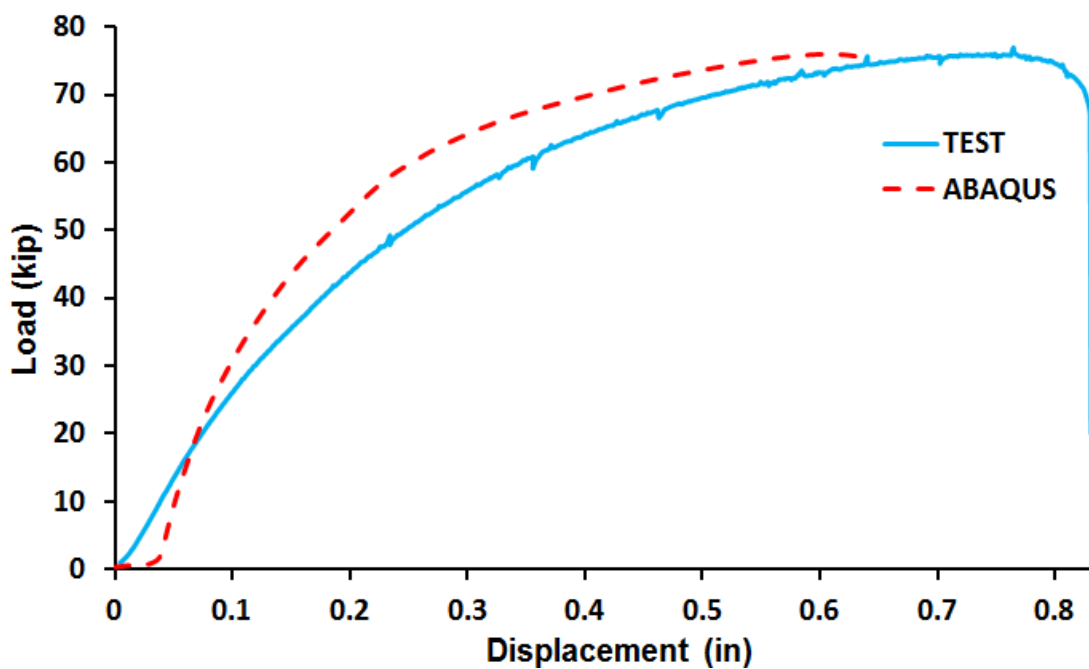


Figure 5.40 Comparison of inclined tension test and finite element analysis - 40°C

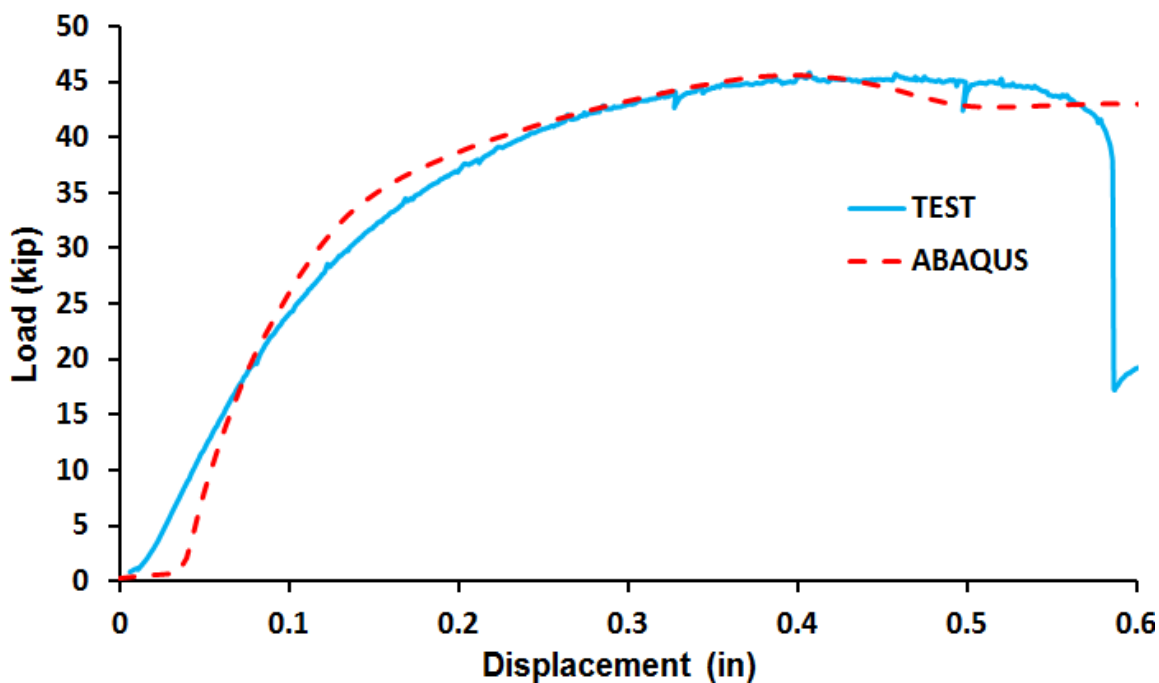


Figure 5.41 Comparison of inclined tension test and finite element analysis - 500°C

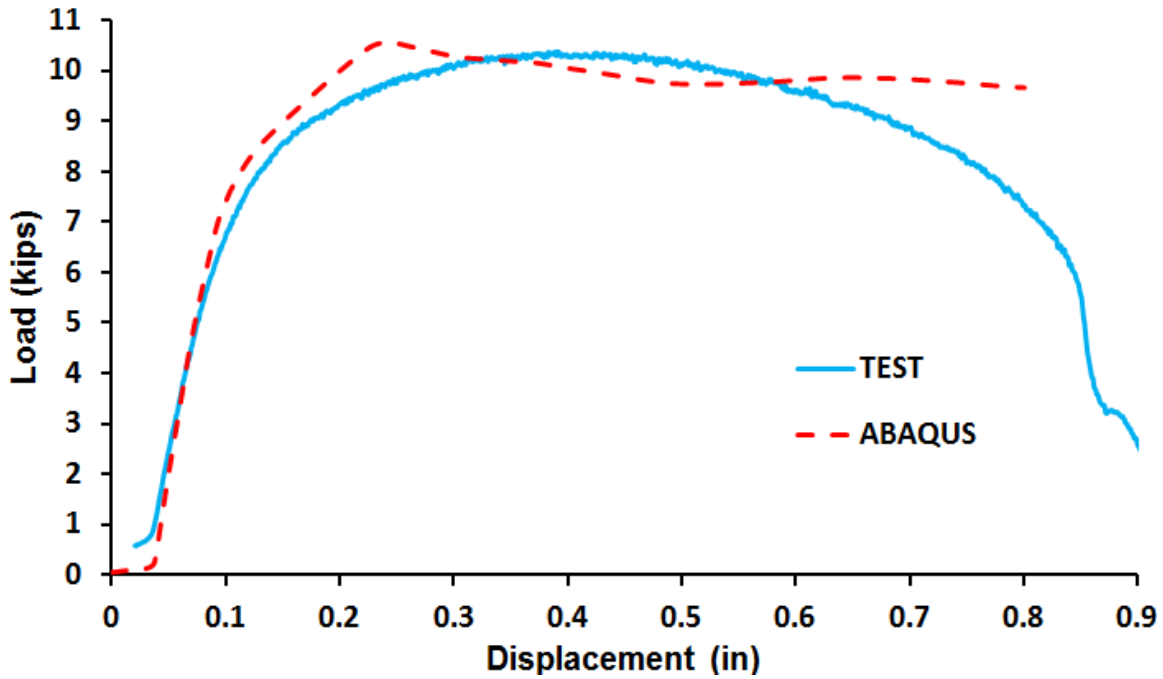


Figure 5.42 Comparison of inclined tension test and finite element analysis - 700°C

5.8 SIMPLIFIED PREDICTIONS OF CONNECTION STRENGTH

One of the objectives of this research is to examine simplified methods to predict connection strength at high temperatures. In this section, the resistance of the tested connections is evaluated using design equations in the AISC Specification (2005).

5.8.1 Bearing Failure

In the AISC Specification (2005), nominal bearing strength at a standard size bolt hole is specified as:

$$R_n = 1.2L_c tF_u \leq 2.4dtF_u \quad (5.1)$$

where d is nominal bolt diameter, F_u is specified minimum tensile strength of the connected material, L_c is clear distance in the direction of the force between the edge of the hole and the edge of the adjacent hole or edge of the material, and t is the thickness of connected material.

Equation 5.1 is valid when deformation at the bolt hole at service load is a design consideration. If it is not a design consideration, Equation 5.2 can be used:

$$R_n = 1.5L_c t F_u \leq 3.0dtF_u \quad (5.2)$$

The above equations were developed based on experimental data and are specified for use at ambient temperature. At elevated temperatures, the bearing failures were controlled by the same failure mechanism as at ambient temperature (Yu 2006). Therefore, the equation for the connection bearing strength calculations at elevated temperatures can be modified as:

$$R_{nt} = 1.5L_c t F_{ut} \leq 3.0dtF_{ut} \quad (5.3)$$

$$F_{ut} = k_{ut} F_u \quad (5.4)$$

where k_{ut} is reduction factor of tensile strength at specified temperature t . In this study, k_{ut} is obtained from the test results in Figure 3.2.

For the inclined tension test, in which the load and bearing failure path is not perpendicular to the beam cross-section, bearing strength can be modified from Equation 5.3 to:

$$R_{nt} = 1.5L_c^* t F_{ut} \quad (5.5)$$

$$L_c^* = \frac{L_c + d/2 + 1/32}{\cos\theta} - \frac{d + 1/16}{2} \quad (5.6)$$

Equation 5.6 is simply the clear distance from the edge of the hole to the edge of the connected part (beam web) in the direction of the load θ . The value of θ is 37° in this study.

5.8.2 Bolt Shear Failure

In the AISC Specification (2005), shear rupture strength of a bolt with threads excluded from the shear plane is specified as:

$$R_n = 0.5F_b A_b \quad (5.7)$$

where F_b = specified minimum tensile strength of the bolt, and A_b is the area of the unthreaded portion of the bolt.

At elevated temperatures, Equation 5.7 can be modified as:

$$R_{nt} = 0.5F_{bt}A_b \quad (5.8)$$

$$F_{bt} = k_{bt}F_b \quad (5.9)$$

where k_{bt} is the reduction factor of bolt strength at specified temperature t . In this study, k_{bt} is obtained from Yu's tests (Yu 2006).

The limit state of bearing failure and bolt shear failure were calculated using Equations 5.3, 5.5 and 5.8. A comparison of calculated resistances with the ultimate loads obtained from the tests is shown in Table 5.8 and Table 5.9. In general, the strength prediction from the AISC equations are conservative compared to the test results, but considering the simple approach used to compute connection strength, the agreement between computed and measured connection strength is reasonable.

The strength of the connection with 3/4 inch A325 bolts under axial tension using the above equations was obtained and shown in Figure 5.43. It can be clearly seen that at relatively low temperatures the connection strength is limited by bearing failure, while at high temperatures the strength is limited by bolt failure, and the transition of the failure modes occurs at about 400°C (intersection of the two solid lines). Therefore, although the strength predicted from the modified AISC equations is mostly conservative, these equations generally predict the correct failure mode.

The strength of the connection with 3/4 inch A325 bolts under inclined tension using the above equations was obtained and shown in Figure 5.44. It should be noted that this method predicts that at a temperature higher than about 330°C for the connection under such loading condition bolt shear failure, rather than bearing failure, dominates, which is consistent with the test results.

5.8.3 Block Shear Failure

Block shear fracture failure was only observed in one connection test, which is connection with 1 inch diameter bolt subject to inclined tension at 700°C. The mechanism caused this failure at such temperature is not clear at current stage, and should be further investigated in future study. Once the failure mechanism and fracture path is understood, the connection resistance can be then evaluated using simplified design equations in specifications.

Table 5.8 Comparison of results for connections with 3/4 inch A325 bolts

Specimen	Temperature (°C)	Test Peak Load (kip)	Strength by AISC (kip)	FEA Max Load (kip)
Connection under Tension				
W12×40	20	109.4	108.8	110.8
W12×40	600	20.6	19.5	22.0
W12×26	20	75.3	65.6	81.0
W12×26	400	70.1	56.4	67.4
W12×26	500	47.4	33.4	46.2
W12×26	550	33.5	26.5	-
W12×26	700	10.8	11.1	11.1
Connection under Inclined Tension				
W12×26	20	80.2	90.1	97.1
W12×26	400	76.7	56.4	76.0
W12×26	500	46.2	33.4	45.6
W12×26	700	10.5	11.1	10.6

Table 5.9 Comparison of results for connections with 1 inch A325 bolts

Temperature (°C)	Test Peak Load (kip)	Strength by AISC (kip)
Connection under Tension		
20	74.8	58.3
500	52.7	39.1
700	14.9	11.7
Connection under Inclined Tension		
400	79.3	64.9
500	55.5	55.5
700	15.8	16.6 (Bearing)

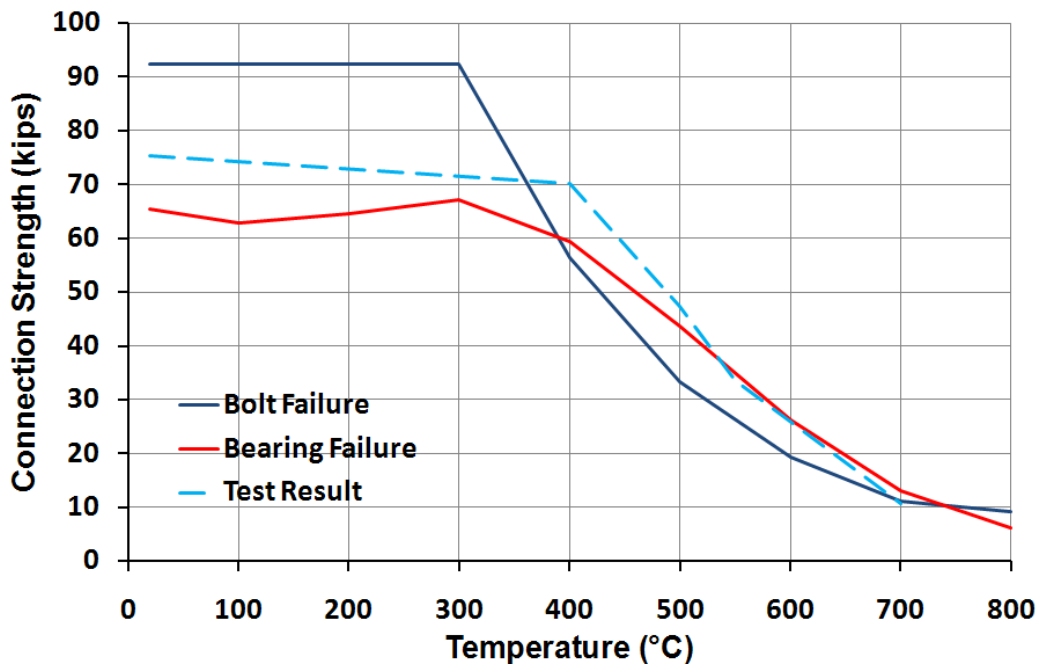


Figure 5.43 Calculated connection strength under axial tension – 3/4 inch A325 bolts

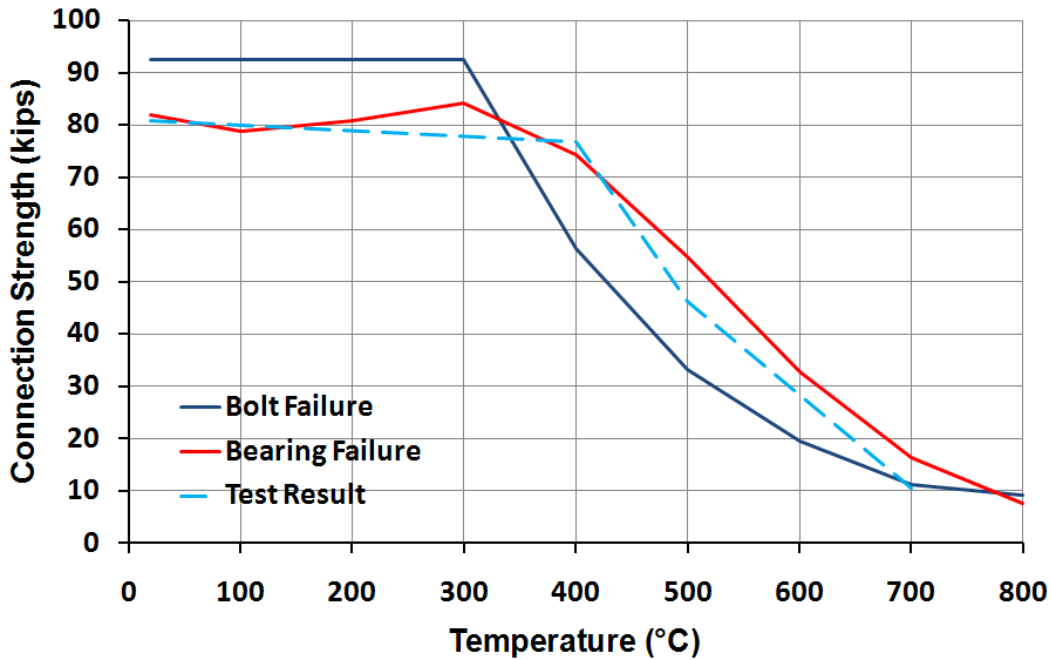


Figure 5.44 Calculated connection strength under inclined tension – 3/4 inch A325 bolts

5.9 SUMMARY

This chapter has presented experimental investigations on the behavior of steel shear tab beam end connections at elevated temperatures. A test program was introduced to study the connection performance. Tests on shear tab connections subject to axial tension and inclined tension at elevated temperatures were conducted to obtain data and insights into connection behavior. From the conducted tests, connection strengths and deformation capacities at elevated temperatures were obtained, failure modes were evaluated, and load-deformation curves were presented.

Connection strengths at elevated temperatures were also evaluated using finite element analysis and modified equations of the AISC specification, and reasonable agreements were obtained between test results, FE analysis and AISC equation

predictions. It appears that using the modified simple AISC equation can predict the connection strength and failure mode quite well.

As observed from the test results, structural bolts are potentially more vulnerable than other connection components at high temperatures, as bolts lose more strength than structural steel with increasing temperature. In addition, results from the inclined tension tests showed that the connection experiences a sequential failure under a combination of tension, shear and rotation. As a result, the connection has a fairly large rotation capacity before final failure is achieved. The large rotations that occur after fracture of the first connection component may help to relieve the thermally induced deformations and forces in the beam, thereby potentially relieving the demands on the connection prior to final failure. As long as final failure does not occur, the beam is still connected to the supporting members and can carry some gravity load. Damaged shear tab connections surviving in large building fires have been observed in past fire events and fire tests as described in Chapters 1 and 2. The large deformation capacity of the connection between first component failure and final failure may help connections survive severe fires.

CHAPTER 6

Analysis and Parametric Studies of Shear Tab Connection Performance in Fire

6.1 OVERVIEW

In this chapter, finite element analysis is used to conduct a series of studies on the behavior of beams with shear tab connections subjected to fire. The overall goal of these studies is to gain further insight into key factors that affect beam and connection performance in fire, and identify areas for further detailed future research. Three-dimensional finite element models on ABAQUS will be developed for these studies, using the modeling techniques described in Chapter 4.

The finite element modeling techniques used in this study were evaluated by comparison with experimental data reported in the literature in Chapter 4 and by comparison with the connection tests conducted as part of this research program reported in Chapter 5. These comparisons showed that the finite element models provided reasonably accurate predictions of the experimentally measured connection load-deformation response, including a reasonably accurate prediction of peak resistance. However, since fracture was not explicitly modeled, the FE analysis was not capable of predicting connection performance after fracture of the first connection component (bolt shear fracture, bearing tear-out fracture, etc.). As discussed in Chapter 5, shear tab connections may have substantial deformation capacity after first component fracture. This post-fracture deformation capacity may be significant in fire scenarios, since these deformations may help relieve thermally induced forces at the connection. While this modeling limitation can be overcome by more advanced modeling techniques and solution algorithms, the post-fracture modeling of connections was beyond the scope of this current research project, and represents an important future research need. An additional limitation of this current study is that the concrete floor system was not

included in the models, with the exception of considering its effect on temperature distributions in the beam. Most steel buildings are provided with composite concrete floor systems on ribbed metal deck and the floor system can potentially have a significant effect on the force and deformation demands on a shear tab connection in fire. However, accurate modeling of a composite concrete floor system introduces numerous modeling challenges, and was also outside of the scope of this current study. Finally, although a large number of FE analyses were conducted as part of study, it was still only possible to examine a small number of variables, considering the very wide range of design variables involved in actual building design. However, despite these simplifications and limitations, it is anticipated that significant insights into connection behavior in fire can still be achieved from these studies.

In the remainder of this chapter, a series of 3-D finite element models of typical floor beams with bolted shear tab connections are created and analyzed. These models are used to examine the effects of several loading variables and boundary conditions on the behavior of the shear tab connections in fire. Further, a number of connection details that may affect connection performance in fire are investigated.

6.2 MODEL AND ANALYSIS

6.2.1 Model Description

In this study, a W16×36 steel floor beam with three-bolt shear tab beam end connections at the ends was simulated in fire conditions. The beam and connection layout is shown in Figure 6.1. The temperature distributions in the beam and connections were assumed to be uniform. A325 bolts were used in the model, and the elevated temperature strength values reported by Yu (2006) were applied in the FE model (Figure 4.37). For the initial analysis, standard bolt holes were used, in which the hole diameter is 1/16 inch larger than the bolt diameter. Welds were not explicitly modeled. The steel beam was assumed to be made of ASTM A992 steel, which is the most common grade of structural steel currently used for wide flange shapes in the US. The stress-strain relationship of

A992 steel at elevated temperatures employed in the FE model was based on the test results presented in Chapter 3, and the curves are simplified to multi-linear shapes and shown in Figure 6.2. The shear tab was assumed to be made from A36 steel, and the elevated temperature properties used in the FE model were also simplified from test results of the investigator (Figure 6.3). Uniformly-distributed loads were applied on the top of the beam in all analyses. The magnitude of the uniform load was chosen to produce a moment equal to a certain ratio of the nominal plastic moment capacity of the beam. Lateral movement of the beam top flange was restrained to simulate the lateral brace effect of a concrete slab. Transient-state analyses were performed, meaning that in each analysis, the load applied on the beam was held constant, while temperature was changing. In the analyses of connection behavior in the cooling phase of a fire, the temperature was increased first and then cooled back down to 20°C.

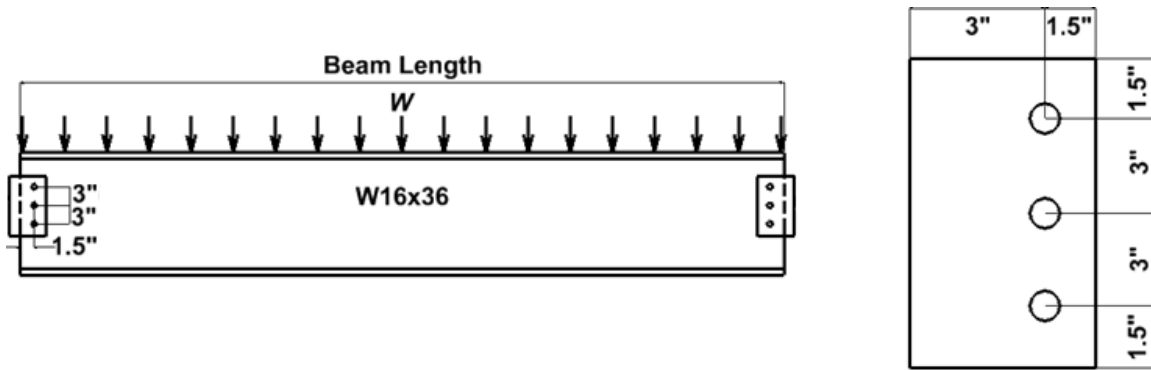


Figure 6.1 Layout of steel beam and shear tab connections for FEA (not to scale)

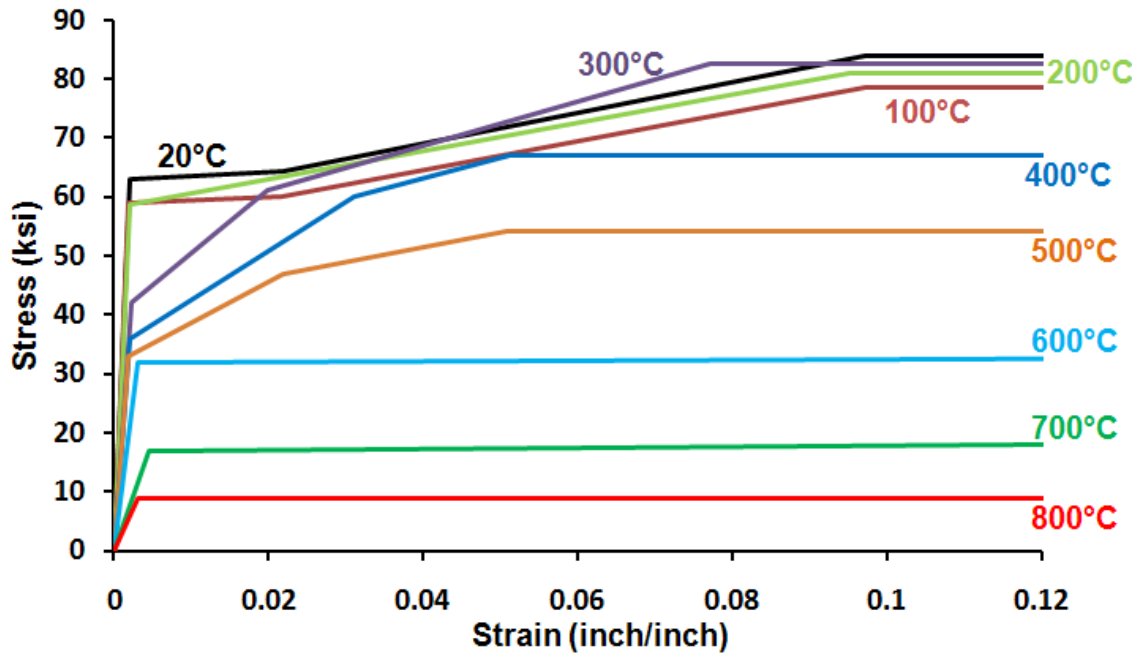


Figure 6.2 Stress-strain relationship of A992 beam material used in FE model

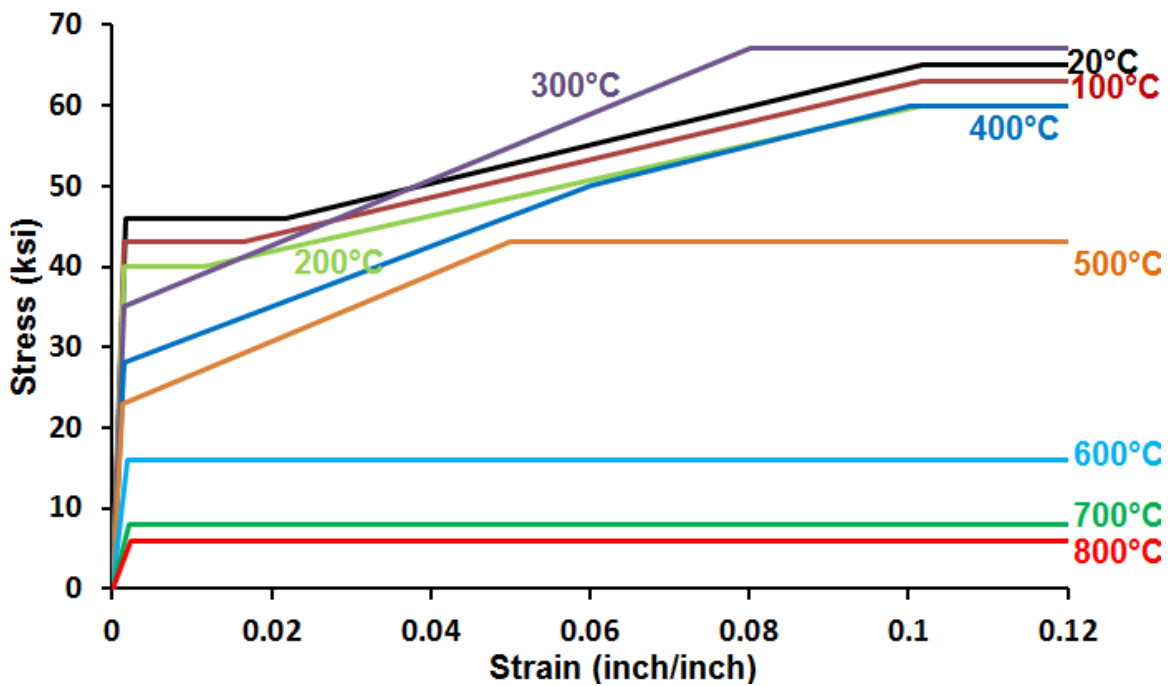


Figure 6.3 Stress-strain relationship of A36 plate material used in FE model

Figure 6.4 shows the typical deformed shape of the bolt holes and local buckling in the shear tab, the beam web and the beam bottom flange from FE analysis during fire. This type of analysis was conducted using detailed 3-D finite element models. To further understand the importance of the detailed connection model in this study, the beam described above was also modeled using simplified beam elements without connections. With the same loading conditions and material properties, the two models are compared in Figure 6.5 and Figure 6.6. It is clear from the figures that the performance of a beam in fire is highly dependent on the beam end connection performance. Modeling beams without consideration of the effect of the end connections can lead to potentially large errors. Further, the FE model using beam elements cannot capture the individual bolt behavior and local buckling behavior of the beam web and shear tab due to the large compression in the heating stage of a fire. Therefore, a detailed connection model using 3-D solid elements is used in this current study.

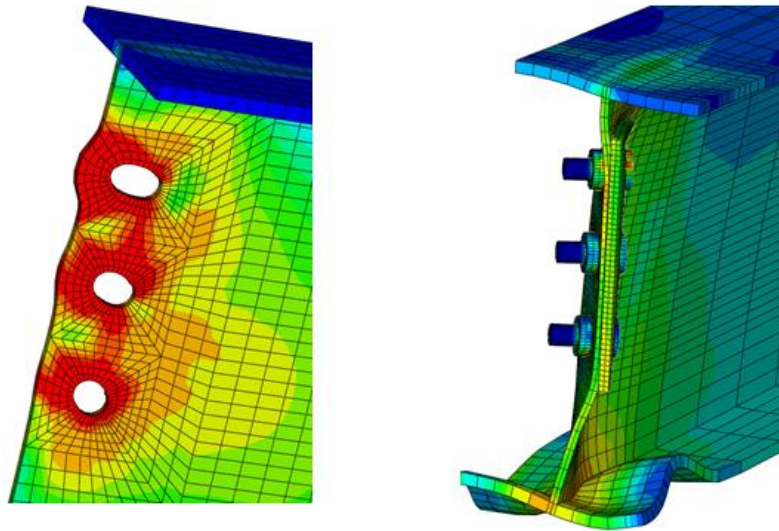


Figure 6.4 Deformed shape and stress contour of the shear tab connection

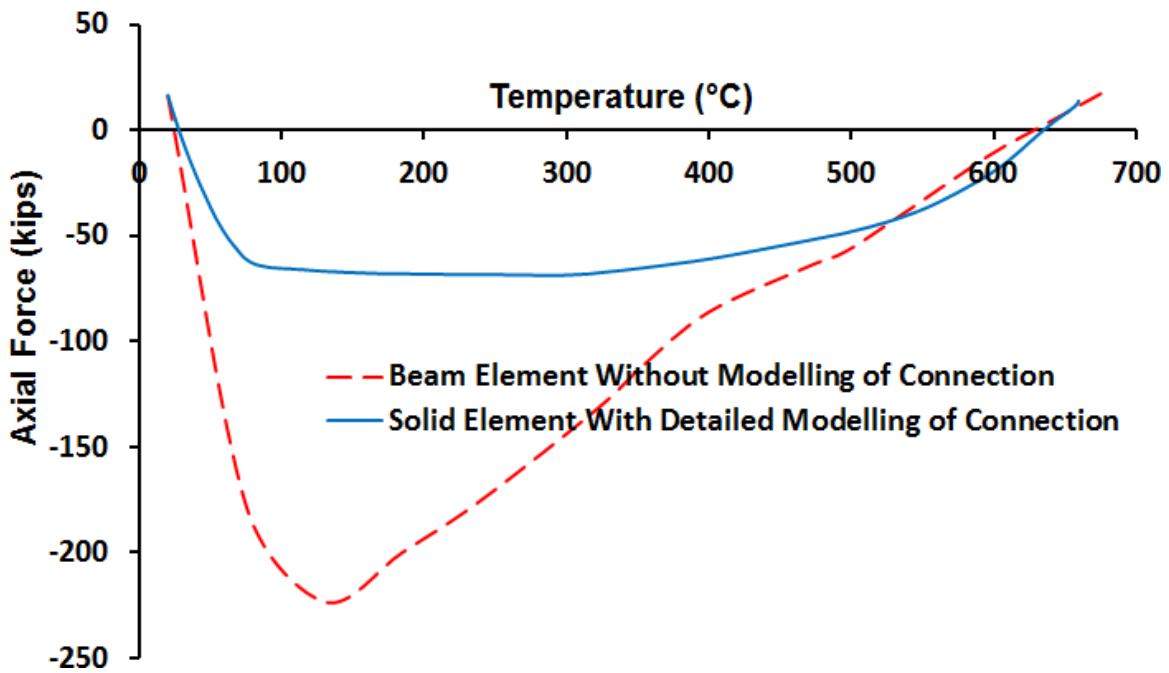


Figure 6.5 Beam Axial force – temperature response comparison between model with beam element and model with solid elements

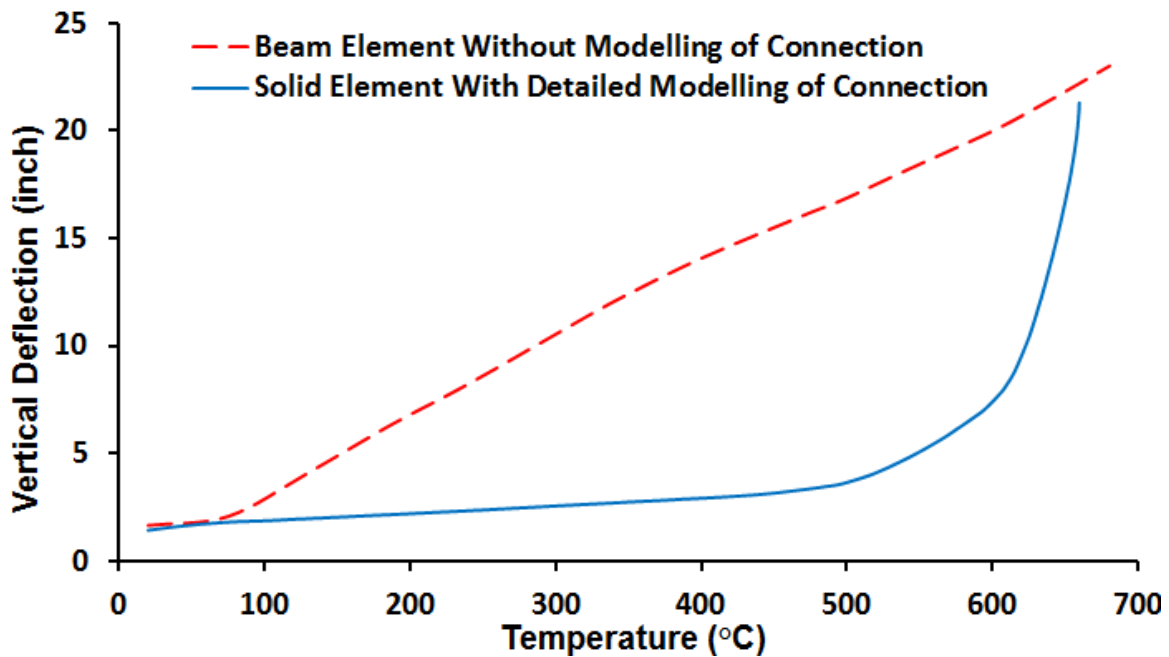


Figure 6.6 Beam deflection – temperature response comparison between model with beam element and model with solid elements

6.2.2 Behavior of Shear Tab Connections

Finite element analysis results of connection axial force and connection rotation during the heating and cooling phases of a fire are shown in Figure 6.7 and Figure 6.8, respectively. In this fire scenario, the temperature of the beam and connection increase from 20°C to 650°C and then reduce back down to 20°C. From Figure 6.7, it is noted that during the heating stage (red solid line in the figure), due to thermal expansion, large axial compression can be produced at the beam end connections with temperature increase. The magnitude of the compression is limited by the local buckling capacity of the shear tab and beam web at elevated temperatures. As the temperature in the beam keeps increasing, significant steel strength and stiffness loss occurs and lead to large deflections of the beam and large rotations of the connections. When the beam sags, the compression caused by thermal expansion will be compensated by the beam deflections until axial tension is developed in the beam and connections due to catenary action. In the whole process, the axial force demands and rotation demands on the connections can be large, as shown in the figures. In the cooling stage (dashed blue line in the figure), large tension can be produced in the beam, and the magnitude of tension increases rapidly with temperature decrease. This large tension force during cooling can potentially cause connection failure.

Large connection rotations and beam deflections can occur during a fire. In Figure 6.8, it is noted that if the beam has already entered the “run-away” stage and experiences large deformations during heating (solid red line), the beam end rotation can only be partially recovered in the cooling phase (dashed blue line), resulting in the beam with a large permanent residual deflection after the fire.

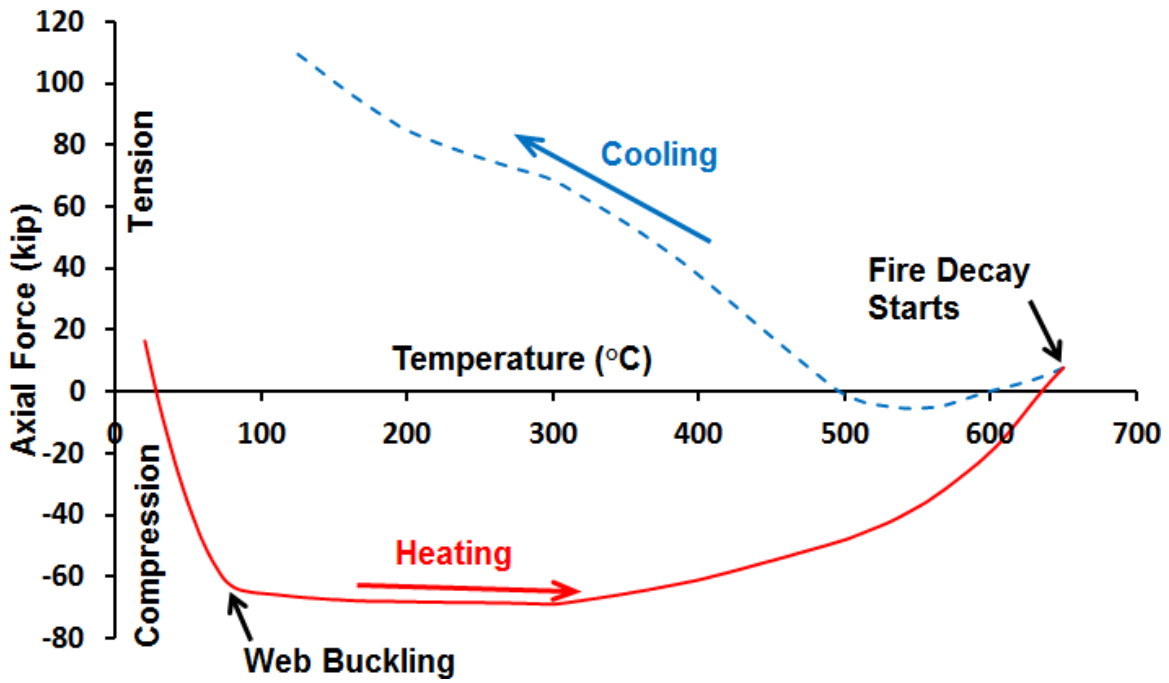


Figure 6.7 Connection axial force - temperature response in fire

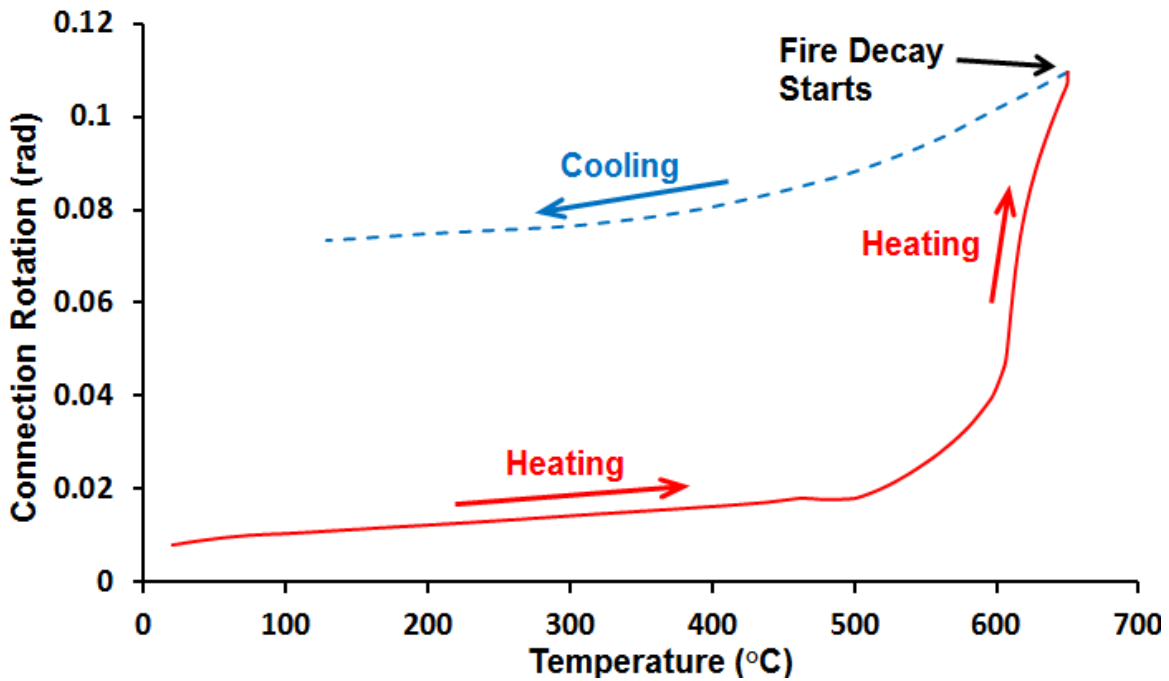


Figure 6.8 Connection rotation - temperature response in fire

6.2.3 Behavior of Bolts

The resultant shear forces in the three bolts during the heating and cooling stages obtained from FE analysis are shown in Figure 6.9 and Figure 6.10, respectively. Also plotted on these figures is the variation of tested bolt shear strength with temperature. In the heating stage, the top bolt experiences a larger shear force than the other two under most of the temperature range. For this specific analysis, the largest shear force on the top bolt occurs at temperatures in the range of 300°C to 400°C, when the beam is still expanding outward and the connection is under compression. However, bolt shear failure does not occur at this point, as the bolt shear strength is still relatively high at these temperatures. With further increases in temperature, bolt shear force decreases significantly due to large connection rotations caused by the degradation of material strength and stiffness in the beam. After the temperature reaches 600°C, catenary action starts develop in the beam, and the bolt shear force increases again slightly when the connection is in tension. The increasing bolt shear force may cause connection failure if the temperature keeps increasing and larger catenary forces develop. However, if the fire stops before failure of the connection and the temperature starts to cool down, shear forces in all bolts will significantly increase with temperature decrease, as shown in Figure 6.10. However, bolt shear strength also increases as temperature decreases. It is noted that in the fire cooling phase, under this large tension, the top bolt still experiences the largest shear force among the three bolts. Also, as illustrated in Figure 6.9 and Figure 6.10, predicting bolt shear failure in a fire is complex since both the bolt shear force and bolt shear strength vary with temperature. Consequently, bolt shear failure does not necessarily occur when the bolt shear forces are at their highest. Similarly, bolt shear failure may not occur when the bolt shear strength is at its lowest. Finally, Figure 6.10 illustrates the important observation that connections can be most vulnerable to failure during the cool down phase of a fire. For all the analyses in cooling phase, bolt shear strengths were assumed to be same with those in heating phase. However, as observed by previous researchers (Kirby 1995, Yu 2006), when bolts are exposed to high temperatures

and then cool, they can experience a reduction in strength. Bolt strength is therefore not only temperature dependent, but also temperature history dependent. This phenomenon suggests that bolts may be even more vulnerable to failure during the cooling stage of a fire. It is also important to recall, as discussed earlier, that failure of a single bolt does not mean that the connection has failed.

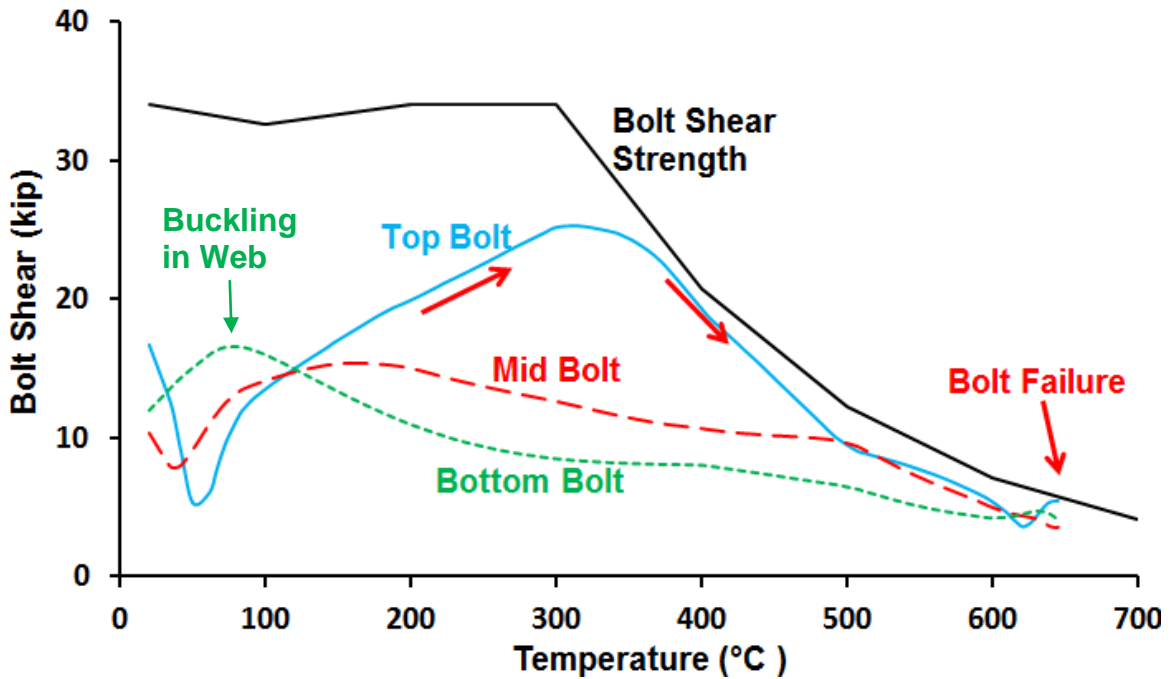


Figure 6.9 Bolt shear forces during heating

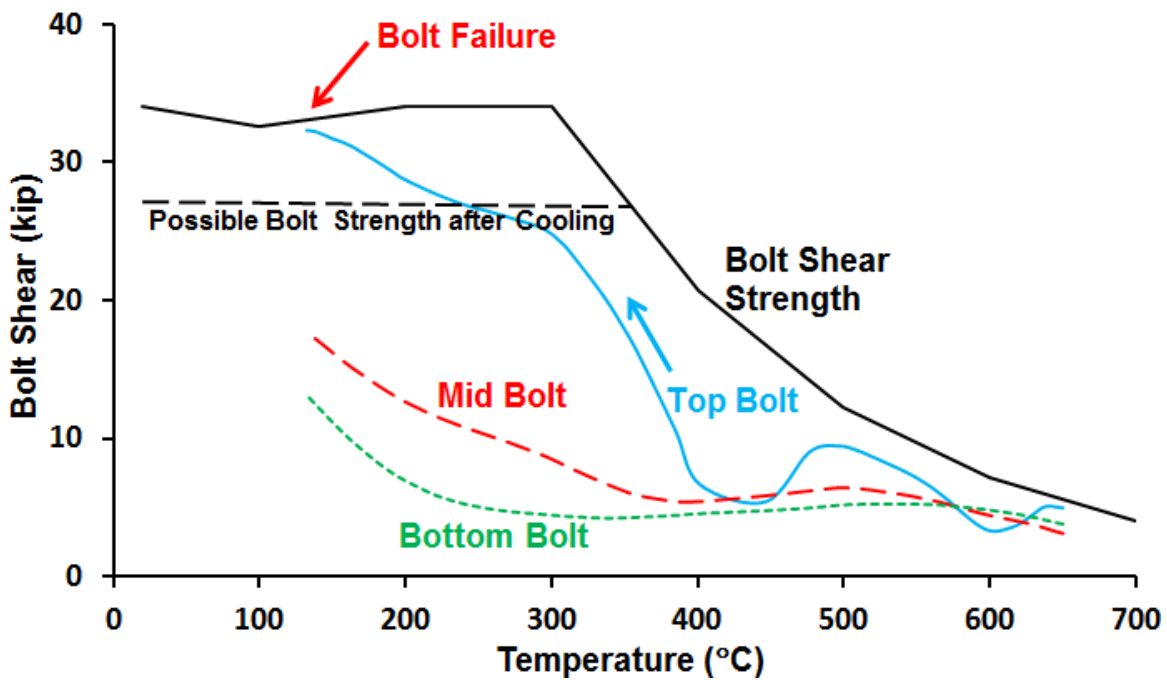


Figure 6.10 Bolt shear forces during cooling

6.3 PARAMETRIC STUDY

In the following sections, some key factors that may affect connection behavior in fire are examined, including load ratio, beam length, stiffness of the adjacent structure, initial cooling temperature and others. The analyses consider variations of the W16×36 beam with shear tab connections shown in Figure 6.1.

6.3.1 Load Ratio

A 30-ft long beam was chosen in this investigation, as this represents a fairly common span length used in typical building construction practice. The beams are loaded with a uniformly distributed load, as shown in Figure 6.1. The load ratio is defined as the ratio of maximum moment in the beam to the nominal plastic moment capacity of beam section, M_p at ambient temperature. Three load ratios were studied, 1.0, 0.5 and 0.25. Thus, for a load ratio of 0.25 for example, the magnitude of the uniform load on the beam is chosen so as to produce a maximum moment of $0.25M_p$ in the beam at ambient

temperature, and assuming that the beam is simply supported (so the maximum moment is $wL^2/8$). The shear tabs were assumed to be attached to a rigid boundary, which has infinite stiffness to achieve the possible largest axial force in the connections.

Figure 6.11 plots the variation of axial force on the connection with beam temperature. It can be observed that higher loading produces less compression in the beam, but higher tension when catenary action develops. It can also be noted that the beam can survive at significantly higher temperature under lower loading, as might be expected. Another observation is that, at a relatively lower temperature stage, compression in the connections develops rapidly with temperature increase until local buckling occurs on the beam web or shear tab. This observation indicates that the shear tab connections with relatively small axial stiffness can limit the axial compression and may potentially prevent connection failure at the very early stages of fire growth. From a load ratio of 0.5 to 0.25, compression in the connection changes little, implying that under realistic loading, the impact of load ratio on the axial force developed in the connections may not be significant. The variation of connection rotation with temperature for different load ratios is shown in Figure 6.12. Larger loads produce larger rotations as expected. Note that the predicted rotations are substantial, exceeding 0.1 radian.

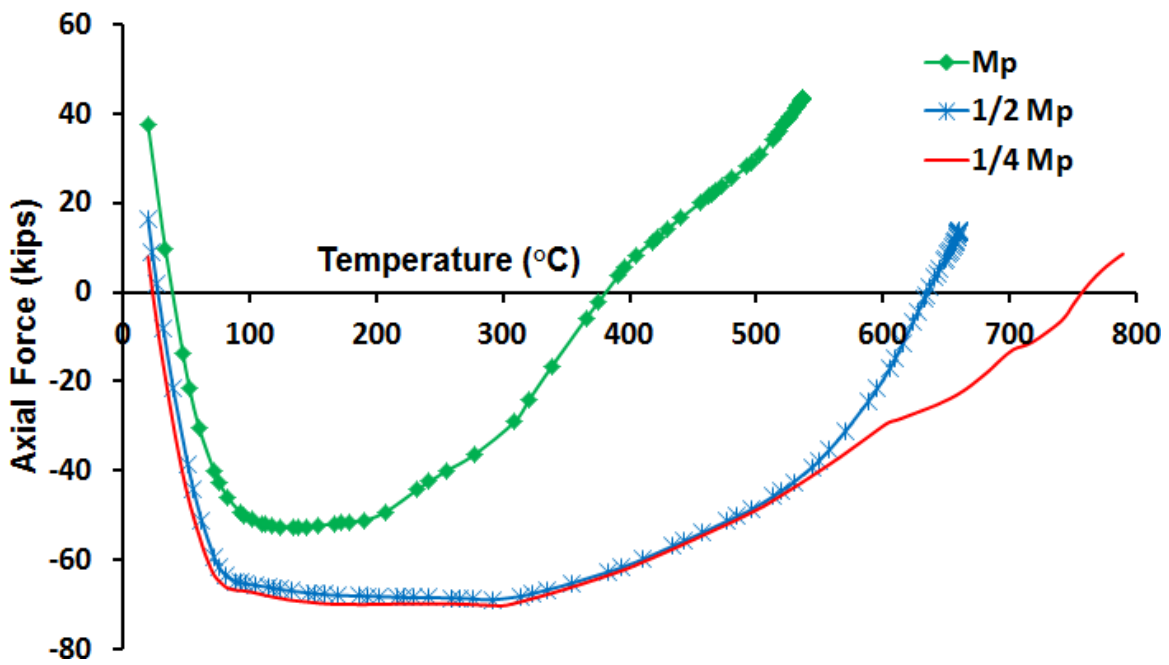


Figure 6.11 Connection axial force - temperature response for different load ratios

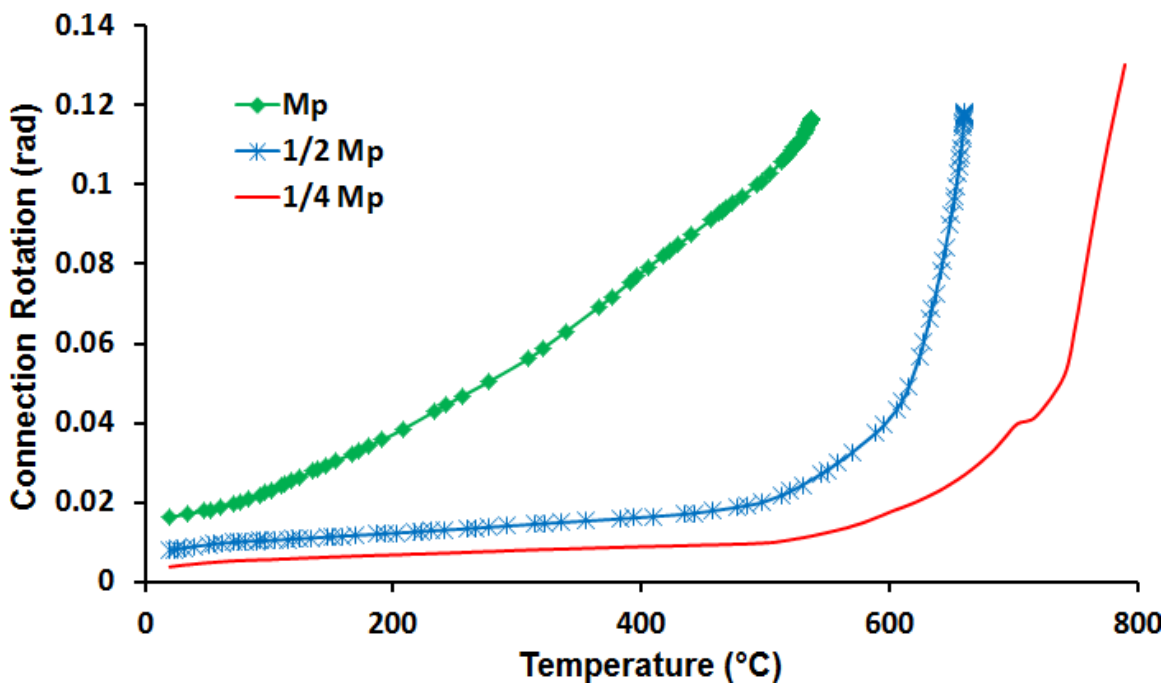


Figure 6.12 Connection rotation - temperature response for different load ratios

6.3.2 Beam Length

Thermally induced forces and deformations can be large in beams and beam end connections during a fire. It would be expected that beam length will have an effect on thermally induced forces and deformations. For a given steel beam section and a certain temperature increment, a longer member will expand more in length, and in turn, produce larger axial force if restrained by the beam end connections with same stiffness. Therefore, a study on the effect of beam length on the connection behavior in fire is of interest.

Figure 6.13 shows connection axial force versus beam temperature for beam lengths of 20 feet, 30 feet and 40 feet. Load ratios for the three beams are all 1/3. It can be observed from the analysis results that the longer beams generate higher peak compression forces in the heating stage. The peak tension forces in the three beams are almost the same. As the beam length changed from 30 feet to 40 feet, the peak compression forces were nearly the same. This may have occurred because the ultimate capacity of the connection under compression was approached and limited that axial force. Figure 6.14 shows a comparison of the connection rotations for the three beams, where longer beams generate larger connection rotation with the same load ratio.

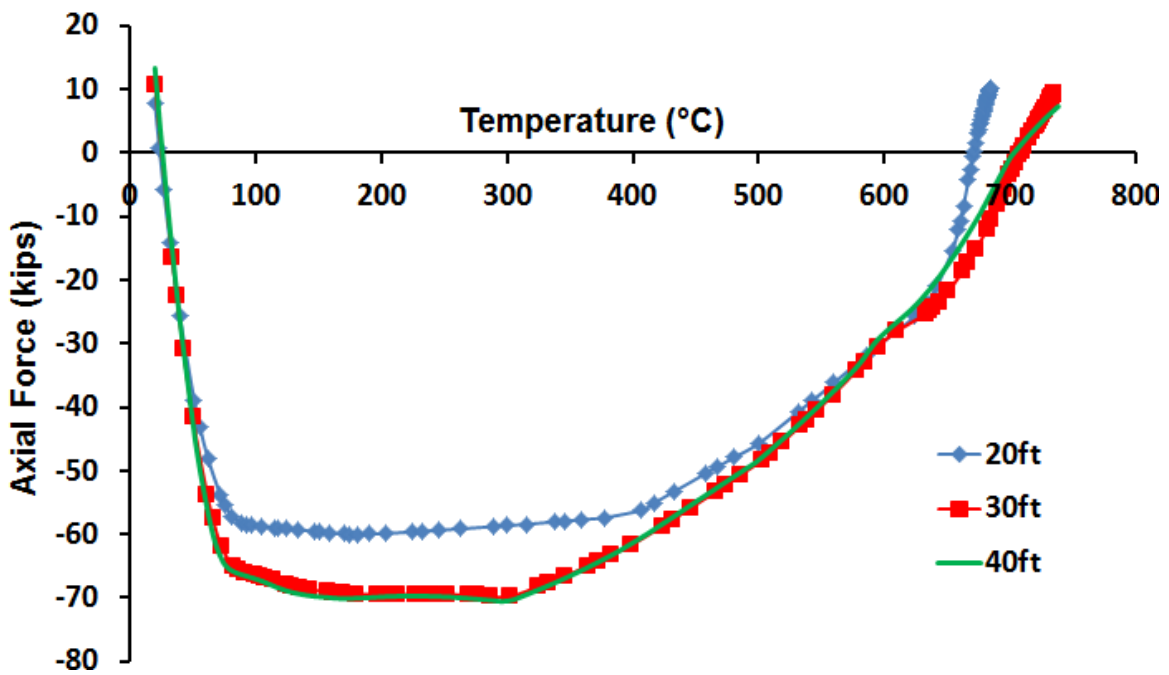


Figure 6.13 Connection axial force - temperature response for different beam lengths

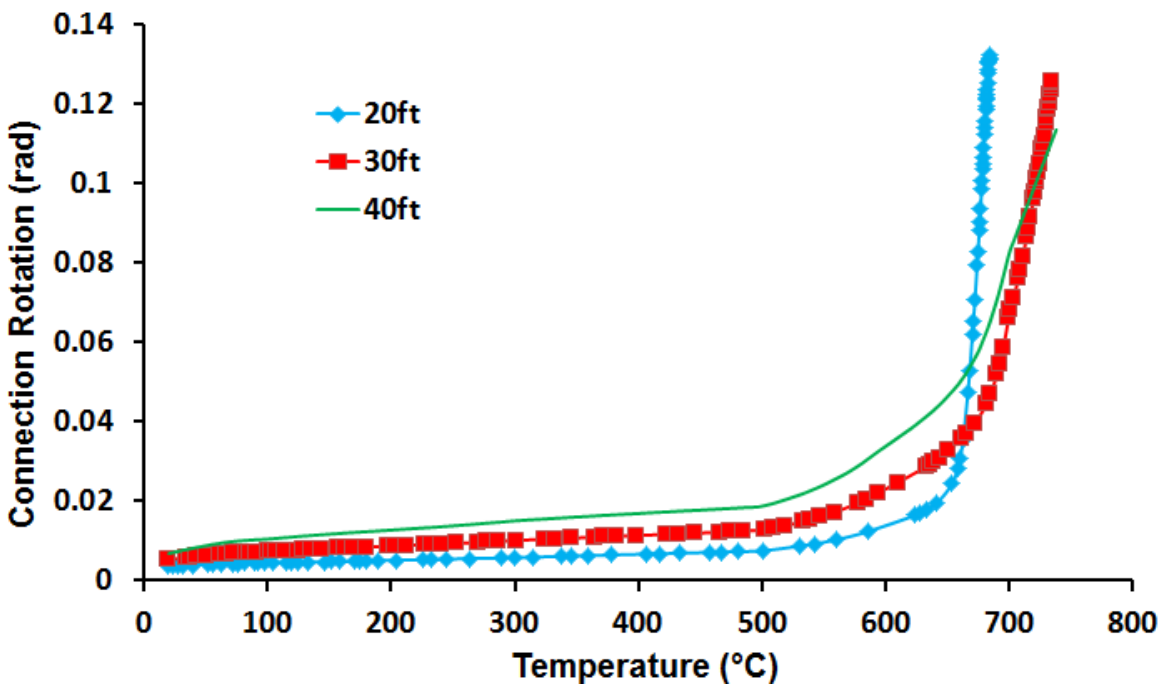


Figure 6.14 Connection rotation - temperature response for different beam lengths

6.3.3 Stiffness of the Adjacent Structure

In steel structures, shear tabs are welded to other elements, such as a column flange, a column web or a beam web. These supporting members provide varying degrees of translational and rotational restraint to the connections. In order to study the effect of boundary stiffness on the behavior of the connections in fire, a W14×90 steel column was modeled and attached to the shear tab. The column was assumed to be protected by insulation material and thus kept at ambient temperature during the fire. Three cases were investigated (Figure 6.15):

1. Rigid boundary conditions;
2. The shear tab attached to the flange of the W14×90 column, which means the axial deformation of the beam and connection is resisted by the strong axis of the attached column;
3. The shear tab attached to the web of the W14×90, which means the axial deformation of the beam and connection is resisted by the weak axis of the attached column and is also affected by flexibility of the column web.

The column height was taken as 10 feet with both columns ends completely fixed. The beam was taken to be 30 feet long with a load ratio of 0.5. Figure 6.16 shows the variation of the connection axial force with temperature during heating and cooling for the three cases. It can be seen that the stiffness of the adjacent structure has a large impact on the axial forces developed in the connections exposed to a fire, particularly at the lower temperatures near the beginning and end of the fire. The stiffer the boundary conditions, the larger the force. At very high temperatures, however, the stiffness of the adjacent structure has little effect on the connection axial force. Plots of connection rotation versus temperature for the three boundary conditions are shown in Figure 6.17. The stiffness of the boundary has less effect on connection rotation than on connection axial force.

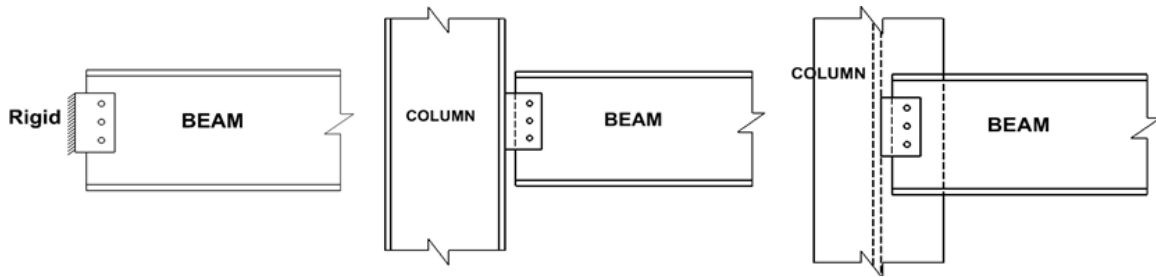


Figure 6.15 Beam connects to different boundaries

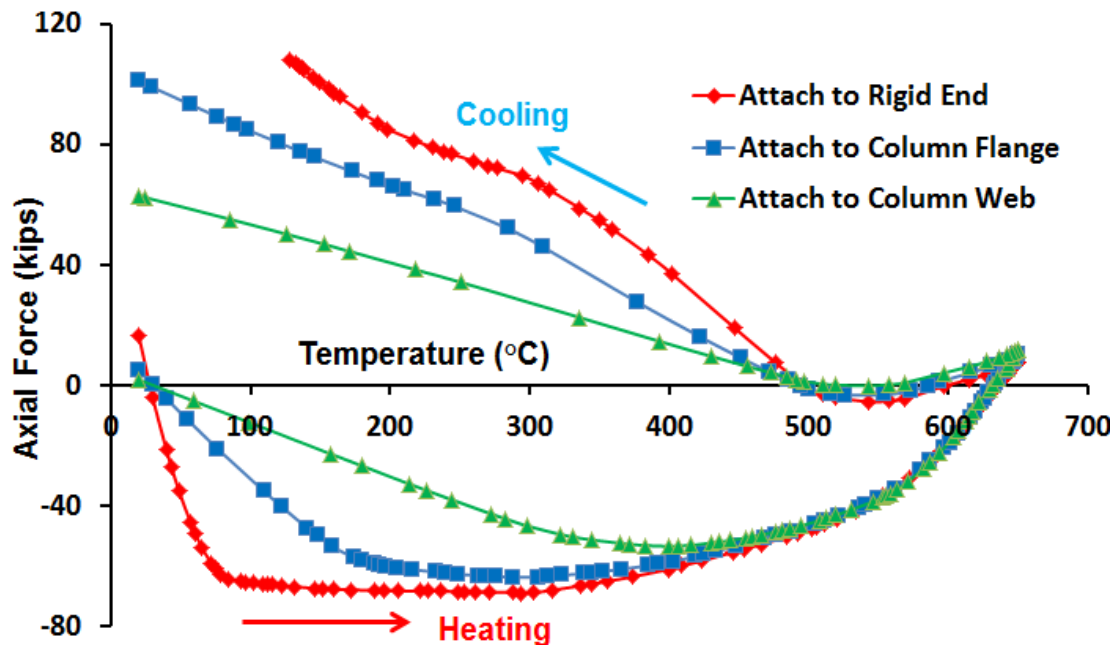


Figure 6.16 Connection axial forces - temperature response for different stiffness levels of adjacent structure

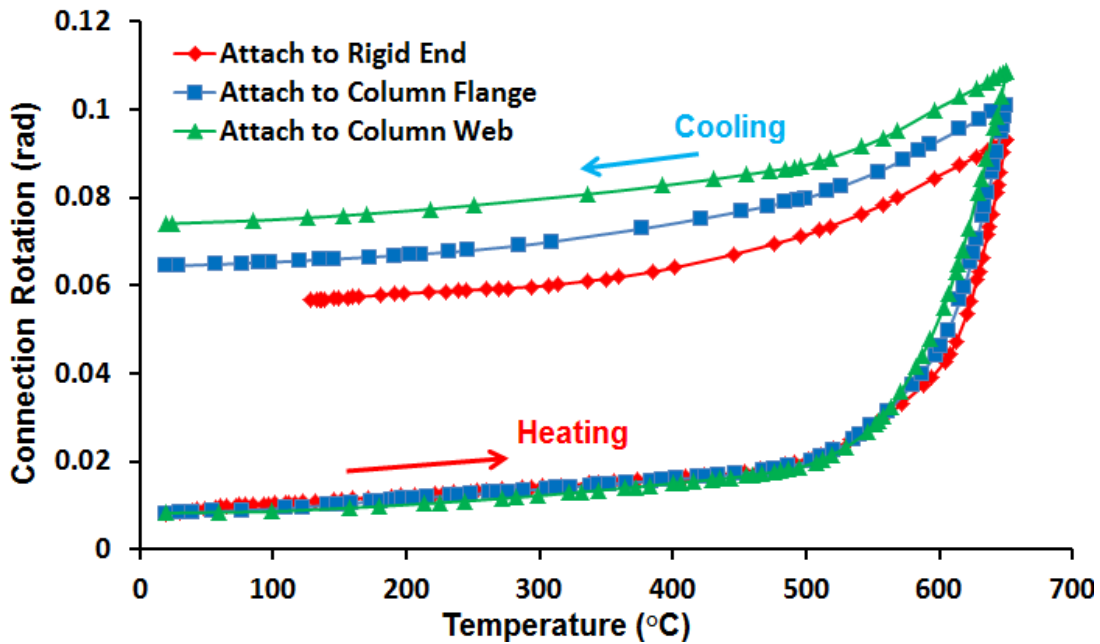


Figure 6.17 Connection rotation - temperature response for different stiffness levels of adjacent structure

6.3.4 Initial Cooling Temperature

The initial cooling temperature in the decay phase of a fire is defined as the maximum temperature in a fire event, after which the temperature decreases. In different fire events, the highest temperature reached in a beam can vary considerably and thus, lead to significant differences in the connection behavior. To study the effect of the initial cooling temperature on the behavior of connections and beams, a 30-ft beam model with a load ratio of 0.5 was used. Initial cooling temperatures of 400°C, 500°C, 600°C and 650°C were investigated. Figure 6.18 shows the axial force in the connection versus temperature. It can be clearly observed that higher initial cooling temperatures will produce larger axial tensile force during cooling and larger residual forces after the beam completely cools down. Even for the rather low initial cooling temperature of 400°C, the final axial tension after cool down is very large.

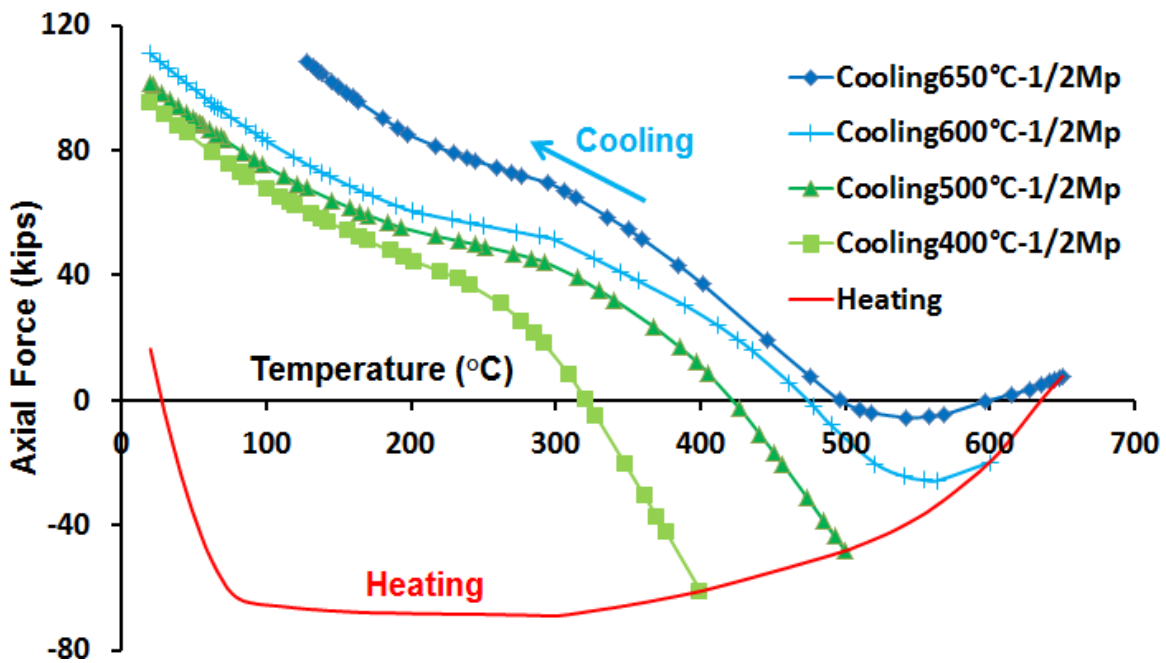


Figure 6.18 Connection axial force - temperature response for different initial cooling temperatures

6.3.5 Non-Uniform Temperature Distribution

In an actual structure subjected to a fire, steel members are not heated uniformly due to different fire exposures, variations in member sizes, non-uniformity of insulation materials, presence of a concrete floor, etc. In the Cardington fire tests, temperatures were measured at different locations on the steel beams, and significant temperature gradients were recorded (Wald et al 2006). Therefore, the behavior of shear tab connections on steel beams under non-uniform temperature distributions is of interest. In this study, finite element analysis was conducted on the same 30-foot long steel beam and shear tab connections described above with a non-uniform temperature distribution. A load ratio of 1/4 was assumed in the analysis. Non-uniform temperature distributions were obtained by conducting finite element thermal analysis (described in Chapter 4) using the fire gas temperatures measured in one of the Cardington tests (Figure 6.19). In the thermal analysis, it is assumed the top flange of the beam is covered by concrete

material, so it is not exposed to fire directly. Therefore, significant temperature gradient exists in the beam, and the bottom flange has the highest temperature during heating as expected. The temperature difference between the bottom flange and top flange is about 200°C during the most of the heating stage. A plot of connection axial force versus beam mid-span temperature is shown in Figure 6.20. In this figure, the average temperature of the beam cross-section at mid-span is plotted. It can be observed that the connection axial forces for the two temperature conditions are similar. Compare to the uniform temperature condition, it appears the temperature gradient on the steel beam did not change the axial forces developed at the connection significantly, as long as the average temperatures are similar. Connection rotation versus beam mid-span temperature is shown in Figure 6.21. As expected, the temperature gradient on the steel beam will significantly increase the beam end connection rotation.

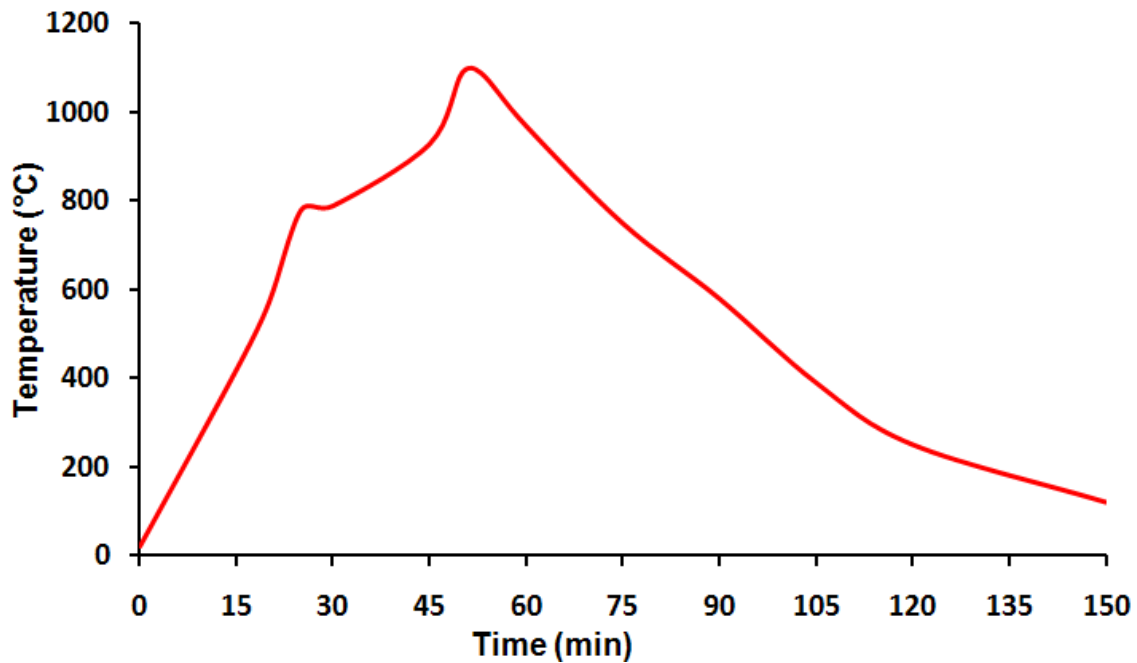


Figure 6.19 Gas temperature of Cardington fire test (Wald et al 2006)

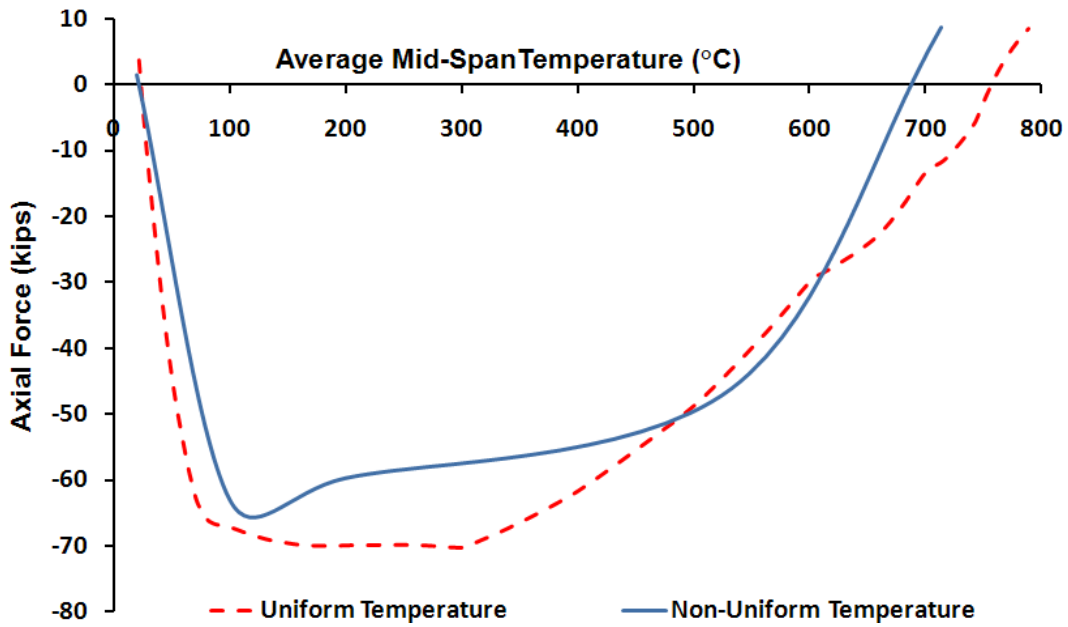


Figure 6.20 Connection axial force for uniform and non-uniform temperature distribution

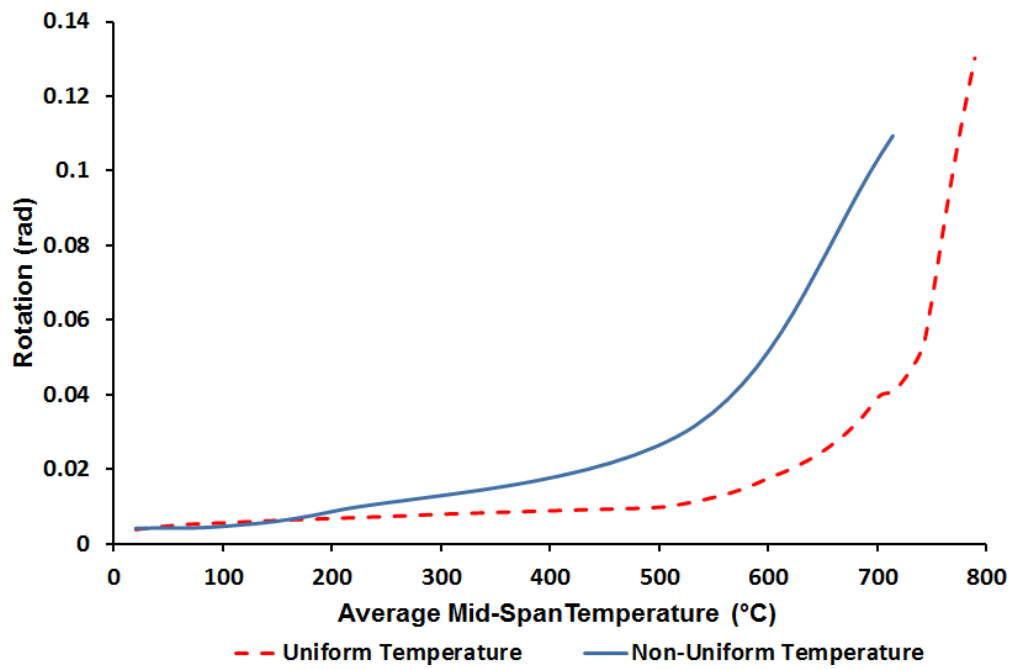


Figure 6.21 Connection rotation for uniform and non-uniform temperature distribution

6.4 EFFECT OF CONNECTION DETAILS

6.4.1 Short Slotted Bolt Holes

The large axial forces generated at the beam end connections are due to thermal expansion and contraction of the member in the heating and cooling phases of the fire. It is reasonable to assume that some flexibility in the horizontal restraint can help reduce these large axial forces. As discussed above, the stiffness of the adjacent structure has a significant impact on the axial force developed at the connections. However, in an actual building, the stiffness of the structure to which the beam connects varies greatly, and usually cannot be easily predicted or controlled. Therefore, a more practical solution may be some modifications to the connection itself to change the horizontal stiffness of the connection.

According to the AISC Manual of Steel Construction (2006), in addition to standard bolt holes, short-slotted holes are also permitted to be used in the horizontal direction in shear tab connections. To study the effect of short horizontal slotted holes on the behavior of the shear tab connections in fire, a new FE model was built according to the nominal bolt hole dimensions in Table J3.3 of the AISC specification (2005). In this model, holes in both the shear tab and beam web are short-slotted in the horizontal direction. The lengths of the slots were 1/4 inch greater than the bolt diameter. Figure 6.22 shows the FE mesh of standard holes and short-slotted holes in this study.

Figure 6.23 shows the comparison of the two types of holes on the response of connection axial force versus connection temperature in the heating phase. It can be seen that during the initial stages of heating, the connection with short-slotted holes develops significantly less axial compression than the one with standard holes. However, with continued temperature increase, the bolt comes into bearing against the edge of the slotted hole, and the magnitude of the axial compression increases rapidly after the connection reaches 100°C and reaches the same level of the standard holes at about 250°C. Similar phenomenon can be observed in Figure 6.24, which shows the variation of shear force in the top bolt with temperature for the standard hole versus the short

slotted hole. From this limited analysis, it appears that the use of short slotted holes may not be an effective means for reducing bolt forces during the heating phase of a fire because the slots are too small compared to the thermal deformation of the beam ends. It is reasonable to assume that bolt shear forces could be reduced more by using long-slotted holes. However, the use of long slotted holes may adversely affect the bracing provided to the columns by the beam.

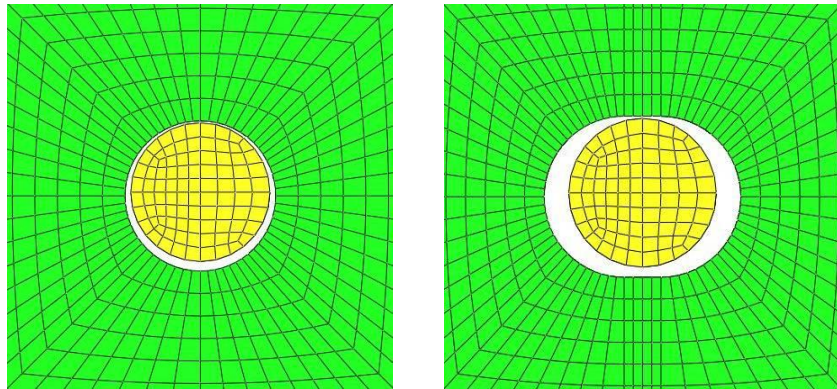


Figure 6.22 FE mesh of standard holes and short-slotted holes

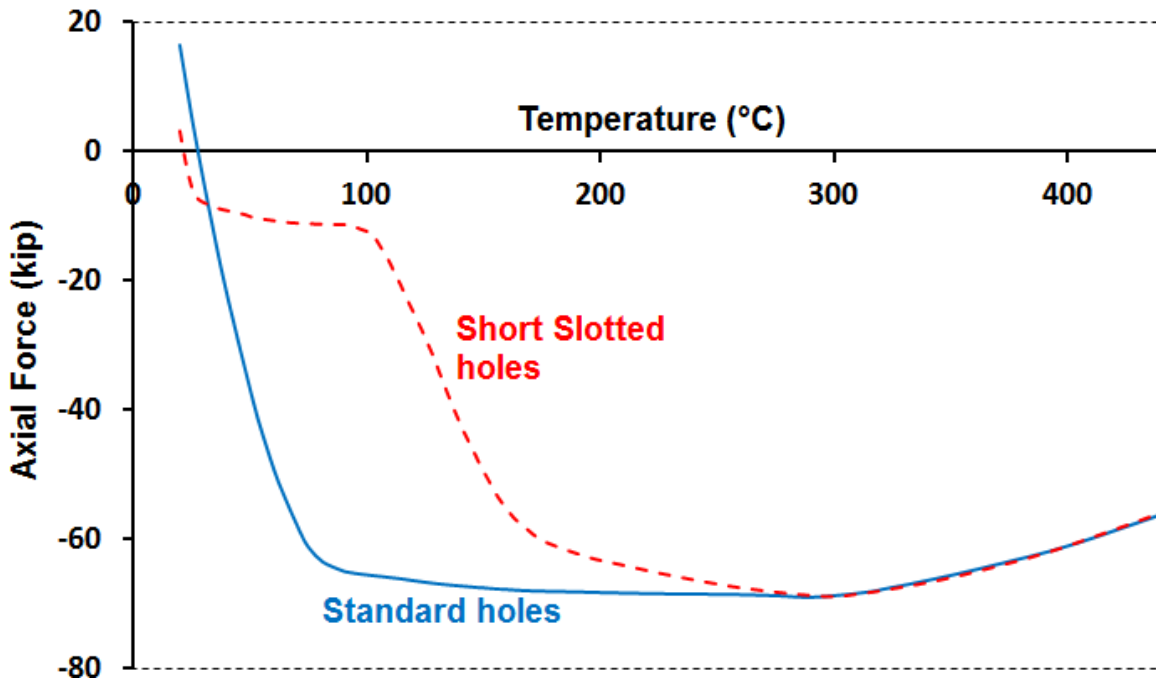


Figure 6.23 Connection force for standard holes and short-slotted holes

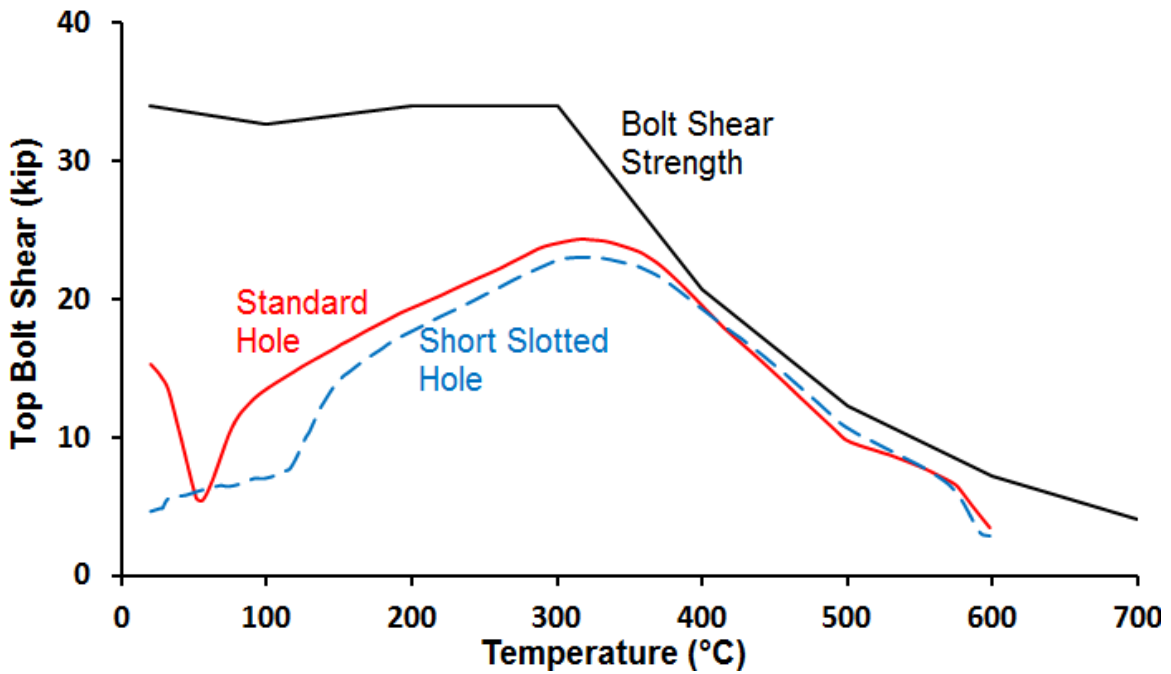


Figure 6.24 Top bolt shear for standard holes and short-slotted holes

6.4.2 Pretension in Bolts

In most shear tab connections in the US, the bolts are usually installed by using the “snug tight” method, which means little or no pretension exists in the bolts. However, slip critical connections are also sometimes used, so it is of interest to examine the effects of bolt pretension on the behavior of shear connections in fire.

To understand the load-displacement behavior of slip critical bolted connections, Yu’s twin-bolt connection test at ambient temperature (Yu 2006), which was discussed in Chapter 2, was remodeled using snug-tightened bolts and pretensioned bolts in ABAQUS. The pretension was assumed to be 30 kips for each bolt. Load-displacement curves are presented in Figure 6.25 comparing connection response with snug-tight versus pretensioned bolts. For the connection using snug-tightened bolts, after initial slip, the bolts bear against the bolt holes, resulting in a smooth load-displacement curve. For the connection using pretensioned bolt, slip occurs at about 20 kips when friction at the plate faying surface is overcome, after which it shows similar behavior to the snug-tight case. This result can be roughly verified by hand calculation, taking into account a coefficient of friction of 0.35.

To study the effect of pretension on the behavior of connections in fire, 30 kips pretension was applied to the bolts in the connection model described in Section 6.2.1. As expected, the connection using pretensioned bolts showed no noticeable difference with the one using snug-tightened bolts on the behavior in both heating and cooling. It may be concluded that the effects of pretension in the bolts are negligible. This probably is due to the fact that the axial force generated in the beam during heating is much larger than the slip load of the connection. Consequently, the bolts go into bearing early in the fire. It must be noted that in this analysis, a constant frictional coefficient of the contact surfaces was assumed. However, according to Yu’s test (Yu 2006), the slip coefficient varies with the temperature. Nonetheless, even if with a temperature varying coefficient of friction, the impact of bolt pretension on connection performance in fire is not likely to be significant.

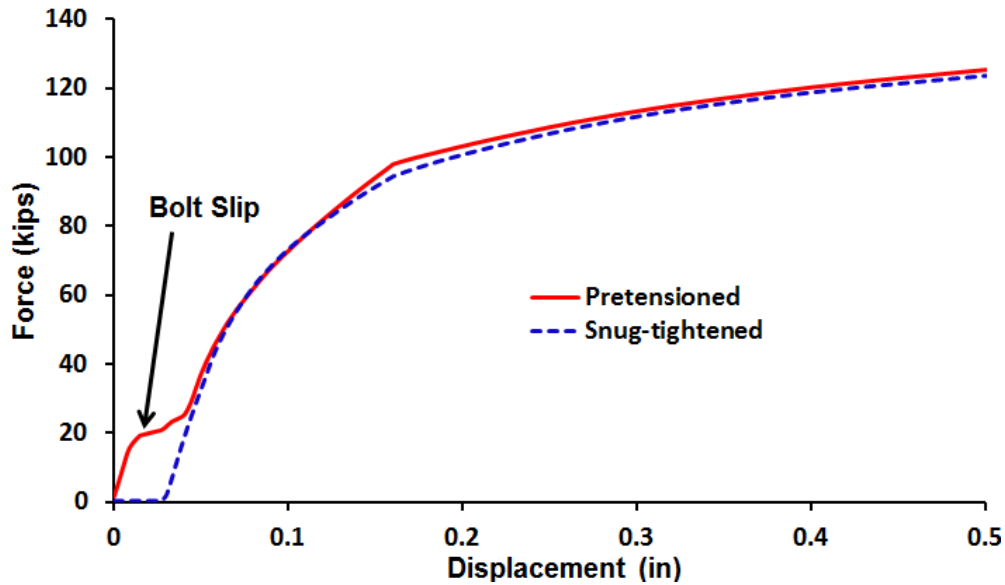


Figure 6.25 Load-displacement behavior of Yu's twin-bolt connection at ambient temperature by FEA (bolt with and without pretension)

6.4.3 Shear Tab Location

Due to beam end rotations, horizontal forces exist in the bolts even at room temperature without thermal loading. The horizontal bolt force is a function of the location of the bolt with respect to the center of rotation. The larger the distance of the bolt from the center of rotation, the greater the horizontal force. This horizontal force, in turn, reduces the capacity of a bolt to resist vertical shear force (Ashakul 2004). At room temperature, this horizontal force is generally small compared to the vertical shear force. However, in a fire, when large axial force is generated in the beam, the location of the shear tab or bolt group with respect to the neutral axis of the beam may have significant impact on the connection capacity.

Typically, the shear tab is located at the upper portion of the beam web. Therefore, in this study, the shear tab and bolt group was moved up 1.25 inch and 2.75 inch from mid height of the beam web, respectively. Top bolt shear forces versus temperature are plotted in Figure 6.26. It is clear from the figure that with an offset of

1.25 inch, the maximum bolt force will increase significantly, but the failure temperature of this connection is not affected. However, when the shear tab and bolt group are 2.75 inch above the mid height of the beam web, as shown in the green line, much larger bolt forces will be generated and significantly earlier bolt failure occurs; at less than 300°C in this study. Therefore, it appears that the shear tab and bolt groups should be located near the mid height of beam web to obtain better performance of the connection in fire.

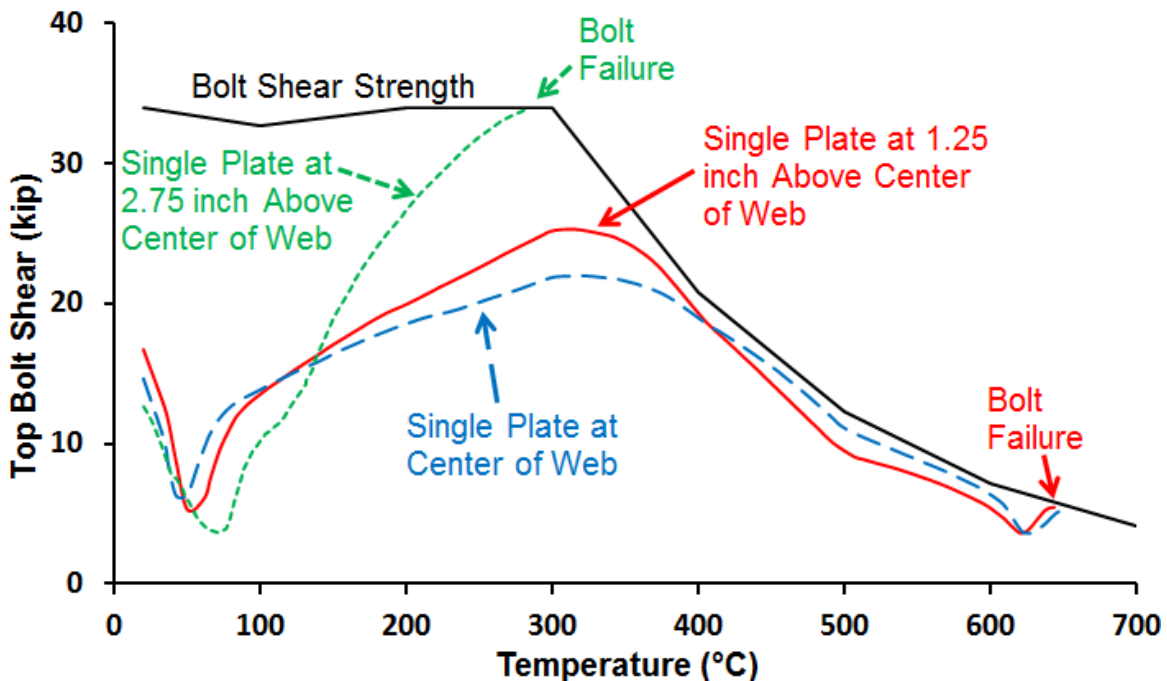


Figure 6.26 Top bolt shear for different shear tab locations

6.4.4 Shear Tab Thickness

Besides bolt shear failure, shear tab connections can also have bearing type failures after catenary action starts to develop and the beam goes into axial tension, as shown in the picture of the bolted shear tab connections tearing out in World Trade Center Building No. 5 (Figure 1.3). Increasing the shear tab thickness is a solution to increase the bearing capacity of the connections. However, based on the finite element

analysis, shown in Figure 6.27, increasing plate thickness from 3/8 inch to 1/2 inch will significantly increase the bolt shear force when the connection is under compression. Therefore, simply increasing plate thickness alone may potentially adversely affect connection performance in fire.

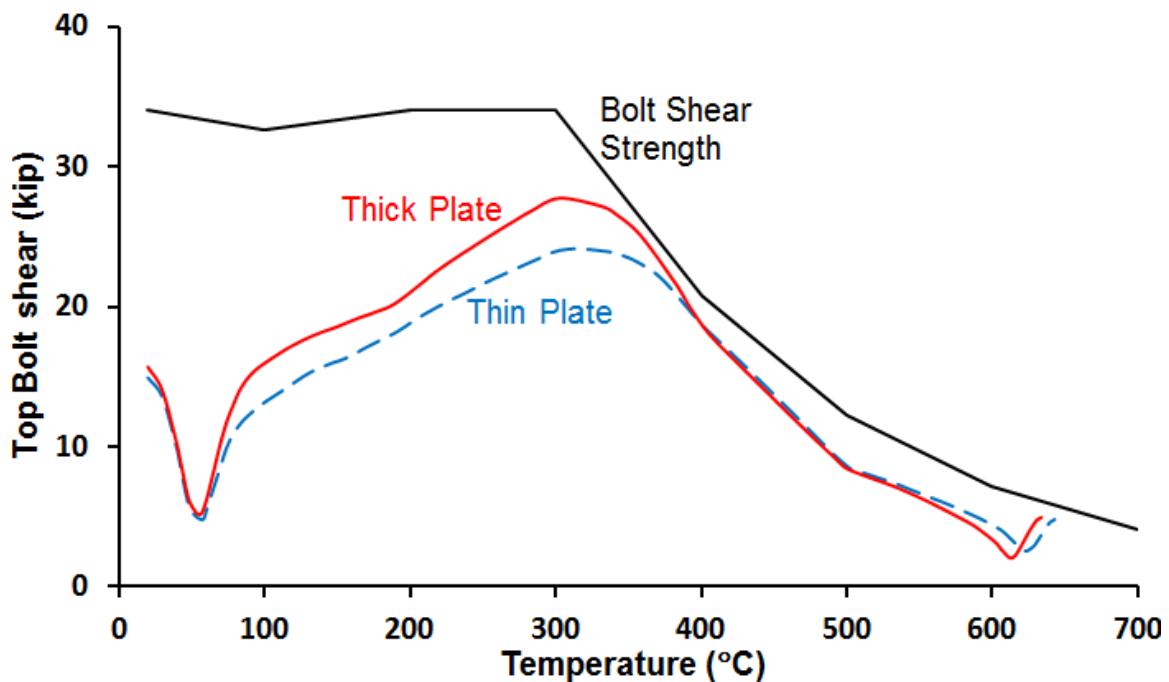


Figure 6.27 Top bolt shear for thick and thin plates

6.4.5 Shear Tab Width

In addition to the properties of bolts and holes, the dimensions of the shear tab can also influence connection performance in fire. In the literature and in steel connection design guides, the width of the shear tab varies significantly, resulting in different gap lengths between beam ends and supporting members. In the AISC Manual of Steel Construction (2006), the length of this initial gap is not specified for shear tab connections. Even so, based on the dimensions of conventional configurations of shear tab connections recommended by AISC, this length can be as large as 1.5 inch. However,

in both Yu's test (Yu et al 2009) and the fire tests on the 8-storey steel–concrete composite frame building at the Cardington laboratory (Wald et al 2006), significantly narrower shear tabs were used. In these tests, initial gaps were only 10 mm (0.4 inch) (Figure 6.28). The difference of the shear tab width may cause significantly different behavior of the connections in fire. As discussed above, the connection axial stiffness, which is related to the local buckling capacity of the shear tab, may change for different plate dimensions. In addition, as noted before, after the connection experiences large rotation, the beam end may come into contact with the supporting member. It appears that the initial gap length may have a significant effect on this phenomenon. Therefore, it is important to examine the effects of shear tab width on the connection performance.

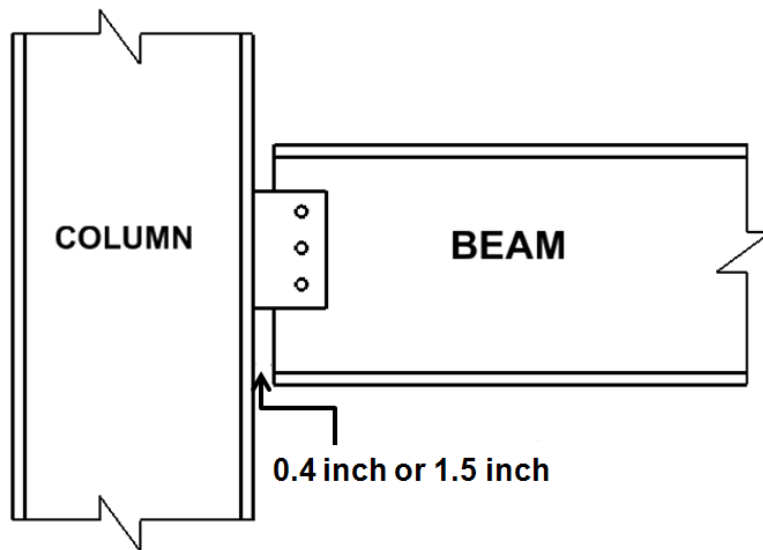


Figure 6.28 Initial gap length of shear tab connection assembly

The response of connection rotation versus temperature for different shear tab widths is compared in Figure 6.29. It can be seen that after early contact, the connection rotation is reduced with temperature increase (blue line at 200°C to 500°C). This is because the thermal expansion of lower portion of the beam is restrained by the supporting member, whereas the upper portion of the beam still expands due to heating. Consequently, this

causes a rotation of the connection in the opposite direction, which helps reduce the beam deflection. However, this early contact will usually cause local buckling in the lower beam flange (Figure 1.5 and Figure 6.4) and large forces on the supporting elements (columns or girders).

For fires where structural safety is the primary concern, forces in the connection components are critical. For the beam and connection assembly considered in this analysis, the shear force in the top bolt versus temperature is shown in Figure 6.30. As shown in the figure, the force at the top bolt is very similar for the two different shear tab widths. The maximum top bolt shear for the wide connection plate is slightly smaller than for the narrow plate, probably due to the smaller stiffness of the wide plate.

In summary, results of these analyses suggest that the wider shear tab is generally beneficial over most of the temperature range considered in the analysis, when bolt shear failure is the primary concern. It is also noted that in both figures, at the end of the curves, the difference of the behavior between the two connections are small. This suggests that after the beam enters the “run-away” stage and catenary action starts to develop, the connections with different plate widths or initial gap lengths behave similarly.

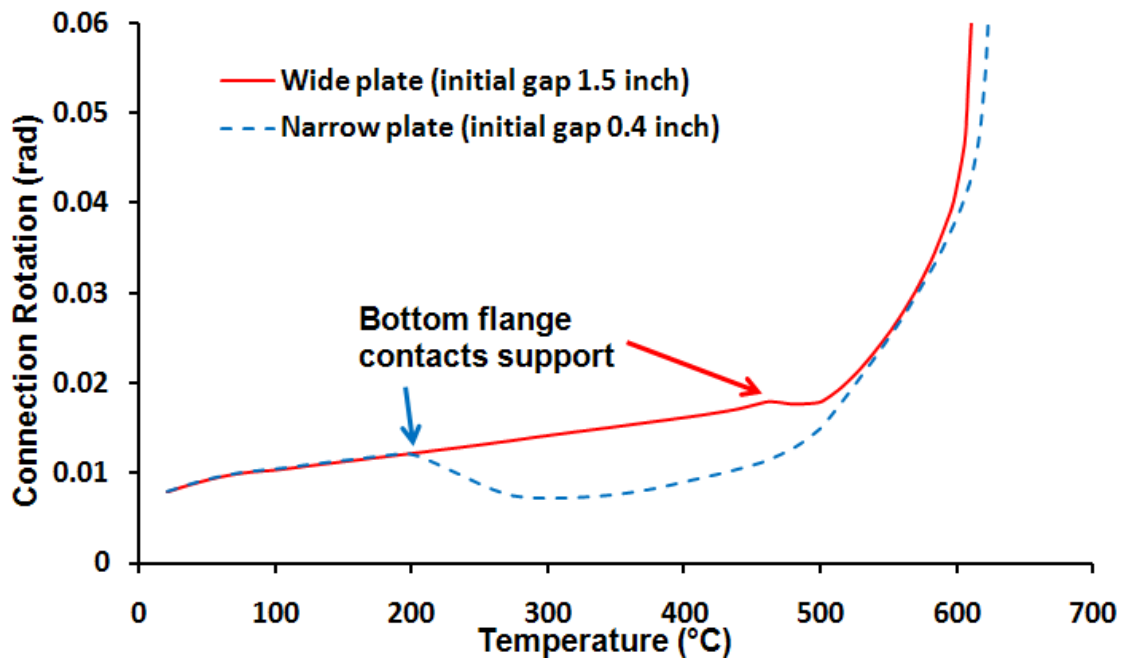


Figure 6.29 Connection rotation - temperature response for different plate width

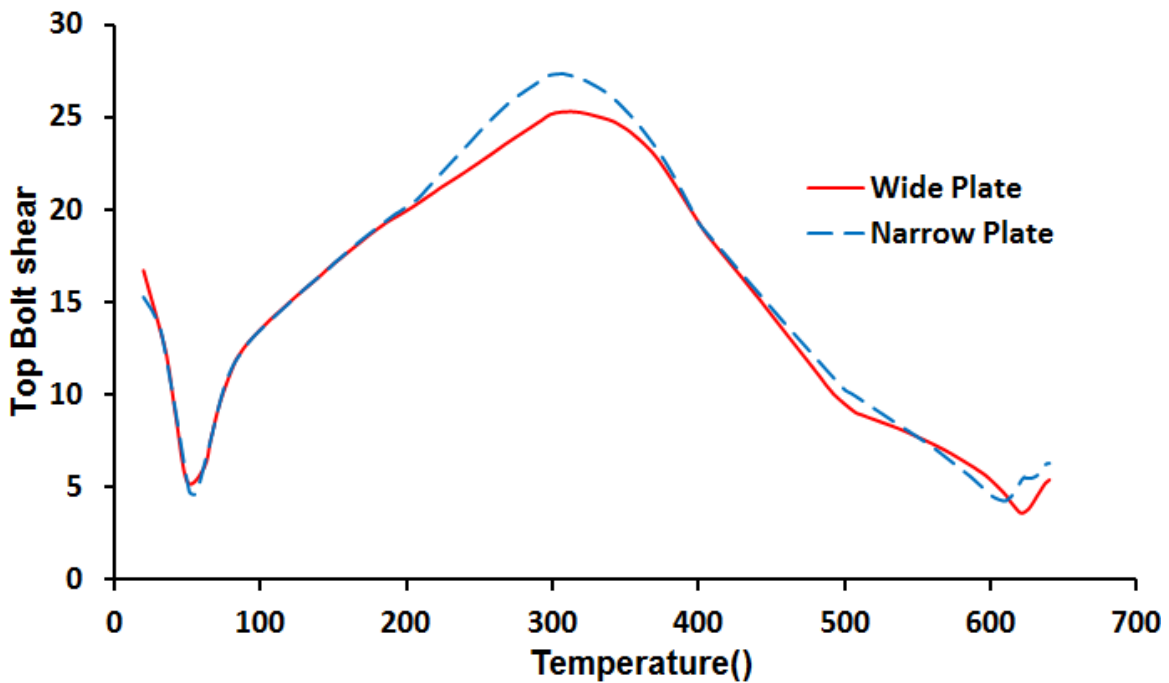


Figure 6.30 Top bolt shear-temperature response for different plate width

6.4.6 Bolt Grade

Based on the test results in Chapter 5, bolts in connections can be more vulnerable to failure than other connection components due to the high strength reduction factors for bolts at elevated temperatures. As demonstrated by the tests in Chapter 5, bolt shear failure often controls connection capacity at elevated temperatures. Consequently, increasing the bolt grade, i.e. using a higher strength bolt, may be an option for improving connection performance in fire. The effect of bolt grade on the connection behavior in fire is directly related to the bolt strength at elevated temperatures. Using higher strength bolts can increase connection strength in fire since most of the structural bolts have similar reduction factors at elevated temperatures. However, the benefits of higher strength bolts may be limited by the occurrence of other failure modes when the beam experiences large deflections, such as block shear (Figure 5.29) or bearing tear out. Therefore, to obtain a significant improvement in connection capacity in fire may require using higher strength bolts in combination with increased edge distances and/or increased plate thicknesses.

6.5 SUMMARY AND OBSERVATIONS

Although only a limited number of FE analyses and parametric studies were conducted for this research, it is clear that predicting the force and deformation demands on beam end connections in fire is complex and is affected by many variables. Some preliminary observations that can be made from these analyses are as follows:

- Very large axial forces can develop at beam end connections during a fire. This is quite different than ambient temperature design, where shear forces are the dominant force in the connection.
- Axial force in the beam, which is transmitted to the connection, is typically compressive in the early stages of a fire, due to thermal expansion of the beam. The peak axial compression force can occur very early in a fire. Early in the fire, the beam has not yet become sufficiently hot to experience a significant reduction in modulus

or yield strength, and therefore maintains a high axial stiffness. However, although reductions in modulus and yield strength do not occur until temperatures of several hundred degrees C are achieved; thermal expansion starts immediately with the start of heating. The combination of thermal expansion and high axial stiffness in the early stages of a fire results in large compressive forces early in the heating. The analyses conducted herein showed that peak axial compressive forces often occur at temperatures on the order of 100 to 200°C. The large axial compression force developed at this stage typically resulted in localized buckling of the shear tab or beam web. This buckling limited any further increase in axial compression.

- As heating continues on the beam, the compression force reduces as the beam loses stiffness (due to the reduction in modulus and yield stress of steel at elevated temperatures) and as the beam begins to sag. The axial force can turn into tension as heating continues and the beam sags and develops catenary action.
- Very large axial tensile forces can develop at the connections during the cooling stage of a fire. During the heating stage of a fire, the beam undergoes permanent geometric changes, including permanent shortening due to yielding under axial compression and permanent bending deformations. Upon cooling, the beam experiences thermal contraction that generates large axial tension.
- The large forces and deformations developed at the beam end connections during the heating and cooling stages of a fire can cause shear fracture of the bolts. Bolt shear fracture is often the controlling limit state for connections subjected to fire. This is because bolts lose strength at a faster rate than structural steel at elevated temperatures, and also suffer a greater degree of permanent strength loss during cooling. Predicting when bolts fail in a fire is complex, since both the forces on the bolts and the strength of the bolts are temperature dependent. Consequently, failure may not occur when bolt forces are largest (typically early in the heating stage or late in the cooling stage) because bolt strength may also be quite large at this stage. Also, bolt failure may not necessarily occur when bolt strength is at a minimum (which

occurs when bolt temperature is at a maximum), because forces on the bolts at this stage may be quite small. Predicting bolt failure is further complicated by the fact that bolt strength is not only temperature dependent, but also temperature history dependent.

- The parametric studies showed the factors having the largest influence on the force and deformation demands on the connection were the stiffness of the adjacent structure, level of vertical load on the beam, peak temperature achieved prior to cooling, and location of shear tab within the depth of the beam web. Factors that had somewhat less influence on the connection force and deformation demands included beam length, presence of a thermal gradient over the depth of the beam, the use of slotted holes, bolt pretension level, and shear tab thickness and width.

The results of these analyses, although preliminary, raise some concerns about structural-fire safety approaches used in current practice. The analyses suggest that connections can be critical elements in which failure can occur during the heating or cooling stage of a fire. Current U.S. practice for structural-fire safety relies on testing of structural components at elevated temperature according to the requirements of ASTM E119 (ASTM 2000). Based on these analyses, there may be several shortcomings with the E119 testing approach. First, ASTM E119 does not require testing of connections. It only requires testing of structural members (beams, girders, columns, etc). Consequently, the performance of connections in fire is not explicitly addressed in U.S. building codes. Secondly, the standard ASTM E119 fire exposure does not include the cooling stage of a fire. As is clear from these analyses, the cooling stage can be the most demanding on a beam end connection, and failure can occur during cooling. Finally, a primary criterion for determining the amount of insulation (fireproofing) required for a beam according to ASTM E119 is to limit the temperature of the beam to about 600°C. This is based on the assumption that the beam will retain sufficient strength at this temperature to maintain support of gravity loads. However, as shown by these analyses, very large connection forces are developed at temperatures well below 600°C. Consequently, even though beam

is insulated to satisfy the ASTM E119 testing criteria, connections may still be vulnerable to failure in a fire. Overall, there is reason to question the adequacy and safety of current U.S. building code requirements when it comes to beam end connections.

In terms of developing improved design practices for structural-fire safety of steel buildings, developing simplified methods for estimating connection force and deformation demands represents an important need. In this research, the forces and deformations developed at connections during a fire were estimated by using very detailed three-dimensional finite element models. This approach is impractical for routine design practice. Considerable further study is needed to develop approaches for evaluating connection performance in fire that are suitable for design practice.

CHAPTER 7

Conclusions and Future Work

7.1 BRIEF SUMMARY OF WORK COMPLETED

This dissertation has presented results of research on the behavior of steel simple shear beam end framing connections in fire. Studies were conducted using both experiments and finite element numerical analysis. The primary focus of the research was shear tab connections, which are commonly used in U.S. practice.

Two sets of experimental studies were completed in this investigation. The first was a series of elevated temperature tension coupon tests on samples of ASTM A992 steel. The second was a series of elevated temperature tests on connection subassemblies. High temperature testing equipment, techniques and procedures were discussed in detail. From the material tests, full stress-strain curves at elevated temperatures were obtained. From these curves, estimates of elevated temperature mechanical properties were derived, including modulus, yield strength, and tensile strength. From the connection tests, connection strength and deformation capacities at elevated temperatures were measured, and failure modes were evaluated. The connection test results were also used to further validate the developed finite element model.

The numerical studies include developing thermal and structural finite element models for analysis of steel beams and beam end connections in fire. This included the development of detailed three-dimensional FE connection models incorporating contact, geometric nonlinearity and temperature dependent material nonlinearity. The capabilities and limitations of the developed FE model was then evaluated by comparison with test results reported in the literature. The model was further evaluated by comparison with the connection subassembly tests conducted as part of this investigation. The finite element model was then used to conduct a series of parametric studies to gain further insights into the behavior of shear tab connections in fire.

7.2 CONCLUSIONS

Key conclusions from this research are as follows:

- The elevated temperature tests on ASTM A992 steel showed that the reductions in modulus, yield strength and tensile strength with temperature are similar to that of other structural steels reported in the literature. The variations of these properties with temperature agree fairly well with the recommendations provided by Eurocode 3 and by the AISC Specification. The largest apparent discrepancies occurred in the elevated temperature values of yield strength. If the yield strength is defined using a conventional 0.2-percent offset method, the measured yield strength values for A992 are substantially lower than the values specified by Eurocode 3 and by AISC for temperatures below about 600°C. A review of the background of Eurocode 3 suggests that the yield stress values were defined as the stress at a total strain of 2-percent. If this definition of yield strength is adopted, then the yield strength values for A992 match Eurocode 3 and AISC quite closely. However, the justification for using the Eurocode 3 definition of yield strength is unclear and is contrary to more commonly used definitions. Further research and discussions may be needed on the development of an appropriate definition of yield strength of steel at elevated temperature, for structural-fire engineering applications.
- Eurocode 3 also provides recommendations for elevated temperature stress-strain curves for steel for use in finite element analysis and other advanced analysis methods. The stress-strain curves recommended by Eurocode 3 matched quite well with the measured stress-strain curves for A992 steel for strains up to about 15-percent. Beyond this, the test data showed significantly higher strain capacities than predicted by the Eurocode 3 curves.
- The tests on A992 steel showed that the stress-strain curves at elevated temperatures are loading rate dependent. For sustained loading, creep effects also

become increasingly important at higher temperatures. Detailed investigation of loading rate effects and creep effects were beyond the scope of this study, but deserve more detailed investigation in the future.

- The temperatures of steel members in fire can be predicted with reasonable accuracy by finite element heat transfer analysis. The thermal properties of steel (thermal conductivity and specific heat) are well characterized. For insulated (fireproofed) steel members, there is greater uncertainty in the heat transfer analysis and the predicted steel temperatures, because thermal properties of commercially available insulation materials are not well documented in the literature and generally not available from manufacturers.
- The structural response of steel beams and connections at elevated temperatures can also be predicted with reasonable accuracy using finite element analysis. When subject to fire, steel elements can undergo very large deformations and experience yielding at low load levels. Consequently, predicting the elevated temperature structural response of steel members and connections generally requires consideration of nonlinear geometry, inelasticity, and temperature dependent nonlinear material properties. These factors can be accommodated by advanced finite element programs such as ABAQUS, which was used in this study. These capabilities, however, are generally not available in commercial structural analysis software typically used for building design. This likely represents a barrier to the more widespread use of engineered structural fire safety solutions for most building design applications.
- Very detailed three-dimensional finite element models were developed for the beam end connections in this study. These models included the allowance for movement of the bolt within the bolt hole, the use of contact constraints to model bearing of the bolt head and nut on adjoining plate elements, contact between the bolt and the edge of the bolt hole, contact between the shear tab and the beam

web, contact between the beam flange and the column at large rotations, and the inclusion of pretension in the bolts. Significant model development effort was required to include all of these items. The subsequent analysis showed that many of these items can have an important effect on connection response in fire. However, one of the key factors not included in the analysis was explicit modeling of fracture phenomena in the connection, such as bolt shear fracture, bearing tear out fracture, block shear fracture, etc. The occurrence of fracture in the first component of the connection could be approximately inferred from the model from predictions of very large localized deformations in an element. However, the behavior of the connection after first fracture, say for example after the first bolt fracture, could not be predicted by the finite element model developed for this research.

- The elevated temperature tests on connection subassemblies showed that bolt shear fracture is a common failure mode at elevated temperatures. This is because bolts lose strength at a faster rate at elevated temperature than structural steel, and also experience greater permanent strength loss upon subsequent cooling. As a result, the limit states that control connection strength may be different at elevated temperature than at ambient. The connection tests performed with inclined tension on the specimens showed that there can be large deformations that occur between fracture events. For example, after the first bolt fractures, the connection can sustain large deformations before the next bolt fractures. This observation is potentially significant for fire performance of connections. The large deformations that occur between fracture events may serve to relieve the thermally induced forces in the beam, and thereby reduce the force demands on the connection. This, in turn, may help the connection survive the fire event.
- Comparisons were made between the experimental data from the connection subassembly tests with connection strength computed using simplified design

- equations from the AISC Specification, adjusted for elevated temperature material properties. This comparison showed that these equations predicted the peak connection resistance reasonably well, and errors were generally conservative.
- Comparisons were made between the experimental data from the connection subassembly tests with corresponding predictions of the finite element model. These comparisons showed that the finite element model provided good predictions of peak connection strength and connection load-deformation response up to the point where the first connection component fractured. The model was not able to predict connection performance after first component fracture. The development of models that can predict connection performance after fracture of the first component is important. Fracture of the first component does not equate to failure of the connection in a fire, and the tests suggest that the connections have substantial deformation and load capacity after fracture of the first component.
 - The finite element analysis showed that the load-deformation characteristics of beam end connections have a large influence on the load-deformation response of the beam itself. Consequently, analysis models for computing the response of structures to fire that do not include the load-deformation characteristics of the connections can lead to significant errors. The simple beam end framing connections considered in this study are normally modeled as pins for structural design at ambient temperature. This type of simplification may not be appropriate for structure-fire analysis.
 - The analyses showed that during a fire, large axial compression and tension forces can be produced at the beam end connections. The magnitude of the compression is limited by the local buckling capacity of the shear tab and beam web at elevated temperatures. Large connection rotations can occur during a fire. During the cooling phase of the fire and after complete cool down, very large tensile forces

can develop in the beam and the beam end connections. These large tensile forces can cause connection failure. Significant residual forces and deformations may remain in the beam and connections after a fire. Note that the large axial compression and tension forces developed in a beam during a fire not only affect the connections, but also affect the adjoining elements connected to the beam. For example, very large forces can be transmitted from the beam to the adjoining columns.

- The behavior of connections in fire is complex and affected by many variables. Load ratio, beam length and initial cooling temperature can affect the connection force and deformation demands. The stiffness of the adjacent structure has a large impact on the connection forces developed during the heating and cooling phases of a fire.
- As noted above, bolts can be vulnerable elements in connections during a fire. As expected, using higher strength or larger diameter bolts can increase connection strength. However, the benefits of higher strength and larger diameter bolts may be limited by the occurrence of other failure modes when the beam experiences large deflection, such as bearing tear out failure. Therefore, to obtain a significant improvement in the connection capacity in fire may require using higher strength or larger diameter bolts in combination with increased edge distances and/or increased plate thicknesses. Pretension in the bolts and short slotted bolt holes do not appear to influence connection performance in fire significantly. Therefore, there is little benefit obtained by using slip critical bolted connections or using short slotted bolt holes.
- After heating and cooling, connection strength can be reduced. Exposed to 800°C and lower, after cooling the connection strength reduction is mainly caused by the strength loss in the structural bolts. Exposed to 900°C and 1000°C, the strength loss of A992 steel after cooling needs to be considered. This loss of strength after

heating and cooling may be significant when evaluating the condition and safety of a steel structure after a severe fire.

- The results of this study suggest that it may be possible to compute the capacity of connections at elevated temperature using relatively simple equations. However, predicting the demands on the connection during a fire appears to be much more difficult. In this study, force and deformation demands on the connections were computed using advanced finite element models. It is not clear how these demands can be predicted with more simplified approaches. Thus, at this point, it appears that we can predict the capacity of a connection using simplified approaches, but we cannot predict the forces for which the connection needs to be checked by simplified approaches. The need to use advanced finite element models to predict connection demands during a fire will likely be a major barrier to more widespread application of structural fire engineering analysis in routine building design applications.

7.3 FUTURE WORK

Based on the results of this research investigation, several issues have been identified where further study or research is needed. These issues are as follows:

- Further work is needed to fully characterize the time dependent effects on the elevated temperature stress-strain response of structural steel.
- Further work is needed in developing a uniform definition of yield strength of steel at elevated temperatures. Because steel loses its characteristic yield plateau at elevated temperature, defining yield strength becomes more subjective. The literature review indicated that previous researchers as well as building standards (Eurocode 3 and AISC Specification) have used a variety of different definitions of yield strength. This can lead to significantly different values of yield strength for the same stress-strain curve. Further, since the elevated temperature yield strength values are used in design equations for elevated temperature strength of structural steel members and

connections, the inconsistency in yield strength definitions results in inconsistencies in member strength calculations. Advancing the practice of structural-fire engineering would likely benefit from a uniform definition of yield strength.

- A factor that introduces considerable uncertainty in heat transfer analysis of steel members subjected to fire is the lack of data on temperature dependent thermal properties of commercially available insulation materials, including spray applied fire resistive materials, gypsum board, fiber board, intumescent coatings, etc. The data needed includes thermal conductivity, specific heat capacity, and density. These properties are needed over the full range of temperatures of interest in structural-fire engineering analysis; typically up to about 1000°C. Further work is needed to develop this data.
- Bolts play a critical role in connection performance at both ambient and elevated temperatures. Bolt behavior at elevated temperature is not only dependent on temperature but also strongly dependent on temperature history. The temperature history dependence of bolt strength can be particularly significant during the cooling stages of a fire, where the force on the bolts can be very large. Further work is needed to better characterize the relationship between bolt strength and temperature history.
- The behavior of beam end connections during a fire is closely interrelated with the behavior of the beam. It would be highly beneficial to conduct elevated temperature experiments on complete assemblies of beams together with their end connections. This would allow study of the beam and connection system under more realistic conditions.
- This study investigated the behavior of beam end framing connections in fire, but did not consider the influence that a composite concrete floor slab has on this behavior, other than its effect on the temperature distribution in the beam. Future research should consider the influence of the concrete floor slab on connection performance in fire.

- The experiments on connection subassemblies conducted in this investigation showed that shear tab connections can have a very large deformation capacity after the first connection element fractures and prior to complete failure of the connection (where the beam is completely separated from the adjoining column or girder). This large deformation capacity may be beneficial in fire. The finite element modeling techniques used in this study were not able to capture the behavior of the connection after fracture of the first connection elements. Future research should consider the use of more advanced analysis techniques that can predict connection behavior through the full sequence of fracture events that occur prior to complete failure.
- The results of this study showed that the behavior of beam end framing connections in fire is affected by many variables. Advanced finite element models provide a useful tool for studying this behavior. Ultimately, however, simpler analysis techniques are needed to evaluate the adequacy of connections in building subjected to fire. Considerable additional work is needed to develop simpler approaches for connection evaluation under fire conditions that are suitable for design practice.

It is clear from this research that modeling, predicting and understanding the behavior of beam end framing shear connections during a fire event is a difficult and complex problem. Connections are critical elements that affect the safety of a structure during and after a fire. Consequently, a thorough understanding of connection behavior during fire events is essential for developing appropriate analysis and design approaches that are needed as the US moves toward performance-based structural fire safety design.

References

1. ABAQUS Version 6.7 User's Manual. 2007. Hibbitt, Karlsson, & Sorensen, Inc., Pawtucket, RI.
2. Adams, C. and Beese, J.G. 1974. "Empirical Equations for Describing the Strain-Hardening Characteristics of Metals Subjected to Moderate Strains," *Journal of Engineering Materials and Technology*, 96(4): 123-126.
3. AISC. 1993. "Steel Construction Manual, Load and Resistance Factor Design," American Institute of Steel Construction, 2nd Ed., Chicago, IL.
4. AISC. 2005. "Specification for Structural Steel Buildings," Standard ANSI/AISC 360-05, American Institute of Steel Construction, Inc., Chicago, IL.
5. AISC. 2006. "Manual of Steel Construction," 13th Edition, American Institute of Steel Construction, Inc., Chicago, Illinois.
6. Al-Jabri K.S., Burgess, I.W., Plank R.J. 1996. "The Behavior of Semi-rigid Steel Beam to Column Connections under Fire Conditions," Progress Report. Sheffield: Department of Civil and Structural Engineering, University of Sheffield.
7. Al-Jabri K.S., Lennon, T., Burgess, I.W., Plank R.J. 1998. "Behavior of Steel and Composite Beam-column Connections in Fire," *Journal of Constructional Steel Research*, 46:1-3.
8. Al-Jabri K.S., Davison, J.B., Burgess, I.W. 2007. "Performance of beam-to-column joints in fire—A review," *Fire Safety Journal*, 43:50-62.
9. Anderburg, Y. 1988. "Modeling Steel Behavior," *Fire Safety Journal*, 13(1):17-26.
10. Ashakul, A. 2004. "Finite Element Analysis of Single Plate Shear Connections," Ph.D. Dissertation, Virginia Polytechnic Institute and State University.
11. Astaneh, A. "Demand and Supply of Ductility in Steel Shear Connections," *Journal of Constructional Steel Research*, 1989.
12. Astaneh, A., Liu, J., and McMullin, K. M. 2002. "Behavior and Design of Single Plate Shear Connections," *Journal of Constructional Steel Research*, Vol. 58, 1121 – 1141.

13. ASTM. 2000. "Standard Test Methods for Fire Tests of Building Construction and Materials," Standard No. E119-00a, American Society for Testing and Materials, West Conshohocken, PA.
14. ASTM A370-08B. 2008. "Standard Test Methods and Definitions for Mechanical Testing of Steel Products," American Society for Testing and Materials, West Conshohocken, PA.
15. ASTM E 21-05. 2005. "Standard Test Methods for Elevated Temperature Tension Tests of Metallic Materials," American Society for Testing and Materials, West Conshohocken, PA.
16. Bailey, C.G., Burgess, I.W., Plank, R.J. 1996. "The Lateral-Torsional Buckling of Unrestrained Steel Beams in Fire," *Journal of Constructional Steel Research*, 36(2):101-19.
17. Beedle, L., Tall, L. 1960. "Basic Column Strength," *Journal of the Structural Division, ASCE*, V 86, N7, pp. 139-173.
18. Buchanan, A. 2002. "Structural Design for Fire Safety," John Wiley and Sons, Ltd., England.
19. Buchanan, A., Moss, P., Seputro, J., Welsh, R. 2004. "The Effect of Stress-strain Relationships on the Fire Performance of Steel Beams," *Engineering Structures*, (26):1505-1515.
20. Burgess, I.W., El-Rimawi, J.A., Plank, R.J. 1990. "Analysis of Beams with Non-uniform Temperature Profile Due to Fire," *Journal of Constructional Steel Research*, 16:169-192.
21. Cardington Fire Test Report. 1998. "The Behavior of Multi-storey Steel Framed Building Subject to Fire Attack," *Experimental Data*, British Steel, Swinden Technology Center.
22. Cardington Fire Test Report. 2003. "Client Report: Results and Observations from Full-Scale Fire Test," *Experimental Data*, BRE Cardington.
23. CERF. 2004. "Fire Protection of Structural Steel in High-Rise Buildings," *Civil Engineering Research Foundation*, American Society of Civil Engineers.
24. Chen, J., Young, B. 2006. "Stress-strain Curves for Stainless Steel at Elevated Temperatures," *Engineering Structures*, Vol. 28, #2, pp 229-239.
25. Cooke, G.M.E. 1988. "An Introduction to Mechanical Properties of Structural Steel at Elevated Temperatures," *Fire Safety Journal*, Vol. 13, pp 45-54.

26. Cox, G. ed. 2001. "The Technical Basis for Performance-Based Fire Regulations: A Discussion of Capabilities, Needs, and Benefits of Fire Safety Engineering," United Engineering Foundation, New York, NY.
27. Daryan, A.S. and Yahyai, M. 2009. "Behavior of Welded Top-seat Angle Connections Exposed to Fire," *Fire Safety Journal*, Vol. 44, pp 603-611.
28. Dharma, R.B. and Tan, K.H. 2007. "Proposed Design Methods for Lateral Torsional Buckling of Unrestrained Steel Beams in Fire," *Journal of Constructional Steel Research*, 63:1066-1076.
29. Dieter, G. E. 1986. "Mechanical Metallurgy," 3rd edition, McGraw-Hill, New York.
30. El-Housseiny, O. M., Abdel Salam, S., Attia, G. A. M. and Saad, A. M. 1998. "Behavior of Extended End Plate Connections at High Temperature", *Journal of Constructional Steel Research*, 46 (1-3): p.299.
31. El-Rimawi, J.A., Burgess, I.W., Plank, R.J. 1997. "The Influence of Connection Stiffness on the Behavior of Steel Beams in Fire," *Journal of Constructional Steel Research*, 43(1-3):1-15.
32. El-Rimawi, J.A., Burgess, I.W., Plank, R.J. 1999. "Studies of the Behavior of Steel Subframes with Semi-rigid Connections in Fire," *Journal of Constructional Steel Research*, 43(1-3):1-15.
33. Eurocode 1: Actions on Structures – Part 1.2: General Actions – Actions on Structures Exposed to Fire, British Standards Institution, BS EN 1991-1-2:2002, November 2002, London, pp. 60.
34. Eurocode 3. 2006. Design of steel structures. Part 1-2: General rules. Structural fire design, EN 1993-1-2 European Committee for Standardization. CEN.
35. FEMA. 2002 "World Trade Center Building Performance Study: Data Collection, Preliminary Observations, and Recommendations," FEMA 403, Federal Emergency Management Agency, Washington, DC.
36. Fields, B.A. and Fields, R.J. 1989. "Elevated Temperature Deformation of Structural Steel." Report NISTIR 88-3899, National Institute of Standards and Technology, Gaithersburg, MD.
37. Fields, B.A. and Fields, R.J. 1991. "The Prediction of Elevated Temperature Deformation of Structural Steel under Anisothermal Conditions." Report NISTIR 91-4497, National Institute of Standards and Technology, Gaithersburg, MD.

38. Franssen J.M. 2005. "SAFIR. A Thermal/Structural Program Modeling Structures under Fire", *Engineering Journal, AISC*, 42(3):143–158.
39. Franssen, J.M., Kodur, V., and Zaharia, R. 2009. "Designing Steel Structures for Fire Safety." CRC Press.
40. Fujimoto, M., Furumura, F., Ave, T., and Shinohara, Y. 1980. "Primary Creep of Structural Steel (SS41) at High Temperatures," *Trans. of Architectural Institute of Japan* 296: 145-157.
41. Fujimoto, M., Furumura, F., and Ave, T. 1981. "Primary Creep of Structural Steel (SM50A) at High Temperatures," *Trans. of Architectural Institute of Japan* 306: 148-156.
42. Galambos, T.V. Editor 1998. "Guide to Stability Design Criteria for Metal Structures," 5th Edition, New York: John Wiley & Sons, Inc.
43. Garlock, M., and Selamet, S. 2010. "Modeling and Behavior of Steel Plate Connections Subject to Various Fire Scenarios," *Journal of Structural Engineering, ASCE*, V 136. N7, pp 897-906.
44. Gayle, F.W., Fields, R.J., Luecke, W.E., Banovic, S.W., Foecke, T., McCowan, C.N., McColskey, J.D., Siewert, T.A. 2005. "Federal Building and Fire Safety Investigation of the World Trade Center Disaster-Mechanical and Metallurgical Analysis of Structural Steel (Draft)," Report NCSTAR 1-3, National Institute of Standards and Technology, Gaithersburg, MD.
45. Gonzalez F., Lange J. 2008. "Material Behavior of High Strength Grade 10.9 Bolts under Fire Conditions," Fifth Conference on Steel and Composite, Graz, Austria.
46. Hall, Jr. 2008. "The Total Cost of Fire in the United States," National Fire Protection Association; Fire Analysis and Research Division, Quincy, MA.
47. Harmathy, T.Z. 1967. "A Comprehensive Creep Model", *Journal of Basis Engineering Transactions, ASME*, 396-502.
48. Harmathy, T.Z., Stanzak, W.W. 1970. "Elevated-Temperature Tensile and Creep Properties of Some Structural and Prestressing Steels," *Fire Test Performance, ASTM STP 464*, American Society for Testing and Materials, pp 186-208.
49. Hanus F., Zilli G. and Franssen J.-M. 2010. "Experimental Investigations and Analytical Model for the Behavior of Grade 8.8 Bolts and Butt Welds Under Heating and Subsequent Cooling," *Sixth International Conference Structures in Fire*, East Lansing, MI, USA.

50. Hill, H.N. 1944. "Determination of Stress-Strain Relations from "Offset" Yield Strength Values," NACA Technical Note No. 927, February 1944.
51. Hollomon, J.H. 1945. "Tensile Deformation," Transactions of Metallurgical Society, AIME, 162:268-290.
52. Hosford, W. 2010. "Solid Mechanics," Cambridge University Press, New York.
53. Hu, G. and Engelhardt, M.D. 2009 "Studies on the Behavior of Steel Single Plate Connections in Fire," Proceedings, the Second International Workshop on Performance, Protection & Strengthening of Structures under Extreme Loading, Hayama, Japan.
54. Hu, G. and Engelhardt, M.D. 2009. "Effect of Connection Details on The Response of Steel Single-plate Connections in Fire," Proceedings, 4th International Conference on Protection of Structures against Hazards, Beijing, China.
55. Hu, G., Morovat, M.A., Lee, J., Schell, E. and Engelhardt, M.D. 2009. "Elevated Temperature Properties of ASTM A992 Steel," Proceedings of ASCE Structure Congress 09, Austin, TX, USA.
56. IASIE. 2005. World Fire Statistics, International Association for the Study of Insurance Economics, Bulletin 19, Geneva.
57. Incropera, F., DeWitt, D., Bergman, T. and Lavine, A. 2007. "Fundamentals of Heat and Mass Transfer," 6th Edition, Wiley.
58. ISO. 1975. "Fire Resistance Tests-Elements of Building Construction," International Organization for Standardization, 834-1975.
59. Kelly, F.S., Sha, W. 1999. "A Comparison of the Mechanical Properties of Fire-Resistant and S275 Structural Steels," Journal of Constructional Steel Research, V 50, N 3, pp. 223-233.
60. Kirby, B.R., Preston, R.R. 1988. "High Temperatures Properties of Hot-rolled Structural Steels for Use in Fire Engineering Design Studies," Fire Safety Journal, Vol. 13, #1, pp27-37.
61. Kirby, B.R. 1995. "The Behavior of High-Strength Grade 8.8 Bolts in Fire," Journal of Constructional Steel Research, 33(1-2): 3-38.
62. Knight D., Skinner D.H., and Lay, M.G. 1971. Prediction of isothermal creep, BHP Melbourne Research Laboratories, Report MRL 18/2, The Broken Hill Proprietary Company Limited Australia, p. 1-14.

63. Kodur, V.K.R, Garlock, M., Iwankiw, N. 2007. "Structures in Fire: State-of-the-Art, Research and Training Needs." Report NIST GCR 07-915, CEE-RR-2007/03 – Proceedings of National Workshop on Structures in Fire. East Lansing, Michigan.
64. Lamalva, K.J., Barnett, J.R., Dusenberry, D.O. 2009. "Failure Analysis of the World Trade Center 5 Building," *Journal of Fire Protection Engineering*, 19:261-274.
65. Latham, D.J. and Kirby, B.R. 1993. "Elevated Temperature Behavior of Welded Joints in Structural Steelwork," Contract ECSC 7210 SA 824.
66. Lawson R.M. "Behavior of Steel Beam-to-column Connections in Fire," *The Structure Engineer*, 68(14):263-271.
67. Lee, J. and Engelhardt, M.D. 2010. "Material Properties of ASTM A992 Structural Steel After Heating and Cooling," Proceedings of US-Korea Conference on Science, Technology, and Entrepreneurship, Seattle, Washington, USA.
68. Lee, B.J., Pessiki, S., Kohno, M. 2006. "Analytical Investigation of Steel Column Fire Tests," ATLSS Report No. 06-23, Lehigh University.
69. Leston-Jones, L.C., Burgess, I.W., Lennon, T., Plank, R.J. 1997. "Elevated-temperature Moment-rotation Test on Steelwork Connections," Proceedings of Institution of Civil Engineers, Structures and Buildings, 122, 410-419.
70. Li, G., Li, M., Yin, Y. 2001. "Experimental Studies on the Behavior of High-strength bolts Made of 20mntib Steel at Elevated Temperatures," *China Civil Engineering Journal*, 34(5):100-104. (in Chinese)
71. Li, G., Jiang, S., Yin, Y., Chen, K., Li, M. 2003. "Experimental Studies on the Properties of Constructional Steels at Elevated Temperatures," *Journal of Structural Engineering*, ASCE, V 129, N 12, pp. 1717-1721.
72. Li, G., Wang, P., Jiang, S. 2007. "Non-linear Finite Element Analysis of Axially Restrained Steel Beams at Elevated Temperatures in A Fire," *Journal of Constructional Steel Research*, 63(9):1175-1183.
73. Li, G. and Guo, S. 2008. "Experiment on Restrained Steel Beams Subjected to Heating and Cooling," *Journal of Constructional Steel Research*, 64(3): 268-274.
74. Lie, T.T. 1992. "Structural Fire Protection," ASCE Manuals and Reports on Engineering Practice No. 78, New York, NY.
75. Lipson, S.L. 1968. "Single-Angle and Single-Plate Beam Framing Connections," Canadian Structural Engineering Conference, Toronto, pp. 141-162.

76. Liu, T.C.H., Morris L.J. 1994. "Theoretical Modeling of Steel Bolted Condition under Fire Exposure," Proceedings of International Conference on Computational Methods in Structural and Geotechnical Engineering Mechanics, Hong Kong.
77. Liu, T.C.H., 1996. "Finite Element Modeling of Behavior of Steel Beams and Connections in Fire," Journal of Constructional Steel Research, 35(3):181-99.
78. Liu, T.C.H., 1998. "Effect of Connection Flexibility on Fire Resistance of Steel Beams," Journal of Constructional Steel Research, 45:99-118.
79. Liu, T.C.H., 1998. "Three-dimensional Modeling of Steel/Concrete Composite Connection Behavior in Fire," Journal of Constructional Steel Research, 45(1-3):361.
80. Liu, T.C.H. 1999. "Fire Resistance of Unprotected Steel Beams with Moment Connections," Journal of Constructional Steel Research, 51:61-77.
81. Liu, T.C.H., Fahad, M.K. and Davies, J.M. 2002. "Experimental Investigation of Behavior of Axially Restrained Steel Beams in Fire," Journal of Constructional Steel Research, 58(9), 1211-1230.
82. Lou G., Yu S. and Wang R. 2010. "Experimental Study of Mechanical Properties of High-Strength Bolts After Fire," Sixth International Conference Structures in Fire, East Lansing, MI, USA.
83. Luecke, W.E., McColskey, J.D., McCowan, C. N., Banovic, S.W., Fields, R. J., Foecke, T., Siewert, T.A. and Gayle, F.W. 2005. "Federal Building and Fire Safety Investigation of the World Trade Center Disaster – Mechanical Properties of Structural Steels (Draft)," Report NIST NCSTAR 1-3D, National Institute of Standards and Technology, Gaithersburg, MD.
84. Mesquita, L.M.R., Piloto, P.A.G., Vaz, M.A.P., Vila Real, P.M.M. 2005. "Experimental and Numerical Research on the Critical Temperature of Lateral Unrestrained Steel I Beams," Journal of Constructional Steel Research, 61:1435-1446.
85. Metzger, K.B. 2006. "Experimental Verification of a New Single Plate Shear Connection Design Model," Master's Thesis, Virginia Polytechnic Institute and State University.
86. Morrison, W. 1966. "The Effect of Grain Size on the Stress-Strain Diagrams," National Bureau of Standards Journal of Research, 9:571-582.
87. Newman, G.M., Robinson, J.T. and Bailey, C.G. 2000. "Fire Safety Design: A New Approach to Multi-Storey Steel Framed Buildings," SCI Publication P288, the Steel Construction Institute, UK.

88. NIST. 2004. "Proceedings; NIST-SFPE Workshop for Development of a National R&D Roadmap for Structural Fire Safety Design and Retrofit of Structures," Report NISTIR 7133, Building and Fire Research Laboratory, National Institute of Standards and Technology, Gaithersburg, MD.
89. NIST. 2005. "Final Report on the Collapse of the World Trade Center Towers", Report NIST NCSTAR 1, National Institute of Standards and Technology, Gaithersburg, MD.
90. NIST. 2008. "Final Report on the Collapse of World Trade Center Building 7," Report NIST NCSTAR 1A, National Institute of Standards and Technology, Gaithersburg, MD.
91. NRC. 2003. "Making the Nation Safe from Fire – A Path Forward in Research," National Academies Press.
92. Outinen, J. 2006. "Mechanical Properties of Structural Steel at Elevated Temperatures and After Cooling Down," Helsinki University of Technology, Laboratory of Steel Structures, Finland.
93. Osgood, W.R. 1932, "Column Curves and Stress-Strain Diagrams," National Bureau of Standards Journal of Research, 9:571-582.
94. Plank, R.J. 2000. "The Performance of Composite Steel Framed Building Structures in Fire," Progress in Structural Engineering and Materials, Vol. 2, John Wiley and Sons, Ltd., p 179-186.
95. Plen, E. 1975. "Theoretical and Experimental Investigation of Point Set Structures", Document D9, Swedish Council for Building Research.
96. Poh, K.W. 1997. "General Stress-Strain Equation," Journal of Materials in Civil Engineering, ASCE, 9(4):214-217.
97. Rahman, A., Hawileh, R., Mahamid, M. 2004. "The Effect of Fire Loading on A Steel Frame and Connection," High-Performance Structure and Materials II, WIT Press, p. 307-316.
98. Ramberg, W. and Osgood, W.R. 1943, Description of Stress-Strain Curves by Three Parameters, NACA Technical Note No. 902, July 1943.
99. Richard, R. M., Gillett, P. E., Kriegh, J. D., and Lewis, B. A. 1980. "The Analysis and Design of Single Plate Framing Connections," Engineering Journal, American Institute of Steel Construction, Vol. 17, 38- 52.

100. Richard, R. M., Kriegh, J. D., and Hormby, D. E. 1982. "Design Single Plate Framing Connections with A 307 Bolts," Engineering journal, AISC, pp 209–213.
101. Robinson J. and Latham, D. 1986. "Fire Resistant Design – the Future Challenge," in Design of Structures Against Fire - Proceedings of the International Conference on Design of Structures Against Fire, Birmingham, UK, Elsevier Applied Science.
102. Santiago, A., Simões da Silva, L., Vila Real, P., Franssen, J.M. 2003. "Effect of Cooling on the Behavior of A Steel Beam under Fire Loading Including the End Joint Response," Proceedings of the 9th International Conference on Civil and Structural Engineering Computing, United Kingdom, paper 65.
103. Santiago, A., Simões da Silva, L., Vila Real, P. 2004. "Three Dimensional Modeling of Beam-column Subassembly under Fire Loading," Proceedings of 10th Nordic Steel Construction Conference, p.567-575, Copenhagen, Denmark.
104. Santiago, A., Simões da Silva, L.S., Vila Real, P., Vaz, G. and Lopes, A.G. 2009. "Experimental Evaluation of the Influence of Connection Typology on the Behavior of Steel Structures under Fire", Engineering Journal, 46(2):81-98.
105. Sarraj, M. 2007. "The Behavior of Steel Fin Plate Connections in Fire," Ph.D. thesis. University of Sheffield.
106. Sakumoto Y. 1993. "Test of fire resistant bolts and joints," Journal of Structural Engineering, Vol. 119 No. 11, ASCE Publications.
107. Selamet, S., Garlock, M.E. 2010. "Robust Fire Design of Single Plate Steel Connections," Engineering Structures, accepted for publication.
108. Scott, D, Lane, B and Gibbons, C. 2003. "Fire Induced Progressive Collapse," Prevention of Progressive Collapse: Report on the July 2002 National Workshop on Recommendations for Future Efforts, Multihazard Mitigation Council of the National Institute of Building Sciences, Washington, D.C.
109. Shi, Y., Zhou, Y. 2006. "ABAQUS Finite Element Analysis Examples," China Machine Press, Beijing.
110. Simões da Silva, L., Aldina, S. and Paulo, V.R. 2001. "A Component Model for the Behavior of Steel Joints at Elevated Temperatures", Journal of Constructional Steel Research, 57: pp1169–1195.
111. Simões da Silva, L. and Santiago, A. 2004. "Behavior of Steel Joints under Fire Loading," Proceedings of the Second International Conference on Steel & Composite Structures, Seoul, Korea.

112. Spyrou S., Davison, B., Burgess, I.W., Plank, R. 2002. "Component-based Studies on the Behavior of Steel Joints at Elevated Temperatures," Proceedings of Third European Conference on Steel Structures, Coimbra: University de Coimbra: p. 1469-78.
113. SSRC. 1987. "Technical Memorandum No. 8: Standard Methods and Definitions for Tests for Static Yield Stress," Structural Stability Research Council.
114. Subramanian, L. 2008. "Parametric Studies on Thermal Properties of Materials in Structural-Fire Engineering." M.S. Thesis, Department of Civil, Architectural and Environmental Engineering, University of Texas at Austin.
115. Swift, H.W. 1946. "Plastic Strain in Isotropic-Hardening Material," Engineering, 162: 381-384.
116. Tan, K.H., Ting, S.K. and Huang, Z.F. 2002. "Visco-elastoplastic Analysis of Steel Frames in Fire", Journal of Structural Engineering, ASCE, 128(1):105-114.
117. Tan, K.H. and Huang, Z.F. 2005. "Structural Responses of Axially Restrained Steel Beams with Semirigid Moment Connection in Fire," Journal of Structural Engineering, 131(4):541-551.
118. Tan, K.H. and Qian, Z.H. 2008. "Experimental Behavior of Thermally Restrained Plate Girder Loaded in Shear at Elevated Temperatures," Journal of Constructional Steel Research. 64(5):596-606.
119. Ticha, A. and Wald, F. 2005. "Temperature Development in Fin Plate Connection under Fire," Center for Integrated Design of Advanced Structures.
120. Twilt, L., Both, C. 1991. "Stress-strain Relationships of Structural Steel at Elevated Temperatures: Analysis of Various Options & European Proposal," SA 112 Part F: mechanical properties.
121. United States Steel. 1972. "Steels for Elevated Temperature Service," United States Steel Corporation, Pittsburg, PA.
122. Usmani, A.S., Rotter, J.M., Lamont, S., Sanad, A.M. and Gillie, M. 2001. "Fundamental Principles of Structural Behavior under Thermal Effects," Fire Safety Journal, Vol. 36, Elsevier Science Ltd., p 721-744.
123. Van der Vegte, G.J., Makino, Y. 2004. "Numerical Simulations of Bolted Connections: the Implicit Versus the Explicit Approach," AISC-ECCS, Connections in Steel Structures, Amsterdam, p. 89-98.

124. Vila Real P.M.M., Cazeli R., Simões da Silva L., Santiago A., Piloto P. 2003. "The effect of residual stresses in lateral torsional buckling of steel I-beams at elevated temperature," *Journal of Constructional Steel Research*. 60(3-5):783-93.
125. Vila Real P.M.M., Piloto, P.A.G., Franssen, J.M. 2003. "A New Proposal of A Simple Model for the Lateral-torsional Buckling of Unrestrained Steel I-beams in Case of Fire: Experimental and Numerical Validation," *Journal of Constructional Steel Research*, 59(2):179-99.
126. Voce, E. 1948. "The Relationship between Stress and Strain for Homogeneous Deformation," *Journal of the Institute of Metals*, 74:537.
127. Wald, F., Chladna, M., Moore, D., Santiago, A., Lennon, T. 2004. "The Temperature Distribution in A Full-Scale Steel Framed Building Subjected to A Natural Fire," *Proceedings of The Third International Conference on Steel & Composite Structures*, Seoul, Korea.
128. Wald, F., Simes da Silva, L., Moore, D.B., Lennon, T., Chadn, M., Santiago, A., Benes, M. and Borges, L. 2006. "Experimental Behavior of Steel Structures under Natural Fire," *Fire Safety Journal* 41 (7), pp. 509-522.
129. Wang, Y.C. 2002. "Steel and Composite Structures – Behavior and Design for Fire Safety," Spon Press, London.
130. Wang, Y.C. 2005. "Performance of Steel-Concrete Composite Structures in Fire," *Progress in Structural Engineering and Materials*, Vol. 7, John Wiley and Sons, Ltd., p 86-102.
131. Williams-Leir, G. 1983. "Creep of Structural Steel in Fire: Analytical Expressions," *Fire and Materials* 7(2): 73-78.
132. Wong, M.B., Ghojel, J.I. 2003. "Sensitivity Analysis of Heat Transfer Formulations for Insulated Structural Steel Components," *Journal of Fire Safety*, (38):187-201.
133. Yin, Y.Z. and Wang, Y.C. 2003. "Numerical Simulations of the Effects of Non-uniform Temperature Distributions on Lateral Torsional Buckling Resistance of Steel I-Beams," *Journal of Constructional Steel Research*, 59:1009-1033.
134. Yin, Y.Z. and Wang, Y.C. 2004. "A Numerical Study of Large Deflection Behavior of Restrained Steel Beams at Elevated Temperatures," *Journal of Constructional Steel Research*, 60(7), 1029-1047.
135. Yin, Y.Z. and Wang, Y.C. 2005. "Analysis of Catenary Action in Steel Beams Using A Simplified Hand Calculation Method, Part 1: Theory and Validation for

Uniform Temperature Distribution,” *Journal of Constructional Steel Research*, 61(2):183-211.

136. Yin, Y.Z. and Wang, Y.C. 2005. “Analysis of Catenary Action in Steel Beams Using A Simplified Hand Calculation Method, Part 2: Validation for Non-uniform Temperature Distribution,” *Journal of Constructional Steel Research*, 61(2):213-234.
137. Yu H., Burgess I.W., Davison, J.B. Plank, R.J. 2008. “Numerical Simulation of Bolted Steel Connections in Fire Using Explicit Dynamic Analysis,” *Journal of Constructional Steel Research*, 64(5):515-525.
138. Yu, H., Burgess, I.W., Davison, J.B., Plank, R.J. 2009. “Experimental Investigation of the Behavior of Fin Plate Connections in Fire,” *Journal of Constructional Steel Research*, 65(3), 723-746.
139. Yu, L. 2006. “Behavior of Bolted Connections During and After a Fire,” Ph.D. Dissertation, Department of Civil, Architectural and Environmental Engineering, University of Texas at Austin.

VITA

Guanyu Hu was born in Chengde, Hebei, China on January 15, 1980, the son of Dashi Hu and Juan Chang. After graduating from No. 1 High School of Chengde, Hebei in 1997, he enrolled in Zhejiang University, Hangzhou, China. He graduated with a Bachelor of Science in Civil Engineering in 2001 from Zhejiang University. In 2002, he entered the graduate school at The University of Akron, and graduated from there with a Master of Science in Civil Engineering in December 2003. He entered the doctoral program in The University of Texas at Austin in 2004. In 2006, he started working as a structural engineer in Butler Manufacturing Company in San Marcos, Texas and obtained his professional engineer license in July 2009. In September 2007, he re-entered the doctoral program in Civil Engineering at The University of Texas at Austin.

Permanent Address:

Banbishan Street, Nanyuan Xiaoqu, Building 13, 2-404

Chengde, Hebei, 067000

P.R. China

This dissertation was typed by the author.